Universität Rostock Traditio et Innovatio

Membranes based on polymerized vinylalkylimidazolium bromides

From ionic liquid monomers to membrane application

Dissertation

to obtain the academic degree

"doctor rerum naturalium" (Dr. rer. nat.)

submitted at the

Faculty of Mathematics and Natural Sciences

University of Rostock

submitted by

Fridolin O. Sommer, M. Sc.

born on August 1st, 1994 in Leverkusen

Rostock, November 2020

https://doi.org/10.18453/rosdok_id00003033

Referees:

1st Referee: Prof. Dr. Udo Kragl
University of Rostock
Institute of Chemistry
Division of Analytical and Industrial Chemistry
Albert-Einstein-Straße 3a
D-18059 Rostock

2nd Referee: Prof. Dr. Dieter Vogt
Technical University of Dortmund
Faculty of Biochemical and Chemical Engineering
Chair for Industrial Chemistry
Emil-Figge-Straße 66
D-44227 Dortmund

Thesis submission: November 13th, 2020

PhD defense: April 13th, 2021

The present work was conducted during the period from June 2017 until September 2020 under the supervision of PROF. DR. UDO KRAGL at the Institute of Chemistry at the University of Rostock.

J'ai pété les plombs, sans abandonner ni baisser les bras

Plus d'nouvelles, batterie faible, malédiction

Dorénavant, je vais de l'avant

C'est ma direction

Bastien Vincent, Djuna Gandhi,
Karim Fall, Adama Diallo, Stany Kibulu

Acknowledgment

I like to take the opportunity to thank the many peoples whose help, support and understanding were necessary to make this work.

First, I like to thank PROF. DR. UDO KRAGL for offering me to work in his research group as well as for supporting me to participate at different conferences and realizing bigger projects. Thank you for this open-minded project in which I could pursue my ideas.

My thanks go to DR. DIRK MICHALIK for the NMR measurements, REGINA LANGE and DR. INGO BARKE for conducting and supporting the AFM experiments. I would also like to thank VICTORIA ALADIN for the measurements and the brief excursion into the field of solid-state NMR.

Foremost all the technical staff, I would like to thank PETER KUMM and MARTIN RIEDEL of the precision mechanics workshop for all the manufactured cells, casting knives, molds, lamps and punching templates. Many thanks for your great willingness so that I could benefit the most from my equipment.

For the welcoming atmosphere, I want to thank the entire research group. I appreciated and had a lot of fun during our coffee breaks. I would like to thank SANDRA DIEDERICH for help with all the smaller problems in daily laboratory life. JANA SOPHIE APPELT and LUKAS TIEDT, thank you for your contribution to this project.

A big thank you to my family for the support and understanding during the past, sometimes crazy and tedious, eight years. Thanks for your confidence, in asking the right (non-scientific) questions and for the many places where I could take some time off.

NATALIE, thank you for the critical questions, your persistence in finding my inaccuracies and your infinite support.

All others, which are not named specifically here, I would like to thank for the short moments that saved the day, distracted me positively from stubborn problems or just endured me the moments I was not in the mood.

Table of contents

List of Symbols and Abbreviations

ABCVA	Azobis(cyanovaleric acid)
ACN	Acetonitrile
AIBN	2,2'-Azobis(2-methylpropionitrile)
BASIL	Biphasic Acid Scavenging utilizing Ionic Liquids
BEE	Benzoin ethyl ether
DGDE	Diethyl glycol dimethyl ether
DMF	Dimethylformamide
DMSO	Dimethyl sulfoxide
DVB	Divinylbenzene
EtOH	Ethanol
H_2O	Water
HPLC	High pressure liquid chromatography
IL	Ionic liquid
LiCl	Lithium chloride
MTBE	Methyl-*tert*-butyl ether
MWCO	Molecular weight cut off
NF	Nanofiltration
NMP	*N*-methyl-2-pyrrolidon
NMR	Nuclear magnetic resonance
PAA	Poly acrylic acid
PEG	Polyethylene glycol
PILs	Polymerized ionic liquids
PVDF	Polyvinylidene fluoride
RAFT	Reversible addition-fragmentation chain transfer
RTIL	Room temperature ionic liquids
ssNMR	Solid-state nuclear magnetic resonance
TEG	Triethylene glycol
TPO	Diphenyl-(2,4,6-trimethylbonzoyl)-phosphine oxide
UF	Ultrafiltration
UV	Ultraviolet
VIm	Vinylimidazole
[VBnIm]Br	3-Benzyl-1-vinyl-1*H*-imidazol-3-ium bromide
[VBuIm]Br	3-Butyl-1-vinyl-1*H*-imidazol-3-ium bromide
[VDodecIm]Br	3-Dodecyl-1-vinyl-1*H*-imidazol-3-ium bromide
[VEtIm]Br	3-Ethyl-1-vinyl-1*H*-imidazol-3-ium bromide
[VHexIm]Br	3-Hexyl-1-vinyl-1*H*-imidazol-3-ium bromide
[VOcdecIm]Br	3-Octadecyl-1-vinyl-1*H*-imidazol-3-ium bromide
[VEOPIm]Br	3-(1-Ethoxy-1-oxopropan-2-yl)-1-vinyl-1*H*-imidazol-3-ium bromide
[VPryIm]Br	3-(Prop-2-yn-1-yl)-1-vinyl-1*H*-imidazol-3-ium bromide

Index of figures and tables

Abstract

The increasing amount of wastewater due to industry, agriculture and domestic endangers the environment as well as health. New and more complex chemicals and residues stress the existing purification and downstream applications towards clean fresh water. Besides established filtration materials, there is a need for innovative, functional materials facing today's challenges.

Ionic liquids represent a class of substances with interesting properties as they are non-flammable, non-volatile, resistant towards aggressive chemicals and highly charged because of their salt character. Due to their synthetic origin, a high number of possible cation and anion combinations is applicable. By polymerizable groups such as vinyl functions, they can be used in material synthesis. Free radical polymerizations of these ionic liquids offer an efficient possibility to synthesize highly functionalized separation materials.

This work presents an universal synthetic approach towards free-standing polymeric membranes consisting of polymerized ionic liquids. Hereby, a membrane formation method was elaborated that does not need to be adapted to the ionic liquids and demonstrating a high reproducibility of the materials. Different vinylalkylimidazolium bromide ionic liquids were used to synthesize membranes and utilize them in aqueous filtration as well as electrodialysis as separation material. Charged substrates such as sugars or dyes were withheld with up to 99% whereby the membrane material was stable up to 2000 hours without a significant loss in efficiency. In electrodialysis, PILs membranes offered a highly stable anion exchange material.

Zusammenfassung

Der steigende Anteil verunreinigter Abwässer aus Industrieanwendungen, der Landwirtschaft sowie dem täglichen Leben gefährden sowohl die Umwelt als auch die Gesundheit nachhaltig. Immer höhere Konzentrationen von Rückständen in diesen Abwässern beanspruchen stark die bestehenden Verfahren der Wasseraufbereitung. Neben dem Scale-up bestehender Prozesse besteht daher auch ein Bedarf an neuen Filtrationsmaterialien, die durch ihre Eigenschaften den aktuellen Problemen entgegenwirken.

Ionischen Flüssigkeiten sind eine nicht-natürliche Stoffklasse, welche nicht-flüchtig, nicht entflammbar, chemisch resistent und geladen sind. Auf Grund ihres synthetischen Ursprungs sind eine Vielzahl von Kombinationen aus unterschiedlichen Anionen und Kationen möglich, wobei auch funktionalisierte Gruppen in die ionische Flüssigkeit eingeführt werden können. Die freie radikalische Polymerisation dieser Stoffklasse bietet eine effiziente Möglichkeit hochfunktionalisierte Materialien herzustellen.

In dieser Arbeit wird ein universeller Ansatz für die Synthese freistehender Polymermembranen aus polymerisierten ionischen Flüssigkeiten vorgestellt. Die Membranen, bestehend aus verschiedenen Vinylalkylimidazoliumbromid ionischen Flüssigkeiten, wurden reproduzierbar und ohne weitere Anpassung an die jeweiligen ionischen Flüssigkeiten synthetisiert und erfolgreich in wässrigen Filtrationen eingesetzt. Nachfolgend wurden geladene Zucker sowie Farbstoffe mit bis zu 99% Effizienz über 2000 Stunden zurückgehalten. In der Elektrodialyse wurde außerdem gezeigt, dass polymerisierte ionische Flüssigkeiten ein hochstabiles Material für Anionenaustauschermembranen darstellen.

1. Introduction

1.1 Membranes

1.1.1 What is a membrane and how to synthesize them?

Membranes are thin materials through which transport by different driving forces is possible.[1] They can be selective barriers for liquids, nanoparticles, (macro-)molecules or gases. Roughly, membranes can be divided into biological and synthetic membranes.

1.1.1.1 Biological membranes

Biological membranes consisting of lipid bilayers execute several functions in nature as they separate the inner cell from the extracellular environment, define reaction comportments or playing a role in responding to external physical and biochemical stimuli and signal transduction.[2,3] Additionally, proteins embedded in the membrane bilayer are responsible for the selective transport of essential or undesired substrates through pores and channels. On the outside, attached proteins assume tasks in signaling, recognition, cell structure, transformation and division.[4]

Compared to artificial membranes, the main drawback of biological ones is the weak stability to sustain needs in industrial applications such as higher pressures, a wider scope of temperature, harsh chemical conditions or a lower permeability. In contrast to natural membranes, synthetic materials are adjustable to different temperatures, pressures or solvents in applications even though the challenges are to imitate biological selectivity and recognition properties.[3]

1.1.1.1 Classification of synthetic membranes

Man-made materials can be classified by several aspects. First, membranes can be differentiated according to their material. Second, the type of filtration operation the membranes are used for is subjected to classify them. Depending on the process design, also the design or shape of the membrane unit are used to differentiate between the materials.

Figure 1 gives an overview of the various types of membranes according to the structure, configuration and material whereby not every combination must be feasible in applications. The most common starting materials for membrane synthesis are glass, ceramic, metals, liquids or polymers, although mixtures of these materials are also used. The configuration in which the material is finally used as a membrane depends on the requirements in the specific application. Possible configurations can be flat, spiral wound or tubular. Additionally, the materials can be subdivided into symmetric and asymmetric structures.[5]

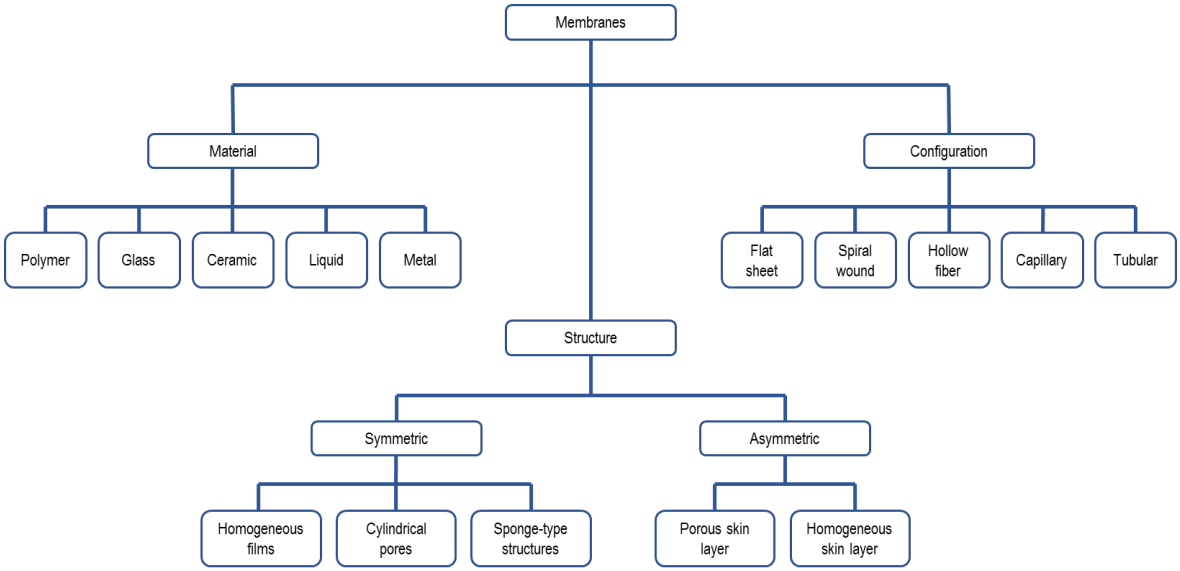

Figure 1: Overview of the various materials, structures and configurations of relevant synthetic membranes.[5,6]

Due to the emphasis of this work, following sections will focus on polymeric membranes. The most common materials for polymer membranes are cellulose, polyvinylidene fluoride, polysulfones, polyamide or polyacrylonitrile. Derivatives of these are used as well. For applications, the membranes are selected by their properties as they should operate in aqueous respectively organic solvents or provide high resistances against certain liquids such as acids, bases or harsh cleaning agents. In addition, the membranes might have a strong hydrophobic or hydrophilic character that is of interest for the application. First commercial polymer membranes were synthesized in 1920 by the German company Sartorius.[7]

1.1.1.2 Membrane processes

Various biological and chemical procedures are possible to enable transport through membranes: pressure, concentration or electric potential gradients. Thus, membrane processes need to be chosen specifically to the application so that for example pores and channels of the materials should be smaller than the substrate size to operate as size exclusion. However, most of the materials have a pore size distribution instead of a discreet value. Within the focus of this work, membranes for pressure-driven liquid-liquid filtrations are reviewed. Figure 2 gives an overview of the basic processes of microfiltration (MF), ultrafiltration (UF), nanofiltration (NF) and reverse osmosis (RO).

Microfiltration (MF) is a widely used, low-cost filtration process also serving as a pretreatment for further purification methods. The large range of 0.1 to 10 µm allows to retain suspended particles, large macromolecules, microorganisms with various applications in *e.g.* food industry or biotechnology.[8] Even though most viruses have a size of 0.02 µm a few of them, such as the poliovirus or coliphage, can be significantly removed by microfiltration.[9,10] Mainly, MF is used in water treatment as it enables high process volumes and removes also blood cells, antifoaming agents or oil.

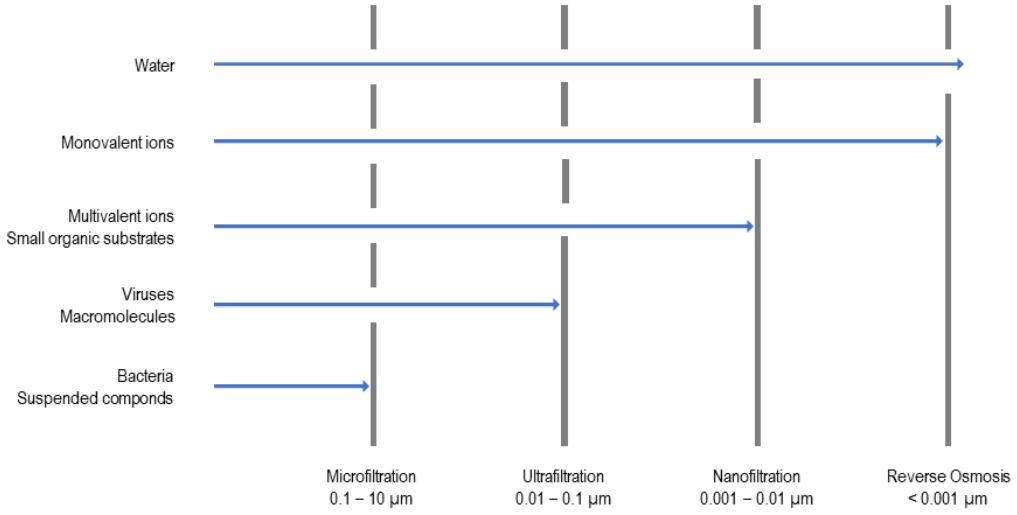

Figure 2: Schematic overview of pressure-driven membrane processes.[11]

Ultrafiltration (UF) membranes with a range of 0.01 to 0.1 µm show increased performance in the removal of macromolecules and viruses.[12] Besides comparable applications to the MF, UF is used in the clarification of juices and biopharmaceutical purification steps as water and buffers pass the membrane.[13]

By rejecting substrates smaller sizes of 0.001 µm, reverse osmosis (RO) membranes are crucial in the desalination of water as it rejects even small inorganic salts. Compared to the other types of filtration, RO is affiliated to high operating pressures to overcome for example the natural osmotic pressure to desalinate seawater. Nanofiltration (NF) is also used to remove very small compounds such as catalysts and ions but with a bigger scale (0.001 to 0.01 µm) than reverse osmosis. Compared to MF and UF, membranes used in NF are classified by the application and the substances to be separated instead of a transport mechanism or structure type. Using lower pressures than at reverse osmosis, nanofiltration applications include the recovery of homogeneous catalysts, active pharmaceutical agents, sugars or organic solvents.[11]

1.1.1.3 Electrodialysis

Electrodialysis is one of several applications for charged ion exchange membranes. To the polymeric membrane backbone fixed charges inhibit ions of the same charge to permeate the layer.[14] End of the 19th century, FRIEDRICH WILHELM OSTWALD and FREDERICK GEORGE DONNAN published fundamental research on chemically modified materials from natural resources[15,16] or resin-, alumina- or resorcinol-formaldehyde impregnated filter papers.[17,18] After World War II, developments in polymer chemistry, such as new catalysts for simplified synthesis, were also beneficial for electrodialysis and the first plants installed.[17,18] These suffered the first two decades of mechanical long-term stability and fouling problems, inhibiting a large scale-up. Even though the reverse electrodialysis process overcame several drawbacks, other technologies took the lead. Still, end of the 1970s an important class of polymeric membranes was established for electrodialysis

applications.[14] With the trade name Nafion®, perfluoro-carbon polymers were invented by DuPont and extended the research towards charged membrane materials. These layers were made of sulfinol fluoride vinyl ether and tetrafluoroethylene with a thickness of 120 µm.[14] Here, a strong hydrophobic backbone is combined with polar groups at the side chain. Nafion® and similar perfluoro-polymers such as Aciplex™ by Asahi Chemical or Tokuyama Soda were used in harsh conditions such as the chlor-alkali electrodialysis (Figure 3).[19]

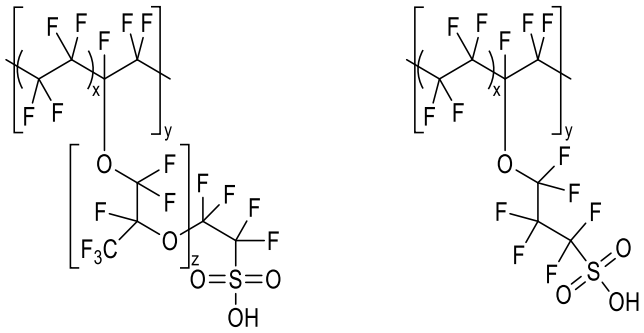

Figure 3: Chemical structures of the perfluoro-polymers Nafion® and Aciplex™.[19]

Early, the electrodialysis was suggested to be an efficient tool to clean up aqueous salt-containing solutions[20], leading to investigations of multilayer arrangements with several anion and cation exchange membranes.[21] These multilayered cell pairs are flushed with salt-containing solutions during application. Due to an electric potential of the membrane's cationic species of the solution passes easily the negatively charged layers towards the cathode and anionic species contrary to the anode. Accordingly, anions and cations cannot pass in the same direction. The space next to the cation and anion exchange membranes is getting ion-rich while the space in between both membranes gets drained of ions.[14] A schematic design of an electrodialysis stack with one ion exchange membrane pair is given in Figure 4.

The distribution of ions in the electrodialysis stack is, even though it is a turbulent flux, not homogenous. Due to the diffusion and rejection of ions at the charged membranes, depleted areas of cations and anions occur. In contrast, these depleted regions have high concentrations of the contrary ion so that a polarization concentration is observed influencing the system efficiency significantly. However, ions can diffuse by higher energy consumption. If increasing energy enables ion flux, the limiting current density is reached and undesired side reactions or destruction of the membrane material is favored.[22]

In industrial applications, hundreds of cell pairs are used to increase the efficiency of the electrolysis. Historically, electrodialysis was mainly used for brackish or seawater purification, in Japan as well for salt recovery from seawater.[23] Also, the steadily increasing amount of nitrate in groundwater can be removed by electrodialysis as nitrate is a harmful chemical towards organisms. Electrochemical reduction enables an up to five times higher reduction of this salt compared to filtration methods. It is one of the most promising approaches as the natural condition of groundwater is preserved by not or only slightly removing various ions, while the nitrate concentration is at least reduced by half.[24]

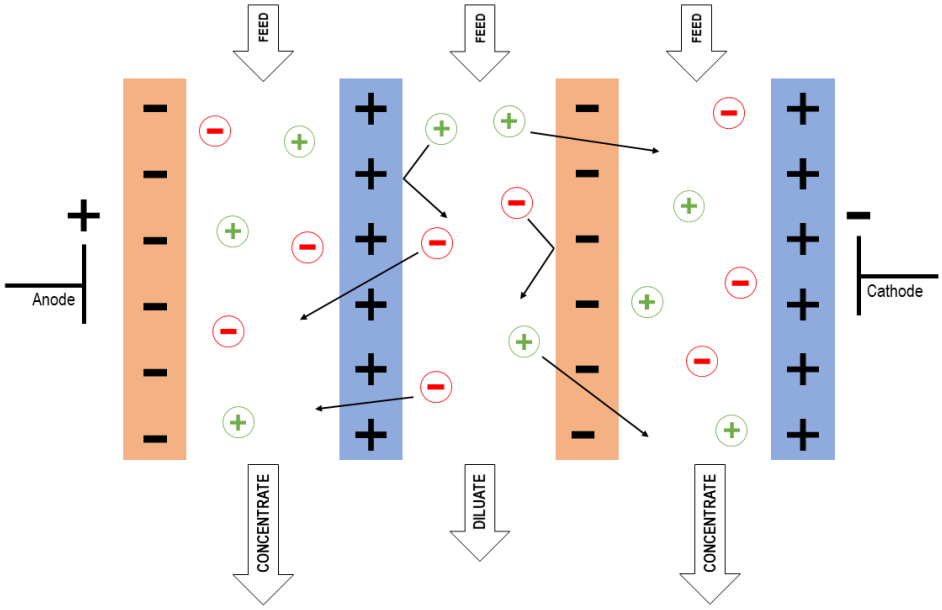

Figure 4: Scheme of electrodialysis without a bipolar membrane (orange: cation exchange membranes, blue: anion exchange membranes).

Alternatively, it is used in the food industry to demineralize whey, pre-treatment of wine[25], deacidification of juice[26,27] or the desalination of soybean sauce. For the demineralization of cheese whey[28], potassium and chloride ions are removed in an early stage. The voltage drop rises by the permeation of citric acid and phosphate so that in industry about a third is additionally removed by ion exchange resins afterward.[29] Comparable process setups with exchange resins in front of an electrodialysis remove up to 80% of undesired ions in the process, softening the feed stream and decrease the operational costs of the electrodialysis.[24] In fermentation processes, experimental setups are scaled-up by installing larger batch processing. Electrodialysis enables a continuous fermentation as charged products are removed from the feed. For example, amino acids are withheld by the anionic and cationic membranes while the used acids diffuse through the layers.[30] The continuous operation increases the economic efficiency as setup times are decreased.

Further development of the electrodialysis is the bipolar procedure (Figure 5). Using a membrane triplet with a bipolar membrane, three different cells are formed in between the layers when an electrical potential is applied. Between the anion and cation exchange membranes, a salt solution passes the cell. Respecting the charges of the membranes, certain ions can pass into the cells between the ion exchange and bipolar membrane. By electrolytic water splitting protons and hydroxide ions formed and the acid and base of the corresponding salt are generated.

Since the 1990s, bipolar membranes were initially used in industry to reduce the energy consumption for the formation of caustic soda solution by two thirds.[31] Despite slightly increased initials costs due to the additional membrane, this refined electrodialysis with bipolar offered a variety of new applications. For instance the production of organic acids such as gluconic[32] or lactic acid[33] from fermentation processes in biotechnology. As the pH value might decrease during fermentation, the addition of bases balances the pH value and prevents

product inhibition. The formed salt is soluble in the broth and is recovered with the produced acid. To increase the efficiency of the fermentation and overcome product loss due to pH adjustments, electrodialysis is used to recycle the base and reobtain the acid.[34] This process management was also applied in wastewater treatment to recover hydrofluoric and nitric acid from steel picking solutions.[22]

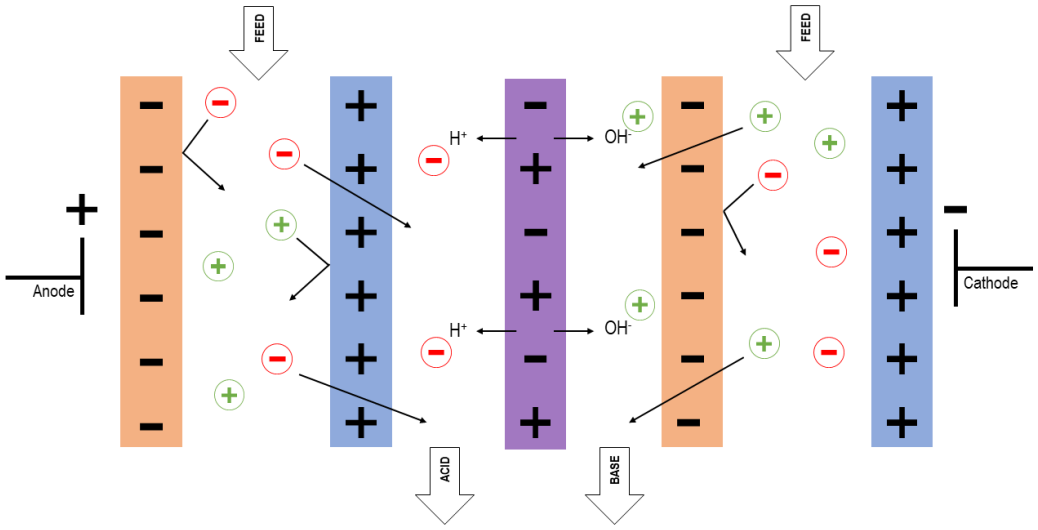

Figure 5: Schematic process of electrodialysis with a bipolar membrane (orange: cation exchange membranes, blue: anion exchange membranes, violet: bipolar membrane).

1.1.1.4 Fabrication of polymeric membranes

The synthesis of membranes is described manifold in literature.[35–37] Fundamental techniques are phase inversion, sol-gel order extruding processes using diverse materials as organic polymers, ceramics or composite materials.[6] The different manufacturing methods thus enable a wide number of structures, functions, transport mechanisms and properties.[5] Besides, basic properties such as the molecular weight or the chain flexibility are already given by the selection of the polymer. For example, carbon-carbon single bonds in the polymer backbone lead to flexible overall structures while carbon-carbon double bonds or phosphorus-nitrogen double bonds result in less flexible, rigid polymers. In addition, thermal and chemical properties are hereby defined where non-covalent interactions in branched polymers are also significant.[5]

Table 1 gives an overview of these fabrication methods, their advantages and disadvantages. Hereby, Table 1 does not specify synthetic routes towards composite, inorganic or liquid-liquid membranes that are also made by dip-coating, interfacial polymerization or sol-gel processes as these will not be part of this work. Further information on the fabrication methods of these membranes can be found in the literature.[38–42]

Table 1: Types of membranes formation with their advantages and disadvantages.[43,44]

Method (Filtration type)	**Advantages**	**Disadvantages**
Electrospinning	- One-step process - High porosity and tunable pore size - Generating nanostructures as core-sheath, trilayer nanofibers	- Diameters lower 100 nm hard to obtain - Slow process yield
Sintering (MF)	- Symmetric membranes with pore size of 0.1-10 µm - Suitable for application in harsh conditions - No solvents required	- Only 10-20% porosity - High process temperature - Need of particles with narrow size distribution
Stretching (MF)	- Symmetric membranes with pore sizes of 0.02-3 µm - Porosity up to 90% - Suitable for chemical stable materials (PTFE, PE, PP)	- High process temperature
Track-etching (MF/UF)	- Symmetric membranes with pore sizes of 0.02-10 µm - Cylindrical pores - Narrow pore size distribution	- High cost - Low porosity (5-10%) - Suitable polymers limited
Template leaching	- Symmetric membranes with pore sizes of 0.5-10 µm - High flux - Extreme narrow pore size distribution	- High cost - Difficult to scale up - Complex process
Phase inversion (all types of filtration)	- Usable for a wide number of polymers - Easy process and simple to scale up - High porosity (80%) - Small pores on surfaces and large pores inside	- Solubility and non-solubility of polymer in different liquids must be given
Solution coatings (NF/gas separation)	- Composite of selective layers	- Solubility and non-solubility of polymer in different liquids must be given

For clarity, the number of possibilities is limited to phase inversion for this work. Phase inversion is an universally applied method to produce membranes from all types of polymers.[45] In general, a layer with a thickness of up to several hundred micrometers is applied onto a plate or production line[46] as support.[47] Also

the application, that is performed as pouring or casting of a solved polymer, is feasible onto commercial microporous membranes as support.[5] The following immersion of this film with the support in a precipitant or coagulation bath separates the polymer film into a polymer-rich solid and a solvent-rich liquid phase. Often, the precipitant or so-called non-solvent is water or an aqueous phase.[48]

As phase inversion is not limited to a certain type of polymer, other settings specify the properties of the obtained membranes that are the concentration of the polymer in the dope solution, the ratio of solvent and co-solvent and the evaporation of the solvents before the precipitation.[49] Casting solution and precipitant temperature[5] as well as the choice of the phase-inversion method are important and influence the resulting membrane and its properties.[47]

Phase inversion is described by a liquid-liquid demixing mechanism in which the polymer-rich phase solidifies. By the preparation of the polymer-containing phase and the technique by which the phase separation is performed, the resulting membrane in its morphology and properties are influenced.[47] Figure 6 shows a schematic phase diagram of a polymer-solvent casting solution in a non-solvent. The stable region of the polymer solution is between the solvent-polymer axis and the binodal (dotted curve) while the area right of the binodal shows the unstable section.[50] A meta-stable zone would be represented between the binodal and spinodal that was omitted to simplify the matter. The point A represents the mixture of the polymer in the solvent. At point B on the binodal curve, first units of polymer precipitates from which an increasing amount of solvent dissolve in the non-solvent. The polymer-rich phase rises in its viscosity until it is high enough to be classified as solid (point C). Overall, the polymer film shrinks as the polymer is not the main part of the starting solution. The solvent is exchanged by the non-solvent being in the channels and pores of the precipitated polymer (point D). Most time, this exchange takes place in a few seconds nonetheless, as well as the formed structure can be controlled by the set-up and conditions chosen.[51,52]

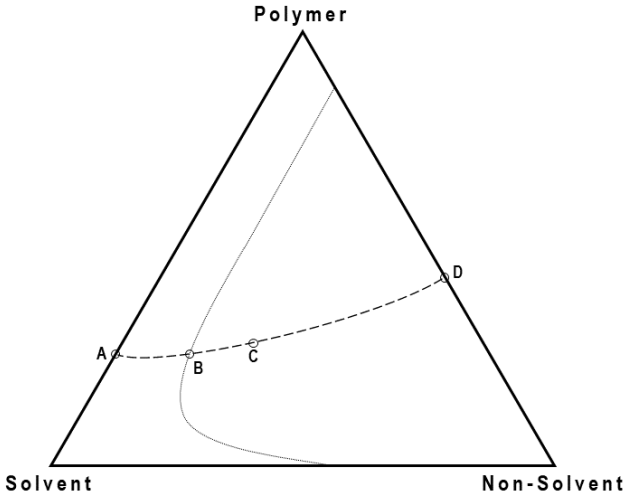

Figure 6: Phase diagram of a polymer-solvent-non-solvent mixture (A: mixture of polymer and solvent, B: first polymer precipitates, C: classified as solid, D: completed precipitation).[51,52]

Alternatively, the precipitation could be performed by thermally induced separation. Different types are possible such as evaporation[53], freeze-drying[54] and vapor-induced.[43] In the evaporation technique, a casting solution of the polymer in a mixture of a volatile solvent and a non-volatile non-solvent is heated up after the casting. The increasing lack of solvent enriches the polymer in the non-solvent phase which then causes precipitation.[52]

In general, the polymer concentration in dope solutions is about 15 to 30wt%.[5] Increasing the polymer concentration often results in denser polymeric membranes and lower permeability. MERTENS *et al.* recognized for polyvinylidene fluoride (PVDF) solutions that also the viscosity is significantly increasing at a concentration between 17 and 24wt% (from 14.3 $Pa \cdot s^{-1}$ to 145.5 $Pa \cdot s^{-1}$). Above these concentrations, even heterogeneous mixtures of PVDF and *N*-methyl pyrrolidone (NMP) occurred so that higher concentrations of the polymer were not feasible.[49]

Solvents of the polymer solution are among other dimethyl formamide (DMF), NMP or dimethyl sulfoxide (DMSO) while 1,4-dioxane, acetone, tetrahydrofuran (THF) or diethyl glycol dimethyl ether (DGDE) might be used as co-solvent. In experiments with P84 polyimide, SOROKO *et al.* noticed that a co-solvent is not necessary to form NF membranes in general. Still, volatile and non-volatile co-solvents in the dope solution guarantee higher rejections, as well as longer evaporation time of volatile co-solvents, lower permeability and porosity.[55] In general, good soluble polymers in the solvent lead to more porous membranes while low miscibility of polymer and solvent result in nonporous layers.[56]

However, the evaporation time of the co-solvent might influence the properties of the membrane. PVDF solved in NMP with slight amounts of THF benefited from a short evaporation time of THF as the retention and permeability increased.[49] In contrast, the evaporation time did not influence the rejection of P84 membranes in the NF range while air humidity during the casting process does. In casting P84 membranes, humidity's higher than 90%, compared to about 40% at standard laboratory conditions, resulted in less permselective membranes with higher fluxes under otherwise equal conditions.[55]

Besides these adjustments, also additives in the dope solution or the coagulation bath can be used to influence membrane characteristics.[50,56] LEE *et al.* added lithium chloride (LiCl) to poly(amic acid) solved in NMP and observed significant changes in solution and resulting membrane properties. Due to strong salt-solvent interactions, the viscosity was increased meanwhile less poly(amic acid) was dissolved, promoting aggregation of the polymer in the organic solvent. Casting dope solutions with increased LiCl amount lead to membranes with smaller pore sizes and increased porosity.[57] Polyvinyl pyrrolidone and polyethylene glycol (PEG) were investigated in dope solution to increase the permeability at constant selectivity. The effective thickness could be decreased through the pore density increased.[58] Casting solutions of cellulose acetate in NMP were enriched with different amounts of PEG resulting in increased permeability, permselectivity and chemically more stable membranes. Simultaneously, the temperature of the coagulation bath was increased from 0° to 25° C showing similar tendencies.[59,60]

However, the influence of nanoparticles is limited by concentration. High amounts risk to aggregate in the layers, providing inhomogeneous distribution, mechanical instability and potential leakage of non-eco-friendly materials.[56]

1.1.2 The need for filtration processes and membranes

Globalization, the increasing worldwide demand for goods and growing environmental awareness are raising the demands on industrial processes. Established and new plants are challenged by new raw materials, high safety standards, more efficient down-stream processing steps and reduced capital costs to be competitive and are summarized in the term of process intensification.[61]

Into the first half of the 20th century, membrane research was only done on a small scale and based on natural and animal materials. Reproducible nitrocellulose and collodion membranes were invented but did not gain that much attention till the demand for clean water was raised due to world wars and increasing population[23] as it is essential for life on earth.[62] These natural water resources are affected by contamination due to industry pollution by heavy oils, metals, pesticides or inorganic matter.[63] But also domestic contaminations appearing by viruses, organic or pathogenic matter declines the water quality[64] why high efficient, safe and low-cost membranes were needed.[62]

Elsewhere, membranes such as cellulose acetate were only used on a laboratory scale with a small economic market of up to 20 million US$. Main disadvantages of membranes were the high costs, lack of selectivity, slow process speed and unreliability.[23] By the progress of LOEB and SOURIRAJAN[65–67] in cellulose ester membrane fabrication, most of the disadvantages were settled such as the flux was increased 10 times higher than the state of the art. This work was a cornerstone for the development of reverse osmosis, micro- and ultrafiltration and their industrialization in the 1980s.[68] Since then, membrane modules and their processes offered a large number of solutions to downstream issues. Long-term use of low-cost membranes in the food and pharmaceutical industry assumes an essential part in the production of for example wine, oils, juices or drugs.[69] In petrol industry, liquids such as solvents or refinery fractions of processes are recovered by different types of reverse osmosis and nanofiltration, substituting more complex phase separation.[70,71] A rapidly increasing field of membrane applications is the gas separation. Since the developments in 1980, a broad range of processes in separating oxygen and nitrogen from the air[72], carbon dioxide from combustion and natural gas[73,74] but also water from air in drying steps were established.[75]

Besides the development of industrial applications, medicine related field gained interest in using membranes. In 1944, KOLFF and coworkers presented an artificial kidney, which became available on a commercial scale in 1960.[76] Artificial organs were mostly based on these membrane developments and became a significant life-saving technology. Quickly, the economic volume of membranes used in medicine exceeded the economic scale of industrial applications.[68]

In summary, membranes are one of the tools to increase efficiency in industrial processes. Besides their potential application in reactive systems to control the addition of substrates, separate or make contact of two phases, immobilize or be itself the catalyst, membranes are also widely used in purification. Different approaches like membrane distillation, extraction, crystallization, adsorption, stripping or pervaporation are feasible.[77] Besides the industrial applications, membrane extraction is also crucial for daily life as it is used on large scale in water treatment. The membrane market is a multi-billion US-dollar market with strongly increasing tendencies in the future (Figure 7).

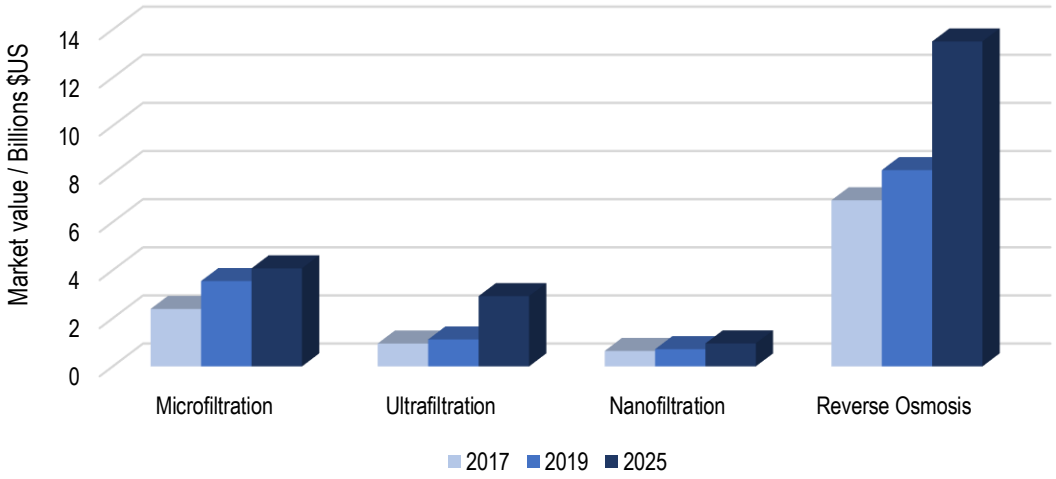

Figure 7: Market value of microfiltration (MF)[78,79], ultrafiltration (UF)[80–82], nanofiltration (NF)[83,84]and reverse osmosis (RO)[85] in 2017, 2019 and estimated in 2025.[86]

1.2 Ionic liquids

1.2.1 Where do they come from?

In 1914, PAUL WALDEN published the synthesis of ethylammonium nitrate[87] proposing a new class of substances which, however, was not of interest for the following decades. Today, this work is considered as the starting point for research in the field of ILs.[88,89] ILs are substances composed of cations and anions with a melting point at or below 100 °C[90] whereby the choice of temperature has no physical or chemical significance.[89] These salts are of particular interest due to their unique properties as low vapor pressure, non-flammability, non-volatility, high ion density and ion conductivity.[90–93] In contrast to molecular organic solvents, ILs are relatively viscous or solid[94] but showing excellent solubility and miscibility properties.[95]

After twenty years, these molten organic salts were used in patents describing the formation of new solutions that were made of cellulose and halide-containing nitrogen bases such as 1-benzylpyridinium chloride[96] to produce films or threads of cellulose.[89] The progress on the usage and synthesis of ILs proceeded slowly, so it wasn't until the late 1940s that new publications and patents appeared.[97,98] Here, the ionic liquids were composed and limited to alkylpyridinium cations and aluminum chloride anions (Figure 8).[99] However, large

differences in the melting temperature were observed of varying ratios of both substances to each other. While equal mixtures of ethyl pyridinium chloride and aluminum chloride lead to a melting point of 88 °C, a surplus of the pyridinium cation decreased it to – 40 °C whereat 45 °C was obtained by 1:2 mixtures. Summarized, ratios with 10 to 75 mol% of aluminum chloride could be ranked as IL with a melting point lower than 100 °C.[98] In 1975, electrochemical studies on organometallics and alkyl aromatic compounds were done in this ionic liquid. The redox behavior was examined in the 2:1 mixture of aluminum chloride and ethylpyridinium bromide, advantaged by room temperature conditions and a solvent-free of water, protons and oxygen.[99] To overcome the experimental drawback of having limited ratios of aluminum chloride and ethylpyridinium bromide mixtures that are liquid at room temperature, butylpyridinium bromide was used in electrochemical and spectroscopic studies instead.[100]

TOM WELTON reasoned the slow progress in discovering ionic liquids and the different approaches by the unawareness of the research groups among each other. Further, there was a lack of technology that ameliorates scientific communication worldwide.[101]

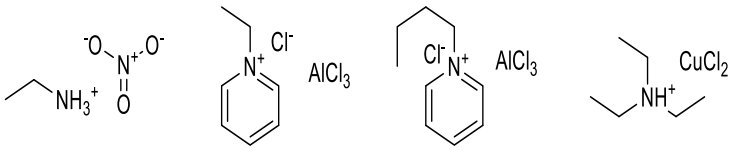

Figure 8: Structure of the first ILs reported in literature and patents (*left to right*: ethylamine nitrate, ethylpyridinium chloride aluminum chloride, propylpyridinium chloride aluminum chloride, triethylamine copper chloride).[87,98–100,102]

Begin of the 1990s, the synthesis of ionic liquids was refined from inert conditions towards bench chemistry. Besides, the number of possible anions increased resulting in numerous newly synthesized and published ILs. Also, the technologic revolution facilitated scientific communication that increased the frequency in synthesizing new ionic liquids.[101] Ten years after 'prediction'[103], air and water stable imidazolium ionic liquids were published in 1992. The 1-ethyl-3-methylimidazolium cation was combined with several anions such as borate, sulfate, nitrate or carbonate whose products were also liquid at room temperature (room temperature ionic liquids, RTIL).[104] Varieties based on the imidazolium cation were investigated as auspicious solvents for photovoltaic devices or electrochemical and synthetic applications. As triflates (TfO^-) already shown good electrochemical properties[105], also trifluoracetate (TF), bis((trifluoromethyl)sulfonyl)amide (NTf_2) and bis(fluorosulfonyl)amide (FSI) became of interest (Figure 9). Especially more complex anions lead to ILs which have a significantly higher thermal decomposition temperature of over 400 °C.[106] The choice of cation has likewise an influence on the physical properties. SUN *et al*. reported the differences in ammonium bis((trifluoromethyl)sulfonyl)amide ILs with increasing side alkyl chains of the cation. Generally, the NTf_2 anion is lowering the melting point compared to the halides. However, tetraalkylammonium cations with methyl to propyl side chains are no ILs (melting points 105-133 °C) while longer alkyl chains lead to RTILs. Compared to the corresponding triflates (Tf) salts, imide salts showed higher conductivities.[107]

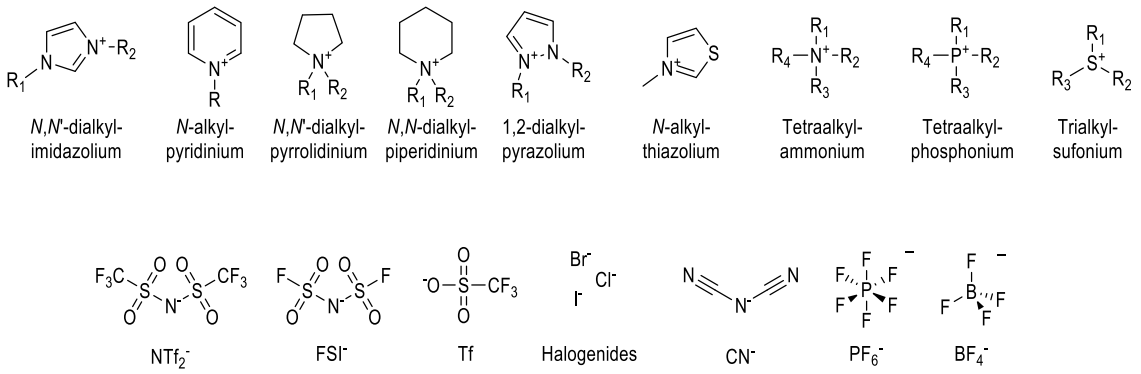

Figure 9: Examples of used cations and anions for ILs.

The development of phosphonium-based ionic liquids has long been limited by synthesis, which could not be performed on a sufficiently large scale.[108] At once, there was a similar interest in this type of ILs even though it started decades later than for ammonium or imidazolium ones.[109] Based on these beginnings in the synthesis of ionic liquids up to 10^{18} ion combinations and ILs are theoretically possible.[110]

1.2.2 Application of ionic liquids

Besides the use as a solvent in electrochemical experiments, ILs became of interest as a solvent in organic chemistry either.[101] Diels-Alder reactions were performed in ethylammonium nitrate where it replaced water as a solvent. Albeit the endo-selectivity was increased compared to results in nonpolar organic solvents but not to those in water, the main advantages of this new system was a higher solubility of neutral organic compounds in the IL[111] and the wider temperature range that could be applied. With a decreased stereo-selectivity this reaction was performed in other ILs such as butylmethylimidazolium tetrafluoro borate[112] or ethylmethylimidazolium tetratfluoro borate. In contrast to the lithium perchlorate in ether solvent system, the reactions were biphasic which facilitated product isolation by organic phase separation.[113] Additionally, the reactions were performed with regioselectivities up to 95%.[112] Similar behavior could be observed in replacing dipolar aprotic solvents in dialkylations.[114]

As ILs became more and more interesting for academic research due to their properties and facilitated synthesis, the application on an industrial scale was also investigated. In homogeneous catalysis, the solvent takes a crucial part in process design as it should solve all substrates, the catalyst and organic ligands. Concurrent, it should be stable at the process conditions and offer a possibility to recycle the catalytic species and unreacted products. According to these requirements, several approaches such as distillation, filtration, temperature-dependent solvent systems, liquid-liquid extraction using ionic liquids were designed.[115–120]

After first investigations of hydrogenation and hydroformylation in quaternary phosphonium salts[121,122], CHAUVIN *et al.* published 1990 a Nickel-catalyzed dimerization in a mixture of the IL methylbutylimidazolium chloride and aluminum chloride. The product removal was *in-situ* as the alkenes, contrary to the allylnickel catalyst complex, were not soluble in the ionic liquid phase.[123]

Early, in 1996, the Eastman Chemical Company started running a process to obtain 1400 tons per year 2,5-dihydrofuran by dimerization of 3,4-epoxybutene (Figure 10).[124–126] The reaction requires a Lewis basic ionic liquid, trioctyloctadecylphosphonium. The phosphonium IL was chosen due to the higher thermal stability as an extraction medium.[89]

One of the best known and widely presented to the general public is the BASIL® (Biphasic Acid Scavenging utilizing Ionic Liquids) process from BASF.[127] In the former process, triethylamine scavenged the acid and formed the unwanted, dense and insoluble side product triethylammonium chloride.[89] Instead, the more expensive base methyl imidazole, which reacted with the acid hydrochloride to the ionic liquid methylimidazolium chloride (melting point 75 °C), was used. This immiscible colorless liquid can be separated by gravity and recycled (Figure 10).[128] Compared to the conventional process, the implementation of ILs increased the process by a factor of 80000[129], from 8 $kg \cdot m^{-3} \cdot h^{-1}$ to 690000 $kg \cdot m^{-3} \cdot h^{-1}$ and doubling the yield up to 98%.[89,130]

The Institute Français du Pétrole established the Dimersol process to synthesize branched hexenes and octenes from less valuable alkenes such as propene or butene. This process was operated initially solvent-free on a scale of multi tons per year. Using ionic liquid catalyst phase, compared to the solvent-free operation before, the yield, as well as the selectivity, increased while the catalyst leaching was reduced simultaneously. Additionally, the process was able to be adapted to less reactive alkenes and overall costs decreased. The recycling of the homogeneous catalyst was realized similarly to the previously described processes by phase separation that could be retrofitted to existing plants.

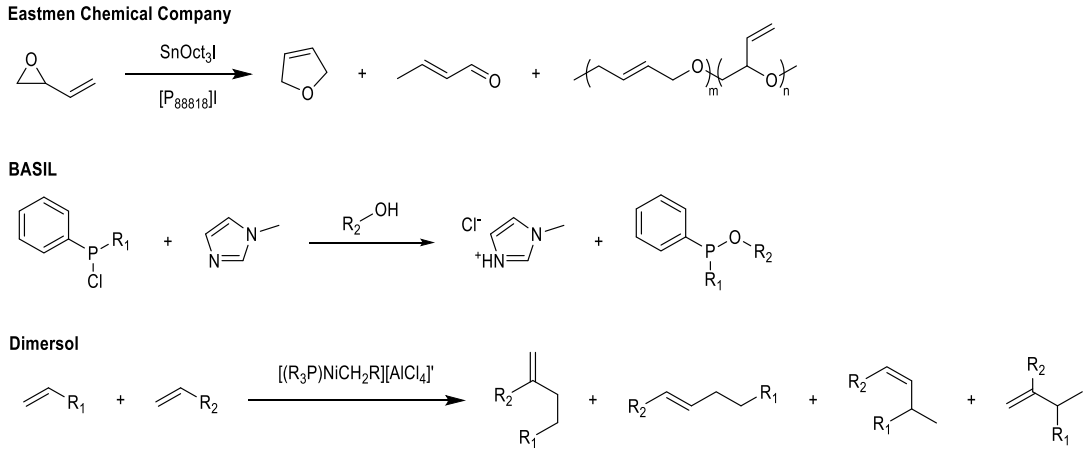

Figure 10: Scheme of the Eastman Chemical Company, BASIL® and Dimersol process.[89]

These multi-phase catalysis using ionic liquids as one of the phases was also appliable to biocatalytic reactions.[131] Often, a part of the reaction system is composed of imidazolium ILs and aqueous buffers. The ionic liquid is mainly used as a substrate phase for poor water-soluble and unipolar raw materials, or *in-situ* product extraction media.[132] For example in the transesterification of rapeseed oil, the ILs Ammoeng 102 and 120 (Figure 11) were used in a solvent system with methanol. As the produced fatty acid methyl ester was not

soluble in the ionic liquid anymore, the product downstream was simplified and the reaction equilibrium postponed to the product side as the product was no longer miscible in the catalyst phase.[133]

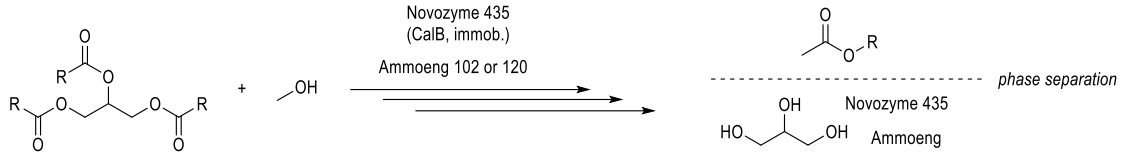

Figure 11: Simplified scheme of the reaction with phase separation of the product.[132]

Even though not all ILs are suitable or showing a general trend to enzymic reactions[134], they might improve stability, selectivity and suppression of side reactions.[135] Instead of using the purified enzyme, whole-cell catalysis benefits of simple preparation and avoidance of co-factors. Still, drawbacks such as cell toxicity of some suitable ILs have to be overcome to exploit *i.e.* stereoselectivity and enantioselectivity in the drug synthesis.[136,137]

Carbohydrate ILs (Figure 12) represents an approach to overcome these drawbacks as they are biocompatible. Thus, Reiß *et al.* suggest biomedical applications such as using these IL types as additives in coatings of drug-eluting balloons[138] that were successfully investigated before with ionic liquids.[139,140] Also, carbohydrate-conjugated ILs could be used as chiral catalysts for example in a Michael addition.[141] Besides, enantiomers such as the Tröger's base are achievable cost-effectively and more efficiently compared to common synthesis.[142] This opens up new and interesting possibilities for synthesis.

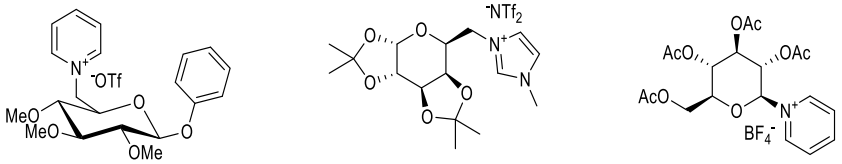

Figure 12: Examples of carbohydrate ionic liquids (*left to right*: β-phenyl glucosidemethylpyrridine trifluoromethylsulfon[138], D-galactose derived IL[141], glucose-containing pyridinium ionic liquid[142]).

1.2.3 Polymerized ionic liquids

Introducing polymerizable groups in the synthesis of ionic liquids opens a new class of materials: polymerized ionic liquids (PILs, also: poly(ILs), polymeric ILs).[143] Apart from a few exceptions[144], PILs are solids with fixed and coordinated charges.[88] Even though they and their possible industrial applications in microreactors for catalyzed hydrolysis were known[145–147], PILs did not gain much attention end of the 20th century (Figure 13). Here, also the lack of communication technology[101] and inconsistent naming decelerated developments. Since then, synthetic strategies, new structures and applications were investigated.

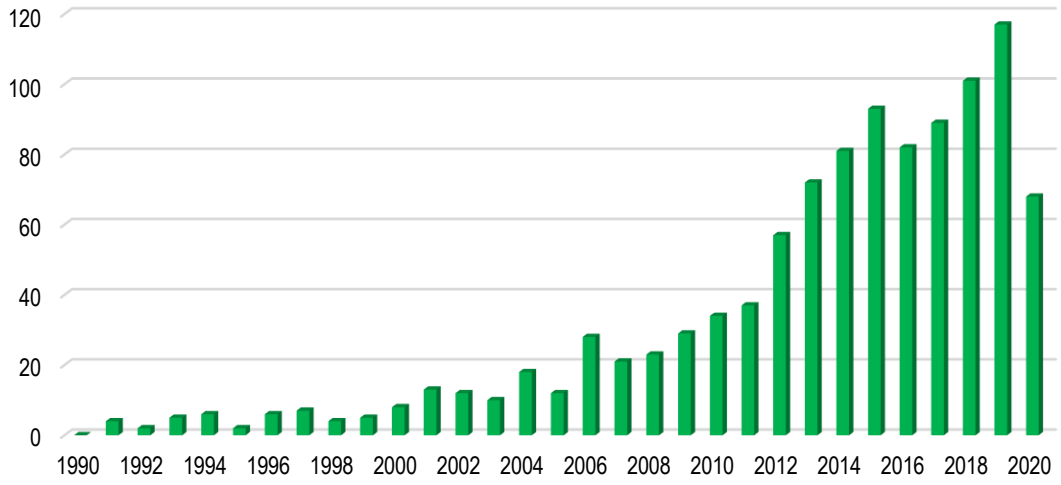

Figure 13: Number of publications on polymerized ionic liquids. According to Web of Science, September 2020.[148]

The polymer structure of PILs can be various (*e.g.* linear, branched, star-shaped) even though using the same monomer. Also, neutral monomers or other charged non-IL polymers may be used towards a tremendous number of polymers.[149] Figure 14 shows exemplary possible structures.

In general, PILs are obtained by polymerization of charged IL monomers or post-modification of uncharged polymers without changing the overall structure of the polymer. Polymerized ionic liquids are tunable in reactivity or solubility by anion exchange. They combine the advantages of ionic liquids (compare 1.2.2) with those of polymers. By various known shapes and properties of polymeric materials, a variety of applications is feasible as well as an improvement of deployed materials.

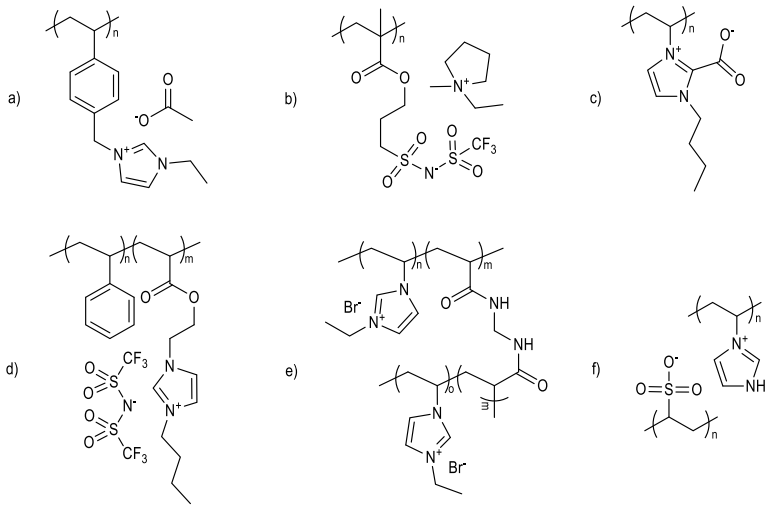

Figure 14: Structurally different types of polymerized ionic liquids: a) polycationic[150], b) polyanionic[151], c) zwitterionic[152], d) copolymeric[153], e) crosslinked[154] and f) complexed PILs[155].[90]

1.2.3.1 Application of PILs

Polymerized ionic liquids can be used in different applications as catalyst, immobilization or filtration material. The following parts will show exemplary uses in organocatalysis, electrochemical devices or downstream processes.

LAMBERT *et al.* used a copolymer of styrene and an ionic liquid as an air-stable precursor for *in-situ* *N*-heterocycle carbene catalysts. The thermally activated carbene catalyzed different reactions with full conversion and high yields.[150,152] As well as the reactivity of the PILs-catalyst[156], the solubility of PILs is affected by anion exchange which enables a downstream and recycling after the reaction.[157,158]

Besides the advantages mentioned above, often there is a lack of reactivity of PILs catalysts. A promising approach to combine the advantages and overcome the low efficiency is to immobilize a known catalyst in PILs. GROßEHEILMANN *et al.* used a vinylethylimidazolium bromide containing hydrogel for embedding a quinine-organocatalyst. The catalyst was accessible to the substrates in an asymmetric nitroaldol reaction that could be performed in water-miscible organic solvents.[159] This encapsulation method is suitable for enzymes as well and even increases the activity compared to non-immobilized enzymes.[160] Recycling of enzymes in these materials without loss in activity makes them economical to industry.[161]

In general, these types of hydrogels used by GROßEHEILMANN *et al.* are obtained by free radical polymerization of the IL and the crosslinker *N,N'*-methylenebisacrylamide in water (Figure 15). Compared to hydrogels of calcium-alginate, PILs hydrogels provide higher thermal stability and mechanical flexibility. Thereby, the properties are mainly influenced by the choice of monomer relating the length of the alkyl chain or the anion size and not the choice of the crosslinker. Adjustments of the mechanical properties can be made by a variation of the ratio of monomer and crosslinker.[162] For example, fabrication of hydrogels with the longer crosslinker poly(ethylene glycol) diacrylate 700 instead of 170 lead to softer material that allowed more deformations before being destructed.[163]

In-vitro applications as tissue models or drug-delivery materials were proposed but needed further investigation as the biocompatibility was uncertain[154] Recently, CLAUS *et al.* confirmed a good to excellent biocompatibility of imidazolium- and sulfopropylmethacrylate-containing hydrogels. The synthesized hydrogels showed no leaching of harmful residuals after reaction[162] while promising antimicrobial properties were discovered.[164]

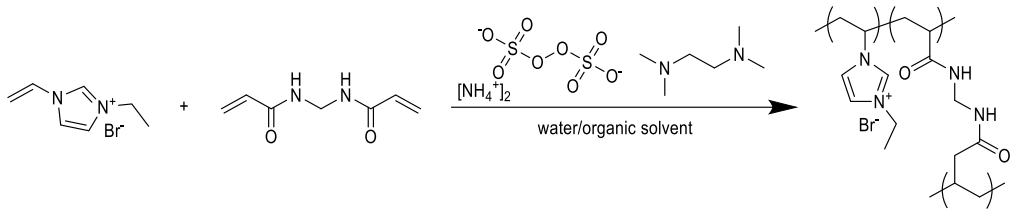

Figure 15: Reaction scheme of the imidazolium-sulforpropylmethacrylate hydrogel synthesis.[159]

Early, PILs became a lot of attention in electrochemical applications as polymer electrolytes (liquid, gel-like and solid-state) as well as the films were less conductive than the monomers. Still, they benefit from the advantages of a solid but flexible material compared to the liquid.[93] Besides the previously presented shapes of PILs materials such as solved powder, often flat sheet polymers of ionic liquids are used in electrochemical applications. Compared to lithium-ion batteries and devices with liquid electrolytes, PILs are not explosive, inflammable and easier to handle.[165] WANG *et al.* synthesized a free-standing, all-solid electrolyte by casting the polymer solution. Due to the arrangement of the bis((trifluoro)sulfonyl)imide anion in the polymer, a higher ionic conductivity was observed. Also, it improved the interfacial behavior between the polymeric and lithium layer so that a small LED could be supplied with energy (Figure 16).[166]

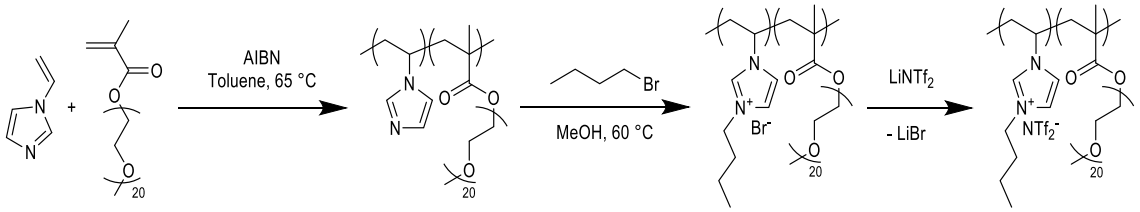

Figure 16: Synthesis of solid polymer electrolytes usable as battery material.[166]

Apart from batteries, polymerized ionic liquids are also potential materials to produce photovoltaic cells.[167] Alkylimidazolium bromide ionic liquids were widely investigated, due to the tunability by the length of the hydrocarbon side group. Shorter alkyl chains improved the electrical conductivity[168] as well as the imidazolium-based crosslinker increased thermal stability.[169] CHEN *et al.* reported that using these bicationic crosslinkers in polymers resulted in higher efficiencies with up to 6% in conductivity and provided longer stability than the corresponding ionic liquid electrolyte.[170] The so-called quasi-solid-state dye-sensitized solar cells additionally prevented recombination effects at the titan dioxide/electrolyte surface which occurs in photovoltaic modules.[171]

1.2.3.2 PILs in downstream applications

Polymerized ionic liquids in downstream applications have different shapes and compositions. PILs can be nanoparticles or likewise compounds that are used as adsorbents in applications. Therefore, they are grafted onto *e.g.* silica or carbon particles and applicated as a dispersion. In contrast, polymerized ionic liquids can also be used as solid, free-standing material. Chemically, the PILs can be a homo- or co-polymer depending on the desired properties. These materials might be supported by a carrier layer such as a silicon polymer or a microfiltration polyacrylic membrane. In addition, these materials can be doped with additional amounts of ionic liquids or other additives to enhance the desired functionality or mechanical stability.

In downstream applications, ionic liquids itself were already used as a membrane material in gas separation. Highly of interest are amine- ILs which are implemented in commercial CO_2 capture processes.[172] Since 1999 it is known, that longer alkyl side chains of the imidazolium ionic liquids increase the solubility of carbon

dioxide. Liquid IL membranes show a positive relationship between the acidity of gases and the polarity of the used IL described by the Kamlet-Taft β parameter, which enables selecting task-specific ILs.[173] Including the simple recovery of the membrane material, IL membranes were used in different combustion and gas capture processes.[174]

Compared to ionic liquid membranes or supported ionic liquid membranes, due to the polymer matrix, PILs membranes have a lack of gas permeability and diffusivity in gas separation. In 2008, PILs-IL-mixed membranes were proposed as a synthetic solution.[175] Hereby, gas mixtures of N_2/CO_2 could be separated selectively.[176] As mentioned above, nitrogen-containing PILs are more suitable for this process, although there are differences between different nitrogen compounds. TOMÉ *et al.* revealed that ammonium structures showed better performances than pyridinium and imidazolium. The permeability, solubility and diffusion of gases in the membrane materials were depended on the cationic polymer backbone.[177] By adding a silver salt to the same PILs-IL-membrane (Figure 17), the application was expandable to the permselective filtration of ethylene and propene. While ethylene is forming a complex with the silver cation and remains in the material, the paraffin passes and is separated from the ethylene.[178]

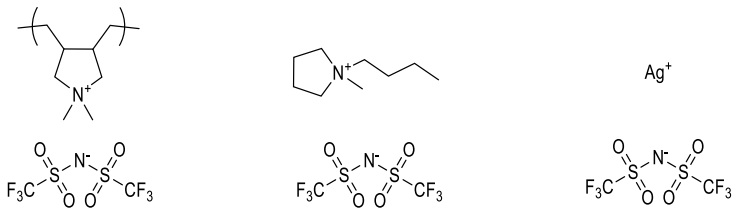

Figure 17: PILs, IL and silver salt for mixed membranes used by TOMÉ *et al.*.[178]

Alternatively, already existing membranes could be postmodificated so that theoretically an IL monomer was "used". CHOULIARAS *et al.* postmodified a chlorostyrene-acrylic acid-blockcopolymer with methylimidazole or gas permeation (Figure 18). Besides the features of PILs as membranes so far, the amount of the neutral compound acrylic acid had a positive impact on gas separation.

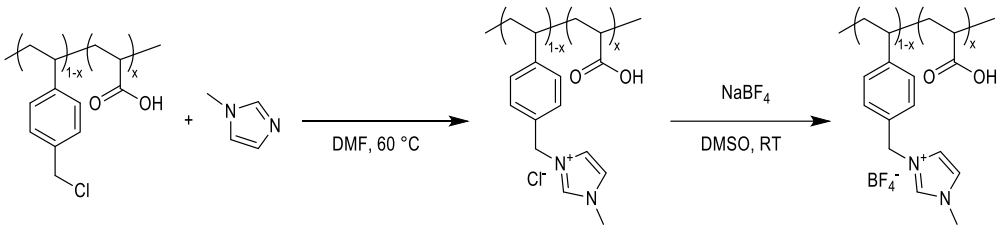

Figure 18: Postmodification of an uncharged polymer towards a gas separation membrane containing an IL.[179]

Since the synthesis of Nafion®, charged membranes are also of interest in filtration processes. If any charged monomers were used, the postmodification of polymers enabled charged membranes.[180–184] Nevertheless, poly(ionic liquids) offered a new synthetic route towards charged filtration materials. Besides the mentioned techniques to optimize membranes in general, also the charges offer new properties by modifying the structure. TÄUBER *et al.* used different benzoic acids to synthesize nanoporous asymmetric PILs membranes.

By increasing valency of the benzoic acid, the pore size was decreased from 2.6 µm to 80 nm. The multivalent benzoic acids function as a crosslinker between the positively charged imidazolium heterocycles.[185]

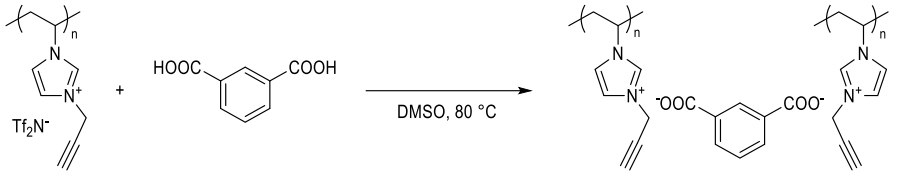

Figure 19: PILs layers using multivalent benzoic acids as an ionic crosslinking agent.[185]

PILs membranes are of interest as they provide solvent and heat resistant materials due to their containing IL monomers. Same separation steps can profit from both, Donnan and size exclusion. Therefore, dye rejections were examined with PILs early. In 2008, Li *et al.* investigated the performance of poly(diallyldimethylammonium chloride) (PDDA) containing membranes obtained by the layer-by-layer method. Onto a hydrolyzed polyacrylonitrile membrane with a molecular weight cut off about 200,000 Da, up to 20 layers of PDDA and sulfonated poly(ether ketone) (SPEEK) were applied (Figure 21). The resulting material has successfully retained the dyes Rose Bengal and Acid Fuchsine at 99%.[186] Charged dyes with the opposite charge to the fixed ones in the polymer backbone are more likely to be adsorbed to the surface than rejected. A composite of polyethersulfone and the positively charged polymer of vinylbutylimidazolium bis(trifluoromethylsulfonyl)imide were preferably used to filter out Methyl Green or Ferroin Red (Figure 20).[187] These materials represent an approach to new possibilities in dye removal and the associated protection of the environment from hazardous and environmentally harmful chemicals.[188]

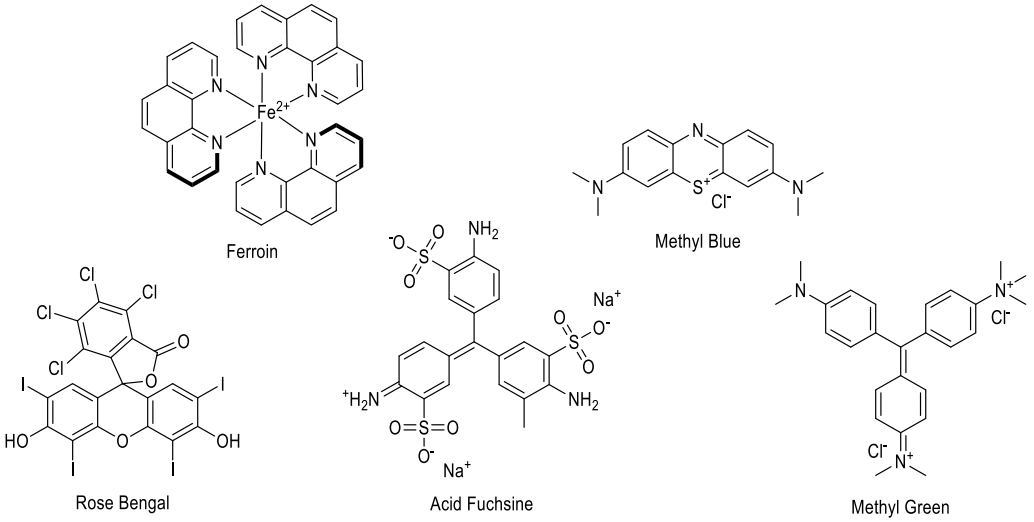

Figure 20: Dyes used in separations with PILs.[186,187,189,190]

Water purification by PILs was also accomplished by encapsulation. Synthesized in a two-step process, poly(N-imidazole-3-propylmethacrylamide) built up vesicles by the hydrophobic side group in aqueous phases. The vesicle encapsulated Rose Bengal and transferred it to an organic phase (Figure 21).[189] Grafted onto polypropylene mesh, polymers of vinylalkylimidazolium bromide showed remarkable properties in oil-water

separation, dye absorption and antimicrobial applications. Oils such as vegetable oils could be separated from water with an efficiency of > 99%, while also showing the possibility to absorb Methyl Blue up to 400 $mg \cdot g^{-1}$. After the contact with the grafted PILs, the bacterial viability of *Escherichia coli* and *Staphylococcus aureus* decreased to 20% in the first and completely after two hours.[190]

The ionic conductivity character of PILs hydrogel was used as a smart draw agent in water desalination. In a forward osmosis application, the thermosensitive material withdrew the water at 4 °C and released the desalinated water with increasing the temperature up to 60 °C. This repeatable process allows obtaining tap water from brackish water. Combined with a waste heat recovery system, this represents an energy-efficient and sustainable process. Possible leaching of the hydrogel materials could be neglected.[191]

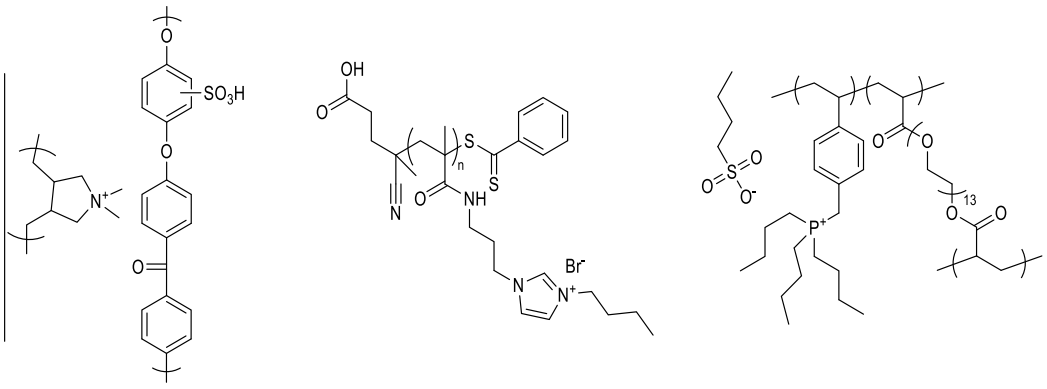

Figure 21: PILs filtration materials (left to right: multi-PDAA-SPEEK-layer membrane with support[186], two-step polymer for vesicles[189], smart draw agent[191])

Summarized, ionic liquids expand the possibilities in material synthesis to approach current challenges. Thereby, the application field is not limited to a specific area of research as they were successfully tested in electrochemical devices, separation and purification applications, catalytic processes as well as in biomedical technology. Due to the almost limitless synthetic possibilities and variability in ion pairs, further task-specific research is needed.

2. Aim of the work

Environmental damage is caused by a multitude of hazardous substances in natural water. The origin of these pollutions are complex mixtures of for example dyes, bacteria, oils or drug metabolites that are not removed effectively. Multifunctional filtration materials are needed to clean up waste and industrials waters.

This work aims to develop a methodology to synthesize solid, free-standing polymer membranes consisting of polymerized ionic liquids. This requires the selection of suitable ILs in terms of formation and commercial or simple synthetic accessibility. In addition to these aspects, the polymerization reaction and set-up for membrane formation should allow a scale-up afterward and plays a key role.

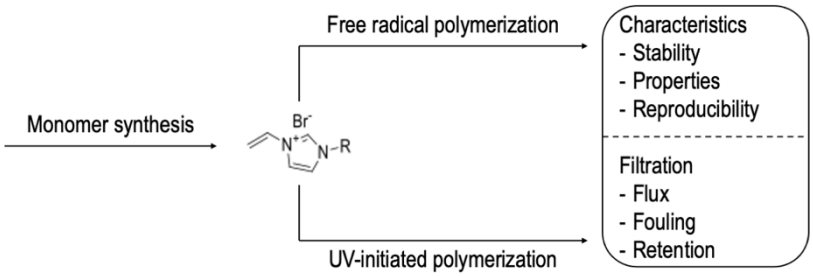

Figure 22: Graphical summary of this work.

Ionic liquids have beneficial properties as they are inflammable, chemical resistant and highly charged. Due to the well-known properties in material synthesis and the possibility to be polymerized by free radical polymerization, vinylalkylimidazolium ionic liquids are selected. These ILs are accessible by one-pot reactions in small and large batches.

First investigations concern the possible polymerization reactions. For this purpose, two synthetic ways of free radical polymerization by using thermal- and UV-initiated initiators will be pursued. Hereby, different initiator concentrations in organic and aqueous solvents, as well as solvent-free conditions will be investigated.

Second objective is to transfer the polymerized ionic liquids by free radical polymerization to the shape of a polymeric layer. Depending on the polymerization mechanism two methods are feasible: polymerization in molds with defined sizes or casting of the compounds. The casting allows using solutions of the already existing PILs polymer as well as a monomer solution followed by thermal or UV initiated activation of the initiator. Requirements to the membrane formation process are an adjustable size for varying applications as well as a possibility to define and control the thickness of the layer.

The third part of this work elaborates on the applications of polymerized ionic liquid membranes. The objective is to investigate nanofiltration with these charged polymeric layers and potential applications to remove organic substrates from aqueous solutions. Besides process parameters such as permeance and efficiency, also the influence of the charges to the application should be considered. As further opportunities, electrochemical applications are established.

3. Materials and methods

3.1 Chemicals

All chemicals were used as purchased from *Sigma-Aldrich* (Steinheim, Germany), *Acros Organics* (Geel, Belgium), *TCI* (Tokyo, Japan), *Merck* (Darmstadt, Germany), *Fisher Scientific* (Loughborough, United Kingdom) and *Alfa Aesar* (Kandel, Germany). Technical grade ethanol and diethyl ether were purified by rotary evaporation before use. Precipitation baths were filled with ultrapure water.

3.2 Synthesis of ionic liquids

The synthesis of ionic liquids is broadly described in the literature.[143,152,154,158,164,192–194] The synthesis of vinylethylimidazolium bromide ([VEtIm]Br), vinylbutylimidazolium bromide ([VBuIm]Br), vinylhexyl-imidazolium bromide ([VHexIm]Br) and vinylbenzoilimidazolium bromide ([VBnIm]Br), vinyldodecanyl-imidazolium bromide ([VDodecIm]Br) and vinyloctadeylimidazolium bromide ([VOcdecIm]Br) were performed under same conditions. Into a flask equipped with a magnetic stirrer 1 equivalent of 1-vinylimidazole (VIm), 1.25 equivalent of the corresponding bromide and 250 mL·mol$_{VIm}^{-1}$ of purified EtOH were added (Figure 23). Then, the solution was purged with argon for one hour at room temperature before the reaction took place for at least 96 hours at 70 °C in an oil bath.

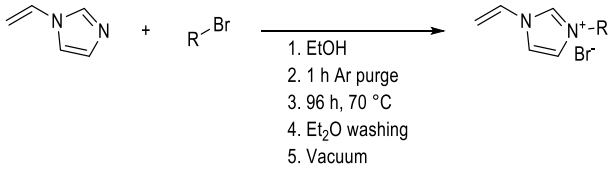

Figure 23: General scheme of the IL synthesis.

After the reaction, the solution was washed several times with diethyl ether till a clear organic phase was obtained and all the unreacted substrates are removed. The remaining solvents were removed by rotary evaporation and vacuum. If the ILs did not precipitate, the already washed reaction solution was first cooled to –28 °C in a freezer overnight and finally in liquid nitrogen. The frozen solution was crashed with a spattle and washed immediately with diethyl ether while thawing. Thus, unremoved substrates of the reaction were solved in the organic phase. The ionic liquids were obtained as a white solid with yields between 54% and 89%.

3.3 Synthesis of polymerized ionic liquids

To synthesize polymerized ionic liquids, different techniques were used such as free and controlled radical polymerization in different solvents as well as UV-initiated polymerization.

3.3.1 Free radical polymerization

3.3.1.1 Polymerization in organic solvents

To obtain polymers by free radical polymerization, different types of reactions were used by varying the solvent and initiator. The most common type is the free-radical polymerization using 2,2'-azobis(2-methylpropionitrile) (AIBN) in organic solvents. Figure 24 shows a general reaction scheme utilizing AIBN purified by recrystallization in methanol.

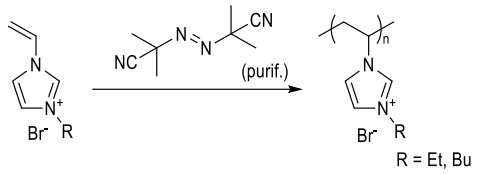

Figure 24: Scheme of the free radical polymerization using AIBN as initiator and [VEtIm]Br or [VBuIm]Br as monomers.

Adapted from literature[158,193,195–202], different reaction conditions were tested (Table 2). Here, the radical initiator was used in concentrations of 0.1-2 mol% depending on the used IL. Dimethyl sulfoxide (DMSO), chloroform, acetic acid, methanol, ethanol and dimethylformamide (DMF) were used as solvents. All components were added in a flame-dried flask and purged for one hour with argon before the reaction took place at 60-75 °C in an oil bath for 1-24 hours. The precipitated solid was washed with chloroform and dried by vacuum.

Table 2: Conditions of the free radical polymerizations of ILs using AIBN as initiator.

Reaction	$n_{[VEtIm]Br}$ / mol	Initiator	$n_{Initiator}$ / mol	Solvent	T / °C	t / h	Preparation and work up
A[158]	0.02	AIBN	0.0004	30 mL $CHCl_3$	70	3	- Solution purged with argon for 1 h - Precipitate washed several with $CHCl_3$ - Solvent evaporation
B[198]	0.01	AIBN	0.0005	14 mL EtOH	70	24	- Three freeze-pump-thaw cycles - Purification by dialysis for 3 d in H_2O - Solvent evaporation by freeze-drying
C[199]	0.00948	AIBN	0.00000948	7.62 mL glacial acetic acid	65	24	- Flushed with argon for 0.5 h - Precipitation in acetone - Reprecipitation in acetone after solving in methanol - Dried 18 h under reduced pressure
D[193,200]	0.016	AIBN	0.0000185	24.5 mL DMSO	65	24	- Purging solution with argon for 0.5 h - Precipitate dried under reduced pressure
E[201]	0.0148	AIBN	0.000148	16.26 mL dry DMF	60	20	- Reaction stopped by cooling with liquid nitrogen - Precipitation from methanol in excess of acetone - Dried under reduced pressure
F[202]	0.0065	AIBN	0.000065	7.15 mL DMF	60	20	- Performed in flame-dried Schlenk flask - Precipitated in a large excess of acetone - Dried under reduced pressure

3.3.1.2 Reversible addition-fragmentation chain-transfer polymerization

Potassium ethyl xanthogenate (1.2993 g, 0.0081 mol) and ethyl-2-brompropionate (1.106 mL, 0.0081 mol) were used to synthesize a chain transfer agent according to literature (Figure 25).[202] The potassium salt was solved in EtOH (16.2 mL, 2 mL·mmol^{-1}) before the ethyl-2-bromopropionate was added slowly. After five hours of stirring, 30 mL H_2O was added to separate phases and isolate the product in the organic phase while the potassium bromide remained in the aqueous phase. The organic phase was washed several times with 35 mL of diethyl ether and dried with magnesium sulfate. Finally, the product was obtained as a white solid by evaporating the ether.

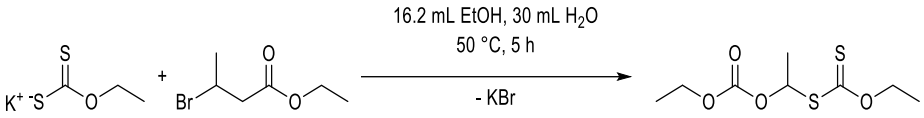

Figure 25: Synthesis of the chain transfer agent using potassium ethyl xanthogenate and ethyl-2-brompropionate.[202]

To perform the reversible addition-fragmentation chain-transfer polymerization (RAFT), [VEtIm]Br (1.5 g, 0.0065 mol), AIBN (0.0107 g, 0.000065 mol) and the chain transfer agent O-ethyl-S-(ethoxycarbonyl) ethyldithiocarbonate (0.0286, 0.00013 mol) were mixed in 7.15 mL DMF in a heat-treated Schlenk flask. The solution was additionally treated by three freeze-pump-thaw cycles before the reaction took place at 60 °C for 20 hours. The polymer was obtained by precipitation in a large excess of acetone and dried under reduced pressure.

3.3.1.3 Polymerization in aqueous systems

4,4'-Azobis(4-cyanovaleric acid) (ABCVA) was used as a water-soluble initiator in aqueous reaction solutions as already described in the literature (Figure 26).[158,203–208] They were performed as described without further modifications using 1.5-10 mol% ABCVA. After 3-20 hours at 70-85 °C, the polymer was obtained by precipitation in *tert*-butylmethyl ether (MTBE). The obtained white solid was washed with chloroform and dried by vacuum.

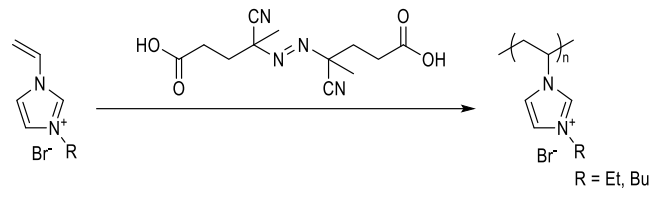

Figure 26: ABCVA as an initiator in aqueous free radical polymerization using the monomers [VEtIm]Br and [VBuIm]Br.

Table 3: Conditions of the free radical polymerization of ILs using ABCVA as initiator.

Reaction	$n_{[VEtIm]Br}$ / mol	Initiator	$n_{initiator}$ / mol	Solvent	T / °C	t / h	Preparation and work up
G[158]	0.02	ABCVA	0.0004	30 mL $CHCl_3$	70	3	- Solute purged with argon for 1 h - Precipitate washed several with $CHCl_3$ - Solvent evaporation
H[203]	0.01	ABCVA	0.00015	40 mL H_2O	85	20	- Solution purged with argon for 1 h - Precipitate washed several with H_2O - Solvent evaporation
I[204–206]	0.01	ABCVA	0.001	13 mL 0.75 M HCl	75	6	- Solution flushed with argon for 1 h - Dialysis in H_2O for 3 d - Solvent evaporation by lyophilization
J[208]	0.005	ABCVA	0.000072	10 mL H_2O	85/68	24	- Purged with argon for 1 h - Precipitation in ice-cold tetrahydrofuran - Precipitate washed with tetrahydrofuran - Dried 18 h at 80 °C under reduced pressure

Alternatively, the reaction was performed in 0.75 M chloride acid aqueous solution for six hours at 75 °C. Then purification was performed by dialysis (3.5 kDa dialysis bag, Spectra/Por®, *Repligen*, Ravensburg, Germany) in deionized water for three days whereupon the product was obtained by freeze-drying.[206,207] All reactions performed are listed detailed in Table 3.

3.3.1.4 Anion exchange of PILs

Solubility properties of the polymerized ionic liquids are mainly influenced by the anion. Bromide containing PILs are well soluble in aqueous solutions and water. An exchange of bromide (Figure 27) allows to make the polymerized ionic liquids insoluble in water and soluble in some organic solvents instead. Several combinations of vinylalkylimidazolium-based PILs and organic solvents are known in the literature.[158]

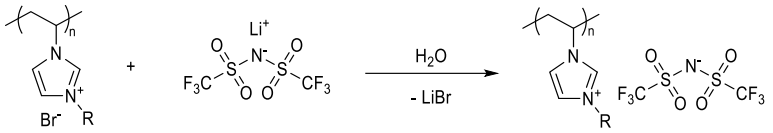

Figure 27: Example of anion exchange of bromide and bis(trifluoromethylsulfonyl)amide.

For the anion exchange, 4.0616 g of poly([VEtIm]Br) (0.02 mol related to the molecular mass of the monomer) was solved in 20 mL of deionized water. Also, 1.15 equivalent of lithium bis(trifluoromethylsulfonyl)amide (6.3954 g, 0.023 mol) were solved in 20 mL of deionized water. Under stirring, the salt was added to the polymer solution, whereby a white solid is formed. After 30 minutes of stirring, the anion exchange is completed and no further solid is formed. The poly([VEtIm]NTf_2) was removed by filtration and dried under vacuum. The desired, white-yellow polymer was obtained with a yield of 80%.

The reaction was performed with different anions to exchange. Under similar conditions, various polymer-solvent combinations were feasible that are summarized in Table 4.

Table 4: Solubility of poly[VEtIm]$^+$ and poly[VBuIm]$^+$ with different counterions adapted from literature.[158]

Polymer		Solvent				
		H_2O	MeOH	Acetone	THF	EtAc
Poly[VEtIm]$^+$	Br^-	+	+	-	-	-
	BF_4^-	-	-	-	-	-
	PF_6^-	-	-	+	-	-
	NTf_2^-	-	+	+	+	+
Poly[VBuIm]$^+$	Br^-	+	+	-	-	-
	BF_4^-	-	-	+	-	-
	PF_6^-	-	-	+	+	+
	NTf_2^-	-	-	-	+	+

3.3.1.5 Casting of polymer solutions

To obtain neat free-standing layers of the purified polymer, a phase inversion technique was used. The required casting solution was made of triethylene glycol (TEG, 2.375 g, 47.5 wt%), *N*-methyl-2-pyrrolidon (NMP, 1.8 g, 36 wt%) and the polymer (0.8 g, 16 wt%). As the precipitation took place in aqueous media, only polymers that were insoluble in water after an anion exchange were used. All components were mixed by shaking and cast by a TQC AB3407 film applicator and the corresponding casting knife (both *TQC Sheen B.V.*, Capelle aan den IJseel, Netherlands, Figure 28). 300 µm was used as the gap of the casting knife so that all films were cast reproducibly onto clean, non-scratched glass plates. Afterward, the plate was immersed in the non-solvent water to precipitate the layer.

Figure 28: Film applicator TQC AB3407 (left) and casting knife (right).

Alternatively, the phase inversion was performed in a 0.2 wt% aqueous ammonia solution for 2 hours. The casted polymer film was composed of dimethylformamide (DMF, 3 mL), the polymer of [VBuIm]Br (0.2 g, 0.0005 mol) and polyacrylic acid (PAA, 0.12 g, 0.0005 mol, 100 kDa with 35 wt% H_2O). After the casting procedure, the resulting film was heated by the integrated Peltier heater to 80 °C for 1 hour. In a slightly basic environment, the layer precipitated the same time as an ion exchange of bromide and the deprotonated polyacrylic acid took place.[197]

3.3.2 UV-initiated polymerization

3.3.2.1 Scope of UV lamps

UV-initiated polymerization was principally carried out as described by ZHENG *et al.*.[209] The experimental procedure was performed with a molar mixture of 20% [VBuIm]Br, 20% styrene and 60% acetonitrile. Additionally, 10wt% divinylbenzene (DVB) as a crosslinker and 10 wt% photo initiator (benzoin ethyl ether, BEE) were used, where the weight percentage was related to the mass of ionic liquid (Figure 29).

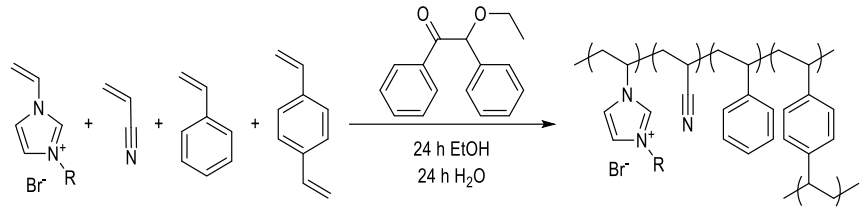

Figure 29: General scheme of the UV-initiated polymerization.

In a 20 mL vial, all reagents were mixed, blended for about 30 seconds and then sonicated for 30 minutes to obtain a homogeneous solution. Afterward, the solution was poured out onto a clean, non-scratched glass plate and irradiated by a UV lamp till the liquid film became solid. The lamp was placed 3.5 cm above the glass plate and covered by a box lined inside with aluminum foil. The yet solid film was immersed first in ethanol, then a water bath for 24 hours each to wash the layer.

For the irradiation the following UV lamps were used: the high-performance Xenon lamp MAX-303 (*Asahi-Spectra Co. Ltd*, Tokyo, Japan), the Dulux® S BL350 UV-A light bubble (*Osram*, Munich, Germany) and the Onfuro IP66 UV blacklight (*Onfuro*, London, United Kingdom, Figure 30).

Figure 30: Different UV-lamps used in polymerization experiments (left: MAX-303, center: Osram Dulux® light bulb, right: Onfuro IP66).

3.3.2.2 Investigation of the polymerization support

To control the thickness of the layers during the polymerization, molds with known areas were used. By the volume of the monomer solution and the area of the mold, the thickness could be approximately calculated. Three different molds were used that are shown in Figure 31.

Figure 31: Molds being used as a support for the UV-induced polymerization (*left to right*: mold A, mold B, mold C).

The left mold has an area of 25 cm^2 so that 1 mL of the monomer solution was used to obtain a layer 400 µm thick. The synthesis was performed as described in 3.3.2.1. Therefore, the chemicals [VBuIm]Br (0.5374 g, 0.00233 mol, 20 mol%), ACN (0.464 mL, 0.00699 mol, 60 mol%), styrene (0.267 mL, 0.00233 mol, 20 mol%), DVB (0.012 mL, 0.000084 mol, 2 wt%) and BEE (0.0537, 0.00022 mol, 10 wt%) were mixed in a vial. After the pretreatment, the homogeneous solution was poured into the mold and irradiated by a Dulux® S BL350 9W UV-A lamp (*Osram,* Munich, Germany) at 3.5 cm. As mentioned, a cover was used. The mold was then immersed first in the ethanol, then the water bath. To obtain the layer, a knife was used to detach and hoist it from the mold.

In contrast, the mold in the center was designed to simplify the procedure as the outer edge could be pushed down. Hereby, the layer could be peeled off carefully with a knife. The third design (mold C, Figure 31) is based on a casting mold with a diameter of 4.7 cm and a height of 400 µm. This mold was covered by a simple glass plate that let the UV light pass. Experiments with the second and third mold were conducted as described for the first mold.

3.3.2.3 Casting process of substrate solution

Type I Homo-PILs

The TQC AB3407 film applicator and the casting knife (Figure 28) ensured a reproducible and homogenous casted monomer film on a non-scratched glass plate. Therefore, 0.7165 g [VBuIm]Br (0.0031 mol, 20 mol%), 0.617 mL ACN (0.0093 mol, 60 mol%), 0.354 mL styrene (0.0031 mol, 20 mol%), 0.016 mL DVB (0.00011 mol, 2 wt%), 0.0717 g BEE (0.00021 mol, 10 wt%) were mixed in a 20 mL vial. After the same treatment as in 3.3.2.1, the homogeneous solution was cast with the TQC at room temperature using a gap of 300 µm and a casting speed of 10 $mm \cdot s^{-1}$. The film was then irradiated at a distance of 3.5 cm with the Dulux® UV light bubble (Figure 30) for 30 minutes before the glass plate with the solid film was immersed into ethanol and

afterward in water for 24 hours each. The film became white and loosed itself from the support. To applicate the layer, it was cut by a hole puncher.

Type II Hetero-PILs

Heteropolymers were synthesized like the homopolymers with the same total molar amount of IL. In an exemplary experiment (Figure 32) 1.0748 g [VBuIm]Br (0.00465 mol, 15 mol%), 0.5319 g [VDodecIm]Br (0.00155 mol, 5 mol%), 1.234 mL ACN (0.0186 mol, 60 mol%), 0.71 mL styrene (0.0062 mol, 20 mol%), 0.0353 mL DVB (0.00025 mol, 2 wt%), 0.0803 g diphenyl(2,4,6-trimethylbenzoyl)phosphine oxide (TPO, 0.00025 mol, 5 wt%) were used.

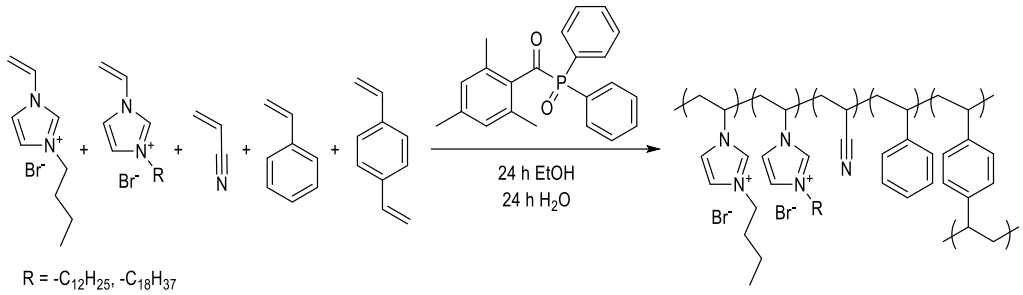

Figure 32: Schematic overview of the UV polymerization using two different ionic liquids and TPO as initiator.

As described for Type1 PILs, the solution was mixed, pretreated and cast. Instead of one Dulux® S BL350, a self-made lamp box with eight light bubbles was used to maximize the irradiated area (Figure 33). The irradiation of the casted monomer film was increased by lining the inner surface of the box with a rescue blanket. Afterward, the layer was washed and cut comparable to Type I PILs.

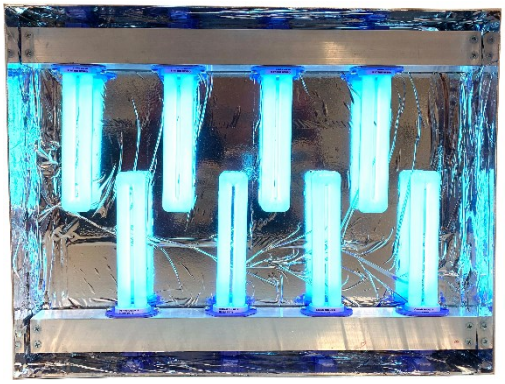

Figure 33: Self-constructed UV lamp consisting of eight Osram Dulux® light bulbes.

The mixtures of [VBuIm]Br and [VDodecIm]Br tested were 95:5, 75:25 and 50:50, whereby 95%, 75% or 50% of [VBuIm]Br was used.

Type III Hetero-PILs

In comparison to Type 2 PILs, the layer was not immersed in ethanol after irradiation. Instead, it was kept at ambient air for two hours before getting immersed in water for 10 minutes. The layer peeled off itself and was ready to use. Similar to Type II PILs, 1.6122 g [VBuIm]Br (0.006975 mol, 15 mol%), 0.7978 g [VDodecIm]Br (0.002325 mol, 5 mol%), 1.85 mL ACN (0.0279 mol, 60 mol%), 1.064 mL styrene (0.0093 mol, 20 mol%), 0.053 mL DVB (0.00037 mol, 2 wt%), 0.0723 g TPO (0.00021 mol, 3 wt%) were mixed in a 20 mL vial till the casting solution became homogenous.

This experiment was scaled up by factor three so that an area of 18x40 cm with a thickness of 300 µm.

3.4 Filtration setup

3.4.1 Dead-end filtration

All measurements of dead-end filtration experiments were performed in a stirred *Schleicher&Schuell* filtration cell (now: *Whatman*, London, United Kingdom; Figure 34). These cells have an effective membrane area of 14.88 cm² with a diameter of 43.53 mm. Pressurized air, used as driving force in the filtration experiments, was limited to 6 bar as a glass body is a part of the setup.

Figure 34: *Schleicher&Schuell* filtration cell used for dead-end experiments.

A homogenous flow and mechanical stability are ensured by a polyethylene sinter plate (70 µm pore diameter, 1.6 mm strong, purchased from *Reichelt Chemietechnik GmbH*, Heidelberg, Germany) as support. The PILs layers were inserted in a wet environment to avoid drying. The flux of deionized water was determined by the amount of water passed the layer at a certain time.

In separation experiments, an initial concentration of 0.025 mol·L^{-1} of the sugars was used. For this, the layer was inserted in an aqueous environment to avoid drying. To assess the proper concentration over the filtration time, a sample of the vessel was taken at the beginning and every fourth filtrate sample. The concentration

was determined by HPLC with internal calibration. For experiments with a steady concentration in the cell, the filtrated volume was replaced by water after each sample collection.

3.4.2 Crossflow filtration

The experiments in a crossflow setup were performed with a self-made module (Figure 35). The effective membrane area was 25.5 cm² and a HPLC pump (*Knauer Wissenschaftliche Geräte GmbH*, Berlin, Germany) was used with a flow rate of 50 mL·min^{-1}. This setup could be pressurized up to 60 bar.

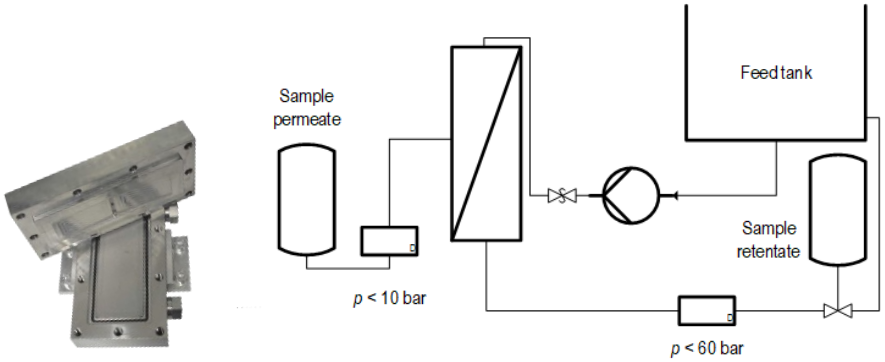

Figure 35: Self-made crossflow module (*left*) and the corresponding flow chart of the filtration setup (*right*).

3.5 Electrodialysis

Electrodialysis was performed in an EDL03 quattro (Figure 36) from *Hescon GmbH* (Engstingen, Germany) in a setup with bipolar membranes. For reference experiments bipolar, cationic, anionic exchange membranes based on modified polystyrene and a 0.2438 mol·L^{-1} sodium acetate solution were used. Experiments were performed with one to three cell triple each consisting in sequence of a cation exchange membrane, a spacer (polyvinyl chloride), a bipolar membrane, a spacer, an anion exchange membrane and a spacer. In addition to the cell triples, the electrolysis stack consists of two electrode endplates. These are equipped with all the necessary connections for the loops of the diluent, concentrates and electrolyte (1 wt% sodium hydroxide solution). In addition, the electrode chamber has an axial connection each for the anode and cathode. Experiments in conventional electrodialysis setups without a bipolar membrane were performed with a 2.5 wt% sodium sulfate solution.

In experiments using anion exchange membranes made of polymerized ionic liquids, two spacers were placed in front and behind the PILs layer. Due to the limiting number of spacers only up to three cell triples in the stack were feasible. Experiments were conducted with sodium acetate (0.2438 mol·L^{-1}), calcium gluconate (0.0465 mol·L^{-1}), sodium gluconate (0.0917 mol·L^{-1}) and potassium gluconate solutions (0.0854 mol·L^{-1}). PILs layers were synthesized as described for Type III PILs and used at voltages of 3, 6, 10 and 15 V. Samples were taken each 10 minutes and analyzed by HPLC (compare A2).

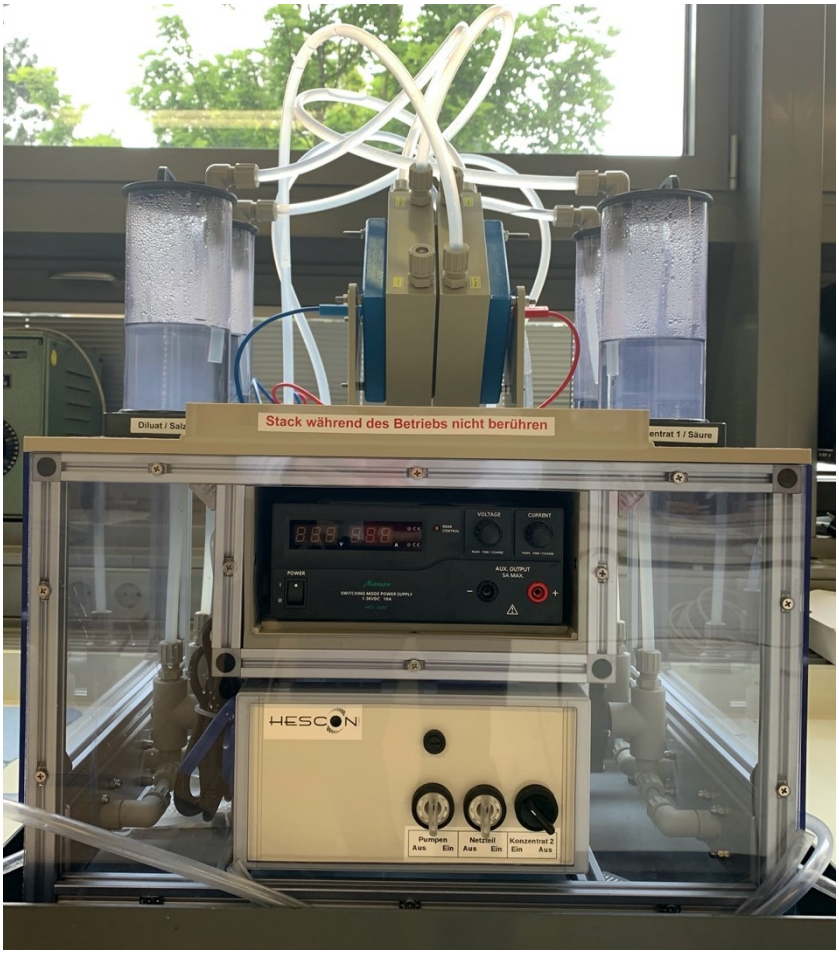

Figure 36: EDL03 quattro from *Hescon GmbH*.

4. Results and Discussion

The following section will present and discuss the results of this work beginning with the synthesis of ionic liquid monomers and possible strategies to form free-standing polymeric layers. Subsequently, material and performance properties of polymerized ionic liquid membranes were investigated and compared regarding the utilized substrates. Potential applications will focus on the retention of charged compounds in different operation modes as well as electrochemical applications.

4.1 From monomers to polymers

4.1.1 Vinylalkylimidazolium ionic liquids

The synthesis of ionic liquids is widely described in the literature.[160,162,164,210] Different strategies were developed to suit the different substrates that are differing fundamental in the use of solvents, inert atmospheres, stochiometric and purification procedures (compare 3.1)

Vinylalkylimidazolium bromide ILs were chosen as they show desired behavior in material synthesis (compare 1.2.3). The reaction was modified based on previous procedures.[154,159] Ethanol proved to be an appropriate solvent for the synthesis of imidazolium bromide ionic liquids with different side groups (Figure 37) with a focus on linear hydrocarbons.

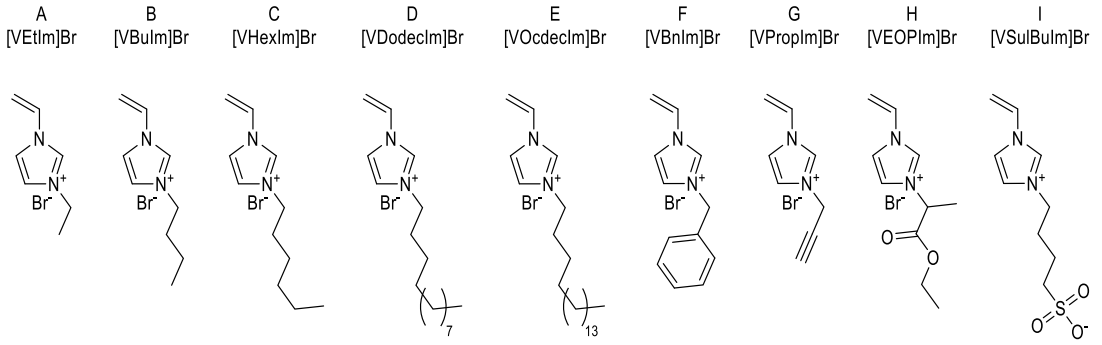

Figure 37: Ionic liquids synthesized and used in membrane formation.

The use of a solvent instead of a solvent-free synthesis and extended reaction times up to 96 h increased the yields up to 89%. The reaction system has tolerated the utilization of technical ethanol, simple mixing of the components and possible presence of oxygen as it was only purged with argon. Additionally, it was applicable to synthesize ionic liquids with sterically complex, charged and chiral side groups (see appendix A1).

In summary, the chosen reaction system offered an efficient, multipurpose usable and economic monomer synthesis.

4.1.2 Free radical polymerization

To form polymeric layers with different starting materials phase inversion technique was used (compare 3.3.1). The utilization of these polymers in a casting solution involves various needs. Required will be polymers of high molar masses able to form a three-dimensional network and be soluble in the solvent but insoluble in the precipitation bath. Starting from the ionic liquid vinylethylimidazolium bromide, a free radical polymerization was performed according to literature in first place to obtain the homogeneous PILs.[211] Water as a cheap and well available solvent was chosen as precipitation solvent. As the bromide-containing polymerized ionic liquid is water-soluble and an organic solvent as precipitant is neither cost-effective nor ecological reasonable, solubility properties of the PILs were changed by anion-exchange (Figure 38).[158] The obtained polymer was soluble in several organic solvents (dimethylformamide, dimethyl sulfoxide, *N*-methylpyrrolidone, dimethylacetamide) that could be used to form a casting solution.

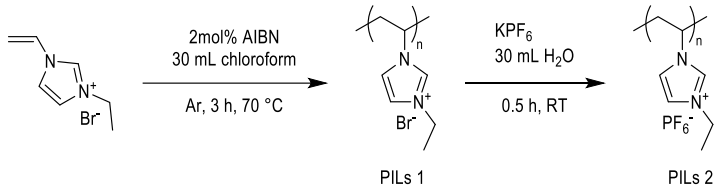

Figure 38: Free radical polymerization of [VEtIm]Br with AIBN and proceeding anion exchange to obtain poly([VEtIm]PF_6^-) from PILs 1.

The casting solution was composed of the polymer PILs 2, the solvent dimethylacetamide and triethylene glycol as an additive to increase the viscosity to make it easier to handle in the casting process (Figure 39). Cast onto a glass plate, the thin film was immersed into deionized water (compare 3.3.2.3). Although the polymer precipitated, it did not form a freestanding layer as desired. Rather it represented swelling polymer artifacts. Changing the polymer concentration of the casting solution, casting speed and thickness, evaporation of the solvent before immersing the film into the water and different casting supports were not effective. In addition, no conclusions could be drawn regarding the influence of the additives either.

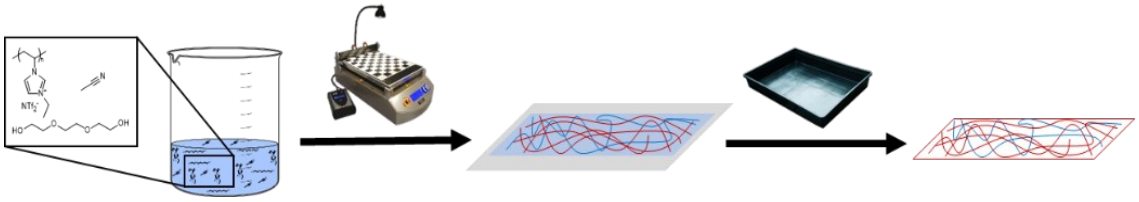

Figure 39: Scheme of the general casting process of layers by phase inversion.

One possibility which prevented the casting could be a low molecular weight of the polymer. Short polymer chains within this system were possibly not able to twist and interact to form a solid material. To obtain higher molecular weights and corresponding chain lengths as in literature, different types of free radical polymerization were performed (compare 3.3.1.1). In general, first investigations concerning the purity and efficiency of the different radical polymerizations were performed by NMR. A representative spectrum of

poly([VEtIm]Br) shows signals of the imidazolium protons (9.0-7.0 ppm), the polymer backbone (4.5-4.0 ppm) and the ethyl sidechain (2.5-1.5 ppm, Figure 40). Signals of the monomeric vinyl group (expected to be at 6.5-5.5 ppm) were not detected, whereas still signals of solvents (MeOH: 3.3 ppm, H_2O: 2.1 ppm) from purification and reaction steps could be observed. Yet, polymer typic broad signals of a purified, linear PILs were observed.

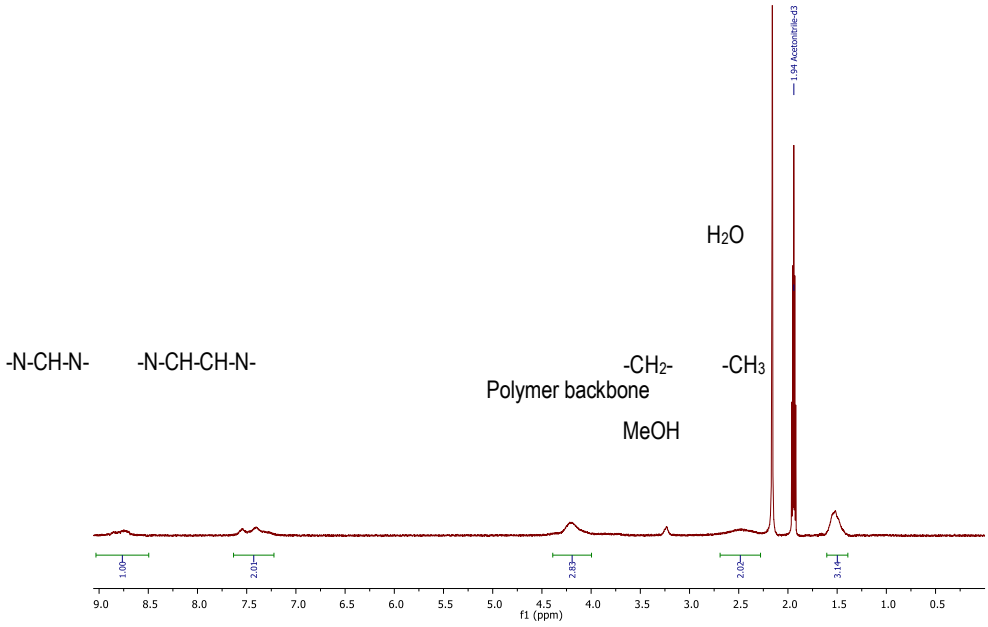

Figure 40: Representative ^{1}H-NMR of poly([VEtIm]Br).

Further analytical investigation by gel permeation chromatography (GPC) should reveal the molecular weight of the polymer before the anion exchange. However, the limited choice of organic solvents appropriate for the polymer, the highly charged character of PILs and a missing reference do not make GPC the most suitable method for molecular weight determination. Polymers obtained by different free radical polymerization reactions (compare 3.3.1 Table 2) were tested as they were reported with high molecular masses.[193,196,203] Also, dialysis bags were used to purify the polymer solution to wash out unreacted monomers and oligomers ensuring high molecular weights. This method has been reported for highly charged polymers similar to those made of ionic liquids.[204,206] Polymers obtained after dialysis should have a molar mass higher than 3500 g·mol^{-1} due to the molecular weight cut off of the used dialysis bag. Neither with the synthesis reported in literature nor with the purification by dialysis bag, the molecular weight of the obtained polymeric solids could be determined by GPC. Since GPC is a relative measurement method, the determination of the molecular weight relies on the calibration substances. Although styrene polymers are often used, they are not comparable to PILs. However, substances for calibration of PILs in GPC do not exist. Further, the influence of charges onto the separation was not determined as ionic interactions might prevent the size exclusion mechanism. Finally, no film of these polymers was successfully precipitated in water after an anion exchange (compare 3.3.1.4).

To overcome stability issues possibly due to a lack of polymer chain interaction or covalent linking, crosslinkers were additionally used in the polymerization. Besides, the well-known divinylbenzene or bisacrylamide, bis(vinylalkylimidazolium bromide) were investigated (Figure 41). Identical procedures in purification, analytical investigation and preparation of the casting solutions were conducted. After anion exchange, no suitable solvent was found to form a homogeneous casting solution.

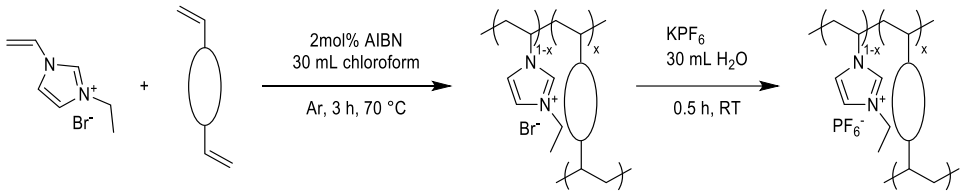

Figure 41: Schematic free radical polymerization of [VEtIm]Br with a crosslinker to obtain the [VEtIm]PF_6-copolymer that precipitates after anion-exchange in water.

Another approach to obtain a stable PILs material is to use an established polymer system as a supporting framework for the membrane formation. Polyacrylic acid with a molar mass of 100,000 g·mol^{-1} was used as reported in the literature to structure the polymer network. Here, the PILs obtained by free radical polymerization were mixed with the polyacrylic acid and a solvent. This casted film was then immersed in a slightly basic aqueous solution enabling precipitation of a polymeric material by anion exchange of bromide with the deprotonated acid (Figure 42).[197]

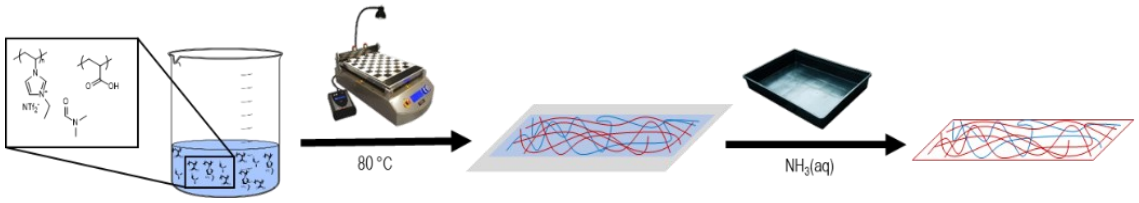

Figure 42: Schematic casting process using polyacrylic acid as “counter-polymer”.

The obtained layer (Figure 43) showed mechanical stability that could even be cut. Therefore, it was scaled-up for used in a stirred dead-end cell as described in 3.4.1 to investigate solvent resistance. The layer showed no type of deformation, dispersion or decomposition in common organic solvents or water for over 28 days have been observed for the layer. Although no holes or breaches were visible, the layer did not perform well in pure water flux simpeding a reliable determination. The high flux suggested physical damage to the layer or a non-homogeneous closed structure.

Figure 43: Layer casted of PILs 2 (compare Figure 38) with deprotonated polyacrylic acid as anion.

4.1.3 UV-initiated radical polymerization

In the literature, different approaches were reported about the photopolymerization of ionic liquids towards membranes.[209,212–215] Styrene and acrylonitrile are often exerted to solve the solid IL and using them simultaneously as comonomers increasing the flexibility and stability of the polymeric layer. Polymerization was initiated by UV light and benzoin ethyl ether. However, details about the synthetic procedure and tools employed are missing.[209,215] The following section intends to consider the various synthetic possibilities and to show UV-initiated synthesis routes that can manufacture large-area polymer layers.

Starting conditions were adapted to the literature[209] and performed with the ionic liquid vinylethylimidazolium bromide. The monomer solution (compare 3.3.2.1) was poured onto a non-scratched glass plate and irradiated by UV light. Since it was not further mentioned in the literature, lamps with an emission spectrum corresponding to the absorption spectrum of the photo initiator were selected. As opposed to the literature[209] a casting solution with IL A ([VEtIm]Br) was feasible by ultrasonic treatment for up to eight hours and 53 °C. However, the polymerization reaction did not take place under any UV light it was exposed to (compare 3.3.2.1) as the casted, liquid film dissolved immediately in the EtOH bath afterward. Further reactions were performed with vinylbutylimidazolium bromide ([VBuIm]Br, IL B) as [VEtIm]Br showed no reactivity under the used conditions with the different lamps.

The experiments pointed out that lamps commonly applied for thin-layer chromatography were generally not powerful enough to initiate the polymerization neither using IL A or B. A more intense light source, the MAX-303 Xenon lamp (Figure 30, *ASAHI-SPECTRA*, Japan), was selected enabling to choose wavelengths from high-energy UV to the visible part of the spectrum. As a layer was obtained after purification the polymerization was successful. Various damages caused by the choice of lamp made these potential membranes not operational. As the setup did not irradiate the entire surface of the layer with even intensity, burned areas occurred (Figure 44). Additionally, a further scale-up is limited by the small area irradiated using the MAX-303. Increasing the distance between the lamp and casted film resulted in inhomogeneous irradiation and an irregular layer occurred.

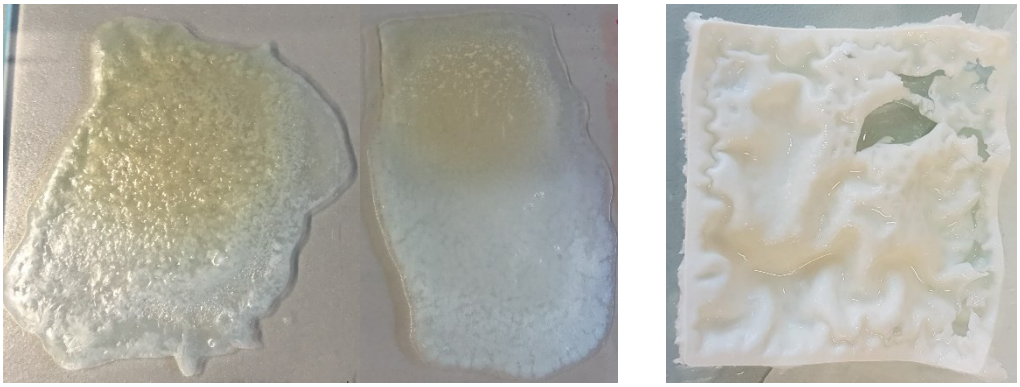

Figure 44: Burned areas after photopolymerization with the MAX-303 (*left*) and damaged layer after being irradiated in a mold (*right*).

Less intense UV lamps were investigated in further experiments. With an UV blacklight and an UV light bulb (3.3.2.1, Figure 30) comparable experiments were successfully performed even though the light intensity was less strong. The poured liquid became solid by irradiation. Since both lamps are equal in use, the light bubble was selected for further experiments as its versatility allows a scale-up. Nevertheless, the received polymeric layers exhibited a lack of mechanical stability.

In the beginning, polymeric, non-adhesive casting supports such as Teflon or poly(oxy methylene) were not considered as they could influence the surface tension of the monomer films by leading to a contraction. Hence, molds were considered as pouring onto the glass resulted in an unwanted thin layer. The thickness was then adjusted by the volume of the monomer solution and the area of the mold. In general, this approach led to a mechanically stable layer. Disadvantages came up by uneven grounds of the mold due to manufacture and leading to irregular layers (Figure 44). Also, the detachment of the layer caused difficulties as there was physical damage to the potential membrane. Improving the mold by an outer ring that can be pushed down overcame these disadvantages (Figure 31). However, the received films were too thick or uneven and thinner films could not be manufactured by this method. For this reason, a film applicator was tested in the next step (Figure 28). Due to the given gap (300 µm) of the applicator and the slightly viscous monomer solution, films were successfully cast. To initiate polymerization, the lamp was placed above the casted monomer film inside a box lined with aluminum foil to reflect the irradiation. The layer was first immersed with the glass support into ethanol and then into an aqueous bath to obtain a free-standing polymer film (Figure 45). Although benzoin ethyl ether is known as a suitable photo initiator[209,215–218], TPO was applied as it showed high reliability in the formation of a polymeric layer while using different ionic liquids.

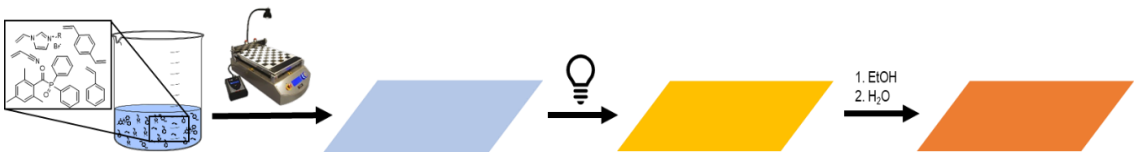

Figure 45: Overview of the casting process including the UV-initiated polymerization.

The use of alkyl side chains longer than butyl resulted in homogeneous PILs. Through the film applicator used, the thickness could be theoretically adjusted between 1 and 3000 µm by the choice of the corresponding casting knife. Initial experiments to determine the aqueous flux through the membrane (compare 3.4.1) reflected, that a gap of 300 µm was most suitable for the experiments and used as a reference in the casting process. A thicker layer could easily reduce the flux to nil. Vice versa, thinner layers were mechanical instable, which could not be improved by longer irradiation.

Further investigations on polymeric membranes made of polymerized ionic liquids were based on this experimental setup using the TQC film applicator and UV A light bulbs.

4.2 PILs membranes by UV irradiation

4.2.1 Type I PILs membranes

4.2.1.1 Synthesis

The following section characterizes UV-polymerized layers composed of different single or mixed ionic liquids, divinylbenzene as crosslinker and TPO as photo initiator (Figure 32). The use of acrylonitrile and styrene was implemented in the polymer (compare 3.3.2.1) as they were renowned to improve the chemical and physical stability of the polymer.[217] Concurrent, they proffered the possibility to solve the solid compounds towards a homogeneous casting solution.

All presented membranes were manufactured similarly while differing in the IL ratios (compare 3.3.2.3), amount of crosslinker and photo initiator. First, the use of a single IL species in the polymer was investigated. More complex IL side groups, such as benzyl or acrylic functional groups, challenged the reaction system. IL G as well as IL I (Figure 37) were not soluble in the casting solution, neither in low concentration nor with longer pretreatments in the ultrasonic bath of up to eight hours. Especially vinylsulfobutylimidazolium bromide showed good solubility in aqueous solvents due to the sulfonate group, which however were not miscible with the comonomers. This zwitterionic species offered interesting possibilities to the formation of layers as positive and negative charges were fixed to the polymer backbone. To further investigate this assumption, ILs that are not structurally based on vinylimidazolium would be necessary.

The synthesis of IL G was strongly exotherm and the product precipitated immediately. It was impossible to resolve it in the casting solution afterward. IL F always resulted in the formation of big holes in the polymeric layer while the reaction with IL H did not take place. Here, the steric properties of the benzyl and ethyl propionate functions compared to less sterically demanding alkyl side groups might be an explanation. These ILs were not further investigated. The structures of successfully synthesized polymer layers, shown in Figure 46 are PILs B, C and D.

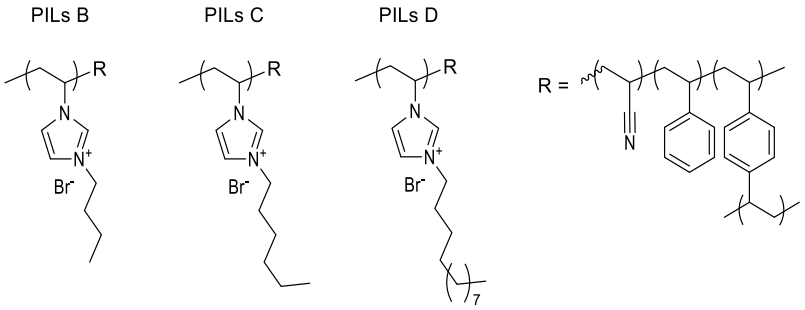

Figure 46: Type I PILs layer with a single IL used in synthesis.

4.2.1.2 Characterization of Type I PILs membranes

Characteristic performance data of membranes are the flux *J* and the permeability *L*. The flux *J* was, after a certain preconditioning time, determined by the amount of water passing the membrane in time depending on the pressure applied. Independent of size, time and pressure different membranes can be compared by the permeability *L*. To classify these data, PILs membranes were compared to commercially available regenerated cellulose ultrafiltration (UF) membranes in identic experimental setups (Figure 47). These experiments were conducted by measuring the volume of pure water passing the membrane per time. After reaching a constant flux at a chosen pressure, it was successively increased.

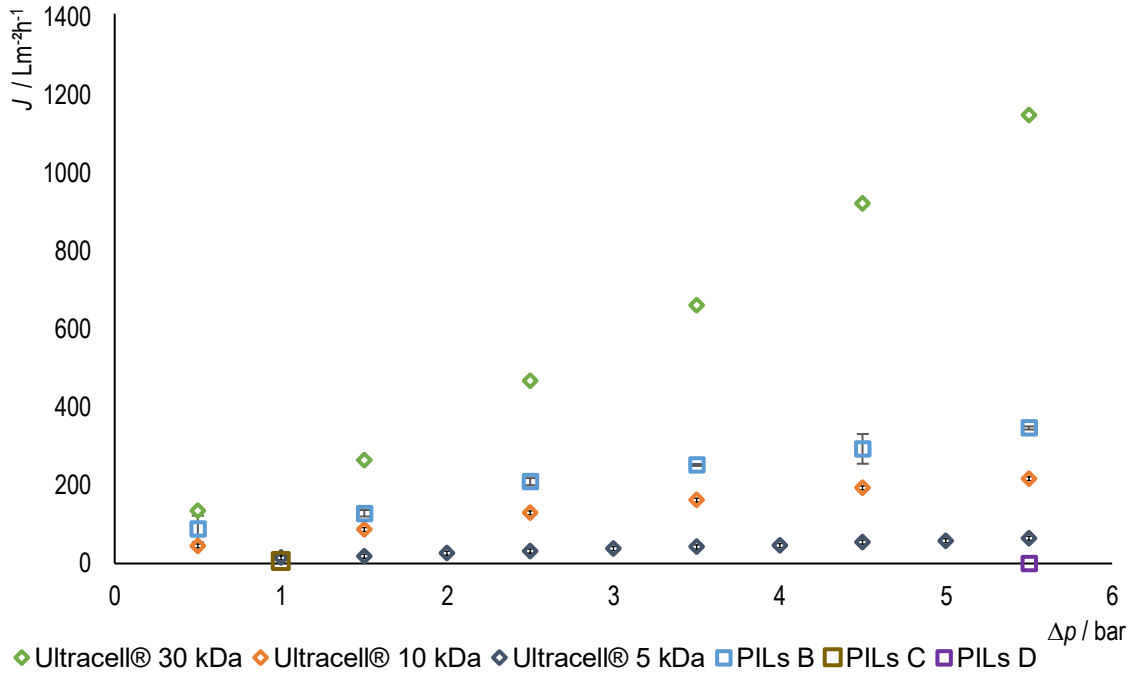

Figure 47: Flux *J* of commercially available regenerated cellulose (rectangles) membranes with different MWCO and PILs B, C and D (squares).

Conditions: $d_{membrane}$ = 43.35 mm, p_{air} = 6 bar, Schleicher&Schuell stirred dead-end cell, n_{IL} = 0.0023 mol, n_{IL} : n_{ACN} : n_{Styr} = 1 : 3 : 1, 5wt% TPO, 5wt% DVB (wt% based on m_{IL}), 0.5 h ultrasonic bath, h_{gap} = 300 µm, 0.5 h UV lamp, 24 h EtOH, 24 h H_2O.

Figure 47 shows a linear behavior of the regenerated cellulose membranes (rectangles) at pressures up to 5.5 bar with negligible errors. As expected, the flux decreases with decreasing molecular weight cut-offs (30 to 5 kDa) of the Ultracell membranes. In experiments with the Ultracell 5 kDa (grey squares), no reliable measurement at 0.5 bar was feasible. A fourth regenerated cellulose membrane with a MWCO of 100 kDa is not pictured, as the flux was significantly higher (450-2600 $Lm^{-2}h^{-1}$). Nevertheless, all commercial membranes are showing a linear behavior of the flux showing an increasing flux with increasing pressure.

PILs B (blue rectangles) was successfully characterized by its flux. It is showing a similar behavior with negligible errors from 0.5 to 5.5 bar. This polymeric layer's data is located between these of Ultracell 30 kDa and 10 kDa even though it is not an indication of the MWCO of PILs B. In contrast, PILs C (brown rectangles) and PILs D (violet rectangles) were not as prosperous. Both are showing higher mechanical stability while implementing them to the setup. Still, no data was realized above 1 bar with PILs C. A possible reason is the microstructure of the membrane has collapsed due to the high applied pressure and the channels were blocked by the membrane material itself. In contrast, no flux was measured under 5.5 bar for PILs D having dodecyl side chains at the imidazolium heterocycle, possibly due to a too dense material. As the experimental setup limited the pressure to 6 bar, the flux could only be quantified for one pressure.

To enable a comparison of the data, permeance *L* can be used. Here, the flux is standardized by the pressure. The results for PILs B, C and D are presented in Table 5.

Table 5: Permeance *L* of Type I PILs layers.

Membrane	L_{H2O} **/ $Lm^{-2}h^{-1}bar^{-1}$**
PILs B	74.090 ± 8.6300
PILs C[a]	5.160 ± 0.5300
PILs D[b]	0.027 ± 0.0021

Conditions: $d_{membrane}$ = 43.53 mm, Schleicher&Schuell stirred dead-end cell, [a]n_{IL} : n_{ACN} : n_{Styr} = 1 : 3 : 1, 5wt% PI, 2wt% CL (wt% based on m_{IL}), 0.5 h ultrasonic bath, h_{gap} = 300 µm, 0.5 h UV lamp, 24 h EtOH, 24 h H_2O. [a]Based on data of 1 bar. [b]Based on 5.5 bar.

The differences in the permeance between the different PILs layers are considerably. By an increasing length of the alkyl side chain, the permeance is dropping more than 90% from PILs B to PILs C. Compared to PILs D, the permeance of PILs B was 2750 times higher. It should be noted, however, that the permeance *L* of PILs C and PILs D only rely on the results of one applied pressure. Although the measurements were feasible, PILs B responded over and over critically to increasing pressures having a lack of mechanical stability in experiments. Short lifetimes and damages occurring during the cutting prevented ongoing experiments.

4.2.2 Type II PILs membranes

4.2.2.1 Synthesis of Type II polymeric layers

As PILs B suffered from a lack of mechanical stability and PILs D was not suitable for experiments due to its dense structure, a layer composed of both IL monomers was investigated at first. The combination of IL B and D should result in a linkage of both, high permeability and mechanical stability. While not changing the total amount of used IL for synthesis, molar mixtures of 95:5, 75:25 and 50:50 of IL B and D were examined (Figure 48). IL B was used in larger quantities as a high flux should be the dominating property.

An increased amount of the other comonomers in the synthesis was not favored. Higher ratios of acrylonitrile and styrene increased the liquidity of the casting solution whereby the casted film did not stay in place and the number of charges would be decreased. Also, the layer got thinner and was not removable from the glass support. In contrast, less of the two liquid comonomers acrylonitrile and styrene and therefore a higher amount of the ionic liquids made a good solution of the solid IL uncertain. The membrane obtained was also very fragile showing an irregular structure. Increasing the concentrations of the crosslinker and photo initiator resulted in denser layers and prevented flux measurement. Lowering the concentrations, the PILs layers were mechanically unstable or the reaction was incomplete.

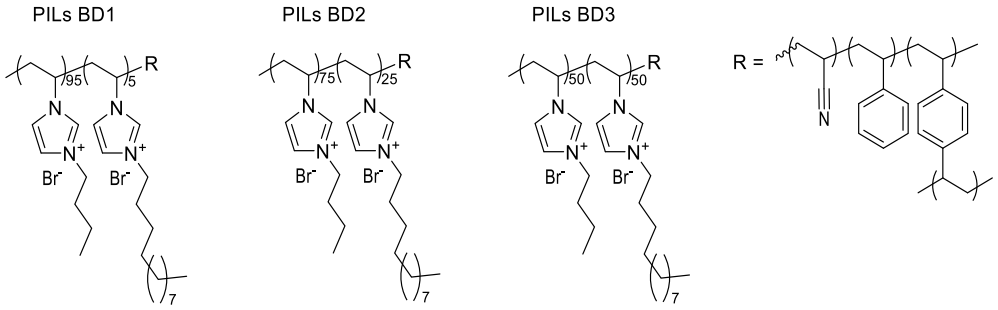

Figure 48: Type II PILs synthesized by UV polymerization.

4.2.2.2 Water flux of Type II PILs layers

Type II PILs layer were tested similarly to Type I (compare 4.2.1.2). All three layers (Figure 48) were successfully characterized and are showing increasing flux while increasing pressure. As a result of the different mixtures of ionic liquids, a tendency in the permeance was observed. Generally, the influence of IL B was less intense than this of IL D so that PILs BD1 has higher permeance than BD2 and BD3. Though the permeance of PILs BD1 and BD2 vary rarely, PILs BD3 has considerably lower permeance (Table 6).

Although a decrease of the flux was expected, it decreased significantly compared to PILs B. Using higher amounts of the longer alkyl chain of IL D resulted in heavy blocking of the polymeric layer preventing any flux. Higher amounts of IL B overcame these problems but did not increase the permeability up to this of PILs B. Permeabilities were up to 180 times lower and just 13 times higher than those of PILs D (Table 6).

Nevertheless, mechanical stability in the cutting the membrane to size as well as longtime resistance in experiments were optimized.

Table 6: Overview of permeance L_{H2O} of Type II PILs membranes.

Membrane	L_{H2O} / $Lm^{-2}h^{-1}bar^{-1}$
PILs BD1	0.291 ± 0.0002
PILs BD2	0.259 ± 0.0041
PILs BD3	0.051 ± 0.0025[a]

Conditions: $d_{membrane}$ = 43.53 mm, Schleicher&Schuell stirred dead-end cell, [a]n_{IL} : n_{ACN} : n_{Styr} = 1 : 3 : 1, 5wt% PI, 2wt% CL (wt% based on m_{IL}), 0.5 h ultrasonic bath, h_{gap} = 300 µm, 0.5 h UV lamp, 24 h EtOH, 24 h H_2O. [a]Based on data at 2.5 bar.

The polymeric layers were also tested in the utilization of common organic solvents such as DMF, alcohols, *N*-methyl-2-pyrrolidone, chloroform, dichloromethane, hydrocarbons, pyridine, diethyl ether, DMSO, acetone, ethyl acetate. As they were fixed in the filtration cell, they were mechanically stable so that any damage could be observed. No evaluable results were obtained as the shape changed due to deformation, which lead to a strongly fluctuating flux over time.

4.2.2.3 Filtration of sugars with Type II PILs

After the initial characterization of the different PILs-containing layers, a separation experiment was conducted to determine the separation efficiency of the membranes. Sugars (Figure 49) were used as a solute for different reasons. All molecular weights apply to nanofiltration as well as they do not differ much in their structure nor their properties. Besides, they are well water-soluble and their functional groups as well as hydrophilicity resemble drug precursors or renewable chemicals. As most of the pharmaceutical substances or intermediates are thermally unstable, aqueous nanofiltration offers a suitable alternative to thermal downstream methods.[219] Afterward, their residues are not fully removed from wastewaters so that new or improved materials are needed to ensure a higher water quality. In addition to the neutral substrates, related charged sugars are accessible. The investigation of these comparable charged compounds provide an insight into charged aqueous NF that gains relevance in withdrawing substances like metabolites or harmful chemicals as arsen oxides.[220]

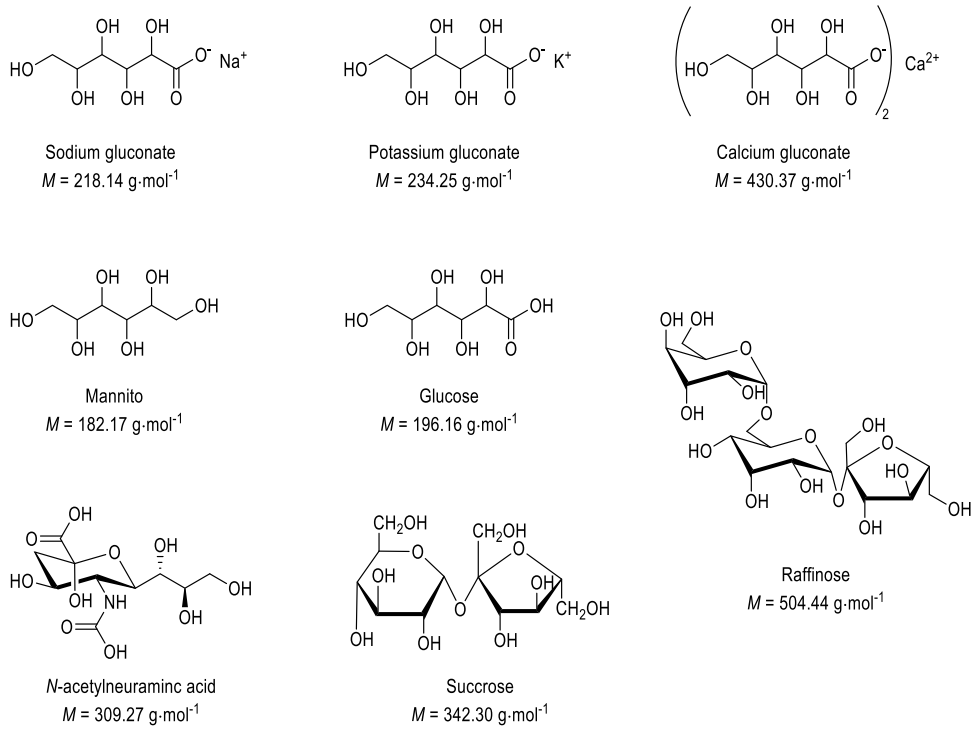

Figure 49: Used neutral and charged sugars in experiments.

Dead-end filtration of neutral sugars using PILs BD2[1]

Separation experiments were conducted using PILs BD2 as this layer had the highest reliability in previous investigations. Since dead-end filtration cells offer the possibility to stir the retentate, the experimental setup was not changed (compare 3.4.1). This guaranteed a homogeneous concentration distribution as well as prevented possible polarization concentration effects that would affect the results negatively.

Figure 50 is presenting the retentions of the sugars glucose, sucrose, raffinose, mannitol and *N*-acetylneuraminic acid (Figure 49) in dead-end filtrations using PILs BD2. The experiments were conducted over a maximal time period of two days and the retentions related to the cell concentration. In the beginning, the retentions are at 100% or nearby, as the PILs layer was implemented in wet conditions to avoid drying and preconditioning the material. The small amount of water remaining at the start of filtrating the sugars deviate between the first samples.

After a few hours, the percentage of retentions are decreasing due to the sugars passing the layer and not being withheld by it. Afterward, the percentage remained constant for the filtration. From mono- to trisaccharide, the retention is about 10% higher with the increasing molecular weight. Of all tested sugars, raffinose had the highest percentage of retention with 23% (compare Table 7: Summarized retentions at the equilibrium of the neutral sugars tested with PILs BD2.). Sugars with similar molecular weights such as glucose

[1] Part of these following results in 4.2.2 were recently published: F. O. Sommer, J.-S. Appelt, I. Barke, S. Speller, U. Kragl, *Membranes* **2020**, 10, *11*, 308.

and mannitol also got withhold with similar efficiency over time. Overall, the PILs BD2 layer was unsuccessful in the filtration of neutral sugars.

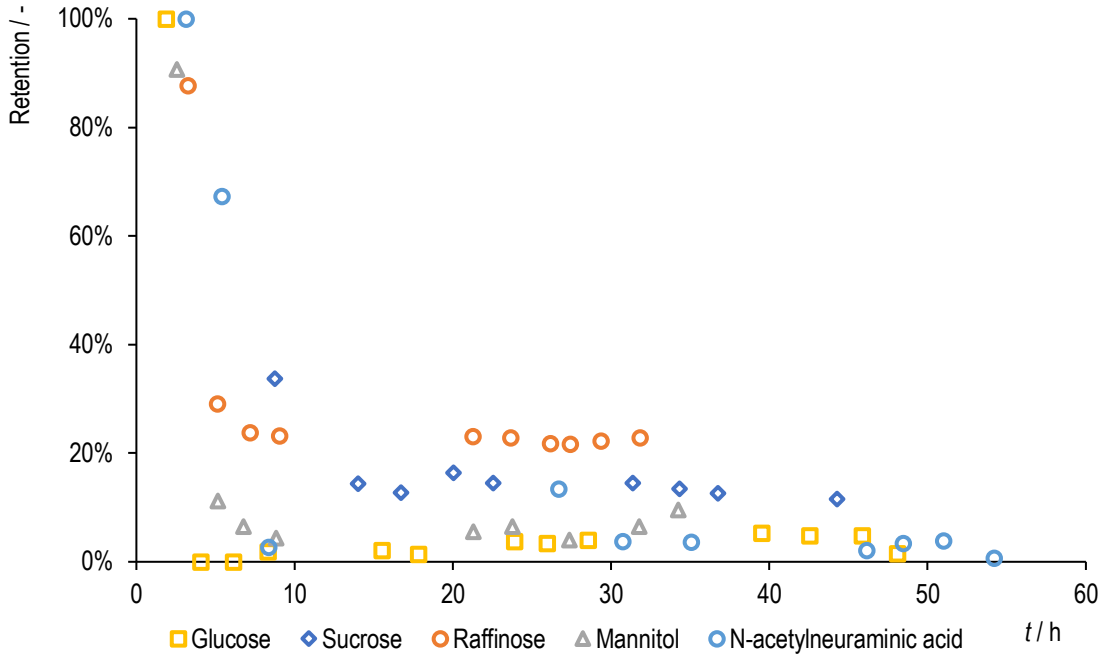

Figure 50: Retention *R* of uncharged sugars in dead-end experiments with PILs BD2.

Conditions: c_{sugar} = 0.025 mol·L^{-1}, $d_{membrane}$ = 43.53 mm, p_{air} = 6 bar, Schleicher&Schuell stirred dead-end cell, n_{IL} = 0.0031 mol, $n_{[VBuIm]Br}$: $n_{[VDodecIm]Br}$ = 0.75 : 0.25, n_{IL} : n_{ACN} : n_{Styr} = 1 : 3 : 1, 5wt% PI, 2wt% CL (wt% based on m_{IL}), 0.5 h ultrasonic bath, h_{gap} = 300 µm, 0.5 h UV lamp, 24 h EtOH, 24 h H_2O.

Due to low retentions, size exclusion or molecular weight cut-off can be rejected as the main mechanism of action. On the contrary, investigations should be made concerning a Donnan exclusion as a mechanism for which a charged solute is used. This exclusion mechanism based on repulsion, also called Donnan effect, occurs when a charged membrane is used in electrolyte solutions. Due to the fixed, impermeant ions in the material, an interface between the membrane and the solution sets up where the ion concentration does not correspond to those in solution.[221] There, the concentration of counter-ions is increased creating a concentration potential. This potential inhibits a trouble-free transport of co-ions to the membrane phase as well as the diffusion of counterions through the material. The latter are, however, attracted by the membrane.[222]

Table 7: Summarized retentions at the equilibrium of the neutral sugars tested with PILs BD2.

Sugar	M / g·mol^{-1}	R / %
D-Glucose	180.16	3
D-Mannitol	182.17	6
N-Acetylneuraminc acid	309.27	6
Sucrose	342.30	14
Raffinose	504.44	23

Conditions: c_{sugar} = 0.025 mol·L^{-1}, $d_{membrane}$ = 43.53 mm, p_{air} = 6 bar, Schleicher&Schuell stirred dead-end cell, n_{IL} = 0.0031 mol, n_{IL} : n_{ACN} : n_{Styr} = 1 : 3 : 1, 5wt% PI, 2wt% CL (wt% based on m_{IL}), 0.5 h ultrasonic bath, h_{gap} = 300 µm, 0.5 h UV lamp, 24 h EtOH, 24 h H_2O.

Dead-end filtration of the charged sugar calcium gluconate using PILs BD1

Calcium gluconate (Figure 49), a charged sugar derivate, was used as a model substrate for charged compounds in aqueous solution. First, calcium gluconate is well known as a food additive[223] and a medical treatment agent.[224] Second, this charged substrate is close to the properties of previously investigated sugars, so that no significant differences due in physicochemical properties are expected. To avoid precipitation of the calcium gluconate by a solubility limit of 0.069 mol·L^{-1}, a 0.025 mol·L^{-1} solution was prepared. To start, the PILs BD1 was initially used as it also provided a good mechanical stability and a high flux as PILs BD2 did.

As mentioned before, the PILs layers forfeit in stability by getting dry, which is why the entire setup was filled with deionized water before the experiment started. This lowered the concentration in the first hours of filtrate sampling (Figure 51 orange dots). The observation is identic in the following experiments.

Over the first 12 hours, the sugar concentration in the filtrate increased continuously. At the same time, the retention of calcium gluconate decreased to 70% (Figure 51 green squares) and collapsed after 12 hours to less than 15%. The concentration of calcium gluconate in the retentate (Figure 51 blue triangles) increased only slightly by 5 mol·L^{-1} over the 20 hours due to the small amounts of sugar withhold successfully by the PILs BD1 membrane. Also, the permeance was decreased in the first half of the experiment from 0.291 with pure water to 0.14 Lm^{-2}h^{-1}bar^{-1} using the sugar solution.

The increasing concentration of calcium gluconate in the filtrate accompanied by decreased retention after 12 hours, expected physical damage of the layer PILs BD1. Resetting the filtration cell, a breach was observed and declared the measured concentrations by HPLC. Figure 51 is showing, that this polymeric layer is not suitable for the application as a membrane over a longer period of filtration due to the mechanical stability.

Nevertheless, the possible equilibrium after 3 hours at about 70% showed, that the retention of charged substrates was increased compared to neutral analytes.

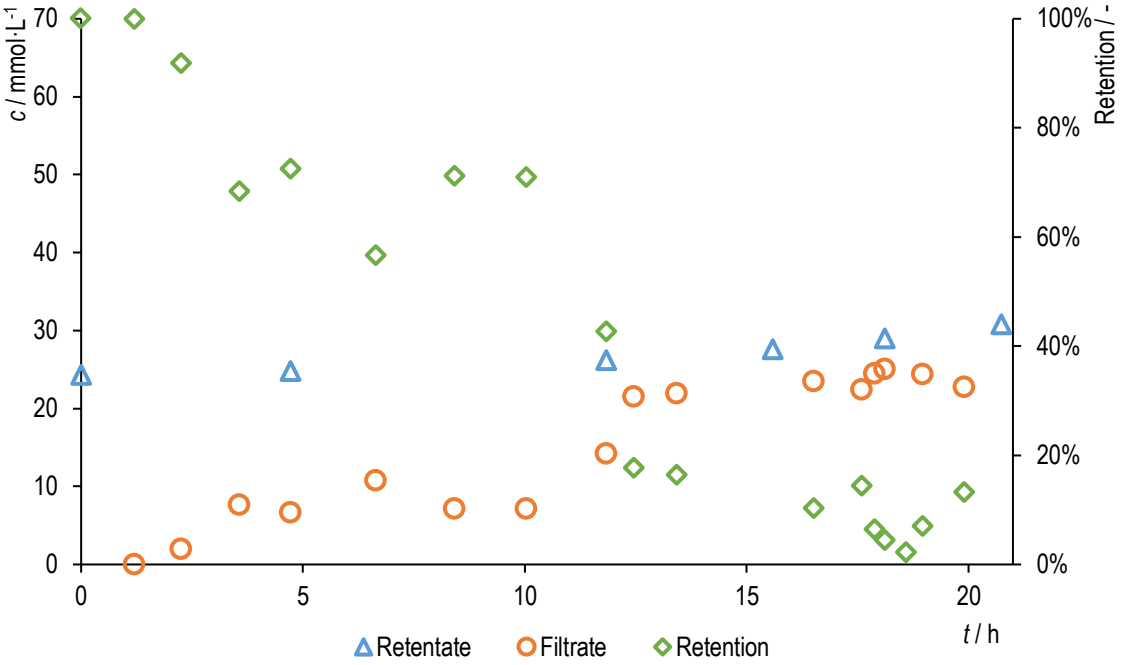

Figure 51: Concentration of calcium gluconate in samples of retentate (blue), filtrate (orange) and retention (green) using PILs BD1 over the filtration time of 20 h.

Conditions: $d_{membrane}$ = 43.35 mm, p_{air} = 6 bar, Schleicher&Schuell stirred dead-end cell, n_{IL} = 0.0031 mol, $n_{[VBuIm]Br}$: $n_{[VDodecIm]Br}$ = 0.95 : 0.05, n_{IL} : n_{ACN} : n_{Styr} = 1 : 3 : 1, 5wt% PI, 2wt% CL (wt% based on m_{IL}), 0.5 h ultrasonic bath, h_{gap} = 300 µm, 0.5 h UV lamp, 24 h EtOH, 24 h H_2O.

Dead-end and diafiltration of calcium gluconate using PILs BD2

To overcome the issue of instability of PILs BD1, a higher proportion of IL D already showed to increase mechanical stability. For that, PILs BD2 was used to filtrate calcium gluconate and evaluate long-term stability (Figure 52). The graph is showing the retention and filtrate concentration of calcium gluconate during dead-end (90-270 h) and diafiltration (270-490 h) in a time-depended manner. The first 90 hours also a similar dead-end filtration was performed but not shown here to reasons of clarity. After 490 hours the experiment was stopped with no visible loss in efficiency or damage to the membrane.

Using the PILs BD2 polymer, the permeance *L* decreased more strongly with about 85% compared to pure water during filtration (here: 0.05 $Lm^{-2}h^{-1}bar^{-1}$, compare Table 6). The filtrate concentration (Figure 52, orange dots) slightly increased in dead-end filtration (90-200 h and 200-270 h), in the same manner as the sugar concentration of the retentate did (Figure 52, blue triangles). As the permeance stayed equal over time during dead-end filtration, a reliance between the cell concentration and efficiency of the polymeric layer was assumed. Starting with a lower retentate concentration (14.45 $mmol·L^{-1}$, ca. 90 hours) this should be

investigated more closely. The concentration of the retentate and filtrate increased coequally in the following 100 hours whereby the increase of both appeared related. The retention declined overall about ten percentage points.

With 10.66 mmol·L^{-1} an even lower starting concentration was chosen at ca. 200 hours. First, the filtration cell was emptying itself due to the experimental time. Second, the reliance described above was reinvestigated at a lower starting concentration to evaluate its influence. Although the first retentions were the highest with 95%, the same straight-line dependency of calcium gluconate concentrations in filtrate and retentate was observed.

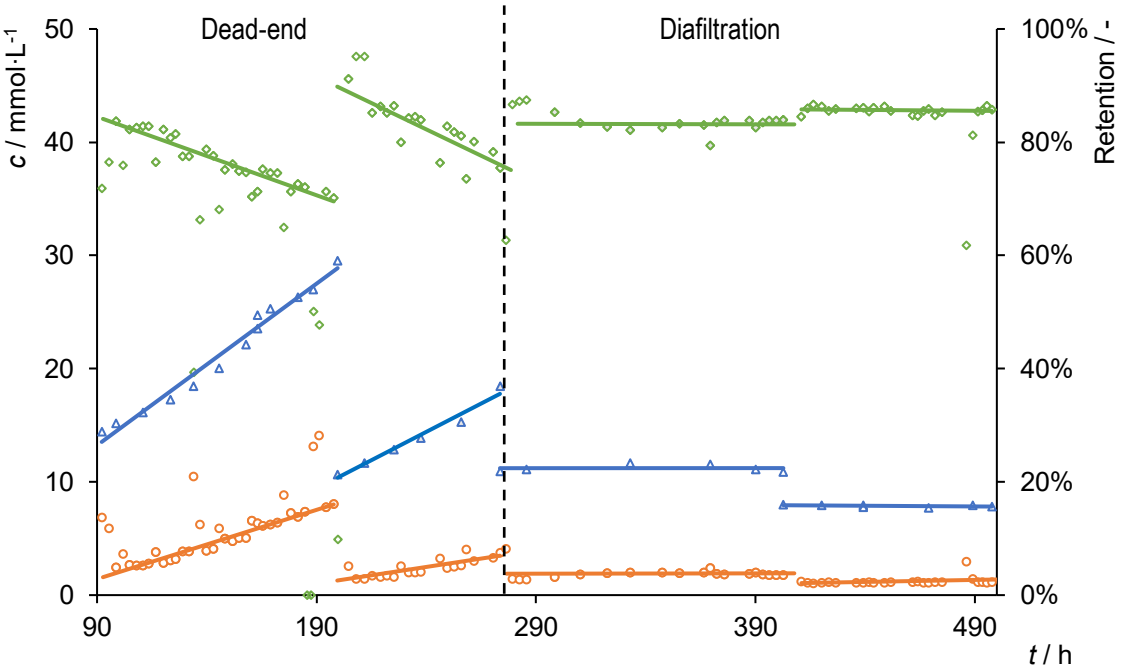

Figure 52: Retentate (blue), filtrate (orange) and retention (green) in dead-end (90-270 h) and diafiltration experiments (270-490 h) using PILs BD2.

Conditions: $d_{membrane}$ = 43.35 mm, p_{air} = 6 bar, Schleicher&Schuell stirred dead-end cell, $n_{[VBuIm]Br}$ = 0.00465 mol, $n_{[VDodecIm]Br}$ = 0.00155 mol, n_{IL} : n_{ACN} : n_{Styr} = 1 : 3 : 1, 5wt% TPO, 2wt% DVB (wt% based on m_{IL}), 0.5 h ultrasonic bath, h_{gap} = 300 µm, 0.5 h UV lamp, 24 h EtOH, 24 h H_2O.

Noteworthy are the outliers of retention and concentration of the sample. These miss fitting data points could be traced back to the experimental setup. Because of the long measurement time, the experiment was paused frequently overnight whereby the pressure was relieved. Small shifts in the overall arrangement of sinter plate, different seals and the membrane might have occurred. Small leaks led to highly concentrated retentate that bypassed the membrane which influenced or even distorted the samples after the resumption of the experiment (Figure 52, 185-200 hours). By steady measurements this detriment was overcome (Figure 52, 200-260 hours).

As the dead-end filtration mode came along with decreasing retention while the concentration of calcium gluconate increased in the retentate, an experiment at steady retentate concentration was aimed. After

280 hours of filtration, the filtration mode was changed from dead-end to diafiltration. Starting off with 11 mol·L^{-1}, the volume of each sample was returned to the cell in the form of deionized water. Measurements of the retentate (blue line) confirmed that the concentration never changed more than ± 5%. Obtaining a retention of 83% (Figure 52, 280-400 hours), the semi-continuous setup was as effective as the previous measurements for comparable concentrations. In contrast, the retention remained constant over time due to the added water and has led to predictable results. Lowering the concentration in the vessel about 25% induced an amelioration of the retention of ca. 5% (Figure 52, 400-490 hours).

Dead-end and diafiltration of sodium gluconate using PILs BD2

Within the filtration of uncharged sugars, a trend between the retention and the molar mass was identified (compare Table 7: Summarized retentions at the equilibrium of the neutral sugars tested with PILs BD2.). A similar structure to calcium gluconate with a smaller molar mass is provided by sodium gluconate. Regarding the previous results, sodium gluconate should be better withheld than the neutral glucose with a similar mass.

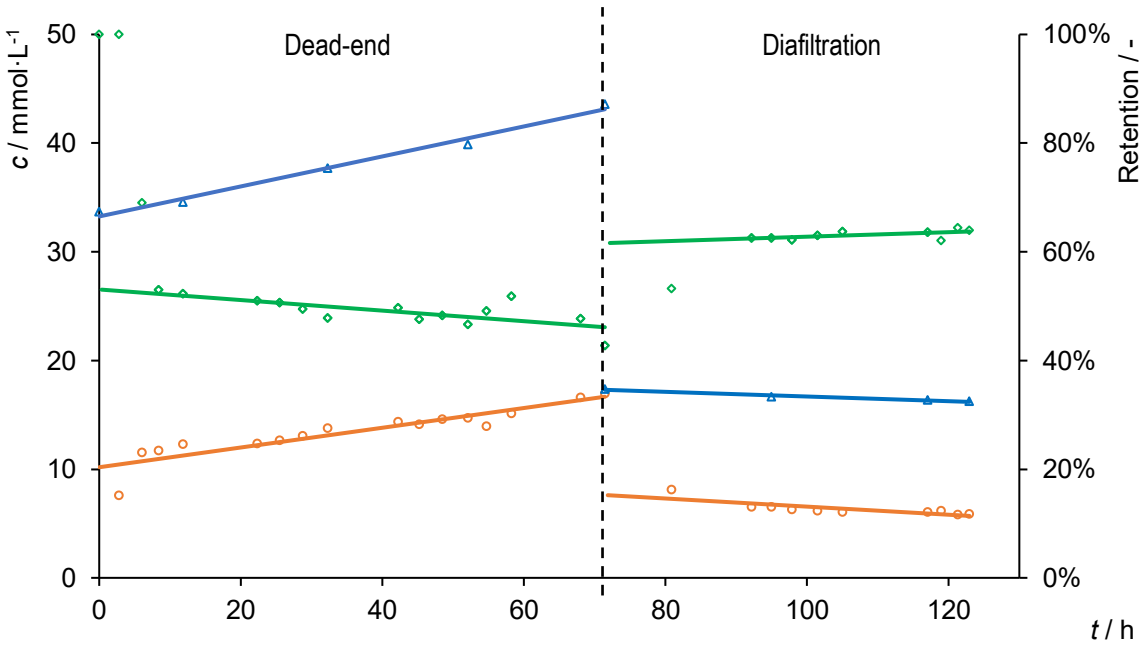

Figure 53: Retentate (blue), filtrate (orange) and retention (green) in dead-end (0-75 h) and diafiltration experiments (75-125 h) with sodium gluconate using PILs BD2.

Conditions: $d_{membrane}$ = 43.35 mm, p_{air} = 6 bar, Schleicher&Schuell stirred dead-end cell, $n_{[VBuIm]Br}$ = 0.00465 mol, $n_{[VDodecIm]Br}$ = 0.00155 mol, n_{IL} : n_{ACN} : n_{Styr} = 1 : 3 : 1, 5wt% TPO, 2wt% DVB (wt% based on m_{IL}), 0.5 h ultrasonic bath, h_{gap} = 300 µm, 0.5 h UV lamp, 24 h EtOH, 24 h H_2O.

The following experiment (Figure 53) was conducted similar to Figure 52 with sodium gluconate for 130 h, since stability of the membrane was approved during calcium gluconate filtration. As both, dead-end and diafiltration mode, reproduced similar graphs the experiment was stopped. The retentate as well as the filtrate concentration increased as the sodium gluconate got withhold by the polymeric membrane. Here, the retention

was about 50% for the dead-end filtration (Figure 53, green squares, 0-75 hours). This value slightly decreased comparable to dead-end filtrations with calcium gluconate but seemed less affected by the increasing retentate concentration. Considering the previous experiments, an onward decrease in retention was estimated, if the experiment would be extended in the dead-end filtration mode. Likewise, the retention is steady when the sample volume is refilled afterward (Figure 53, 75-125 hours). Compared to the neutral glucose, sodium gluconate was withheld in higher amounts. Also, the retention was lower than for calcium gluconate that might be referred to the lower molecular weight of sodium gluconate.

Comparison of dead-end filtration of charged sugars using PILs BD2

64% of sodium gluconate was withheld at a retentate concentration of 16.6 mmol·L^{-1}, whereas 83% of calcium gluconate with a comparable retentate concentration was retained during filtration. Therefore, it should be investigated whether this difference could be a phenomenon of the initial sugar concentration when it is a mono- or bi-charged derivate, or whether it would change at initial concentrations other than 25 mmol·L^{-1}. Additionally, two further charged sugar derivates, potassium gluconate and sodium pyruvate, were tested in the same way as sodium and calcium gluconate. Potassium gluconate should reveal possible influences of the cation towards the performance while sodium pyruvate should demonstrate potential differences by variation of the anion.

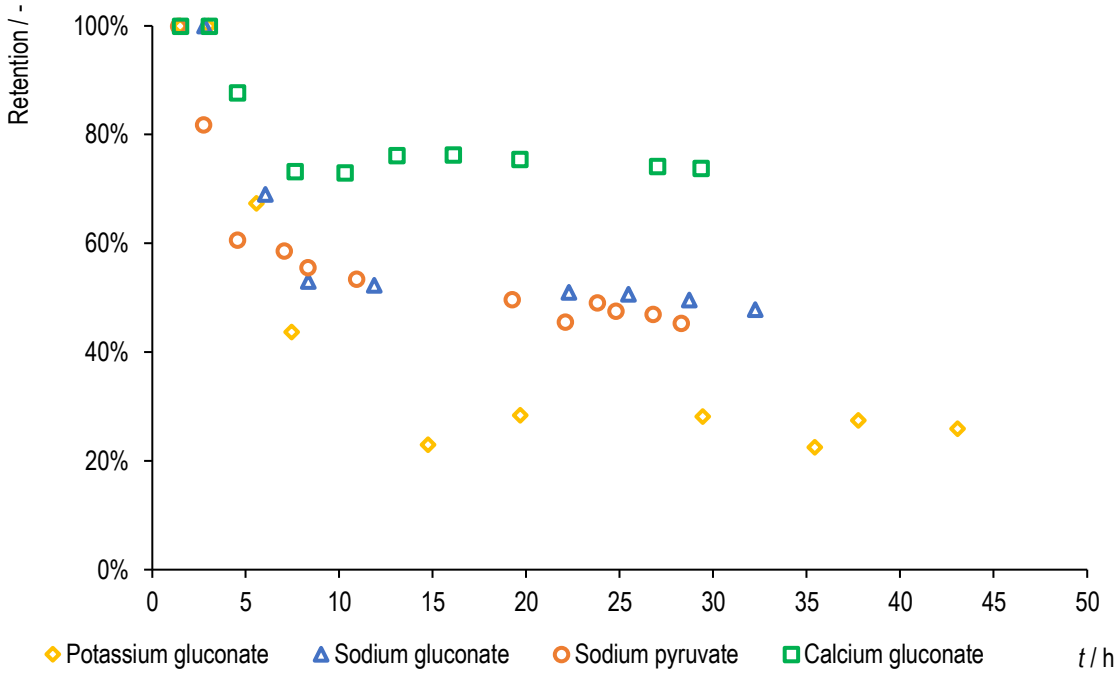

Figure 54: Filtration of charged sugars with PILs BD2 over 50 hours.

Conditions: c_{sugar} = 0.025 mol·L^{-1}, $d_{membrane}$ = 43.53 mm, p_{air} = 6 bar, Schleicher&Schuell stirred dead-end cell, n_{IL} = 0.0031 mol, $n_{[VBuIm]Br}$: $n_{[VDodecIm]Br}$ = 0.75 : 0.25, n_{IL} : n_{ACN} : n_{Styr} = 1 : 3 : 1, 5wt% PI, 2wt% CL (wt% based on m_{IL}), 0.5 h ultrasonic bath, h_{gap} = 300 µm, 0.5 h UV lamp, 24 h EtOH, 24 h H_2O.

Figure 54 is showing the retention of the differently charged sugar derivates over 50 hours of dead-end filtration. Besides the already mentioned difference between the mono and bi-charged gluconate sugars in different retention rates, no additional distinction could be made. For identic monovalent cations with different anions also no difference in the retention was observed. Sodium gluconate and sodium pyruvate showed a similar behavior. The starting retention of up to 100% was due to the experimental setup where the PILs membranes were inserted in cells flushed with pure water to avoid drying of the membrane and conditioning the membrane at the same time.

Regarding the trend of neutral sugars (compare Table 7), the retention increased with increasing molar masses. Conversely, the identic layers showed significantly higher performance just by simply charging molecules of comparable structure and molecular weight (*e.g.* $R_{glucose}$ = 3% < $R_{sodium\ gluconate}$ = 53%). Table 8 shows, that potassium gluconate miss fit in this tendency as it had the lowest percentage of retention at similar retentate concentrations.

Table 8: Summarized retention *R* and molecular weight of the charged sugars tested with PILs BD2.

Sugar	*M* / g·mol^{-1}	*R*
Sodium gluconate	218.14	53%
Potassium gluconate	234.25	25%
Calcium gluconate	448.39	75%
Sodium Pyruvate	110.04	47%

Conditions: c_{sugar} = 0.025 mol·L^{-1}, $d_{membrane}$ = 43.53 mm, p_{air} = 6 bar, Schleicher&Schuell stirred dead-end cell, n_{IL} = 0.0031 mol, $n_{[VBuIm]Br}$: $n_{[VDodecIm]Br}$ = 0.75 : 0.25, n_{IL} : n_{ACN} : n_{Styr} = 1 : 3 : 1, 5wt% PI, 2wt% CL (wt% based on m_{IL}), 0.5 h ultrasonic bath, h_{gap} = 300 µm, 0.5 h UV lamp, 24 h EtOH, 24 h H_2O.

Compared to the uncharged sugars, a size-exclusion trend was remarked. Dissociated, the charged sugar derivatives are differing by their cations and retentions (R_{K+} < R_{Na+} < R_{Ca2+}). Similar effects were reported by CHENG *et al.* for chloride salts. There, the rejection of mono- and bivalent ions depended on the number of used polyelectrolyte multilayers of poly(diallyldimethylammonium chloride) and poly(sodium styrenesulfonate). A larger hydrated radius, a larger charge density and a higher hydration free energy of the solved cations resulted in increased retentions.[225]

The retention of gluconate salts decreased using larger cations (Table 9). Nonetheless, due to smaller cation size and correlated valency effects, a larger hydrate shell is formed. Within this increasing radius the retention increased in experiments either. Concluding, charges seem to be necessary to withhold molecules by PILs membranes, however, the efficiency is determined by the size of cation and anion hydrate shells.

Table 9: Radii of cations and their hydrate shell corresponding to the retention in dead-end experiments.

Cation	r / pm[226]	$r_{\text{hydrate shell}}$ / pm[227]	$R_{\text{gluconate salt}}$
K^+	138	331	25%
Na^+	102	358	53%
Ca^{2+}	100	412	75%

Crossflow filtration

In contrast to the dead-end filtration, crossflow filtration allows passing the liquid feed the membrane tangentially instead of straight onto.[228] This prevents possible fouling products or filter cakes from remaining on the membrane as the feed washes them away. Different techniques to operate crossflow modules are used in the industry.

Due to the good retention of calcium gluconate operating a dead-end filtration cell in diafiltration mode, the crossflow module should simplify the long-term process as a bigger reservoir vessel was used. The driving force in crossflow filtration is the transmembrane pressure that is not identical to the applied pressure in dead-end filtration or the pressure generated by the pump. Figure 55 shows the measured concentration of calcium gluconate in the feed and filtrates as well as the percentage of retention.

Overall, the crossflow filtration of calcium gluconate with PILs membranes was successful. The polymeric layer was stable over 35 hours at pressures of up to 80 bar. The concentration of calcium gluconate in the filtrate decreased over time and was as high as the concentration of the feed as the setup was filled in the beginning. The concentration of the feed did not change over time as the withheld amount of substance of the sugar was too low to influence the feed vessel concentration. After 35 hours, retention increased up to 84%. Under similar experimental conditions, the crossflow filtration performed as good as the dead-end filtration.

The main advantage was the less complex setup as the filtration process did not need to be stopped while taking a sample. Additionally, a refill of the feed vessel was possible at any time. The self-made filtration cell and the corresponding setup was prone to the high pressure needed. A more professional, also bigger setup would overcome this drawback. Also, thinner PILs layer might provide higher fluxed through the membrane. As the estimated transmembrane pressure was significantly lower than the applied pressure in dead-end experiments, less filtrate was generated. Still, crossflow filtrations with PILs membranes should be considered for bigger scale applications.

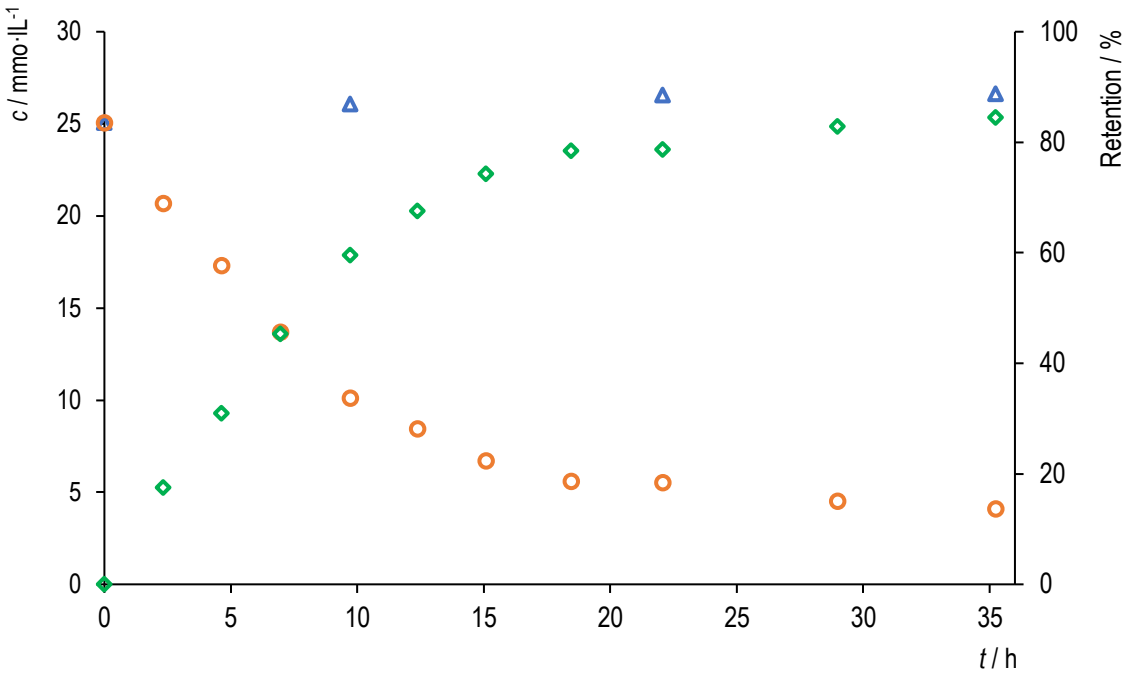

Figure 55: Feed (blue), filtrate (orange) and retention (green) in crossflow filtration of calcium gluconate using PILs BD2.

Conditions: $A_{membrane}$ = 25.5 cm², p_{air} = < 80 bar, self-made cross-flow cell, $n_{[VBuIm]Br}$ = 0.00465 mol, $n_{[VDodecIm]Br}$ = 0.00155 mol, n_{IL} : n_{ACN} : n_{Styr} = 1 : 3 : 1, 5wt% TPO, 2wt% DVB (wt% based on m_{IL}), 0.5 h ultrasonic bath, h_{gap} = 300 µm, 0.5 h UV lamp, 24 h EtOH, 24 h H_2O.

4.2.2.4 Investigation of the surface morphology

Determination of surface morphology by optical microscopy

The surface morphology of membranes significantly influences the properties of permeability and stability.[229] However, rough surfaces favor the potential fouling of particles and thus decrease efficiency. Since the permeability and retention changed considerably, due to different ILs and varying ratios, differences in the membrane surfaces were suspected. Figure 56 shows PILs B with different magnifications pictured by an optical microscope.

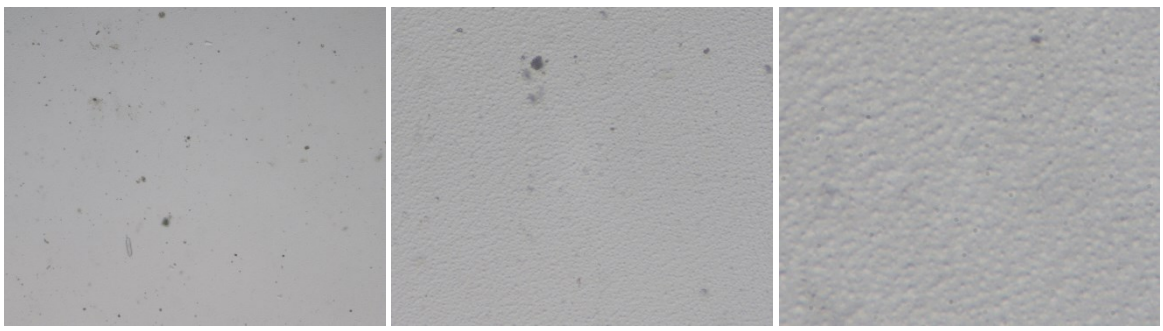

Figure 56: PILs B investigated at 5-, 20- and 50-times (left to right) magnification by optical microscopy.

At first sight, the surface seemed to be even but viewed in a higher resolution, small elevations and hole-like structures were visible. The distribution and sizes of these objects appeared to be even and uniform.

These observations suggested a dominant structure of the PILs surfaces, which is determining main properties as mechanical stability, permeability and the retention of substrates. It is unclear whether different single and mixtures of ILs also lead to structural differences. It can therefore not be excluded that the structural differences may also explain the experimental differences in flux and retention.

Determination of surface morphology by AFM

Hence, the determination of the surface morphology on the micro- and nanoscale was intensified by atomic force microscopy (AFM). Subsequently, the differences between the layers of individual polymerized ionic liquids (PILs B and D) and the mixture of PILs B and D (PILs BD2) were investigated after filtration with pure water. (Figure 57).

In general, all surfaces are showing no superordinate structures and were relatively plane on a larger scale (> 10 µm). Even though height corrugation of less than 100 nm was observed, they showed different morphological characteristics on the subscale. PILs B (Figure 57 a and b) indicated large cavities with a lateral size of 1 µm with a depth of up to 200 nm. Still, this might be limited to the AFM cantilever and its geometry. With heights of 30 to 50 nm, an additional grainy structure is recognized on the microscale (PILs B and BD2, Figure 57 b and c). A closer inspection of PILs BD2 revealed only height corrugation of the grainy structure in the order of 10 nm or smaller (Figure 57 d).

PILs D (Figure 57 e) appeared at first sight alike PILs BD2, as any noticeable holes are visible but are differing as the density and corrugation of the grooves are less pronounced. Albeit the microstructure seems to be comparable, they contradict in two major observations. First, the corrugation heights of PILs D is smaller than those of PILs BD2 observable in comparison to the line profiles. Second, dark spots indicate relatively deep spots onto PILs D (Figure 57 f) which can be also observed in the green line profile. These are not visible or less pronounced when two ionic liquids are used in synthesis. As mentioned above, the detection of their depth is limited to cantilever geometry though it should be at least 30 nm.

Overall, the surface morphology is mainly influenced by the choice and ratio of ionic liquids in the casting process and UV-induced polymerization. The influence of the glass support in the formation process is disqualified as different morphologies are obtained and AFM images of the support itself revealed another shape. Differences in surface shapes of the PILs membrane by variation of the vinyl group or the anion were reported by SENGUPTA *et al.* Using allylbutylimidazolium ionic liquids in the synthesis did not change the overall appearance. Also, chloride anions in synthesis resulted in the formation of holes with similar sizes while increased UV irradiation times lead to decreased diameters.[215]

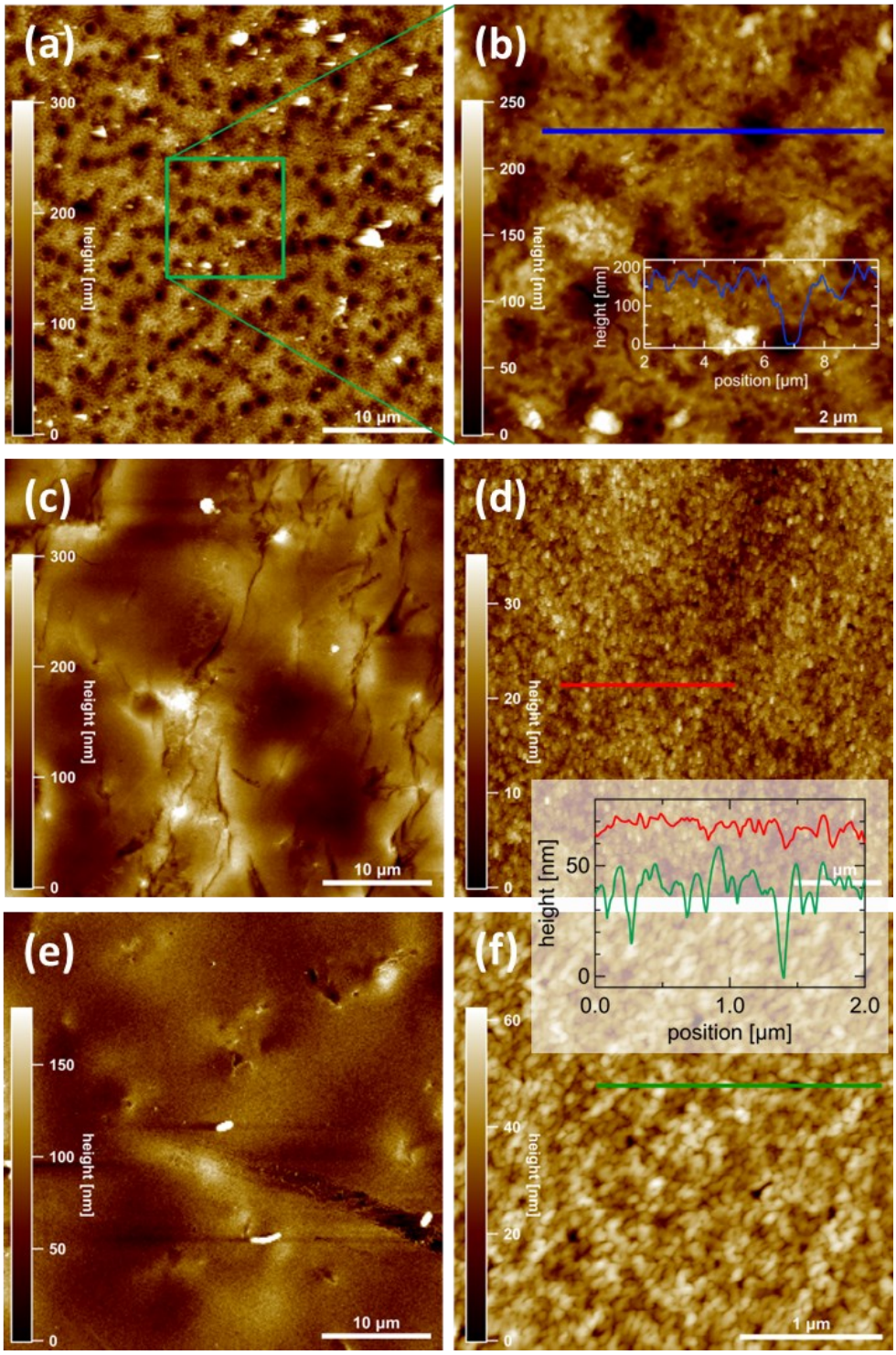

Figure 57: Surfaces of PILs B (a, b), PILs BD2 (c, d) and PILs D (e, f) obtained by AFM. a, c and e correspond to overview images while b, d and f show high-resolution images of the fine structure on the microscale. Heights are indicated by bright (large) and dark (small) colors. Blue, red and green lines indicate locations where profiles are investigated.

Considering the flux data of the different PILs membranes, an interesting correlation towards the morphology and the appearance and size of holes could be perceived (compare Table 5 and Table 6). With the increasing

extent and quantity of holes the flux increases. These observed cavities in the AFM topographies, which are hollow channels in between the grains, therefore are correlated to the main liquid flux channels. This correlation enables to prescreen of future PILs membranes via AFM and avoid an elaborated flux measurement at first instance. Nonetheless, the high number of holes is accompanied by mechanical instability of the membranes and a decreased retention of charged sugars. Therefore, IL mixtures demonstrate to be an optimal intermediate approach of polymerized ionic liquid membranes.

Spot-like patterns with a shape comparable to Figure 57 are known to occur in systems that are subject to distinct microphase separations, e.g. block copolymers.[230] These dark features may occur due to microphase separation of the polymers in the membrane. In general, microphase separations appear by spontaneous segregation and formation of two micro-separated phases. These local demixing occur due to the incompatibility of the chemical compounds in concentrated solutions and restrict locally and refer to e.g. the chain length or molecular weight of the compound.[231]

Although such phenomena on the nanoscale cannot be excluded, topographic AFM as used here is too insensitive to detect these under soft conditions. More precisely methods such as SEM showed for block copolymers of polystyrene and poly(methyl methacrylate), that periodical concentration gradients of both occurred while no domain containing one single polymer species was observed. These gradients on a small scale of up to 3 nm might arise due to the Flory-Huggins parameters of polystyrene and poly(methyl methacrylate) or a bigger copolymer brush.[230] Based on these reported observations and the 300 times larger scale of the given topography, the coexistence of different phases at the surface may be excluded.

Following a filtration experiment with calcium gluconate similar to Figure 51, AFM images of the used PILs membranes were recorded (Figure 58). The aim of this investigation was the determination of surface changes after the filtration of a charged sugar. Compared to the pure water, the flux decreased significantly in the filtration of water. AFM was used as no visible fouling was observed afterwards.

Besides the yet presented morphology, lengthy objects are observed that are like fiber bundles. Compared to the images of PILs BD2 (Figure 57), these objects are a hundred times bigger than the surface corrugation noticeable by the height scale. Most likely, these bundles accumulate onto the surface through the aggregation of charged sugar molecules. In further investigations, this anion exchange could be investigated by the glass transition temperature of newly synthesized and used polymer membranes.

Presumably, these deposits contribute to a time-dependent reduction in permeability through the membrane. This reduction was mainly observed during the first three hours of filtration and stayed equal afterward. Considering the charged character of the solute and the PILs membrane, an anion exchange of the bromide and dissociated gluconate ions is feasible. The bigger gluconate ion blocked the main hollow channels between the grains and decreased the flux recognizable in flux data and AFM images. The possible anion exchange mechanism is shown in Figure 58. Regarding the decreasing permeances filtrating charged sugars (compare 4.2.2.3), an anion exchange might be the reason. Still, in the long-term application of the membrane

at a comparable concentration of the sugar, this should not influence the performance as it did not in diafiltration experiments (Figure 52).

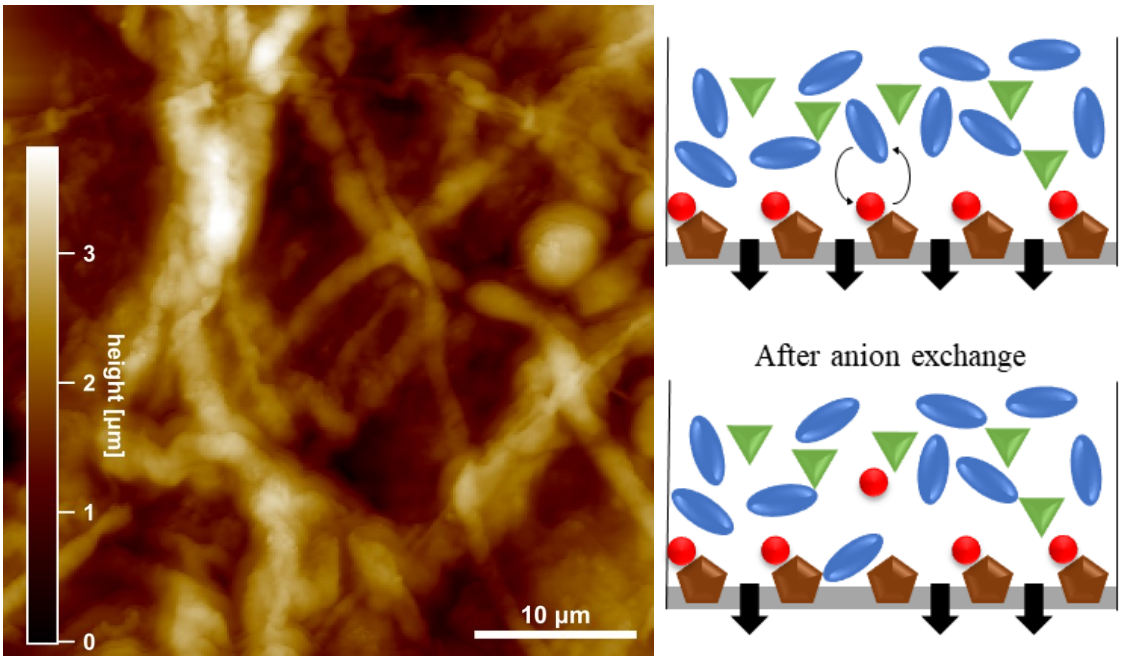

Figure 58: Topside of PILs BD2 membrane after use in filtration experiment with an aqueous calcium gluconate solution (*left*). Hypothetical mechanism of decreasing flux due to anion exchange (*right,* brown: imidazolium cation, green: calcium cation, red: bromide, blue: gluconate).

4.2.3 Type III PILs membranes

4.2.3.1 Synthesis of Type III PILs layers

Following the successful filtration experiments with charged sugars and surface investigation of several PILs layers, a scale-up of membrane synthesis should enable the use of bigger cells. The synthesis was mainly limited by the irradiated area using only one light source. New technical equipment realized a layer size of 30x40 cm by a bigger lamp (3.3.2.3, Figure 33) and casting knives. To reduce the waste in the cutting of the membranes, smaller layers were casted. However, the purification steps educed the efficiency of the layer synthesis. While staying in the ethanol bath, edges of the polymerized film splintered and hardened making them unusable. This was already known from the previous synthesis why high amounts of waste were produced to obtain PILs membranes. Benefiting from the volatility of some compounds, this step was replaced by evaporation in air. Afterward, it remained only 15 minutes in pure water whereby the layer peeled of itself.

Figure 59 shows the investigated PILs layers synthesized following the new proceeding. Besides PILs BD1 and BD2, it shows PILs BE1 that contains longer alkyl chains by implementing the IL vinyloctadecylimidazolium bromide. This new IL should increase stability and permeability.

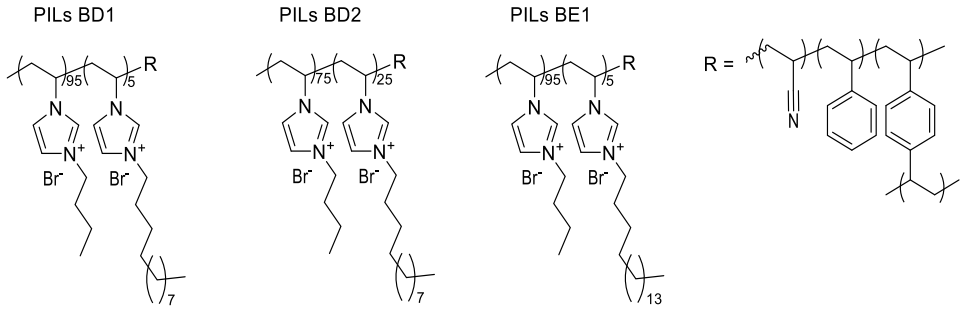

Figure 59: PILs membranes synthesized following the new method.

A layer with only IL E was not fabricable. The solid ionic liquid could only be solved at about 50 °C in the ultrasonic bath and needed also to be handled in a temperature environment. Although the glass support could be heated by the film applicator during the casting and photopolymerization, the layer could not be cut or inserted into the cell. The same occurred with mixtures using more than 5% of the IL E.

The modified synthesis improved the efficiency of the casting process. Therefore, one casting procedure offers the possibility to obtain several pieces for dead-end applications. In addition, a higher outcome was generated as the outer areas of the polymer did not harden or curl. The following section will investigate, if the newly synthesized layers have different properties then Type I and II PILs and determine the influence of the shorten purification process.

4.2.3.2 Water flux of Type III PILs layers

Like 4.2.2.2, the newly synthesized PILs layers were characterized towards their permeance. Of great interest was a possible change of the performance due to the missing ethanol bath as well as the influence of octadecyl side chains. Figure 60 shows the flux of PILs BD1, BD2 and BE1 compared to a commercial nanofiltration membrane.

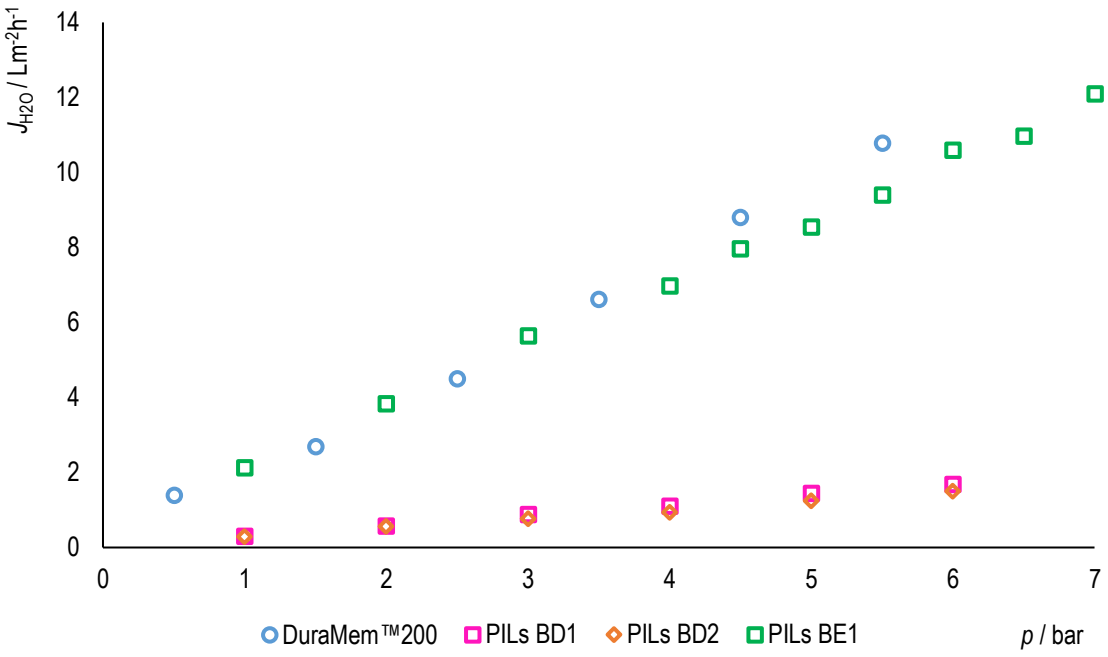

Figure 60: Flux *J* of commercial membrane and synthesized PILs with two ionic liquids membranes compared to the commercial NF membrane DuraMem 200.

Conditions: $d_{membrane}$ = 43.53 mm, p_{air} = 6 bar, Schleicher&Schuell stirred dead-end cell, n_{IL} = 0.0093 mol, n_{IL} : n_{ACN} : n_{Styr} = 1 : 3 : 1, 3wt% PI, 2wt% CL (wt% based on m_{IL}), 0.5 h ultrasonic bath, h_{gap} = 300 µm, 0.5 h UV lamp, 1 h air, 0.25 h H_2O.

As expected, the flux increased linearly with increasing pressure. The changed synthesis had no significant influence the performance of the PILs BD1 and BD2 membranes. An unexpected behavior was observed with PILs BE1. Since the side octadecyl side chain is longer, the flux is higher and correlates to the commercial NF membrane. A comparison of the former and newly synthesized PILs membranes is given in Table 10.

Table 10: Permeability of PILs layer with two ionic liquids and new purification methods.

Membrane	L_{H2O} / Lm^{-2}h^{-1}bar^{-1}	
	Old method	New method
PILs BD2	0.259 ± 0.0041	0.2899 ± 0.0082
PILs BE1	-	1.7312 ± 0.0285

Conditions: $d_{membrane}$ = 43.53 mm, p_{air} = 6 bar, Schleicher&Schuell stirred dead-end cell, n_{IL} = 0.0093 mol, n_{IL} : n_{ACN} : n_{Styr} = 1 : 3 : 1, 3wt% PI, 2wt% CL (wt% based on m_{IL}), 0.5 h ultrasonic bath, h_{gap} = 300 µm, 0.5 h UV lamp, 1 h air, 0.25 h H_2O.

4.2.3.3 Filtration of charged sugars with Type III membranes

To determine possible differences in the properties after modifying the synthesis, the filtration of neutral and charged sugars is reinvestigated. As well as in 4.2.2.3, dead-end filtration with a stirrer was used that ensured a homogeneous concentration in the vessel. Concentration polarization can thereby be excluded. The results are presented in Table 11.

Table 11: Retention of neutral and charged sugars with PILs membranes synthesized by the new method.

Sugar	$R_{\text{Type II}}$	$R_{\text{Type III}}$
D-Glucose	3%	3%
D-Mannitol	6%	7%
N-Acetylneuraminc acid	6%	3%
Sucrose	14%	8%
Raffinose	23%	16%
Sodium gluconate	53%	67%
Calcium gluconate	75%	74%
Sodium pyruvate	47%	24%

Conditions: c_{sugar} = 0.025 mol·L^{-1}, $d_{membrane}$ = 43.53 mm, p_{air} = 6 bar, Schleicher&Schuell stirred dead-end cell, n_{IL} = 0.0031 mol, n_{IL} : n_{ACN} : n_{Styr} = 1 : 3 : 1, 5wt% PI, 2wt% CL (wt% based on m_{IL}), 0.5 h ultrasonic bath, h_{gap} = 300 µm, 0.5 h UV lamp, 1 h air, 0.25 h H_2O.

Overall, the retentions of type III membranes are comparable to those of type II. On the one hand, the retentions of neutral sugars slightly decreased by the new method. Still, they are very low and in the same range. On the other hand, charged compounds were withheld with the same efficiencies, in case of sodium gluconate even better. As previously described, the identic influence of a possible anion exchange onto the permeance was observed.

Equal to Type II membranes, the filtration of calcium gluconate with PILs BD2 synthesized by the modified method was performed on a long-term scale (Figure 61). After a short time of dead-end mode (Figure 61, 0-150 h), the experiment was conducted in diafiltration mode for up to 2000 h. Especially the break of seven weeks after 720 hours due to COVID-19 lockdown should be considered. Here, the experiment was shut down and remained unstirred without pressure. In Figure 61, this interception can be remarked by a 5% drop of retention value. Despite, retention remained stable at 83% over 550 hours. Nevertheless the drop, the retention remained equal for over 1100 hours (720-1850 h). In the last 100 hours, the value dropped even

though no damage or optical alterations were noticed on the membrane surface. Possibly, smaller, local damages allowed low amounts of calcium gluconate to pass.

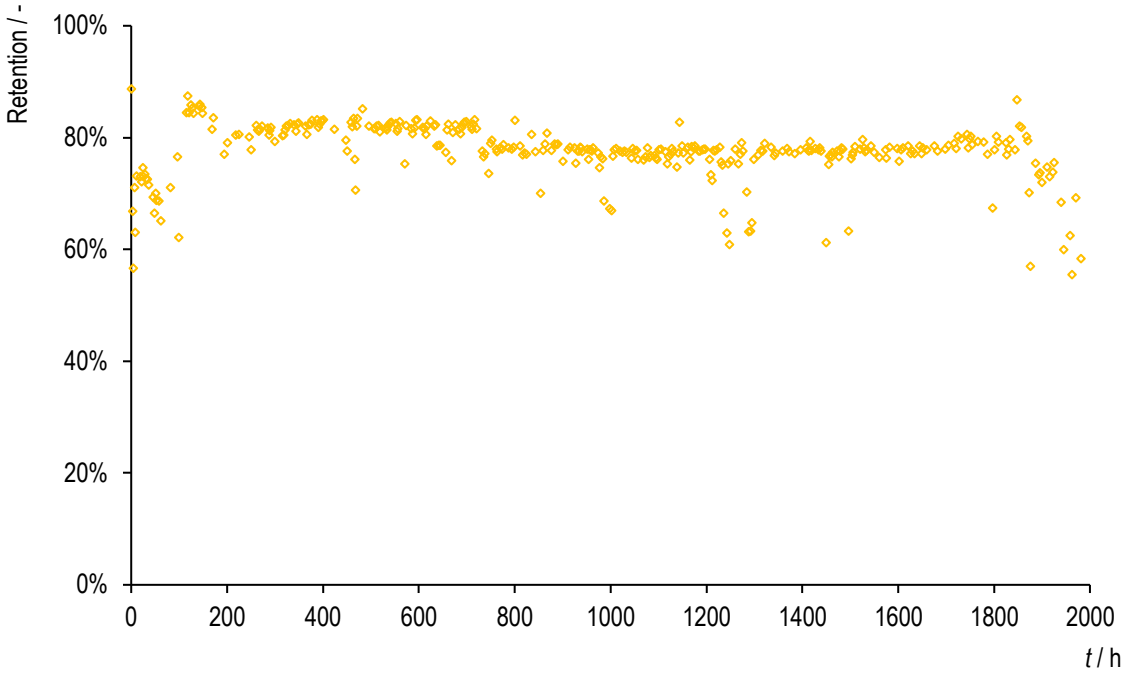

Figure 61: Filtration of calcium gluconate with PILs BD2 synthesized following the new procedure.

Conditions: $d_{membrane}$ = 43.53 mm, p_{air} = 6 bar, Schleicher&Schuell stirred dead-end cell, n_{IL} = 0.0093 mol, n_{IL} : n_{ACN} : n_{Styr} = 1 : 3 : 1, 3wt% PI, 2wt% CL (wt% based on m_{IL}), 0.5 h ultrasonic bath, h_{gap} = 300 µm, 0.5 h UV lamp, 1 h air, 0.25 h H_2O.

4.2.3.4 Filtrations of dyes with Type III PILs layers

Dyes are residues of the textile industry, one of the largest industries consuming water. These wastewaters are complex and varying in their pollution or composition.[232] As the components are poorly biodegradable and harmful to the environment, downstream applications are needed where membrane technology is an efficient method.[233] Ultrafiltration and nanofiltration are used as (pre-)treatment ensuring retentions of up to 99%.[188,234]

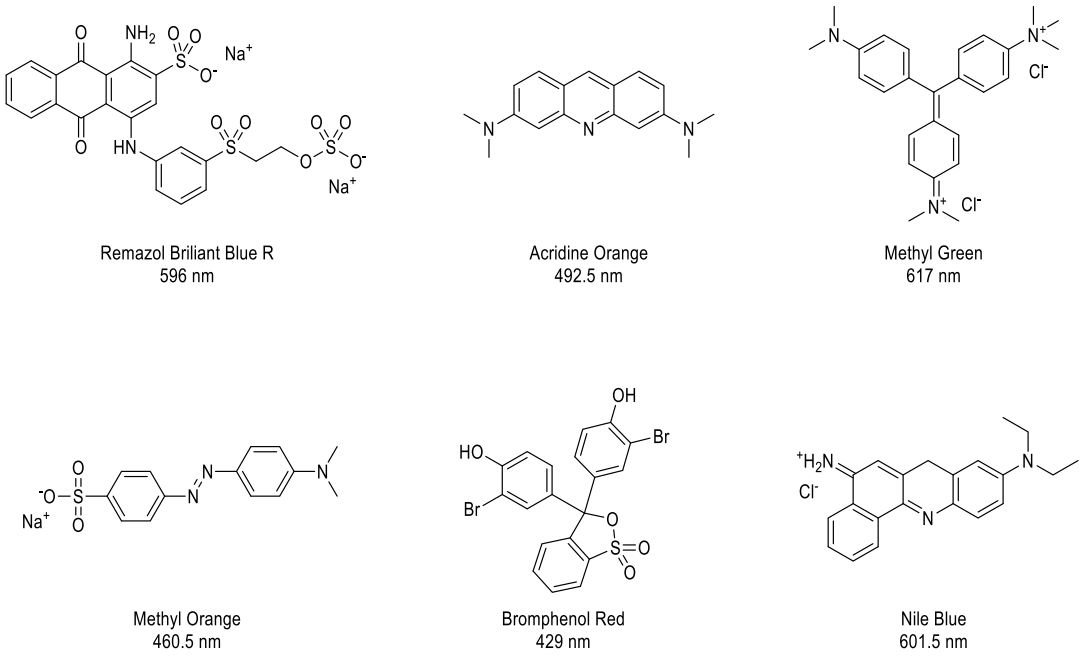

Figure 62: Dyes used in filtration experiments and their adsorption maximum.

In the following section, the retention of dyes by PILs membranes should be investigated. Due to the different properties of the dyes, six structural different dyes with various charges were chosen. The experiments were conducted with concentrations of 2 mg·L^{-1} and analyzed by the absorbance of light.

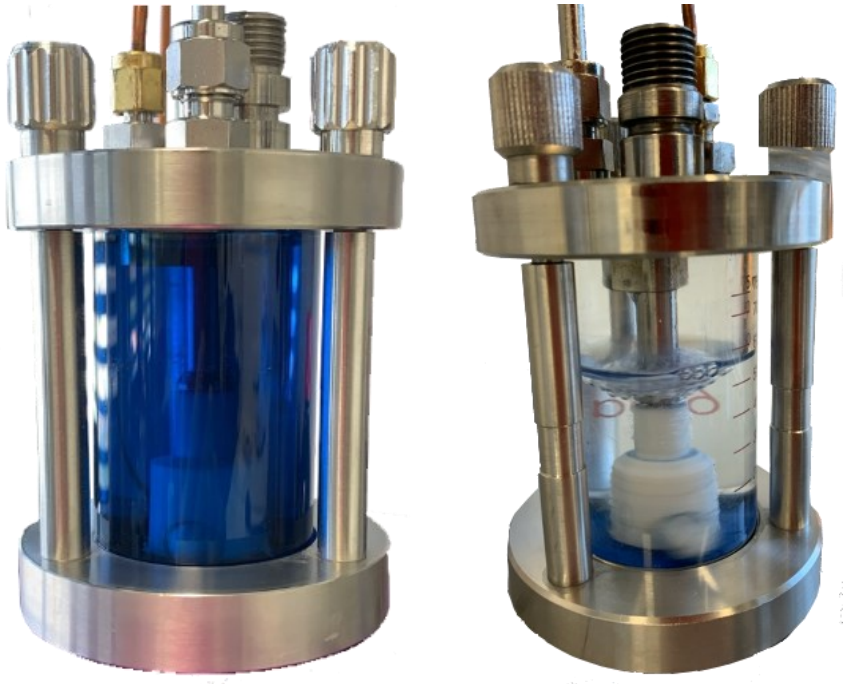

Figure 63: Filtration of Remazol Brilliant Blue R with PILs BD2 at the begin (*left*) and after the filtration (*right*).

Two promising polymeric layers, PILs BD2 and BE1, are used in dead-end filtration (compare 4.2.2.3). Both retained the six dyes with 87% to 99% (Table 12). In general, the PILs layers were very efficient while the permeance did not decrease same as for charged sugars. Within a range of 0.27 Lm^{-2}h^{-1}bar^{-1}, the flow through

the membrane did not get less as dyes were adsorbed at the layer. In particular Remazol Brilliant Blue R was adsorbed almost completely in the first hour of filtration, as indicated by the colorless retentate (Figure 63). This observation was confirmed by measuring optical density. The adsorption of negatively charged dyes on hydrophobic positive-charged PILs hydrogels is known. AL-KHARABSHEH *et al.* used thin-film composite PILs gels of 1-butyl-3-vinyl imidazolium bis(trifluromethanesulfonyl)imide bis(trifluromethanesulfonyl)imide and DVB grafted on PES porous supports as solvent resistant material in nanofiltration with moderate results for neutral dyes.[187] However, anion exchange is also known to reduce the concentration of dyes within the filtration cell.[190]

Filtration of the other dyes did not result in a similar behavior. Indeed, visible adsorption took place in experiments with Nile Blue, Acridine Orange and Bromphenol Red. Nevertheless, the amount of substance adsorbed was low, as the concentrations of filtrate and retentate almost summed up in the initial concentration. Surprisingly, Acridine Orange, either negatively charged with a sulfonic group, still got not adsorbed as Remazol Brilliant Blue R. In contrast, the neutral Bromphenol Red got adsorbed slightly. A direct link between the charge and possible retention or adsorption was not feasible. All results are summed up in Table 12.

Table 12: Retentions of different dyes with PILs BD2 and BE1.

Dye	Charge	Retention	
		PILs BD2	PILs BE1
Remazol Brilliant Blue R	Positive	99%	99%
Methyl Orange	Positive	94%	99%
Acridine Orange	Neutral	97%	93%
Bromphenol Red	Neutral	99%	87%
Nile Blue	Negative	99%	99%
Malachite Green	Negative	92%	92%

Conditions: c_{dye} = 2 mg·L^{-1}, $d_{membrane}$ = 43.53 mm, p_{air} = 6 bar, Schleicher&Schuell stirred dead-end cell, n_{IL} = 0.0093 mol, n_{IL} : n_{ACN} : n_{Styr} = 1 : 3 : 1, 3wt% PI, 2wt% CL (wt% based on m_{IL}), 0.5 h ultrasonic bath, h_{gap} = 300 µm, 0.5 h UV lamp, 1 h air, 0.25 h H_2O.

Further, the stability of PILs membranes was tested in harsh acidic and basic conditions. In comparable experiments, the pH value was lowered to 1 by hydrochloride acid or increased to 13 by sodium hydroxide. The mechanical stability and performance of PILs membranes should be tested at these conditions to evaluate chemical resistance introduced by ionic liquids.

In general, the PILs membranes withstand the acidic and basic conditions excellent and did not suffer from mechanical damages. Remarkably, the permeance decreased slightly in acidic conditions. This observation led to the result that even Malachite Green was successfully filtered. Figure 64 shows the retention of the four dyes by PILs BE1. Malachite Green and Acridine Orange (green and blue circles) were withhold by about 30% and 35%. In acidic conditions, the retentions dropped continuously from the beginning.

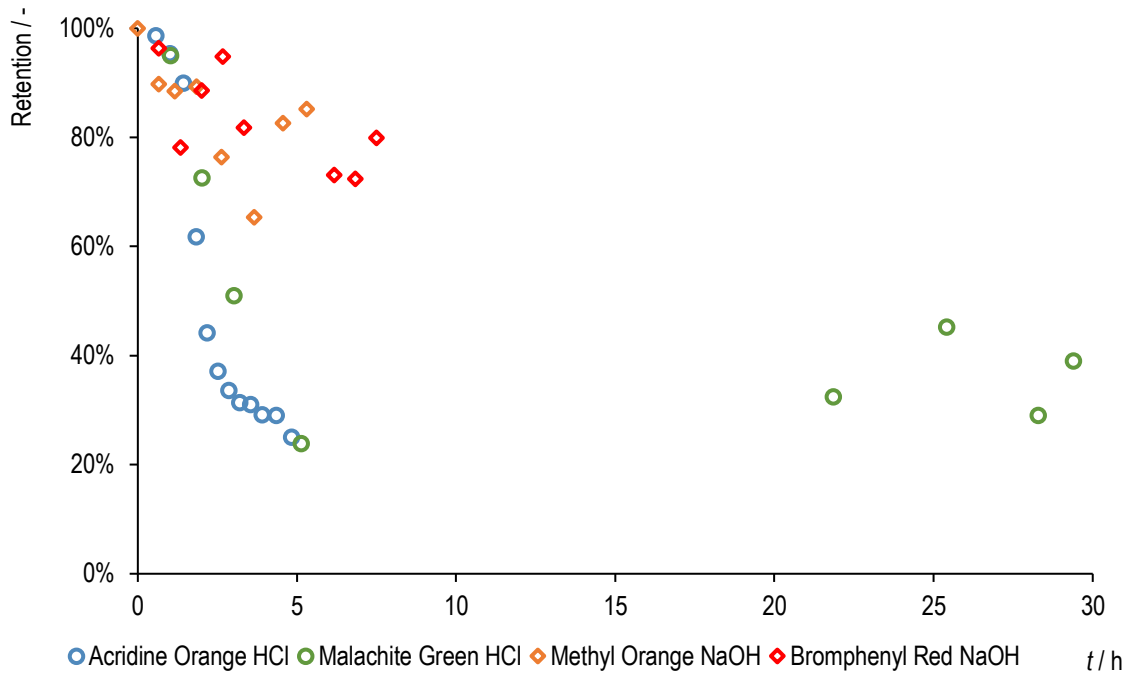

Figure 64: Retention of different dyes in acidic (circles) and basic (rhombuses) conditions using PILs BE1.

Conditions: $d_{membrane}$ = 43.53 mm, p_{air} = 6 bar, Schleicher&Schuell stirred dead-end cell, n_{IL} = 0.0093 mol, PILs BE1, n_{IL} : n_{ACN} : n_{Styr} = 1 : 3 : 1, 3wt% PI, 2wt% CL (wt% based on m_{IL}), 0.5 h ultrasonic bath, h_{gap} = 300 µm, 0.5 h UV lamp, 1 h air, 0.25 h H_2O.

Methyl Orange and Bromphenol Red got slightly less favorable under basic conditions than at pH of 7. With retentions of 75% and 80%, dyes in basic conditions are more withhold than in acidic ones. No physical damage of the layers was observed after the filtration process. Also, the amount of dyes adsorbed on the surface of PILs BE1 was less visible.

Since the presence of charges in the substrate previously had no negative influence on efficiency, protonated or deprotonated functions are excluded as a reason for decreased retention. According to the surface changes during the filtration of calcium gluconate (compare Figure 58), an anion exchange of bromide against hydroxide or chloride ions could have occurred here. Based on this assumption, an exchange against hydroxide ions are influencing the retention of dyes with PILs membranes less than an exchange of bromide and chloride. To confirm this hypothesis, further investigations with acidic and alkaline medias are necessary.

These exchanges can influence the channels and pores that are controlling the permeation of water and rejection of dyes as well as the adsorbance. In these harsh conditions the performance decreased. Still, the

PILs membranes were stable and a separation with moderate results was achieved. Therefore, increased separation yields are to be expected at less harsh conditions. As these conditions are closer to the applications, downstream applications or wastewater management of acidic or basic liquids might benefit.

4.2.3.5 Investigation of the surface morphology of Type III membranes

Here, comparable to 4.2.2.4, the surface was investigated after filtration of pure water by AFM. PILs BD1 and BD2 were chosen to determine differences in membrane formation in regard the new purification procedure. In general, no differences were expected as all monomers in these low concentrations are soluble in water so that unreacted monomers could be removed. No further changes of the experimental set-up of Type III compared to Type II were done. PILs BE1 was additionally imaged to examine the influence of octadecyl alkyl side chains to the surface morphology. An overview and high-resolution images of the three layers are shown in Figure 65.

Compared to Type II layers (4.2.2.4, Figure 57), PILs BD2 showed also a grainy substructure of the surface (Figure 65 c). No grooves were observed as for Type II membranes. Whereas individual, fine heights were previously visible through bright spots, it is now apparent after modified purification that more bulky elevations are imaging. Only a few dark spots are indicating depth why it was examined more closely.

Figure 66 shows a representative height corrugation of PILs BD2 (grey upper line). At first sight, the fluting seemed extreme compared to Type II layers (compare Figure 57) that have differences of less than 10 nm. Neglect the outer areas of the graph that might be this extreme due to the sample arrangement, differences in height of about 200 nm remains. For PILs membranes with 95% of [VBuIm]Br, the corrugations are less pronounced. PILs BD1 (blue middle line) showed elevations of about 100 nm while PILs BE1 (orange lower line) had differences in height of approximately 80 nm. The PILs B and D (Figure 57) showed corrugations in the same range.

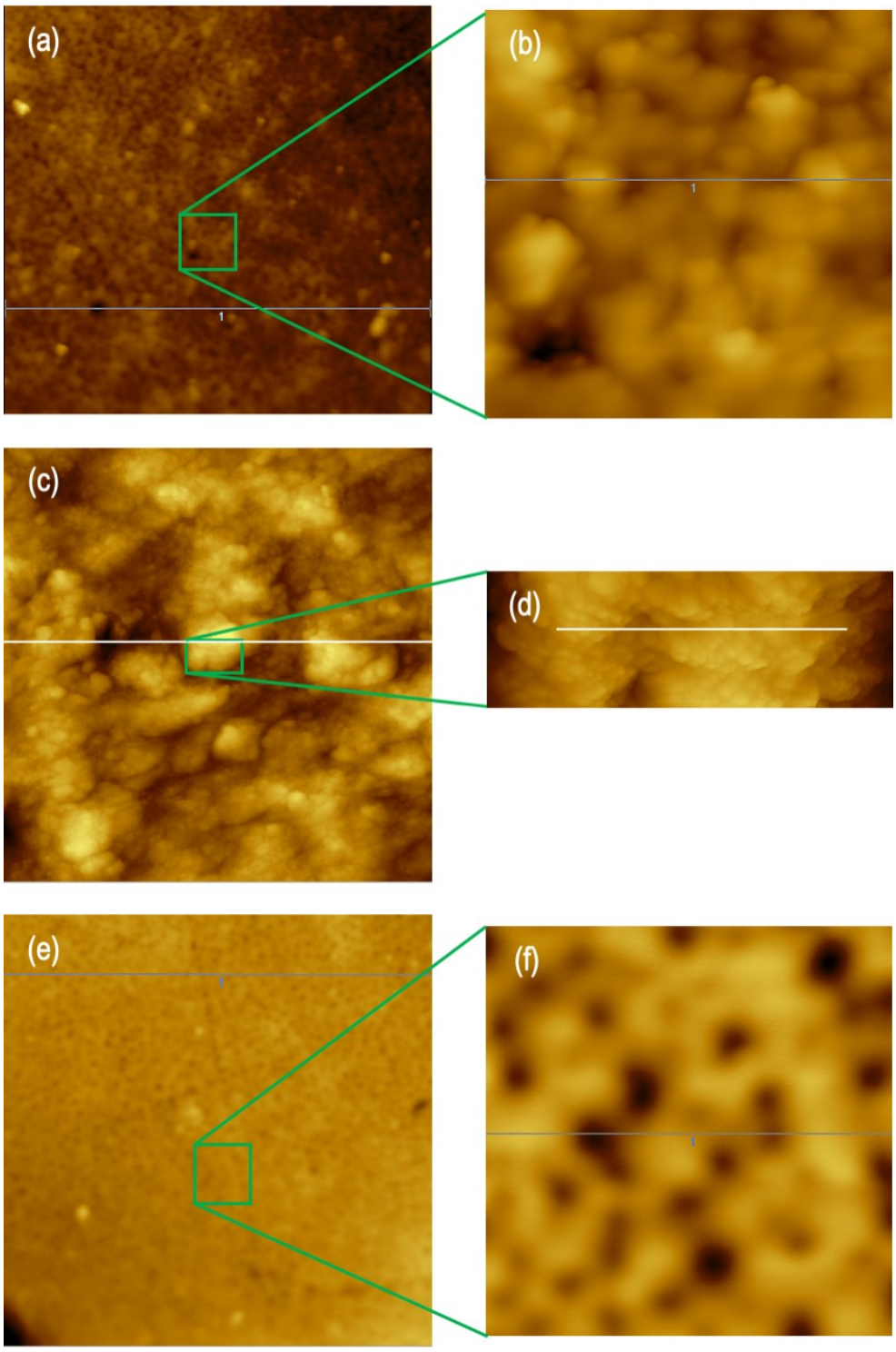

Figure 65: Surfaces of PILs BD1 (a,b), PILs BD2 (c,d) and PILs BE1 (e,f) obtained by AFM. a,c and e correspond to overview images (40 μm^2) while b,d and f show high-resolution images (5 μm^2) of the fine structure. Heights are indicated by bright (large) and dark (small) colors. Blue, red and green lines indicate locations where profiles are investigated.

The big change in elevation of PILs BD2 cannot be further explained. The new membrane formation method of Type III layers by omitting the ethanol bath resulted in a visual change. Large grooves or a mix of grooves

and grainy compartments are no longer visible. As the experienced flexibility of the material increased in the experiment, ethanol acted as a curing agent for the PILs layer. This hypothesis might be verified by ultimate tensile strength experiments between Type II and III PILs membranes.

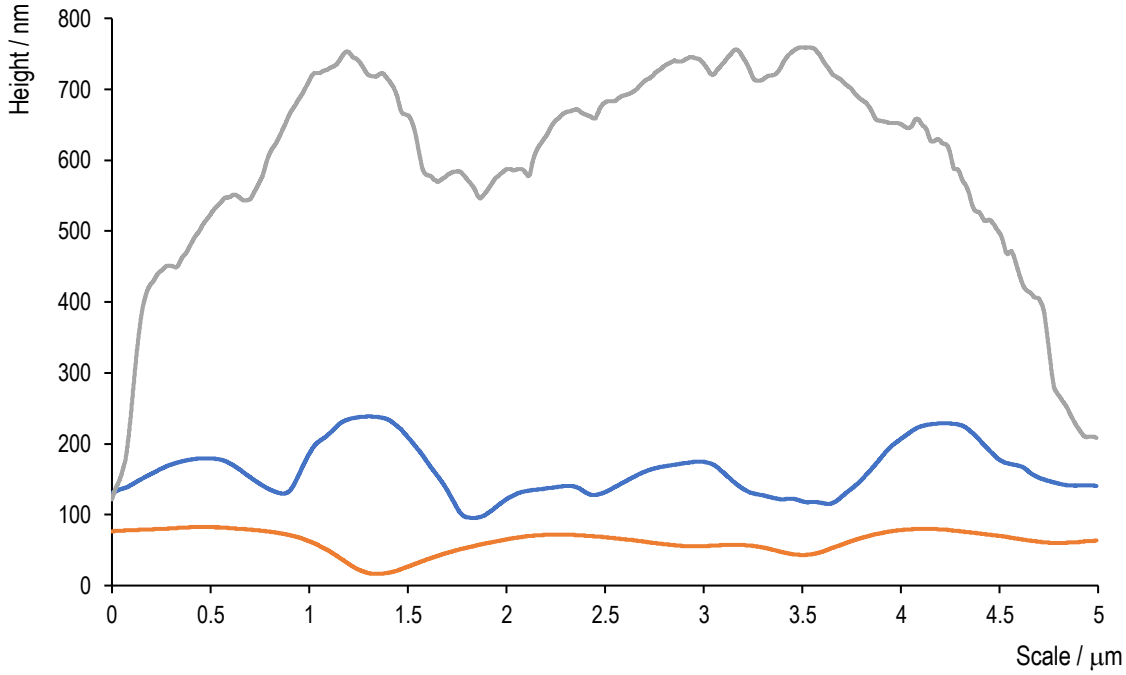

Figure 66: Investigated profiles of the PILs layers BD1 (*middle*), BD2 (*upper*) and BE1 (*lower*) indicated by profile lines in Figure 65.

In membrane application, often only the top side of the layer is of interest. Here, the first separation processes take place and make demands on the surface. For commercial membranes, these side is often called “glossy side” due to their shiny appearance. The reverse side is given a less demanding treatment, as it does no directly participates the separation and retention of substances.

As Type III have been shown more effective but topside images do not indicate it clearly, the lower sides were pictured. A superordinate structure of these membranes was observed. A grainy overall structure defined the appearance of the surfaces. Increasing the amount of [VDodecIm]Br in the polymer from 5% (PILs BD1, Figure 67 a) to 25% (PILs BD2, Figure 67 b), visibly refines the overall structure. It seemed that the number of granular formations is increasing with the increased monomer concentration of [VDodecIm]Br. Similar to the results of surface morphology of Type II layer (Figure 57), longer alkyl side chains smoothen the surface. PILs BE1 (Figure 67 c) that consists also of 95% [VBuIm]Br such as PILs BD1 (Figure 67 a) shows a less granular composition. On the contrary, the corrugations seem smaller, forming bigger holes on the surface (dark spots). In summary, the bottom sides of the three PILs membranes are close to each other in the surface structure. They are indicating a structure correlation when increasing the amount of [VDodecIm]Br. Big differences as on the topsides were not observed. However, these observations cannot explain the variance in performance in filtration applications.

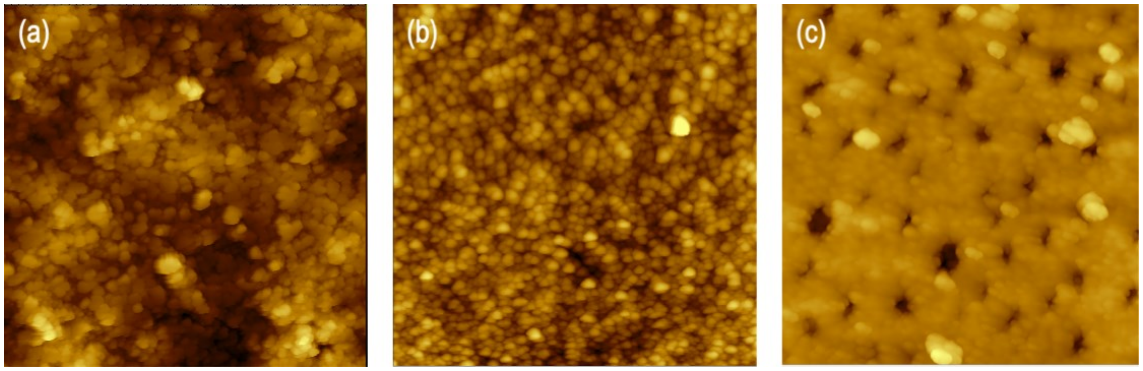

Figure 67: Topographies of membrane bottom side (40x40 µm) of BD1 (a), BD2 (b) and BE1 (c).

4.2.3.6 Composition of Type III layers

Common polymer analytic

In the chapter 4.1.2, two analytical methods (NMR and GPC) were presented to investigate the polymer structure and properties itself. In summary, the successful reaction for PILs by free radical polymerization was confirmed by NMR even though a mass by GPC could not be determined.

Polymerized ionic liquids by UV-induced free radical polymerization are not soluble in organic solvents. Also, aqueous solvents were excluded as water was used for the purification bath. This causes difficulties for analytics as any solvent-based method is unusable. Vapor pressure osmometry, membrane osmometry, viscometry and separation by centrifuges are all dependent on a polymer-solvent mixture. Matrix-assisted laser desorption/ionization (MALDI) determines molecular masses of polymers by ionization and following the detection of the ions. In general, here also a polymer-solvent matrix is needed.[235] As well as there are sample preparation techniques for insoluble polymers, they are limited to fewer complex structures, biopolymers or smaller molecular weights.[236,237]

Another, rather unconventional option to determine the conversion of the UV-induced polymerization and the real distribution of the monomers in the polymer, is to analyze the unreacted monomers. To the best of my knowledge no similar procedure is done in literature. After the reaction time, the unreacted monomers are removed by ethanol or water (compare 3.3.2.3). Acrylonitrile, styrene and divinylbenzene then could be determined by gas or high-pressure liquid chromatograph. The ionic liquids are not possible to be quantified by HPLC due to their special character. Investigations can be done by removing the solvent and analyzing the weight of the remaining IL. A problem with this approach is the experimental setup. As the amount of substance is lower than 300 mmol for each monomer and the purification baths are filled with up to four liters of solvent, concentrations become too small to determine. Additionally, the vapor pressures of the liquid monomers are close to ethanol and lower than water, so it is not possible to evaporate the solvent. Performing the same experiment several times using the same purification bath and expecting an approximation of the conversion, do not overcome the problem of small concentration.

Solid-state NMR

As the solid PILs layers were not soluble in a high number of organic and aqueous solvents at different temperatures and pH-conditions, common solvent-based analytical methods are not applicable as mentioned before. Since the conversion of each monomer was not determinable, solid-state nuclear magnetic resonance spectroscopy (ssNMR) should investigate the ratios of the monomers inside of the polymers. Therefore, it is aimed to identify the ration between butyl and dodecyl (respectively octadecyl) side chains, the nitrile as well as the styrene group. In the end not the yield of the UV-induced polymerization will be determined but rather the actual polymer composition.

ssNMR has evolved towards an analytical method to detect the structure of catalysts, protein and polymers.[238] In general, diluted spins such as the ^{13}C are difficult to observe as the abundance is very low and hard to recognize with a weak signal-to-noise ratio. Additionally, homonuclear dipolar interactions of ^{13}C are missing making the relaxation time significantly longer. Though, several scans need essentially more time.[239] A shorter measurement time is mainly made possible by cross polarization, where weak polarizations are supported by a coupled stronger polarization of another species.[240] This method is based on the easy transfer of magnetization from highly polarized nuclei onto weak polarized ones while being in contact in a suitable manner. The weak and strong polarizable nuclei (mostly ^{1}H) are stimulated by two different radio frequency fields that do not influence the other. The frequencies are selected that both nuclei have the same rotation rate. This allows an energetically neutral exchange of polarization from the strong polarized to the weak polarized species that is investigated.[238]

In the following experiments, the successful UV-induced free radical polymerization of the monomer solution should be confirmed. The liquid monomers (acrylonitrile, styrene, divinylbenzene) could not be investigated by ssNMR. Residues of these liquid monomers are not expected due to the purification steps. Figure 68 shows the measurements of PILs BE1 and the representative ionic liquid [VOcdecIm]Br as well as the photo initiator.

The first spectrum shows the ^{13}C signals of PILs BE1 (blue) and representatively for all ionic liquids IL E (red). The bottom graph picture the photo initiator and PILs BE1. All samples were measured individually, then overlayed. Comparison to the liquid monomers are not part of the investigation here as all liquids are assumed to be removed after drying.

In both spectra, the IL E monomer and photo initiator TPO were measured with discreet signals. Comparable to the liquid phase NMR (Figure 40), the signals were referred to carbon atoms in the ionic liquid. The signals of the IL alkyl side chain (40-20 ppm) were cut off due to the presentability of the spectrum. By a chemical shift of 120 to 100 ppm, the vinylidene carbon atoms are apparent.

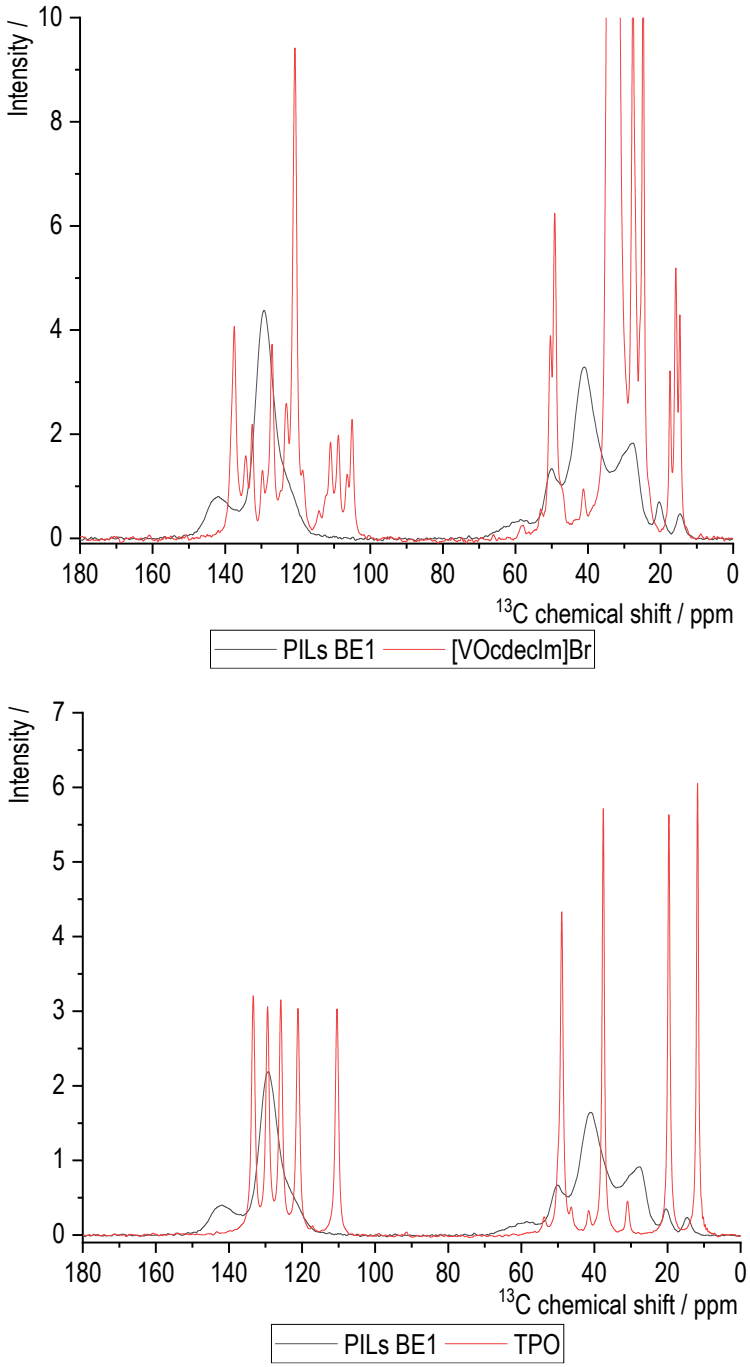

Figure 68: ssNMR of PILs BE1 (*black*) in comparison to the IL E(*top*) and the photo initiator TPO (*bottom*).

The signals of the polymer are less sensitive in comparison to the IL E which can be referred to anisotropic interactions in the polymer. The signals of the alkyl side chain and polymer backbone can be identified by a depth shift of 60-20 ppm. Imidazolium and benzene functions are high field shifted (150-120 ppm). The comparison between the polymer and the monomer reveals, that no signal of the IL monomer can be recognized in the polymer spectrum. Neither a sensitive signal nor an unexpected signal appeared. It suggests, that the polymerization as well as the purification of the membrane was successful.

The cross polarization in solid-state NMR is a suitable analytical method to confirm the PILs polymer since it is insoluble and unsuitable for common methods. Figure 69 shows the spectra of PILs BD2 and PILs BE1. The signals can be separated roughly in two sections: 160-120 ppm and 60-10 ppm. In the first, a combination of signals of carbon atoms from styrene, nitrile and imidazolium functions are expected. A differentiation could not be made. In the second part of the spectrum, the polymer backbone and the imidazolium side chains are estimated. Here, several local maxima are pictured at about 50, 40, 28, 20 and 13 ppm. The last belong to methyl groups at the end of the IL side chains while the other are a combination of methylene groups of the backbone and side chains. A close distinction of these methylene groups is not possible as neither the signals at 50, 40 and 28 ppm are not totally separated, nor the number of different methylene groups corresponds. Differences between the spectrum of PILs BD2 and BE1 could not be made as they only differ in length of one alkyl side chain. Contrary, the signal ratios in between are congruent. Even if the general structure and successful polymerization is confirmed, a determination of the real monomer ratios of each polymer cannot be investigated by ssNMR. Here, the signals are too wide by the anisotropic interactions.

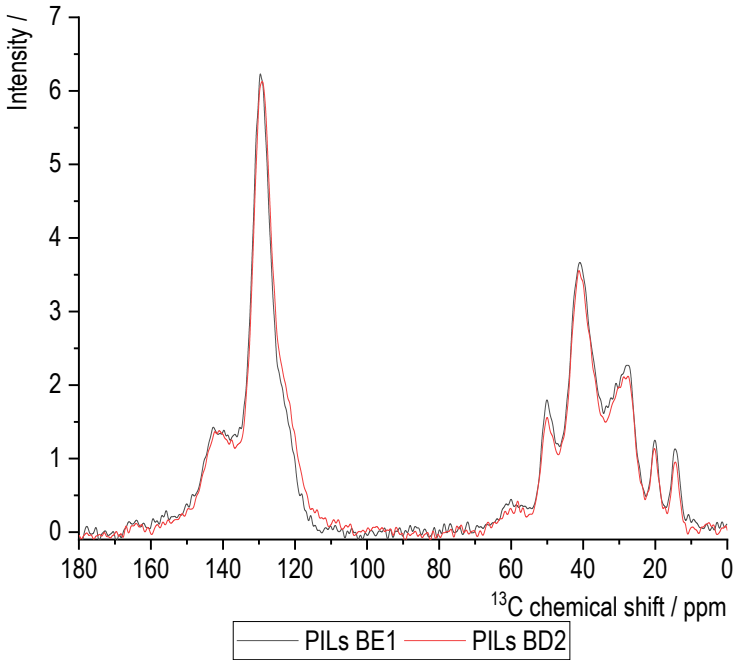

Figure 69: ssNMR spectrum of PILs BE1 and PILs BD2

So far, ssNMR was the only successful analytical method to investigate the chemical structure of the synthesized PILs layers. In different measurements, the polymerization and purification could be confirmed as well as significant polymer functions as backbone, imidazolium ring or alkyl side chain identified. Due to the insolubility of these polymerized ionic liquids and incompatibilities of other techniques, this is the only method so far.

4.2.4 PILs membranes in electrodialysis

As presented in 1.1.1.4, membranes for electrodialysis can be received by using charged polymers in membrane fabrication or by post-treatment of already synthesized membranes. The PILs layers used in aqueous filtration (compare 4.2.2.3 and 4.2.3.3) indicate to be a suitable anion exchange membrane in electrodialysis. This section will examine the possibility using polymerized ionic liquids in electrodialysis as a proof of concept using sodium acetate as an analyte.

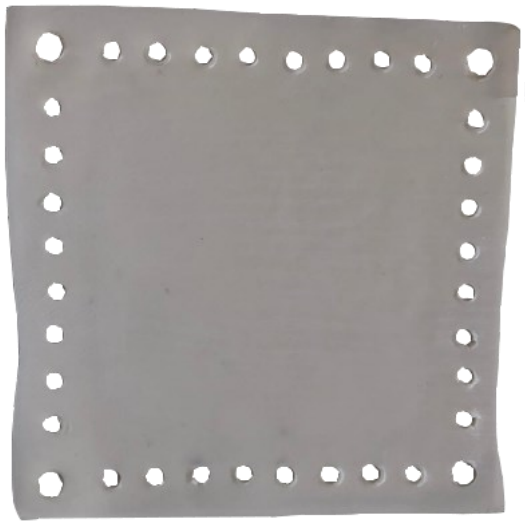

Figure 70: Cut and unused PILs BD2 membrane for electrodialysis.

PILs layers were synthesized and cut to a size of 11x11 cm^2 whereas the efficient area in the experiment is 8x8 cm^2 (0.64 dm^2). The peripheral area of the membrane was used to enable the flux of concentrate, electrolyte and diluent in the device (Figure 70). Each of the membranes used has holes as passages for the flux while spacers in between the layers avoid mixing of the different liquids in the chambers. Since no existing data revealed a suitable voltage, current density or amperage for similar PILs membranes in bipolar electrodialysis, four current voltages in the range of the device were chosen (3, 6, 10 and 15 V). Samples of the concentrations of diluent, concentrate and electrolyte were taken each 10 minutes and measured by HPLC.

4.2.4.1 Electrodialysis of sodium acetate using polymerized ionic liquids

As a representative to the following experiments, Figure 71 shows the course of an electrodialysis of sodium acetate using a PILs BD2 as anion exchange membrane. Sodium acetate was used as preliminary studies on this device were performed with it as well as a chemical proximity towards the charged sugars is given. The descending graph (squares) represents the concentration of the concentrate sodium acetate while the ascending graph (circles) displays the diluent acetic acid. By the different colors, the results for the voltages of 3 (blue), 6 (orange), 10 (grey) and 15 V (yellow) are shown.

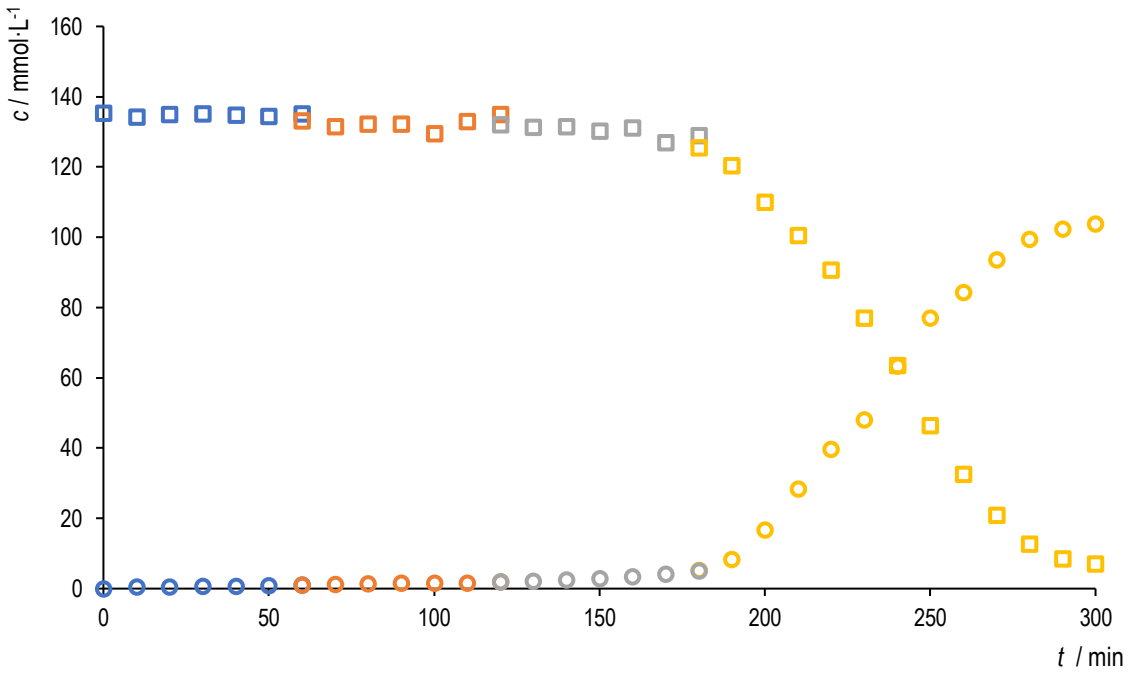

Figure 71: Concentration of acetic acid (circles) and sodium acetate (squares) in electrodialysis using PILs BD2 at increasing voltages (blue: 3 V, orange: 6 V, grey: 10 V, yellow: 15 V).

Conditions: $c_{NaAcetate}$ = 0.2438 mmol·L^{-1}, *Hescon* EDL03 quattro, PILs BD2 membrane triplet, $A_{membrane}$ = 110x110 mm, $n_{IL\ B}$ = 0.022 mol, $n_{IL\ D}$ = 0.0073 mol, n_{IL} : n_{ACN} : n_{Styr} = 1 : 3 : 1, 3wt% PI, 2wt% CL (wt% based on m_{IL}), 0.5 h ultrasonic bath, h_{gap} = 300 µm, 0.5 h UV lamp, 1 h air, 0.25 h H_2O.

The initial concentration of sodium acetate at 0 minutes (135 mmol·L^{-1}) does not correspond to the stock solution of 0.2438 mmol·L^{-1}. Before starting the experiment, the device is flushed with pure water. This serves to wash residues of the UV-initiated reaction, to condition the PILs layer as well as test the tightness of the installed system. As the membrane should be wet and a high dead volume in the tubes in pumps exist, the initial concentration refers not to the stock solution.

For the first two hours, only 1 mmol·L^{-1} of acetic acid was formed at 3 and 6 V. As the separation of ions and formation of the acid succeeded, the process is not considered efficient. By increasing the voltage to 10 V, 3 mmol·L^{-1} of acetic acid has been synthesized in an hour. No physical damage of the membrane was observed during the experiment even not in data. The PILs layers were stable for three continuous hours at this moment.

At 15 V, the concentration of sodium acetate decreased rapidly over two hours. At the same time, the amount of acetic acid increased assimilable. Compared to the previous voltages, about 60 mmol·L^{-1} of acid was obtained in one hour. By this, an equivalent concentration of concentrate and diluent was reached at 240 minutes. After 300 minutes, the reaction seemed to be completed as the graphs flatten.

The difference between the realized 105 mmol·L^{-1} of acetic acid and the theoretical yield of 135 mmol·L^{-1} is referred to inaccuracies in measurement.

Following the positive results of using PILs BD2 as an anion exchange membrane in the electrodialysis of sodium acetate, the efficiency should be improved by using two membrane triplets. Thereby, a triplet contains an anion and cation exchange membrane as well as a bipolar membrane (compare 3.5). The electrodialysis was performed with acetic acid at 15 V. Figure 72 shows the concentration of the diluent (acetic acid) and concentrate (sodium acetate). The circles are representing the data of two membrane triplets. The preceding experiment with one triplet is shown by triangles.

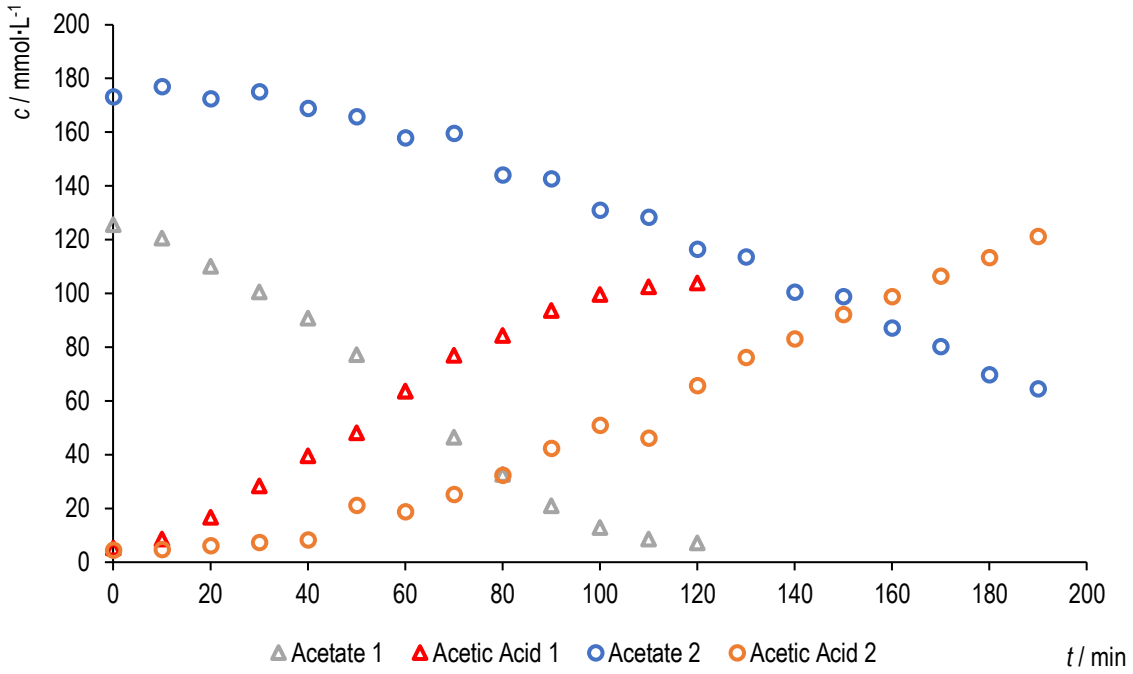

Figure 72: Concentrations of sodium acetate and acetic acid over time using one (triangles) and two membranes triplets with PILs BD2 (circles) at 15 V.

Conditions: $c_{NaAcetate}$ = 0.2438 mmol·L^{-1}, *Hescon* EDL03 quattro, $A_{membrane}$ = 110x110 mm, $n_{IL\ B}$ = 0.022 mol, $n_{IL\ D}$ = 0.0073 mol, n_{IL} : n_{ACN} : n_{Styr} = 1 : 3 : 1, 3wt% PI, 2wt% CL (wt% based on m_{IL}), 0.5 h ultrasonic bath, h_{gap} = 300 µm, 0.5 h UV lamp, 1 h air, 0.25 h H_2O.

Electrodialysis with two membrane triplets (circles) was successfully tested. The concentration of sodium acetate decreased equal to the increasing concentration of acetic acid. After about 150 minutes, half of the concentrate (90 mmol·L^{-1}) was converted. As the HPLC measurement was not made online, the experiment was stopped after 190 minutes and was not conducted completely. The end was expected to be earlier. Regarding the trend, full conversion of sodium acetate would be after about 300 minutes.

Two instead of one membrane triplets were expected to reduce the running time of the electrodialysis. The former experiment using one triplet converted 90 mmol·L^{-1} of concentrate in 80 minutes, 70 minutes less than using two triplets. By the literature and theoretical background (compare 1.1.1.3), this trend cannot be explained in first place. Besides the sample concentration, also the voltage and current were measured each 10 minutes. In both experiments in Figure 72, a similar behavior according to the literature (compare Figure 5) was expected. However, the experiment with two PILs BD2 layers showed different.

Figure 73 shows the voltage *U* (upper grey and blue line) and current *I* (lower red and orange line) during the electrodialysis processes already presented in Figure 72. The rhombuses are related to the use of one membrane triplet with PILs BD2 anion exchange membrane and the squares to the usage of two membrane triplets.

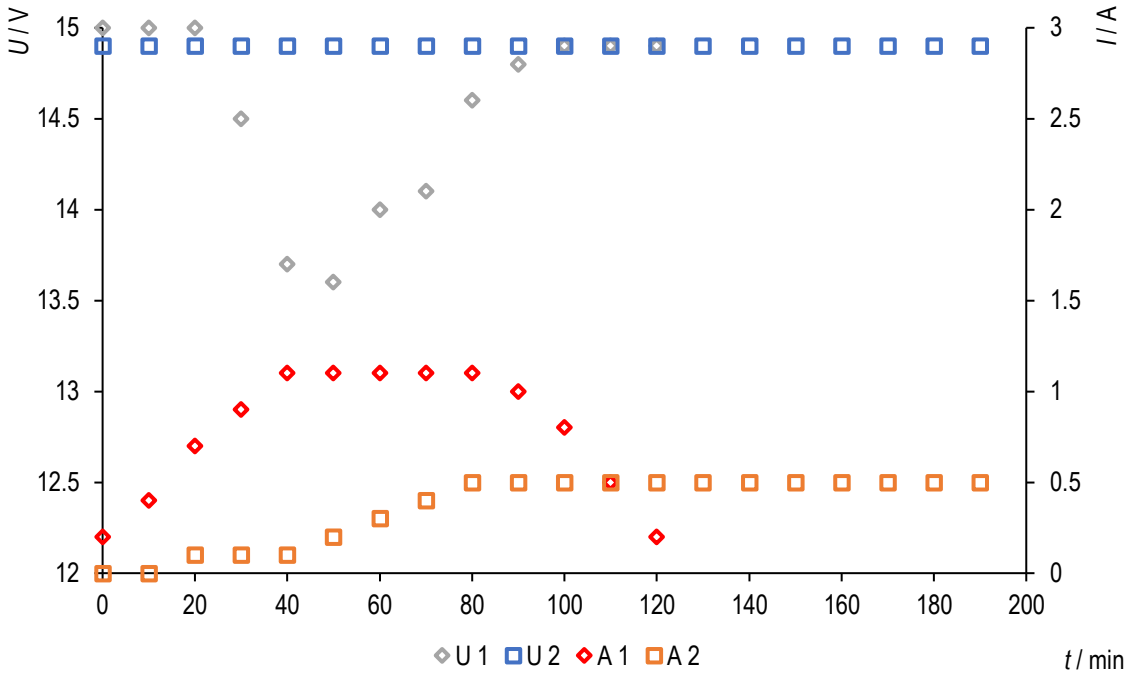

Figure 73: Voltage *V* and current *I* in electrodialysis of sodium acetate over time using one (rhombuses) and two membrane triplets (squares) with PILs BD2 at 15 V.

Conditions: $c_{NaAcetate}$ = 0.2438 mmol·L^{-1}, *Hescon* EDL03 quattro, $A_{membrane}$ = 110x110 mm, $n_{IL\ B}$ = 0.022 mol, $n_{IL\ D}$ = 0.0073 mol, n_{IL} : n_{ACN} : n_{Styr} = 1 : 3 : 1, 3wt% PI, 2wt% CL (wt% based on m_{IL}), 0.5 h ultrasonic bath, h_{gap} = 300 µm, 0.5 h UV lamp, 1 h air, 0.25 h H_2O.

Using one PILs layer (rhombuses) the current (red) increased during the first 40 minutes, then was stable for again 40 minutes. Compared to the concentration of acetic acid in Figure 72, this correlates to the times where the conversion per time increased and was at its highest level. After 80 minutes, the current decreased as also did the conversion rate in Figure 72. The voltage dropped in this experiment from 15 to 13.6 V for the time the current was steady and regain at 15 V afterward. In the experiment with two PILs layers, the voltage was steady at 14.9 V at any time. The current only increased to 0.5 A. As mentioned before, the current is also expected to decrease after full conversion. Nonetheless, no similarity between the two experiments was observed.

In general, the increase and decrease of voltage and current proceed according to Ohm's law stating that the current between two points is directly related to the voltage by the resistance as constant. In this application, the resistance is the sum of the several resistances of different membranes as well as the resistances of the electrolyte, concentrate and diluent. The single resistances of the liquids are directly related to the concentration and are increasing with decreasing ion concentrations.

At the starting point 15 V was set as voltage for both experiments. The ion concentration in the concentrate is very high whereas the concentration of the diluent and electrolyte are low. This results in high single resistances dominating the cell resistance and reason the need for a high voltage at the beginning. As the ion exchange processes take place, the concentration and so the single resistances align and the cell voltage decreased to its lowest data point (50 minutes, 13.6 V) using one PILs BD2. Afterward, the single resistance of the concentrate increased and the ion exchange continued. The cell voltage is increasing as well. The electrodialysis is completed after the voltage assumed the original value and the current decreased from 1.1 A to zero.

The graph of voltage and current can thus be used to monitor the electrodialysis. Already shown in Figure 72, the performance dropped by using two membranes triplets. The voltage did no longer decrease while the current increased only up to 0.5 A (Figure 73). This observation can be explained by a non-completed decrease in conversion (compare Figure 72). Nonetheless, the curves did not behave as expected and seen in the experiment with one PILs layer.

After the electrodialysis with one and two PILs BD2, PILs layers were replaced by a commercial anion exchange membrane based on modified polystyrene. Before the investigations of polymerized ionic liquids in electrodialysis, a reference measurement with commercial membranes were performed. Here, conditions and sodium acetate as the analyte were applied in the same way as for PILs. A comparison of the conversion from sodium acetate to acetic acid between used and unused membranes should reveal the impact of membrane damages.

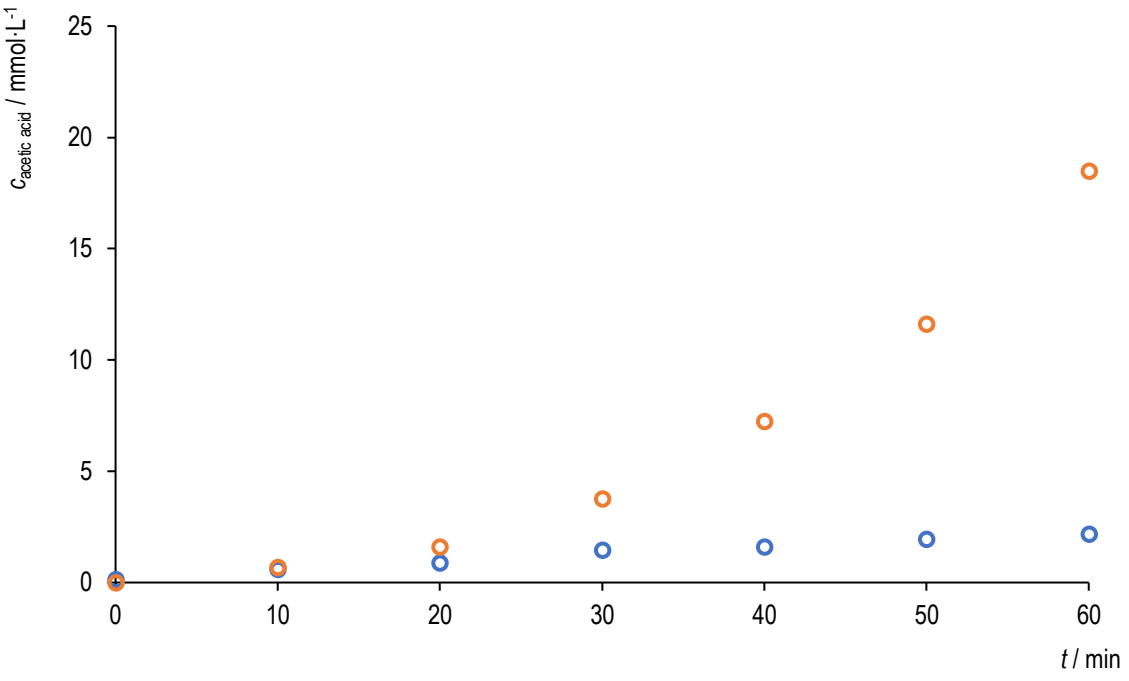

Figure 74: Modified polystyrene membrane triplet unused (orange) and already used (blue) at 15 V.

Conditions: $c_{NaAcetate}$ = 0.2438 mmol·L^{-1}, *Hescon* EDL03 quattro, $A_{membrane}$ = 110x110 mm, U = 6 V.

Figure 74 shows the concentration of acetic acid with a commercial membrane triplet before (orange circles) and after being used with PILs membranes (blue rectangles) at 15 V. An exponential growth of the concentration was observed for 60 minutes by yielding about 18 mmol·L^{-1} acetic acid when idle the unused membranes. For the already utilized membranes at 15 V, this increase is significantly less. Over 60 minutes, only 2 mmol·L^{-1} of acid are formed. Here, the influence of damages due to the high voltages in experiments with PILs membranes is indicated significantly. The loss in efficiency is about 90% explaining the decreased conversion of sodium acetate by using two triplets in Figure 72. It is also expected that this will procure in following experiments.

This decreased performance could also be observed on the membranes after performing experiments. The commercial membranes in Figure 75 possess damages of the material. Small surface discolorations of the bipolar in the middle reveal, that high voltages lead to a change of the membrane material.

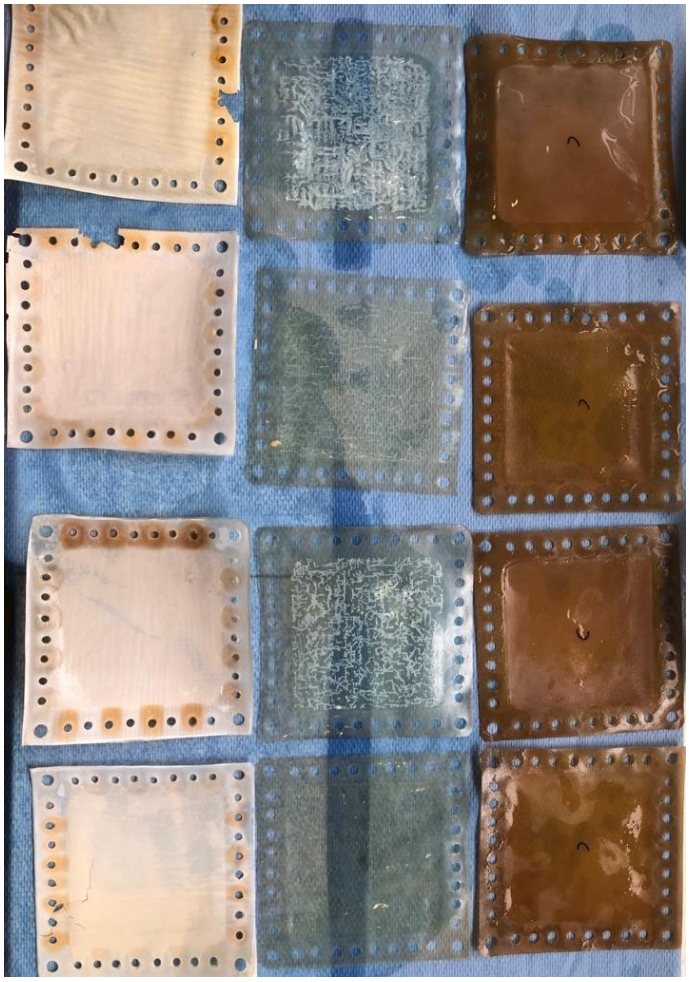

Figure 75: Membranes used at up to 15 V in electrodialysis with sodium acetate (*left*: PILs BD2, *middle*: commercial bipolar membranes, *right*: commercial cation exchange membranes).

Exceeding the limiting current density is a possible explanation for the visible change of the material. The limiting current density is caused by the high conductivity of the membrane compared to the electrolyte. When ions pass the membranes, their concentration decreases in front of the material and forming a laminar

boundary layer. By increasing the current, the concentration of ions in this zone can become nearly zero. Then, on anion exchange and bipolar membranes, water dissociation occurs. The hydrogen and hydroxide ions change the pH-level leading to damages on the membrane materials. Additionally, in the presence of ions such as calcium cations, coatings of calcium hydroxide occur on the surface and decrease the process efficiency by fouling.[241] The last of these was not observed in experiments with PILs membranes.

Some of the PILs membranes (here PILs BD2, Figure 75) show discoloration outside the flow openings after use in electrodialysis. The material became breakable. This could have been caused by short circuits at the openings where the different membranes were not separated precisely from each other. In addition to a decreased current efficiency in the process, it might damage the materials as observed here. Results of further experiments need to be considered with respect to these damages.

Table 13 shows an overview of the formation rates of acetic acid per minute in the electrodialysis with polymerized ionic liquids membranes. Here, PILs BD2 and BE1 were tested with one to three triplets. Additionally, PILs BD3 was tested as monolayer. In aqueous filtration experiments, more dense layers showed no or low flux and were not suitable. These PILs materials were tested in the electrodialysis as a denser material might benefit it.

Table 13: Conversion rates of sodium acetate with different PILs layers in electrodialysis membrane triplets.

Membrane	$\dot{c}_{\text{acetic acid}}$ / mmol·min^{-1}			
	3 V	6 V	10 V	15 V
PILs BD2	0.0153	0.0130	0.0521	0.9890
2x PILs BD2	0.0212	0.0268	0.0256	0.2777
3x PILs BD2	0.0357	0.0388	0.0461	0.0505
PILs BD3	0.0018	0.0018	0.0014	0.0018
PILs BE1	0	0.0214	0.0151	0.0408
2x PILs BE1	0.0069	0.0176	0.0361	0.1476
3x PILs BE1	0.0105	0.0080	0.0336	0.1365

Conditions: $c_{\text{NaAcetate}}$ = 0.2438 mmol·L^{-1}, *Hescon* EDL03 quattro, A_{membrane} = 110x110 mm, n_{IL} = 0.0293 mol, n_{IL} : n_{ACN} : n_{Styr} = 1 : 3 : 1, 3wt% PI, 2wt% CL (wt% based on m_{IL}), 0.5 h ultrasonic bath, h_{gap} = 300 µm, 0.5 h UV lamp, 1 h air, 0.25 h H_2O.

Even though a loss in performance due to the previous mentioned damages must be considered, all experiments showed that higher voltages are beneficial. The highest concentration rates were obtained at 15 V. Increasing the number of triplets, also increased the yield for PILs BD2 and BE1. For example, two

instead of one membrane triplet enhanced the conversion with PILs BE1 by more than the triple (from 0.0408 to 0.1476 mmol·min^{-1} at 15 V). Different from expected, three membrane triplets resulted in similar results at all voltages instead of a higher increased yield. That might be referred to damages of the commercial membranes limiting the reaction. Likewise, the decreasing yield of one (0.9890 mmol·min^{-1}), two (0.2777 mmol·min^{-1}) and three membrane triplets (0.0505 mmol·min^{-1}) at 15 V with PILs BD2 might be led back to it. As the experiments were conducted in sequence and an increasing trend with increasing voltage was expected. The reduced conversion rate can be referred to malfunctions of cation exchange and bipolar membranes.

For both, PILs BD2 and BE1, a distinct increase in the yield from 10 to 15 V was observed. Associated with the observed heat generated, the experimental cell setup needs more energy than formally required for a successful reaction. Therefore, an overpotential is assumed to be the reason for the distinct increase as well as the material changes and damages. Further, more precise investigations of the applied voltages might indicate an ideal operating window for the electrodialysis with PILs BD2 and BE1. In particular, the determination of a limiting current density might be advantageous.

PILs BD3 was not efficient at all compared to PILs BD2 and BE1. A denser PILs material is not suitable for this type of electrodialysis. Mainly, a decreased permeability of ions through the membrane could be reason for the small conversion of sodium acetate. Also, the higher number of charges in the material, may have a repulsion effect onto the substrate inhibiting a permeation as no further difference to PILs BD2 exist.

4.2.4.2 Electrodialysis of charged sugars

After proofing that PILs layers can be used in electrodialysis, larger organic molecules as well as multivalent ions were tested with PILs BD2 and BE1. As in 4.2.2.3 and 4.2.3.3, charged sugars (sodium gluconate, potassium gluconate and calcium gluconate) were used. Like the investigations in 4.2.4.1, the conversion of the sugar into the gluconic acid and corresponding base was measured. All the experiments were conducted with only one membrane triplet. An overview of the results is given in Table 14.

For PILs BD2 membranes, measurements at 3 V yielded in 0.0113-0.0194 mmol·min^{-1} that correspond to the results of sodium acetate in 4.2.4.1, for which no damage of the commercial membranes was known. Experiments at 6 and 10 V were less efficient, in contrast to the previously observed yield. At 15 V, calcium gluconate had the smallest conversion rate with 0.0045 mmol·min^{-1}, the lowest value for the four experiments with this charged sugar. Potassium gluconate had their highest yield in experiments at 15 V (0.0244 mmol·min^{-1}) while the yield of experiments with sodium gluconate was slightly lower than at 3 V (0.0172 mmol·min^{-1}).

Electrodialysis of charged sugars with PILs BE1 was more efficient than with PILs BD2. Here, the data showed that the PILs membrane had a strong influence on the conversion rates. For sodium and potassium gluconate,

the conversion rate was up to 0.0626 mmol·min^{-1} at 3 V which is more than 3 times higher than with PILs BD2. For sodium gluconate, the highest conversion was obtained at 10 V (0.3854 mmol·min^{-1}) and decreased afterwards (0.02801 mmol·min^{-1} at 15 V). The conversion of potassium gluconate increased constantly with increasing voltage and were higher than with sodium gluconate. Here, the highest conversion rates of all experiments with gluconate sugars were obtained at 6 and 10 V (0.7607 and 0.8072 mmol·min^{-1}).

Table 14: Formation of the gluconic acid with one membrane triplet containing PILs BD2 and BE1.

Membrane	Gluconate	$\dot{c}_{\text{gluconic acid}}$ / mmol·min^{-1}			
		3 V	6 V	10 V	15 V
PILs BD2	Na-Gluconate	0.0194	0.0092	0.0087	0.0172
PILs BD2	K-Gluconate	0.0118	0.0050	0.0062	0.0244
PILs BD2	Ca-Gluconate	0.0113	0.0068	0.0050	0.0045
PILs BE1	Na-Gluconate	0.0626	0.0800	0.3854	0.2801
PILs BE1	K-Gluconate	0.0623	0.7607	0.8072	-
PILs BE1	Ca-Gluconate	0.0192	0.0072	0.0072	0.0020

Conditions: $c_{\text{Gluconate}}$ = 20 g·L^{-1}, *Hescon* EDL03 quattro, A_{membrane} = 110x110 mm, n_{IL} = 0.0293 mol, n_{IL} : n_{ACN} : n_{Styr} = 1 : 3 : 1, 3wt% PI, 2wt% CL (wt% based on m_{IL}), 0.5 h ultrasonic bath, h_{gap} = 300 µm, 0.5 h UV lamp, 1 h air, 0.25 h H_2O.

Although the damage of commercial polystyrene membranes at overpotential was known, the conversion rates of charged sugars were higher than those with sodium acetate. In contrast to the aqueous filtration experiments (4.2.2.3), larger cations benefit the electrodialysis. Assorted by the radius of the cation (compare Table 9), the yielded amount of gluconic acid increased with increasing radius from potassium to calcium cation. As all cations were used with the identic gluconate anion, a higher selectivity for monovalent cations than for the bivalent calcium cation with both PILs membranes can be assumed. Similar behavior is already known from monovalent permselective ion exchange membranes.[242] Increased repulsions of bivalent ions and the charged layer decreased the diffusion rate while stronger interactions with the cation exchange membrane occurred. The selectivity towards the monovalent potassium and sodium increased from 3 to 15 V. At 3 V, potassium gluconate was converted three times more than calcium gluconate. At 10 V, the conversion was already over 100 times higher. An explanation is given by the steeper concentration gradient in the boundary layer with increasing current density. That benefit to monovalent cations due to their higher diffusion rate.[243,244] Further investigations should include analytes of mono- and bivalent cations with gluconate anions to substantiate this assumed hypothesis.

4.3 Outlook

The results presented show the great potential of polymerizable ionic liquids in material synthesis and especially membrane formation. Applications in dead-end filtration and first investigation in crossflow filtration revealed high potential in the retention of charged compounds.

To understand the basics of the UV-induced polymerization with ionic liquids, additional analytical techniques must be carried out. In order to resume the distribution of the monomers in the polymer, ultra-HPLC can be used and a specific analytical method developed. In addition, gravimetric and solids analysis provide additional information about the composition. For example, elemental analysis of the polymer could determine the molecular formula and specify the monomer ratios. A deeper understanding of the UV-polymerization mechanism will benefit an efficient material synthesis for example by reducing the irradiation time or using less TPO.

Further development in reducing the thickness of the layer offers a big opportunity to overcome drawbacks such as low permeance. The presented membrane synthesis method allows easily to reduce the casting thickness while no change is needed to be done. Combined with a supporting material, polymerized ionic liquids might be used as a selective layer onto for example polyacrylonitrile UF membrane. This supported asymmetric membrane with a thin and selective PILs layer enables advantages to the fabrication method, too. Less of the cost-intensive ionic liquid is used while the performance of the membrane is expected to be increased.

The set-up to form PILs membranes was designed suitable to further scale-up steps. The actual size is limited by the film applicator. Combined with the supporting material, an automatic casting process is conceivable. Besides the possibility to scale-up the filtration application with larger membrane areas, the fabrication costs might be reduced also.

The characterization of the membrane surface and its properties are of interest. First, by different methods, such as the static sessile drop or pendant drop method, the contact angle could be measured to determine a hydrophilic or hydrophobic character of PILs membranes. Second, intentional anion exchanges might result in new material properties. Filtration experiments with hydrochloric acid and sodium hydroxide showed that the permeance and retention changed in the presence of additional anions. Tensile testing and determination of the glass transition temperature, for example by differential scanning calorimetry, will reveal changes in the material in addition to AFM. Besides mechanical properties, also the performance in nanofiltration or electrodialysis experiments might be improved as the permeability and rejection of substrates are influenced material changes.

Generally, a more demanding filtration system can be used. This work revealed that membranes with polymerized ionic liquids are beneficial in aqueous filtration due to their charged character. In more specialized applications, charged residues of drugs or wastewater streams are of interest especially as high retentions

were obtained at low concentrations. The low concentrations of these hardly separable substances might also be less problematic towards ion exchange reactions with the material.

With larger membranes produced, bigger and continuous applications are of interest. Thinner layers, by adjusting the gap in the casting process, could improve the flexibly of the material with unchanged mechanical stability in addition to higher permeances so that tubular or spiral wound shapes are feasible. These shapes are of interest for big scale applications that are not necessarily limited to the wastewater treatment. Regarding the high retention of dyes and selectivity toward charged species, also downstream should be considered.

In electrodialysis, PILs membranes seemed to be potential materials for further investigations as they resisted the high voltages for hours. Of interest are general characterizations such as the limiting current density of the different polymeric layers, transport numbers and the desalination potential of these materials. Limiting current density of PILs layers were not determined yet. Here, experimental setups from literature can be adapted for example with ammonium nitrate solutions.[245] In future developments, a fixed negative charge to the backbone would be of interest. Besides possible cation exchange membranes, also bipolar PILs layer are thinkable. For both, possible cation exchange and bipolar membranes, properties such as the electrochemical resistance can be improved. Also, the behavior of these layers in electrodialysis might be comparable to the anion exchange membranes presented in this work so that a more efficient system is thinkable.

Further experiments should clarify the relation between the radii of ions and the conversion of the substrate. A broader scope of gluconate salts with for example lithium cations support the investigations. To ensure the findings concerning this relation, experiments with further anions such as acetate or pyruvate are helpful. Here, the developments of the material such as supported or thinner layers will benefit. Regarding the electric energy used, higher efficiencies in electrodialysis might be obtained.

Figure 7 shows that the market value for nanofiltration membranes is comparable low in contrast to reverse osmosis or microfiltration. On the one side, the specialized applications are often not widely used. On the other hand, nanofiltration was not that much developed in the scheduling and engineering of industrial and big scale processes. This could be a large market in the future. So, a cost-effective and large fabrication as schematically presented above is needed to compete with established and far-developed membrane materials.

5. Summary

Within this PhD study, an innovative concept to synthesize neat free-standing polymer membranes using polymerized ionic liquids, as well as the applications of these materials in three different purification processes, were successfully presented. This widely adaptable method to different types of ionic liquids offers an approach to further investigations and a new type of materials.

Membranes are obtained by different methods that are tailored to the final shape or properties of the materials. In this work, film casting was chosen as the preparation method as it offers an universal approach. Layers to the size of 0.12 m^2 are possible to cast with thicknesses between 1 and 3000 µm. Here, 300 µm was chosen as the reference for the experiments. Additionally, the device is heatable that might support the formation process and is not limited to a specific type of raw material. The needed casting solution can be made of a solved polymer with additives or monomers that are brought to reaction afterwards.

Polymerized ionic liquids were obtained by free-radical polymerization. Vinylalkylimidazolium ionic liquids were used as monomer due to their synthetic variability, their adaptable solubility in organic and aqueous solvents and good availability. Free radical polymerization reactions were successfully performed in aqueous and organic solvents as described in the literature. By anion exchange, the solubility properties were adapted enabling precipitation in water. Casting steps with *N*,*N*-dimethylacetamide, triethyl glycol as an additive and the following precipitation in water were unsuccessful towards neat polymer membranes.

A fruitful approach was to cast monomer solutions. Vinylalkylimidazolium ionic liquids were mixed with acrylonitrile, styrene, the crosslinker divinylbenzene and the photo initiator TPO. The other monomers shall contribute to a less rigid and mechanically more stable polymeric layer. The absence of a solvent and further additives increased the environmental friendliness as well as no additional waste is produced or needs to be recycled. The initiator was activated by commercial UV A light bubbles. On the one hand, the polymerization after the casting step was more efficient than using high-quality lamps. On the other hand, investment costs are significantly lower as well as a scale to increase the irradiated area without any effort.

Even though all vinylalkylimidazolium ionic liquids that were soluble in organic solvents or the other monomers, they did not all result in a proper membrane. More demanding side chains of the imidazole, heterocycles such and benzoyl or nitrile, were not applicable as the main monomer. As for [VEtIm]Br, a casting solution was feasible, but no proper layer was formed. The use of one IL in the reaction always came up with drawbacks like low permeability in experiments, mechanical instability in the devices or unreliable polymerization reactions. This was resolved using two ionic liquids (0). Here, the final properties such as permeability and mechanical characteristics were mainly influenced by ILs with longer alkyl side chains so that they were added only in smaller quantities.

First investigations on polymerized ionic liquids membranes were made in dead-end filtration devices. The aqueous flow through the membrane, flux and permeance, were determined. Here, only pure water was used.

PILs layers containing just [VBuIm]Br as ionic liquid showed the highest flux while it decreased notably when using only one IL with longer alkyl chains. Due to the low mechanical stability in the filtration cell, mixtures of [VBuIm]Br with other ILs were investigated. As well as the flux was also low, long-term stability increased significantly. Mixtures of 95% or 75% of [VBuIm]Br and 5% or 25% of ionic liquids with longer alkyl chains ([VDodecIm]Br or [VOcdecIm]Br) were in the same range. Shorter alkyl side chains like [VHexIm]Br were not suitable for mixtures.

Using organic solvents were not suitable in first place. All the polymeric layer crunched and no reliable result onto the permeability was feasible.

Charged and neutral sugar solutions were used to investigate the retention of substrates by PILs membranes. In general, neutral sugars were not retained in moderate or high quantities. With increasing molecular weight, also the retention increased but still, less than 25% were withheld for molecular masses within the range of NF applications. For charged sugars with comparable weight to the neutral ones, the retentions significantly increased. While glucose was retained with about 6%, the retention of sodium gluconate was about 53% for identic concentrations in water.

The cation influenced the retention of gluconate significantly. In dead-end filtrations with PILs membranes, retention increased with decreasing cation radii. At comparable concentrations, the bivalent calcium gluconate was retained more efficient (75%) than monovalent sodium gluconate (53%) and potassium gluconate (25%). The operation of dead-end filtration cells was also tested on long-term use and stability. Without a loss in efficiency or mechanical damage, PILs layers were used 2000 hours at 6 bars. Even though the filtration system was stopped for several absences such as the COVID-19 lockdown, the excellent results did not collapse after the resumption. Nevertheless, small disruptions were recognized after restarting the filtrations. Crossflow filtration was investigated in lab-scale experiments as it offered a continuous filtration. Besides the advantage of reduced workload, crossflow instead of dead-end filtration resulted in equal retentions.

The chemical characterization of the PILs membranes was rather difficult and had several drawbacks. Due to the insolubility of the polymerized layer, various analytical methods such as GPC, NMR or HPLC could not be used to determine a conversion of monomers, identify structural properties or the molecular mass of the polymer. Conclusions from the purification bath residues were also not possible due to the low concentration. Solid-state NMR was used to confirm the successful polymerization and purification of the solid. A ratio of the monomers in the polymer by intensity comparison of the signals was not possible.

By AFM the membrane surface was investigated. Here, differences between the PILs layers were recognized. Depending on the length of the alkyl side chain, different overall structures were formed. Butyl side chains tended to form pores or holes on the surface with a grainy pattern. Dodecyl or octadecyl side chains of the imidazolium heterocycle resulted in even, homogenous surfaces without any structural pattern. A mix of two ionic liquids in the synthesis resulted in combinations of the grainy and even structure, as well as a mix of pores and corrugations. Thereby, a link between the surface structure and permeance measurement was

done. More dense appearing surface pictures were correlated to lower permeance data. Also, an anion exchange onto the surface of bromide and gluconate was determined after the filtration of charged sugars. This anion exchange is a possible reason for the lowered permeance data while the retention of these sugars.

Charged polymerized ionic liquids layers offer a potential application in electrochemical devices. In this work, PILs membranes were successfully tested in the electrodialysis of organic compounds. In classic as well as in bipolar electrodialysis, these polymeric membranes were able to replace commercial anion exchange membranes. Even though commercial cation exchange and bipolar membranes falsify the data, PILs membranes were characterized by good stability for several hours even at high voltages. Here, one membrane triplet with PILs layers could convert up to 60 $mmol \cdot h^{-1}$ of sodium acetate or 48 $mmol \cdot h^{-1}$ of a gluconate sugar.

6. References

[1] In *IUPAC Compend. Chem. Terminol.*, IUPAC, **2020**.

[2] Y. Shi, M. Cai, L. Zhou, H. Wang, *Semin. Cell Dev. Biol.* **2018**, *73*, 31–44.

[3] E. Piacentini, R. Mazzei, E. Drioli, L. Giorno, in *Compr. Membr. Sci. Eng.*, Elsevier, **2017**, pp. 1–16.

[4] A. M. Whited, A. Johs, *Chem. Phys. Lipids* **2015**, *192*, 51–59.

[5] H. Strathmann, L. Giorno, E. Piacentini, E. Drioli, in *Compr. Membr. Sci. Eng.*, Elsevier, **2017**, pp. 65–84.

[6] M. Ulbricht, *Polymer* **2006**, *47*, 2217–2262.

[7] K. Peinemann, S. P. Nunes, in *Membr. Grundlagen,Verfahren Und Ind. Anwendungen* (Eds.: K. Ohlrogge, K. Ebert), Wiley-VCH, Weinheim, **2006**, pp. 1–26.

[8] S. S. Madaeni, in *Encyclopedia of Membranes* (Eds.: E. Drioli, L. Giorno), Springer, Heidelberg, **2016**, pp. 1300–1302.

[9] S. S. Madaeni, *Water Res.* **1999**, *33*, 301–308.

[10] S. S. Madaeni, A. Khorasani, M. Asgharpour, S. A. Ghoreshi, M. Lotfi, *Desalin. Water Treat.* **2013**, *51*, 4313–4322.

[11] P. Luis, *Fundamental Modeling of Membrane Systems: Membrane and Process Performance*, Elsevier, Amsterdam, **2018**.

[12] B. Van der Bruggen, in *Fundam. Model. Membr. Syst. Membr. Process Perform.* (Ed.: P. Luis), Elsevier, Amsterdam, **2018**, pp. 24–70.

[13] H. Lutz, in *Encyclopedia of Membranes* (Eds.: E. Drioli, L. Giorno), Springer, Heidelberg, **2017**, pp. 1947–1950.

[14] R. W. Baker, in *Membr. Technol. Appl.* (Ed.: R.W. Baker), John Wiley & Sons, Chichester, **2004**, pp. 393–423.

[15] W. Ostwald, *Zeitschrift für Phys. Chemie* **1890**, *6U*, DOI 10.1515/zpch-1890-0609.

[16] F. G. Donnan, *Zeitschrift für Elektrochemie und Angew. Phys. Chemie* **1911**, *17*, 572–581.

[17] T. R. E. Kressmann, *Nature* **1950**, *165*, 568–568.

[18] W. Juda, W. A. McRae, *J. Am. Chem. Soc.* **1950**, *72*, 1044–1044.

[19] Kirk, Othmer, in *Encyclopedia of Chemical Technology* (Eds.: J.I. Kroschwitz, M. Howe-Grant), John Wiley & Sons, Chichester, **2004**, p. 543.

[20] E. Manegold, K. Kalauch, *Kolloid-Zeitschrift* **1939**, *88*, 257–273.

[21] K. H. Meyer, W. Straus, *Helv. Chim. Acta* **1940**, *23*, 793–795.

[22] H. Strathmann, in *Compr. Membr. Sci. Eng.*, Elsevier, **2017**, pp. 355–392.

[23] R. W. Baker, *Membrane Technology and Applications*, John Wiley & Sons, Chichester, **2004**.

[24] T. Sata, *Ion Exchange Membranes: Preparation, Characterization and Application*, Royal Society Of Chemistry, Cambridge, **2002**.

[25] F. Gonçalves, C. Fernandes, P. Cameira dos Santos, M. N. de Pinho, *J. Food Eng.* **2003**, *59*, 229–235.

[26] V. A. Shaposhnik, K. Kesore, *J. Membr. Sci.* **1997**, *136*, 35–39.

[27] E. Vera, J. Ruales, M. Dornier, J. Sandeaux, R. Sandeaux, G. Pourcelly, *J. Chem. Technol. Biotechnol.* **2003**, *78*, 918–925.

[28] M. Fidaleo, M. Moresi, in *Adv. Food Nutr. Res.*, **2006**, pp. 265–360.

[29] W. E. Katz, *Desalination* **1979**, *28*, 31–40.

[30] R. Wódzki, J. Nowaczyk, *J. Appl. Polym. Sci.* **1997**, *63*, 355–362.

[31] R. Simons, *J. Membr. Sci.* **1993**, *78*, 13–23.

[32] S. Novalic, J. Okwor, K. D. Kulbe, *Desalination* **1996**, *105*, 277–282.

[33] Y. H. Kim, S.-H. Moon, *J. Chem. Technol. Biotechnol.* **2001**, *76*, 169–178.

[34] C. Huang, T. Xu, Y. Zhang, Y. Xue, G. Chen, *J. Membr. Sci.* **2007**, *288*, 1–12.

[35] T. A. Saleh, V. K. Gupta, *Nanomaterial and Polymer Membranes: Synthesis, Characterization, and Applications*, Elsevier, Amsterdam, **2016**.

[36] A. Basile, S. P. Nunes, Eds. , *Advanced Membrane Science and Technology for Sustainable Energy and Enviromental Applications*, Woodhead Publishing, Philadelphia, **2011**.

[37] K. C. Khulbe, C. Y. Feng, T. Matsuura, *Synthetic Polymeric Membranes*, Springer Berlin Heidelberg, Berlin, Heidelberg, **2008**.

[38] P. S. Goh, A. F. Ismail, *Desalination* **2018**, *434*, 60–80.

[39] A. Kumar, A. Thakur, P. S. Panesar, *Rev. Environ. Sci. Bio/Technology* **2019**, *18*, 153–182.

[40] C. Z. Liang, T.-S. Chung, J.-Y. Lai, *Prog. Polym. Sci.* **2019**, *97*, 101141.

[41] Y. Song, J.-B. Fan, S. Wang, *Mater. Chem. Front.* **2017**, *1*, 1028–1040.

[42] X. Tang, X. Yan, *J. Sol-Gel Sci. Technol.* **2017**, *81*, 378–404.

[43] M. Bassyouni, M. H. Abdel-Aziz, M. S. Zoromba, S. M. S. Abdel-Hamid, E. Drioli, *J. Ind. Eng. Chem.* **2019**, *73*, 19–46.

[44] E. Drioli, *Encyclopedia of Membranes*, Springer, Heidelberg, **2016**.

[45] R. Zsigmondy, W. Bachmann, *Zeitschrift für Anorg. und Allg. Chemie* **1918**, *103*, 119–128.

[46] A. Goetz, *Method of Making Microporous Filter Film*, **1960**, US 2,926,104.

[47] M. Mulder, *Basic Principles of Membrane Technology*, Kluwer Academic Publishers, Dordrecht, **1996**.

[48] C. Wei, Z. He, L. Lin, Q. Cheng, K. Huang, S. Ma, L. Chen, *J. Membr. Sci.* **2018**, *563*, 752–761.

[49] M. Mertens, T. Van Dyck, C. Van Goethem, A. Y. Gebreyohannes, I. F. J. Vankelecom, *J. Membr. Sci.* **2018**, *557*, 24–29.

[50] I. Pinnau, B. D. Freeman, in *Membrane Formation and Modification* (Eds.: I. Pinnau, B.D. Freeman), American Chemical Society, Washington, D. C., **1999**, pp. 1–22.

[51] H. Strathmann, K. Kock, P. Amar, R. W. Baker, *Desalination* **1975**, *16*, 179–203.

[52] H. Strathmann, K. Kock, *Desalination* **1977**, *21*, 241–255.

[53] H. Matsuyama, S. Berghmans, M. T. Batarseh, D. R. Lloyd, in *Membrane Formation and Modification* (Eds.: I. Pinnau, B.D. Freeman), American Chemical Society, Washington, D. C., **1999**, pp. 23–41.

[54] H. C. Park, Y. S. Moon, H. W. Rhee, J. Won, Y. S. Kang, U. Y. Kim, in *Membrane Formation and*

Modification (Eds.: I. Pinnau, B.D. Freeman), American Chemical Society, Washington, D. C., **1999**, pp. 110–124.

[55] I. Soroko, M. Makowski, F. Spill, A. Livingston, *J. Membr. Sci.* **2011**, *381*, 163–171.

[56] B. S. Lalia, V. Kochkodan, R. Hashaikeh, N. Hilal, *Desalination* **2013**, *326*, 77–95.

[57] H. J. Lee, J. Won, H. Lee, Y. S. Kang, *J. Membr. Sci.* **2002**, *196*, 267–277.

[58] J. Marchese, M. Ponce, N. A. Ochoa, P. Prádanos, L. Palacio, A. Hernández, *J. Membr. Sci.* **2003**, *211*, 1–11.

[59] E. Saljoughi, M. Amirilargani, T. Mohammadi, *Desalination* **2010**, *262*, 72–78.

[60] M. Amirilargani, E. Saljoughi, T. Mohammadi, M. R. Moghbeli, *Polym. Eng. Sci.* **2010**, *50*, 885–893.

[61] T. Van Gerven, A. Stankiewicz, *Ind. Eng. Chem. Res.* **2009**, *48*, 2465–2474.

[62] S. Al-Amshawee, M. Y. B. M. Yunus, A. A. M. Azoddein, D. G. Hassell, I. H. Dakhil, H. A. Hasan, *Chem. Eng. J.* **2020**, *380*, 122231.

[63] P. F. Tee, M. O. Abdullah, I. A. W. Tan, N. K. A. Rashid, M. A. M. Amin, C. Nolasco-Hipolito, K. Bujang, *Renew. Sustain. Energy Rev.* **2016**, *54*, 235–246.

[64] S. O. Ganiyu, E. D. van Hullebusch, M. Cretin, G. Esposito, M. A. Oturan, *Sep. Purif. Technol.* **2015**, *156*, 891–914.

[65] S. Loeb, S. Sourirajan, *High Flow Porous Membranes for Separating Water from Saline Solutions*, **1964**, US 3,133,132.

[66] S. Loeb, S. Sourirajan, *Adv. Chem. ACS* **1963**, *38*, 117–132.

[67] S. Sourirajan, *Nature* **1964**, *203*, 1348–1349.

[68] R. W. Baker, in *Membr. Technol. Appl.* (Ed.: R.W. Baker), John Wiley & Sons, Chichester, **2004**, pp. 1–14.

[69] R. W. Baker, Ed. , *Membrane Technology and Applications*, Wiley-VCH, Chichester, **2012**.

[70] G. Cederlof, E. R. Geus, *Continuous Process to Separate Colour Bodies and / or Asphalthenic Contaminants from a Hydrocarbon Mixture*, **2008**, US 7,351,873.

[71] J. T. Scarpello, D. Nair, L. M. Freitas dos Santos, L. S. White, A. G. Livingston, *J. Membr. Sci.* **2002**, *203*, 71–85.

[72] W. Liu, *Membr. Technol.* **2016**, 2.

[73] R. W. Baker, K. Lokhandwala, *Ind. Eng. Chem. Res.* **2008**, *47*, 2109–2121.

[74] T. C. Merkel, M. Zhou, R. W. Baker, *J. Membr. Sci.* **2012**, *389*, 441–450.

[75] W. Liu, in *Encyclopedia of Membranes* (Eds.: E. Drioli, L. Giorno), Springer Berlin Heidelberg, Berlin, Heidelberg, **2016**, pp. 29–30.

[76] W. J. Kolff, H. T. J. Berk, N. M. Welle, A. J. W. Ley, E. C. Dijk, J. Noordwijk, *Acta Med. Scand.* **1944**, *117*, 121–134.

[77] E. Drioli, A. I. Stankiewicz, F. Macedonio, *J. Membr. Sci.* **2011**, *380*, 1–8.

[78] PrescientStrategicMarketresearch, “Microfiltration Membrane Market Overview 2017,” can be found under https://www.psmarketresearch.com/market-analysis/membrane-microfiltration-market, **2020**.

[79] MenaFN, “Microfiltration Membrane Market 2020-2025 Global Review and Outlook,” can be found under https://menafn.com/1099789502/Microfiltration-Membrane-Market-2020-2025-Global-Review-

and-Outlook-Asahi-Kasei-Corporation-X-Flow-Pentair-PLC-NYSEPNR-Totay-KMS, **2020**.

[80] Markets&Markets, "Ultrafiltration Market Global Forecast to 2023," can be found under https://www.marketsandmarkets.com/Market-Reports/ultrafiltration-market-102302816.html, **2020**.

[81] Reports&Data, "Ultrafiltration Market To Reach USD 3.05 Billion By 2026," can be found under https://www.globenewswire.com/news-release/2019/08/20/1904264/0/en/Ultrafiltration-Market-To-Reach-USD-3-05-Billion-By-2026-Reports-And-Data.html, **2020**.

[82] MarketWatch, "Ultrafiltration Membrane Filtration Market Size to Grow at 3.5%+ CAGR to Reach US$ 2920 Mn by 2025," can be found under https://www.marketwatch.com/press-release/ultrafiltration-membrane-filtration-market-size-to-grow-at-35-cagr-to-reach-us-2920-mn-by-2025-2019-04-30, **2020**.

[83] AlliedMarketResearch, "Nanofiltration Membrane Market Outlook - 2025," can be found under https://www.alliedmarketresearch.com/nanofiltration-membranes-market, **2020**.

[84] PRNewswire, "The Global Nanofiltration Membrane Market size is expected to reach $845.2 Million by 2025, rising at a market growth of 5.3% CAGR during the forecast period," can be found under https://www.prnewswire.com/news-releases/the-global-nanofiltration-membrane-market-size-is-expected-to-reach-845-2-million-by-2025--rising-at-a-market-growth-of-5-3-cagr-during-the-forecast-period-300920884.html, **2020**.

[85] AlliedMarketResearch, "Reverse Osmosis Membrane Market Global Opportunity Analysis and Industry Forecast 2018–2025," can be found under https://www.alliedmarketresearch.com/reverse-osmosis-membrane-market, **2020**.

[86] F. Yalcinkaya, E. Boyraz, J. Maryska, K. Kucerova, *Materials (Basel).* **2020**, *13*, 493.

[87] P. Walden, *Bull. Acad. Imper. Sci. (St. Petersburg)* **1914**, *8*, 405–422.

[88] J. Yuan, M. Antonietti, *Polymer* **2011**, *52*, 1469–1482.

[89] N. V Plechkova, K. R. Seddon, *Chem. Soc. Rev.* **2008**, *37*, 123–150.

[90] J. Claus, F. O. Sommer, U. Kragl, *Solid State Ionics* **2018**, *314*, 119–128.

[91] B. S. Sugden, *J. Chem. Soc.* **1928**, 1291–1298.

[92] H. Ohno, *Electrochemical Aspects of Ionic Liquids*, John Wiley & Sons, Hoboken, NJ, USA, **2011**.

[93] H. Ohno, M. Yoshizawa, W. Ogihara, *Electrochim. Acta* **2004**, *50*, 255–261.

[94] S. Werner, M. Haumann, P. Wasserscheid, *Annu. Rev. Chem. Biomol. Eng.* **2010**, *1*, 203–230.

[95] H. Olivier-Bourbigou, L. Magna, D. Morvan, *Appl. Catal. A Gen.* **2010**, *373*, 1–56.

[96] C. Graenacher, *Cellulose Solution*, **1934**, US 1,943,176.

[97] F. H. Hurley, T. P. Wier, *J. Electrochem. Soc.* **1951**, *98*, 207.

[98] F. H. Hurley, T. P. Wier, *J. Electrochem. Soc.* **1951**, *98*, 203.

[99] H. Li Chum, V. R. Koch, L. L. Miller, R. A. Osteryoung, *J. Am. Chem. Soc.* **1975**, *97*, 3264–3265.

[100] J. Robinson, R. A. Osteryoung, *J. Am. Chem. Soc.* **1979**, *101*, 323–327.

[101] T. Welton, *Biophys. Rev.* **2018**, *10*, 691–706.

[102] J. T. Yoke, J. F. Weiss, G. Tollin, *Inorg. Chem.* **1963**, *2*, 1210–1216.

[103] E. I. Cooper, C. A. Angell, *Solid State Ionics* **1983**, *9–10*, 617–622.

[104] J. S. Wilkes, M. J. Zaworotko, *J. Chem. Soc. Chem. Commun.* **1992**, 965–967.

[105] E. I. Cooper, E. J. M. O'Sullivan, **1992**, pp. 386–396.

[106] P. Bonhôte, A. P. Dias, N. Papageorgiou, K. Kalyanasundaram, M. Grätzel, *Inorg. Chem.* **1996**, *35*, 1168–1178.

[107] J. Sun, D. R. MacFarlane, M. Forsyth, *Ionics (Kiel)*. **1997**, *3*, 356–362.

[108] K. J. Fraser, D. R. MacFarlane, *Aust. J. Chem.* **2009**, *62*, 309.

[109] C. J. Bradaric, A. Downard, C. Kennedy, A. J. Robertson, Y. Zhou, *Green Chem.* **2003**, *5*, 143–152.

[110] M. Doble, A. K. Kruthiventi, in *Green Chem. Eng.*, **2007**, pp. 93–104.

[111] D. A. Jaeger, C. E. Tucker, *Tetrahedron Lett.* **1989**, *30*, 1785–1788.

[112] M. J. Earle, P. B. McCormac, K. R. Seddon, *Green Chem.* **1999**, *1*, 23–25.

[113] T. Fischer, A. Sethi, T. Welton, J. Woolf, *Tetrahedron Lett.* **1999**, *40*, 793–796.

[114] M. J. Earle, P. B. McCormac, K. R. Seddon, *Chem. Commun.* **1998**, 2245–2246.

[115] U. Onken, A. Behr, *Chemische Prozesskunde*, Georg Thieme Verlag, Stuttgart, **1996**.

[116] A. Behr, D. W. Agar, J. Jörissen, A. J. Vorholt, *Einführung in Die Technische Chemie*, Springer Berlin Heidelberg, Berlin, Heidelberg, **2016**.

[117] A. Behr, *Angewandte Homogene Katalyse*, Wiley-VCH, Weinheim, **2008**.

[118] J. M. Dreimann, M. Skiborowski, A. Behr, A. J. Vorholt, *ChemCatChem* **2016**, *8*, 3330–3333.

[119] T. A. Faßbach, F. O. Sommer, A. Behr, S. Romanski, D. Leinweber, A. J. Vorholt, *Catal. Sci. Technol.* **2017**, *7*, 1650–1653.

[120] T. A. Faßbach, F. O. Sommer, A. J. Vorholt, *Adv. Synth. Catal.* **2018**, *360*, 1473–1482.

[121] J. F. Knifton, *J. Am. Chem. Soc.* **1981**, *103*, 3959–3961.

[122] J. F. Knifton, *J. Mol. Catal.* **1988**, *47*, 99–116.

[123] Y. Chauvin, B. Gilbert, I. Guibard, *J. Chem. Soc. Chem. Commun.* **1990**, 1715.

[124] S. N. Falling, S. A. Godleski, L. W. McGarry, *Process for the Separation of Oligomeric Materials from a Catalyst Mixture*, **1993**, US 5,238,889.

[125] G. W. Philips, S. N. Falling, S. A. Godleski, J. R. Monnier, *Continuous Process for the Manufacture of 2,5-Dihydrofurans from Epoxybutenes*, **1994**, US 5,315,019.

[126] J. R. Monnier, P. J. Muelbauer, *Selective Monoepoxidation of Olefins*, **1990**, US 4,897,498.

[127] M. Volland, V. Seitz, M. Maase, M. Flores, R. Papp, K. Massonne, V. Stegmann, K. Halbritter, R. Noe, M. Bartsch, et al., *Method for the Separation of Acids from Chemical Reaction Mixtures by Means of Ionic Fluids*, **2003**, WO 03/062171 A2.

[128] K. R. Seddon, *Nat. Mater.* **2003**, *2*, 363–365.

[129] R. D. Rogers, K. R. Seddon, *Science (80-.).* **2003**, *302*, 792–793.

[130] M. Maase, in *Multiph. Homog. Catal.* (Eds.: B. Cornils, W.A. Herrmann, I.T. Horváth, W. Leitner, S. Mecking, H. Olivier-Bourbigou, D. Vogt), Wiley-VCH, Weinheim, **2005**, pp. 560–566.

[131] S. Oppermann, F. Stein, U. Kragl, *Appl. Microbiol. Biotechnol.* **2011**, *89*, 493–499.

[132] L.-E. Meyer, J. von Langermann, U. Kragl, *Biophys. Rev.* **2018**, *10*, 901–910.

[133] B. L. A. P. Devi, Z. Guo, X. Xu, *AIChE J.* **2011**, *57*, 1628–1637.

[134] C. Roosen, P. Müller, L. Greiner, *Appl. Microbiol. Biotechnol.* **2008**, *81*, 607–614.

[135] U. Kragl, M. Eckstein, N. Kaftzik, *Curr. Opin. Biotechnol.* **2002**, *13*, 565–571.

[136] N. L. Mai, Y.-M. Koo, in *Appl. Ion. Liq. Biotechnol.* (Eds.: T. Itoh, Y.-M. Koo), Springer International Publishing, **2018**, pp. 105–132.

[137] M. L. M. Saraiva, S. Costa, P. Pinto, A. Azevedo, *ChemSusChem* **2017**, *10*, 2321.

[138] M. Reiß, A. Brietzke, T. Eickner, F. Stein, A. Villinger, C. Vogel, U. Kragl, S. Jopp, *RSC Adv.* **2020**, *10*, 14299–14304.

[139] S. Petersen, S. Kaule, F. Stein, I. Minrath, K.-P. Schmitz, U. Kragl, K. Sternberg, *Mater. Sci. Eng. C* **2013**, *33*, 4244–4250.

[140] U. Kragl, C. Harder, K. Sternberg, F. Stein, M. Löbler, K.-P. Schmitz, *Ballonkatheter Mit Einer Aktiven Beschichtung*, **2013**, DE 10 2012 200 077 A1.

[141] R. Jayachandra, S. R. Reddy, Balakrishna, *ChemistrySelect* **2016**, *1*, 2341–2343.

[142] R. Yuan, Y. Wang, Y. Fang, W. Ge, W. Lin, M. Li, J. Xu, Y. Wan, Y. Liu, H. Wu, *Chem. Eng. J.* **2017**, *316*, 1026–1034.

[143] A. Eftekhari, T. Saito, *Eur. Polym. J.* **2017**, *90*, 245–272.

[144] H. L. Ricks-Laskoski, A. W. Snow, *J. Am. Chem. Soc.* **2006**, *128*, 12402–12403.

[145] M. F. Hoover, *J. Macromol. Sci. Part A - Chem.* **1970**, *4*, 1327–1418.

[146] S. M. Hamid, D. C. Sherrington, *Polymer* **1987**, *28*, 332–339.

[147] C. Damas, A. Brembilla, F. Baros, M.-L. Viriot, P. Lochon, *Eur. Polym. J.* **1994**, *30*, 1215–1222.

[148] "Web of Science," **2020**.

[149] D.-Z. Zhang, Y.-Y. Ren, Y. Hu, L. Li, F. Yan, *Chinese J. Polym. Sci.* **2020**, DOI 10.1007/s10118-020-2390-1.

[150] R. Lambert, P. Coupillaud, A.-L. Wirotius, J. Vignolle, D. Taton, *Macromol. Rapid Commun.* **2016**, *37*, 1143–1149.

[151] A. S. Shaplov, P. S. Vlasov, M. Armand, E. I. Lozinskaya, D. O. Ponkratov, I. A. Malyshkina, F. Vidal, O. V Okatova, G. M. Pavlov, C. Wandrey, et al., *Polym. Chem.* **2011**, *2*, 2609–2618.

[152] P. Coupillaud, J. Pinaud, N. Guidolin, J. Vignolle, M. Fèvre, E. Veaudecrenne, D. Mecerreyes, D. Taton, *J. Polym. Sci. Part A Polym. Chem.* **2013**, *51*, 4530–4540.

[153] K. M. Meek, Y. A. Elabd, *Macromol. Rapid Commun.* **2016**, *37*, 1200–1206.

[154] J. Bandomir, A. Schulz, S. Taguchi, L. Schmitt, H. Ohno, K. Sternberg, K.-P. Schmitz, U. Kragl, *Macromol. Chem. Phys.* **2014**, *215*, 716–724.

[155] O. Green, S. Grubjesic, S. Lee, M. A. Firestone, *Polym. Rev.* **2009**, *49*, 339–360.

[156] P. Coupillaud, J. Vignolle, D. Mecerreyes, D. Taton, *Polymer* **2014**, *55*, 3404–3414.

[157] M. M. Obadia, B. P. Mudraboyina, A. Serghei, T. N. T. Phan, D. Gigmes, E. Drockenmuller, *ACS Macro Lett.* **2014**, *3*, 658–662.

[158] R. Marcilla, J. A. Blazquez, J. Rodriguez, J. A. Pomposo, D. Mecerreyes, *J. Polym. Sci. Part A Polym. Chem.* **2004**, *42*, 208–212.

[159] J. Großeheilmann, J. Bandomir, U. Kragl, *Chem. - A Eur. J.* **2015**, *21*, 18957–18960.

[160] A. Grollmisch, U. Kragl, J. Großeheilmann, *SynOpen* **2018**, *02*, 0192–0199.

[161] M. Moniruzzaman, K. Ino, N. Kamiya, M. Goto, *Org. Biomol. Chem.* **2012**, *10*, 7707–7713.

[162] J. Claus, A. Brietzke, C. Lehnert, S. Oschatz, N. Grabow, U. Kragl, *PLoS One* **2020**, *15*, e0231421.

[163] J. Claus, T. Eickner, N. Grabow, U. Kragl, S. Oschatz, *Macromol. Biosci.* **2020**, *20*, 2000152.

[164] J. Claus, T. Eickner, N. Grabow, U. Kragl, S. Oschatz, *J. Appl. Polym. Sci.* **2020**, *105*, 135–149.

[165] D.-Z. Zhang, Y. Ren, Y. Hu, L. Li, F. Yan, *Chinese J. Polym. Sci.* **2020**, DOI 10.1007/s10118-020-2390-1.

[166] A. Wang, X. Liu, S. Wang, J. Chen, H. Xu, Q. Xing, L. Zhang, *Electrochim. Acta* **2018**, *276*, 184–193.

[167] B. Lin, T. Feng, F. Chu, S. Zhang, N. Yuan, G. Qiao, J. Ding, *RSC Adv.* **2015**, *5*, 57216–57222.

[168] S.-M. Chen, T.-L. Wang, P.-Y. Chang, C.-H. Yang, Y.-C. Lee, *React. Funct. Polym.* **2016**, *108*, 103–112.

[169] H. Nakajima, H. Ohno, *Polymer* **2005**, *46*, 11499–11504.

[170] X. Chen, J. Zhao, J. Zhang, L. Qiu, D. Xu, H. Zhang, X. Han, B. Sun, G. Fu, Y. Zhang, et al., *J. Mater. Chem.* **2012**, *22*, 18018–18024.

[171] Y. Rong, Z. Ku, M. Xu, L. Liu, M. Hu, Y. Yang, J. Chen, A. Mei, T. Liu, H. Han, *RSC Adv.* **2014**, *4*, 9271–9274.

[172] R. D. Noble, D. L. Gin, *J. Membr. Sci.* **2011**, *369*, 1–4.

[173] X. Zhang, X. Zhang, H. Dong, Z. Zhao, S. Zhang, Y. Huang, *Energy Environ. Sci.* **2012**, *5*, 6668–6681.

[174] M. Ramdin, T. W. De Loos, T. J. H. Vlugt, *Ind. Eng. Chem. Res.* **2012**, *51*, 8149–8177.

[175] J. E. Bara, C. J. Gabriel, E. S. Hatakeyama, T. K. Carlisle, S. Lessmann, R. D. Noble, D. L. Gin, *J. Membr. Sci.* **2008**, *321*, 3–7.

[176] R. M. Teodoro, L. C. Tomé, D. Mantione, D. Mecerreyes, I. M. Marrucho, *J. Membr. Sci.* **2018**, *552*, 341–348.

[177] L. C. Tomé, A. S. L. Gouveia, C. S. R. Freire, D. Mecerreyes, I. M. Marrucho, *J. Membr. Sci.* **2015**, *486*, 40–48.

[178] L. C. Tomé, D. Mecerreyes, C. S. R. Freire, L. P. N. Rebelo, I. M. Marrucho, *J. Mater. Chem. A* **2014**, *2*, 5631–5639.

[179] T. Chouliaras, A. Vollas, T. Ioannides, V. Deimede, J. Kallitsis, *Membranes (Basel).* **2019**, *9*, 164.

[180] L. Setiawan, R. Wang, K. Li, A. G. Fane, *J. Membr. Sci.* **2011**, *369*, 196–205.

[181] Y. Yao, C. Ba, S. Zhao, W. Zheng, J. Economy, *J. Membr. Sci.* **2016**, *520*, 832–839.

[182] C. Ba, J. Langer, J. Economy, *J. Membr. Sci.* **2009**, *327*, 49–58.

[183] M. Amirilargani, M. Sadrzadeh, E. J. R. Sudhölter, L. C. P. M. de Smet, *Chem. Eng. J.* **2016**, *289*, 562–582.

[184] S. Y. Zhang, Q. Zhuang, M. Zhang, H. Wang, Z. Gao, J. K. Sun, J. Yuan, *Chem. Soc. Rev.* **2020**, *49*, 1726–1755.

[185] K. Täuber, Q. Zhao, M. Antonietti, J. Yuan, *ACS Macro Lett.* **2015**, *4*, 39–42.

[186] X. Li, S. De Feyter, D. Chen, S. Aldea, P. Vandezande, F. Du Prez, I. F. J. Vankelecom, *Chem. Mater.* **2008**, *20*, 3876–3883.

[187] S. Al-kharabsheh, R. Bernstein, *Adv. Mater. Interfaces* **2018**, *5*, 1800823.

[188] C. Fersi, M. Dhahbi, *Desalination* **2008**, *222*, 263–271.

[189] K. Manojkumar, D. Mecerreyes, D. Taton, Y. Gnanou, K. Vijayakrishna, *Polym. Chem.* **2017**, *8*, 3497–3503.

[190] Y. Ren, J. Guo, Q. Lu, D. Xu, J. Qin, F. Yan, *ChemSusChem* **2018**, *11*, 1092–1098.

[191] X. Fan, H. Liu, Y. Gao, Z. Zou, V. S. J. Craig, G. Zhang, G. Liu, *Adv. Mater.* **2016**, *28*, 4156–4161.

[192] A. S. Shaplov, D. O. Ponkratov, Y. S. Vygodskii, *Polym. Sci. Ser. B* **2016**, *58*, 73–142.

[193] M. D. Green, D. Salas-de la Cruz, Y. Ye, J. M. Layman, Y. A. Elabd, K. I. Winey, T. E. Long, *Macromol. Chem. Phys.* **2011**, *212*, 2522–2528.

[194] H. Qi, Y. Ren, S. Guo, Y. Wang, S. Li, Y. Hu, F. Yan, *ACS Appl. Mater. Interfaces* **2020**, *12*, 591–600.

[195] K. Täuber, A. Zimathies, J. Yuan, *Macromol. Rapid Commun.* **2015**, *36*, 2176–2180.

[196] M. H. Allen, S. T. Hemp, A. E. Smith, T. E. Long, *Macromolecules* **2012**, *45*, 3669–3676.

[197] Q. Zhao, M. Yin, A. P. Zhang, S. Prescher, M. Antonietti, J. Yuan, *J. Am. Chem. Soc.* **2013**, *135*, 5549–5552.

[198] B. Lin, L. Qiu, J. Lu, F. Yan, *Chem. Mater* **2010**, *22*, 6718–6725.

[199] Y. Ye, J.-H. Choi, K. I. Winey, Y. A. Elabd, *Macromolecules* **2012**, *45*, 7027–7035.

[200] D. Salas-de la Cruz, Morphology and Ionic Conductivity of Polymerized Ionic Liquids, University of Pennsylvania, **2011**.

[201] H. Mori, M. Yahagi, T. Endo, *Macromolecules* **2009**, *42*, 8082–8092.

[202] C. Ladavière, N. Dörr, J. P. Claverie, *Macromolecules* **2001**, *34*, 5370–5372.

[203] K. Grygiel, B. Wicklein, Q. Zhao, M. Eder, T. Pettersson, L. Bergström, M. Antonietti, J. Yuan, *Chem. Commun.* **2014**, *50*, 12486–12489.

[204] B. Schille, N. O. Giltzau, R. Francke, *Angew. Chem. Int. Ed.* **2018**, *57*, 422–426.

[205] B. Schille, N. O. Giltzau, R. Francke, *Angew. Chem.* **2018**, *130*, 429–433.

[206] B. Schille, Studien Zur Verwendung von Polyelektrolyten Und Polymediatoren in Der Organischen Elektrosynthese, University of Rostock, **2019**.

[207] T. Janoschka, N. Martin, U. Martin, C. Friebe, S. Morgenstern, H. Hiller, M. D. Hager, U. S. Schubert, *Nature* **2015**, *527*, 78–81.

[208] I. Spanos, S. Neugebauer, R. Guterman, J. Yuan, R. Schlögl, M. Antonietti, *Sustain. Energy Fuels* **2018**, *2*, 1446–1451.

[209] Z. Zheng, Q. Xu, J. Guo, J. Qin, H. Mao, B. Wang, F. Yan, *ACS Appl. Mater. Interfaces* **2016**, *8*, 12684–12692.

[210] N. Nishimura, H. Ohno, *Polymer* **2014**, *55*, 3289–3297.

[211] W. Qian, J. Texter, F. Yan, *Chem. Soc. Rev.* **2017**, *46*, 1124–1159.

[212] H. Diao, F. Yan, L. Qiu, J. Lu, X. Lu, B. Lin, Q. Li, S. Shang, W. Liu, J. Liu, *Macromolecules* **2010**, *43*, 6398–6405.

[213] J. Guo, L. Qiu, Z. Deng, F. Yan, *Polym. Chem.* **2013**, *4*, 1309–1312.

[214] T. Feng, B. Lin, S. Zhang, N. Yuan, F. Chu, M. A. Hickner, C. Wang, L. Zhu, J. Ding, *J. Membr. Sci.*

2016, *508*, 7–14.

[215] A. Sengupta, S. Kumar Ethirajan, M. Kamaz, M. Jebur, R. Wickramasinghe, *Sep. Purif. Technol.* **2019**, *212*, 307–315.

[216] F. Gu, H. Dong, Y. Li, Z. Sun, F. Yan, *Macromolecules* **2014**, *47*, 6740–6747.

[217] Z. Zheng, J. Guo, H. Mao, Q. Xu, J. Qin, F. Yan, *ACS Biomater. Sci. Eng.* **2017**, *3*, 922–928.

[218] J. Guo, Q. Xu, R. Shi, Z. Zheng, H. Mao, F. Yan, *Langmuir* **2017**, *33*, 4346–4355.

[219] B. Van der Bruggen, M. Mänttäri, M. Nyström, *Sep. Purif. Technol.* **2008**, *63*, 251–263.

[220] T. Siddique, N. K. Dutta, N. Roy Choudhury, *Nanomaterials* **2020**, *10*, 1323.

[221] L. Y. Ng, A. W. Mohammad, C. Y. Ng, *Adv. Colloid Interface Sci.* **2013**, *197–198*, 85–107.

[222] P. Fievet, in *Encyclopedia of Membranes* (Eds.: E. Drioli, L. Giorno), Springer, Heidelber, **2015**.

[223] H. Spencer, J. Scheck, I. Lewin, J. Samachson, *J. Nutr.* **1966**, *89*, 283–292.

[224] L. M. Ruilope, A. Oliet, J. M. Alcázar, E. Hernández, A. Andrés, J. L. Rodicio, R. García-Robles, J. Martínez, V. Laherat, J. C. Romero, *J. Hypertens.* **1989**, *7*, S170-171.

[225] W. Cheng, C. Liu, T. Tong, R. Epsztein, M. Sun, R. Verduzco, J. Ma, M. Elimelech, *J. Membr. Sci.* **2018**, *559*, 98–106.

[226] Y. Marcus, *Biophys. Chem.* **1994**, *51*, 111–127.

[227] E. R. Nightingale, *J. Phys. Chem.* **1959**, *63*, 1381–1387.

[228] W. J. Koros, Y. H. Ma, T. Shimidzu, *Pure Appl. Chem.* **1996**, *68*, 1479–1489.

[229] D. J. Johnson, D. L. Oatley-Radcliffe, N. Hilal, *Desalination* **2018**, *434*, 12–36.

[230] J. Bürger, V. S. Kunnathully, D. Kool, J. K. N. Lindner, K. Brassat, *Nanomaterials* **2020**, *10*, DOI 10.3390/nano10010141.

[231] Y. Matsushita, in *Encyclopedia of Polymeric Nanomaterials* (Eds.: S. Kobayashi, K. Müllen), Springer, Heidelberg, **2014**, pp. 1–6.

[232] S. M. Samaei, S. Gato-Trinidad, A. Altaee, *Sep. Purif. Technol.* **2018**, *200*, 198–220.

[233] A. G. R Ananthashankar, *J. Chem. Eng. Process Technol.* **2013**, *05*, DOI 10.4172/2157-7048.1000182.

[234] D. Y. Koseoglu-Imer, *Desalination* **2013**, *316*, 110–119.

[235] K. J. Wu, R. W. Odom, *Anal. Chem.* **1998**, *70*, 456A-461A.

[236] R. Skelton, F. Dubois, R. Zenobi, *Anal. Chem.* **2000**, *72*, 1707–1710.

[237] S. D. Hanton, D. M. Parees, *J. Am. Soc. Mass Spectrom.* **2005**, *16*, 90–93.

[238] D. D. Laws, H.-M. L. Bitter, A. Jerschow, *Angew. Chem.* **2002**, *114*, 3224–3259.

[239] M. J. Duer, in *Solid-State NMR Spectroscopy* (Ed.: M.J. Duer), Blackwell Science, Oxford, **2002**, pp. 73–110.

[240] A. Pines, M. G. Gibby, J. S. Waugh, *J. Chem. Phys.* **1973**, *569*, 569–590.

[241] H.-J. Rapp, in *Membr. Grundlagen, Verfahren Und Ind. Anwendungen* (Eds.: K. Ohlrogge, K. Ebert), Wiley-VCH, Weinheim, **2006**, pp. 429–452.

[242] X. Xu, Q. He, G. Ma, H. Wang, N. Nirmalakhandan, P. Xu, *Desalination* **2018**, *428*, 146–160.

[243] M. Reig, H. Farrokhzad, B. Van der Bruggen, O. Gibert, J. L. Cortina, *Desalination* **2015**, *375*, 1–9.

[244] Y. Kim, W. S. Walker, D. F. Lawler, *Water Res.* **2012**, *46*, 2042–2056.

[245] N. Káňavová, L. Machuča, D. Tvrzník, *Chem. Pap.* **2014**, *68*, 324–329.

[246] H. E. Gottlieb, V. Kotlyar, A. Nudelman, *J. Org. Chem.* **1997**, *62*, 7512–7515.

Appendix

A1. Nuclear Magnetic Resonance

Bruker Avance 250 II, 300 III and 500 (Ettlingen, Germany) were used to record the NMR spectra of ILs in order to determine the structure and purity of ILs. d_6-DMSO (δ= 2.50 ppm) and *d*-chloroform (δ= 7.26 ppm)[246] were used as solvent.

Solid-state NMR experiments of the dried and crushed educts as well as PILs layers were performed on the Bruker AVANCE III HD spectrometer with a borehole of 89 mm and a proton resonance frequency of 400.2 MHz. A MASWVT400W1 BL4 X/Y/H with a triple resonance channel was used as sample head. The frequency of magic angle spinning (MAS) was 8000 Hz. The samples were rotated in a 4 mm ZrO2 rotor at room temperature. The power of the radio frequency pulses was 83 kHz for ^{1}H and 50 kHz for ^{13}C experiments. For cross polarization experiments a contact time of 1.5 ms was chosen and the decoupling sequence SPINAL64 was used for proton decoupling. The processing was performed by TopSpin 4.0.6 with an exponential apodization with 50 Hz propagation parameter. The spectra were referenced to Adamantane Standard.

The superimposed spectra of the experiments were normalized to the same intensity. Automated base correction was performed with TopSpin 4.0.6 for ^{13}C-CP MAS (CP) and with Origin 2018b Pro for ^{13}C-MAS (DP) experiments.

Table i: Number of experiments per sample.

Sample	Number of experiments
CP 95	10240
CP 98	6144
CP 96	4096
CP 99	10521
DP 95	2816
DP 98	1280
DP 96	1536
DP 99	3071
[VBuIm]Br	5120
[VDodecIm]Br	5120
[VOcdecIm]Br	5120

[VEtIm]Br

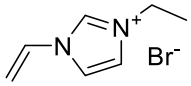

3-ethyl-1-vinyl-1-imidazole-3-ium bromide

$C_7H_{11}N_2Br$ M = 203.08 g·mol^{-1}

Calculated: C: 41.40 H: 5.46 N: 13.79 Measured: C: 41.740 H: 5.753 N: 13.957

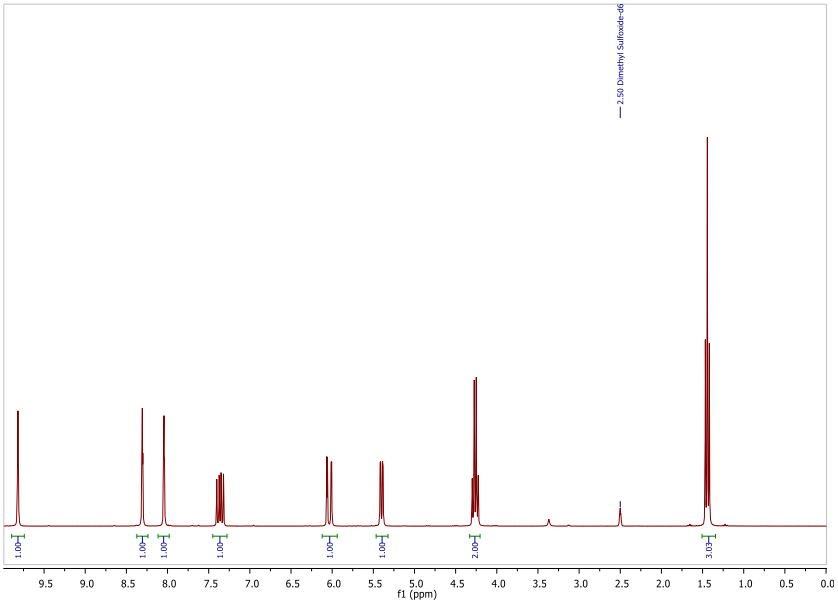

^{1}H NMR (300 MHz, DMSO) δ 9.82 (s, 1H), 8.31 (t, *J* = 1.8 Hz, 1H), 8.04 (t, *J* = 1.7 Hz, 1H), 7.36 (dd, *J* = 15.7, 8.8 Hz, 1H), 6.04 (dd, *J* = 15.7, 2.3 Hz, 1H), 5.40 (dd, *J* = 8.8, 2.3 Hz, 1H), 4.26 (q, *J* = 7.3 Hz, 2H), 1.44 (t, *J* = 7.3 Hz, 3H).

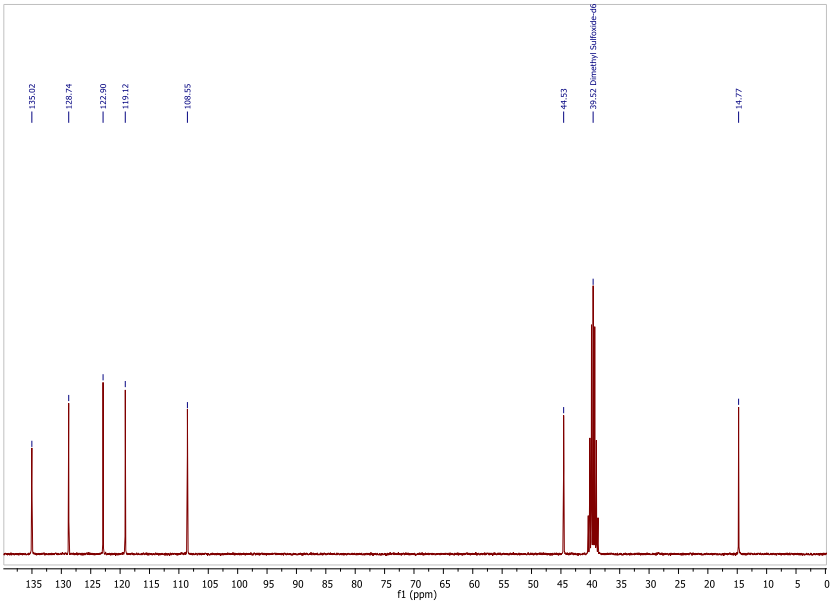

^{13}C NMR (75 MHz, DMSO) δ 135.02, 128.74, 122.90, 119.12, 108.55, 44.53, 14.77.

[VBuIm]Br

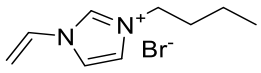

3-butyl-1-vinyl-1-imidazole-3-ium bromide

$C_9H_{15}N_2Br$ M = 231.14 g·mol^{-1}

Calculated: C: 46.77 H: 6.54 N: 12.12 Measured: C: 46.824 H: 6.438 N: 12.125

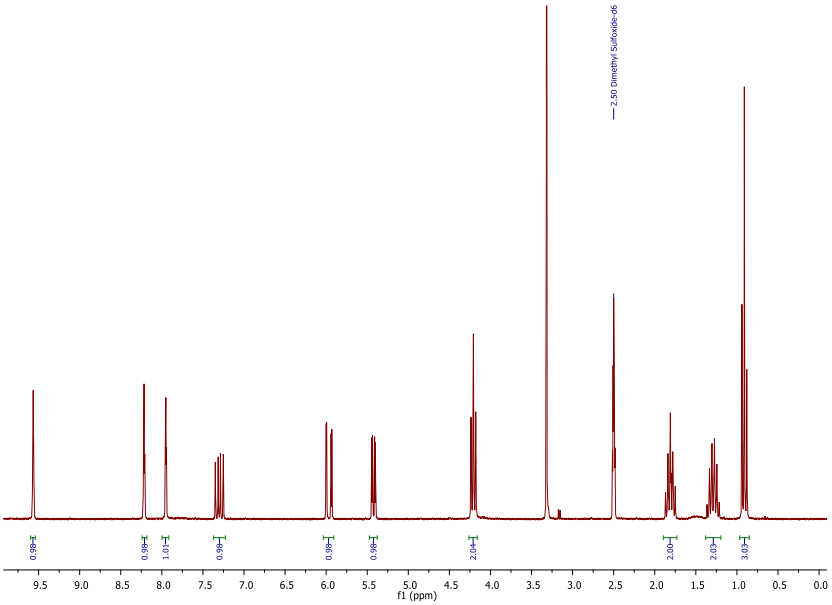

^{1}H NMR (250 MHz, DMSO) δ 8.21 (s, 1H), 7.94 (s, 1H), 7.25 (s, 1H), 5.93 (s, 1H), 5.40 (s, 1H), 4.19 (d, *J* = 7.1 Hz, 1H), 1.80 (s, 1H), 1.77 (d, *J* = 7.4 Hz, 1H), 1.26 (d, *J* = 7.3 Hz, 1H), 1.24 – 1.22 (m, 1H), 0.90 (d, *J* = 7.3 Hz, 1H).

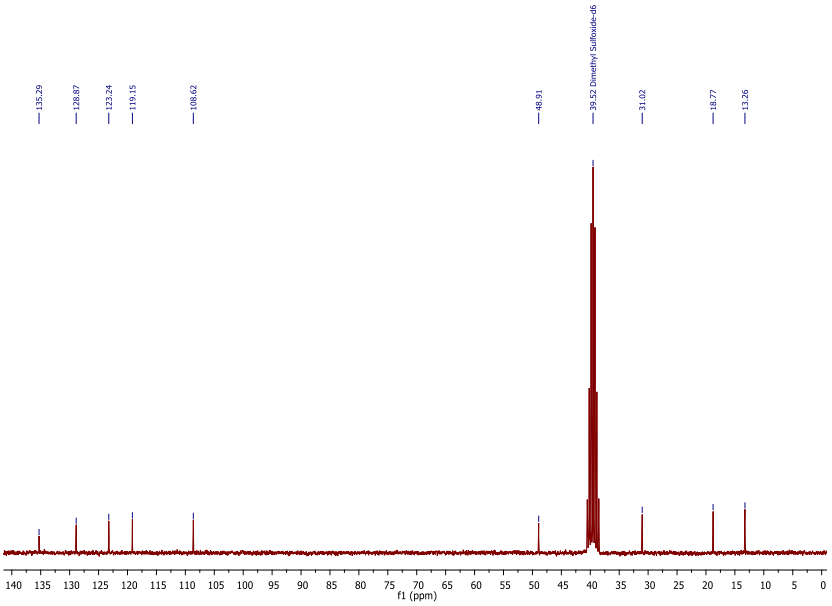

^{13}C NMR (63 MHz, DMSO) δ 135.29, 128.87, 123.24, 119.15, 108.62, 48.91, 31.02, 18.77, 13.26.

[VHexIm]Br

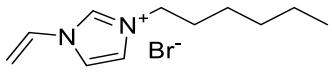

3-hexyl-1-vinyl-1-imidazole-3-ium bromide

$C_{11}H_{19}N_2Br$ M = 259.19 g·mol^{-1}

Calculated: C: 50.97 H: 7.39 N: 10.81 Measured: C: 51.048 H: 7.665 N: 11.113

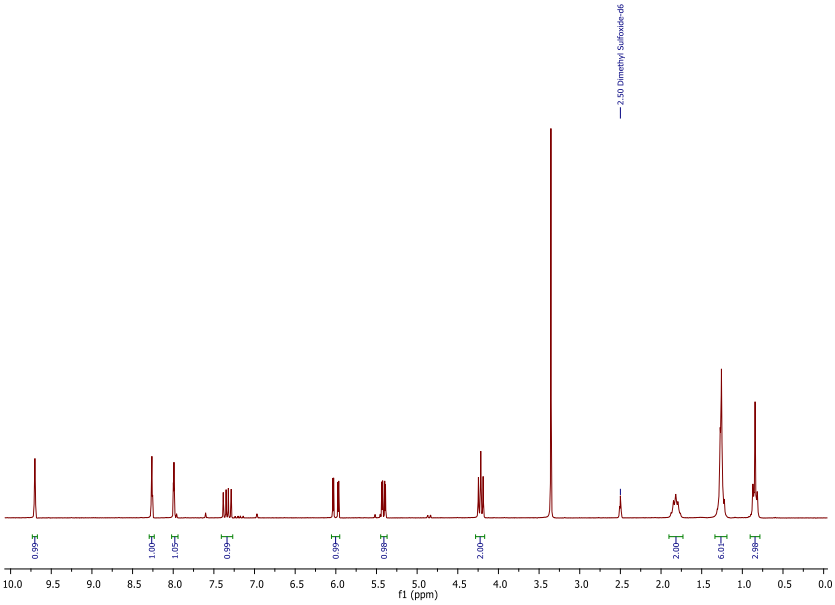

^{1}H NMR (250 MHz, DMSO) δ 9.70 (t, *J* = 1.5 Hz, 1H), 8.26 (t, *J* = 1.8 Hz, 1H), 7.98 (dd, *J* = 5.8, 4.1 Hz, 1H), 7.34 (dd, *J* = 15.7, 8.8 Hz, 1H), 6.00 (dd, *J* = 15.6, 2.4 Hz, 1H), 5.41 (dd, *J* = 8.7, 2.3 Hz, 1H), 4.22 (t, *J* = 7.3 Hz, 2H), 1.83 (dd, *J* = 13.8, 7.0 Hz, 2H), 1.34 – 1.19 (m, 6H), 0.90 – 0.78 (m, 3H).

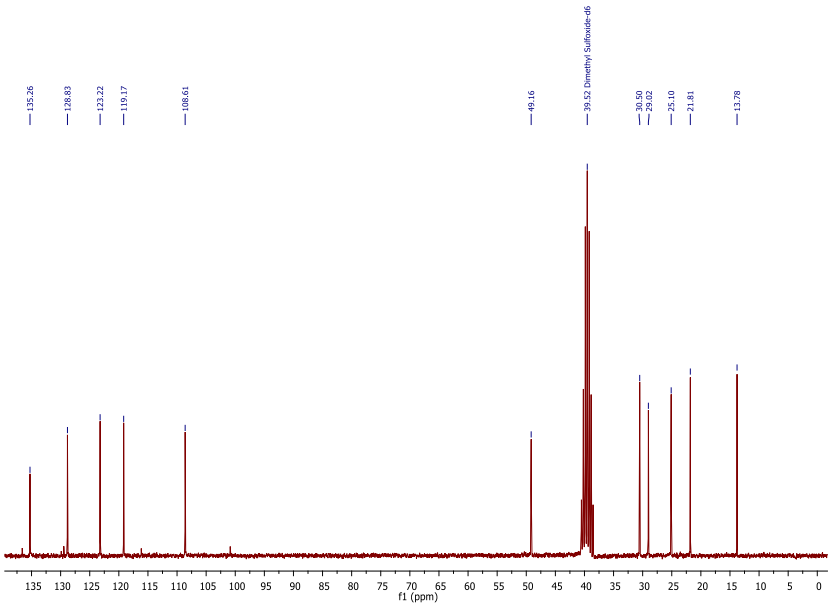

^{13}C NMR (63 MHz, DMSO) δ 135.26, 128.83, 123.22, 119.17, 108.61, 49.16, 30.50, 29.02, 25.10, 21.81, 13.78.

[VDodecIm]Br

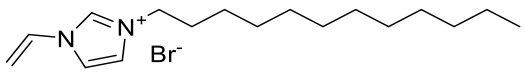

3-dodecyl-1-vinyl-1-imidazole-3-ium bromide

$C_{17}H_1N_2Br$ M = 343.35 g·mol^{-1}

Calculated: C: 59.47 H: 9.10 N: 8.16 Measured: C: 60.552 H: 9.257 N: 8.672

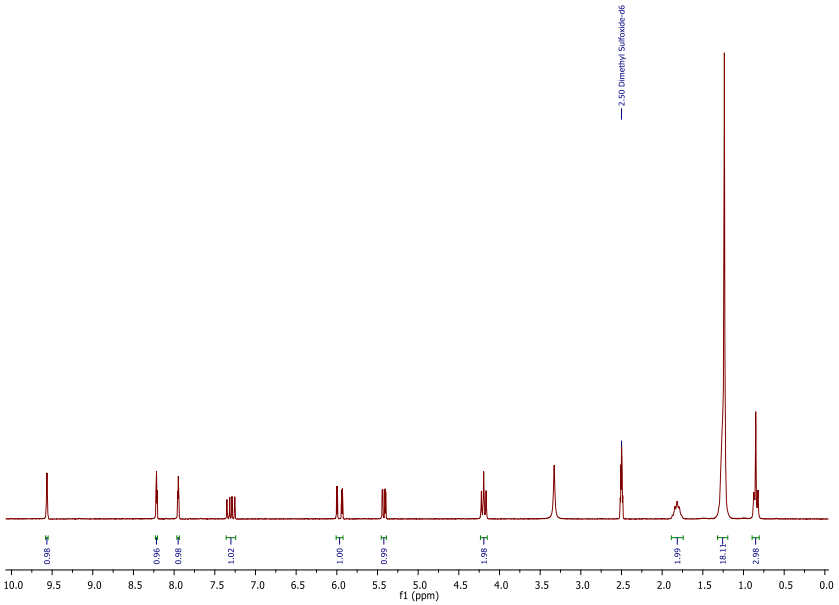

^{1}H NMR (250 MHz, DMSO) δ 9.56 (t, *J* = 1.5 Hz, 1H), 8.22 (t, *J* = 1.9 Hz, 1H), 7.95 (t, *J* = 1.7 Hz, 1H), 7.30 (dd, *J* = 15.6, 8.8 Hz, 1H), 5.97 (dd, *J* = 15.6, 2.3 Hz, 1H), 5.42 (dd, *J* = 8.7, 2.3 Hz, 1H), 4.19 (t, *J* = 7.2 Hz, 2H), 1.89 – 1.74 (m, 2H), 1.24 (s, 18H), 0.89 – 0.81 (m, 3H).

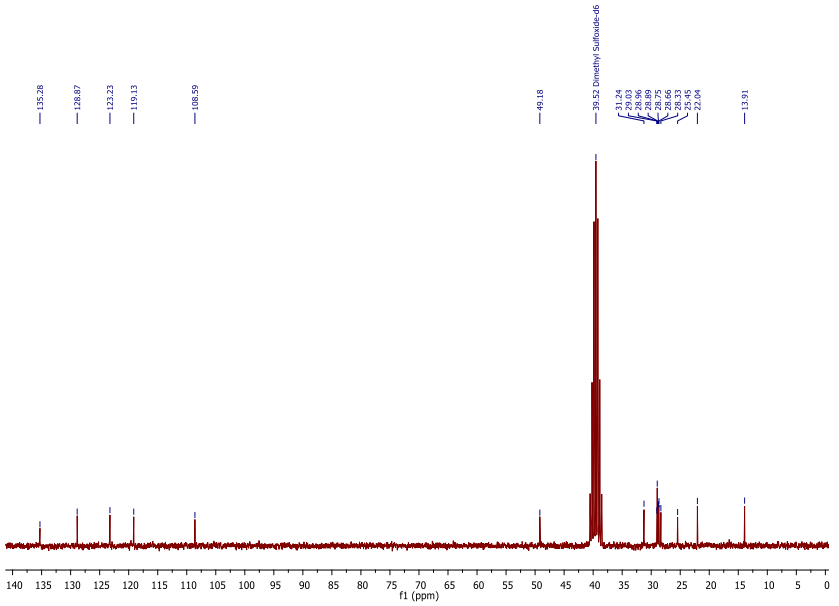

^{13}C NMR (63 MHz, DMSO) δ 135.28, 128.87, 123.23, 119.13, 108.59, 49.18, 31.24, 29.03, 28.96, 28.89, 28.75, 28.66, 28.33, 25.45, 22.04, 13.91.

[VPrylm]Br

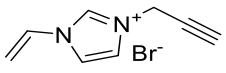

3-(prop-2-yn-1-yl)-1-vinyl-1-imidazole-3-ium bromide

$C_8H_9N_2Br$ M = 213.08 g·mol^{-1}

Calculated: C: 45.10 H: 4.26 N: 13.15 Measured: C: 45.149 H: 4.423 N: 13.288

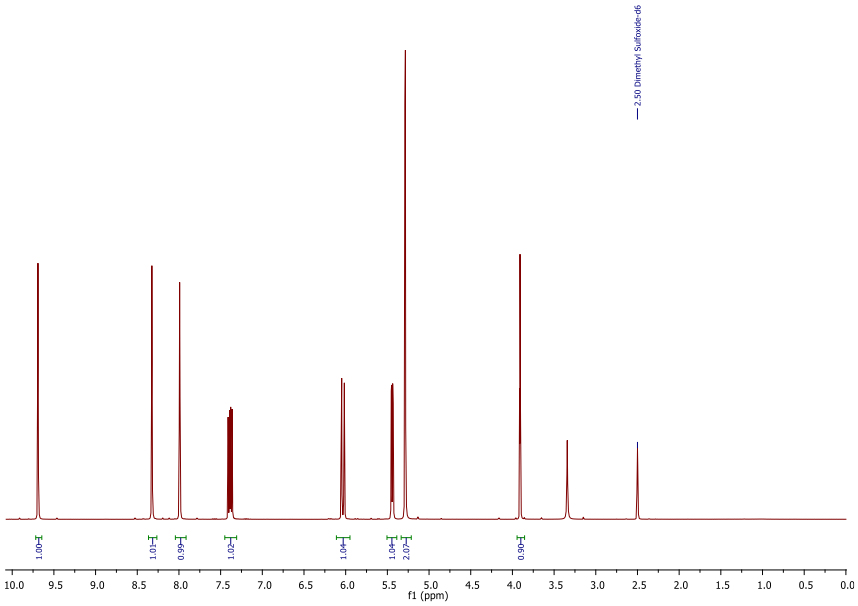

^{1}H NMR (500 MHz, DMSO) δ 9.69 (s, 1H), 8.32 (t, *J* = 1.7 Hz, 1H), 7.99 (s, 1H), 7.39 (dd, *J* = 15.7, 8.8 Hz, 1H), 6.03 (dd, *J* = 15.7, 2.4 Hz, 1H), 5.44 (dd, *J* = 8.7, 2.4 Hz, 1H), 5.29 (d, *J* = 2.5 Hz, 2H), 3.91 (t, *J* = 2.5 Hz, 1H).

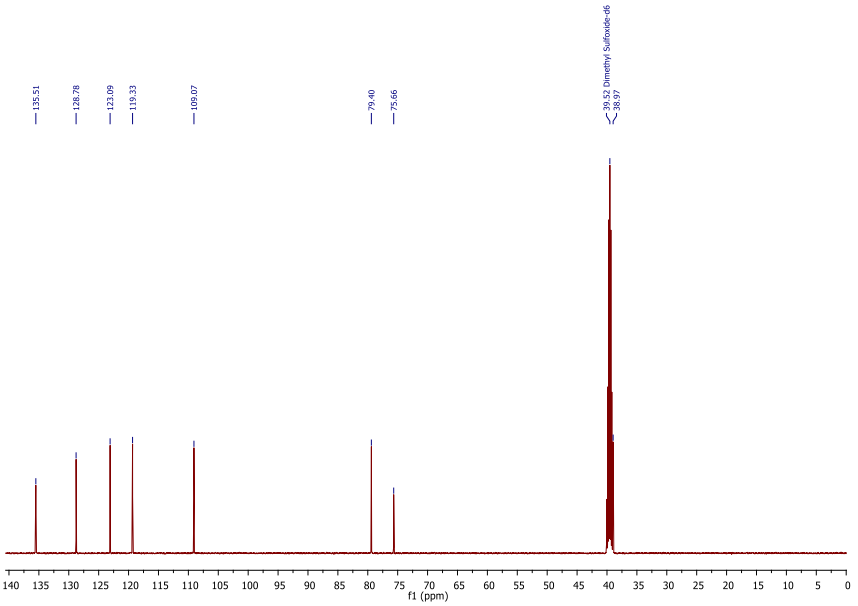

^{13}C NMR (126 MHz, DMSO) δ 135.51, 128.78, 123.09, 119.33, 109.07, 79.40, 75.66, 39.52, 38.97.

[VBnIm]Br

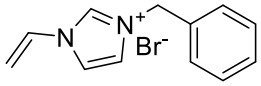

3-benzyl-1-vinyl-1-imidazole-3-ium bromide

$C_{12}H_{13}N_2Br$ M = 265.15 g·mol^{-1}

Calculated: C: 54.36 H: 4.94 N: 10.57 Measured: C: 54.464 H: 5.565 N: 10.050

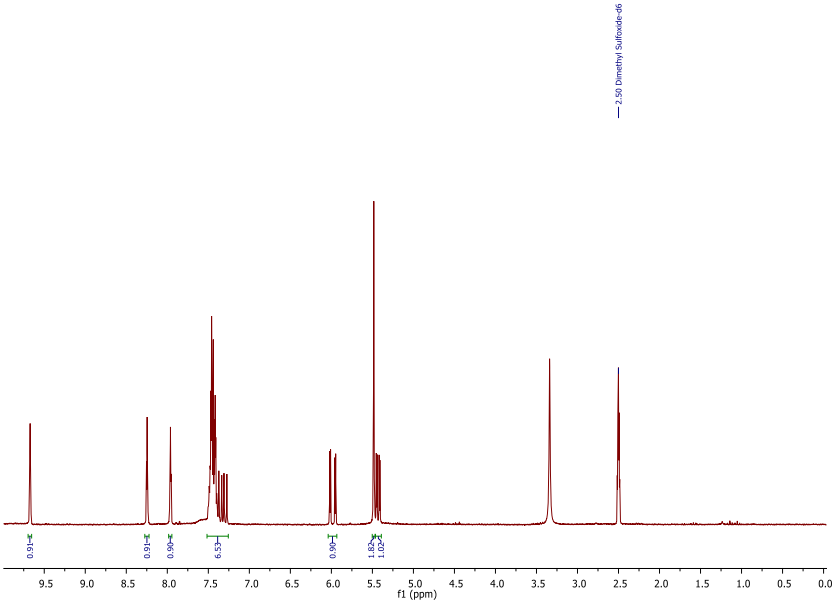

^{1}H NMR (250 MHz, DMSO) δ 9.67 (s, 1H), 8.25 (t, *J* = 1.8 Hz, 1H), 7.96 (t, *J* = 1.7 Hz, 1H), 7.52 – 7.26 (m, 7H), 5.98 (dd, *J* = 15.6, 2.4 Hz, 1H), 5.48 (s, 2H), 5.43 (dd, *J* = 8.7, 2.4 Hz, 1H).

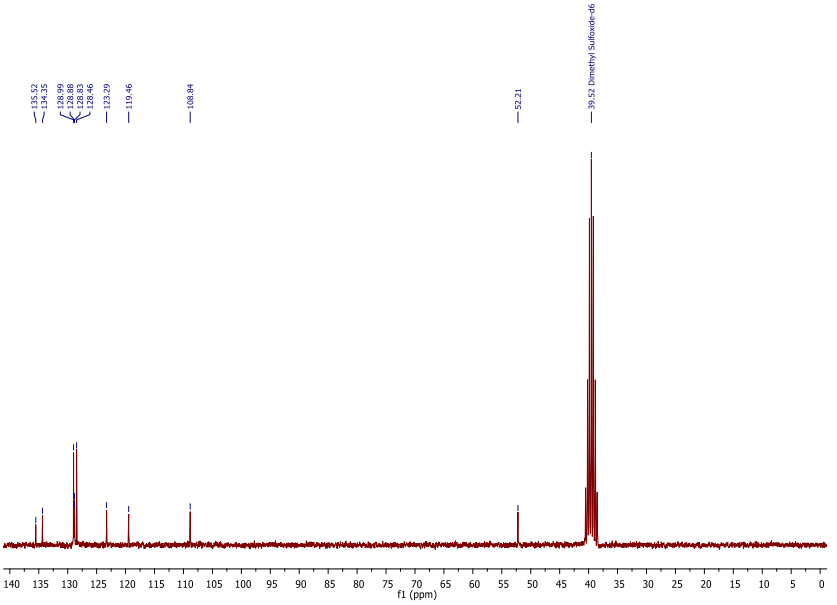

^{13}C NMR (63 MHz, DMSO) δ 135.52, 134.35, 128.99, 128.88, 128.83, 128.46, 123.29, 119.46, 108.84, 52.21.

A2. High Pressure Liquid Chromatography

Calcium gluconate concentrations were analyzed by HPLC and internal calibration using a RI detector K-2301, a degasser, a HPLC pump (all from *Knauer*, Berlin, Germany), a HyperREZ XP carbohydrate H+ 8µm column (*Phenomenex*, Aschaffenburg, Germany), a *Smartline* autosampler 2800 and Eurochrom 2000 (both Knauer, Berlin, Germany) as analyzing software.

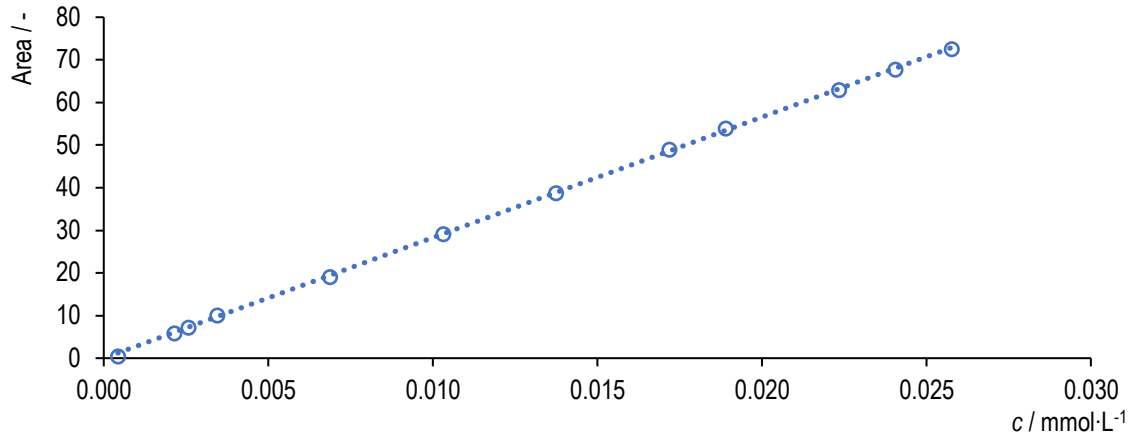

Figure i: Calibration of calcium gluconate ($y = 2828.3 \cdot x$, $R^2 = 0.9998$).

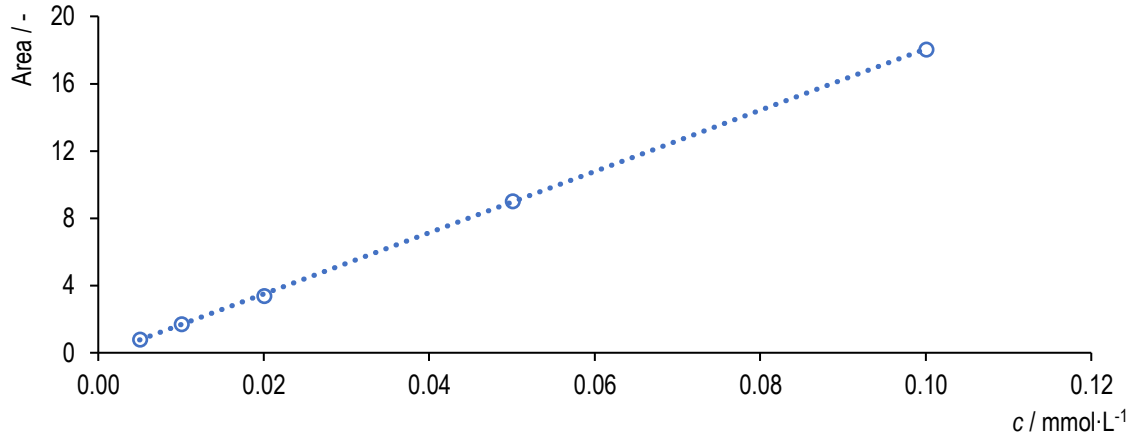

Figure ii: Calibration of D-glucose ($y = 182.09 \cdot x - 0.1454$, $R^2 = 0.9999$).

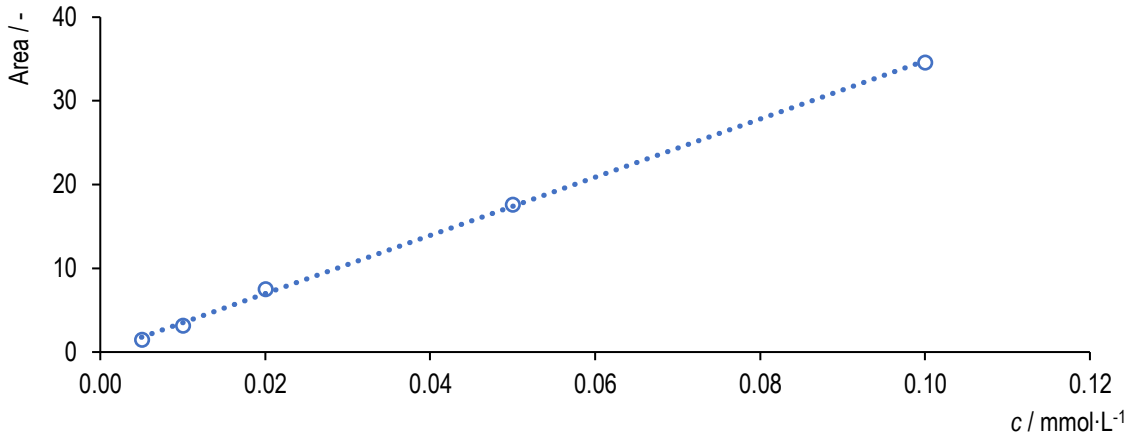

Figure iii: Calibration of sucrose (y = 347.5·x + 0.0295, R^2 = 0.9992).

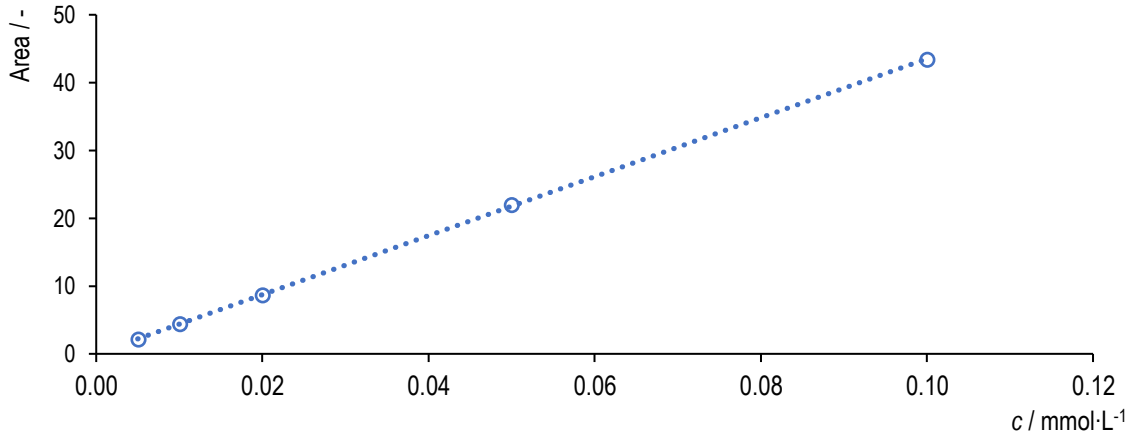

Figure iv: Calibration of raffinose (y = 434.74·x + 0.0348, R^2 = 0.9999).

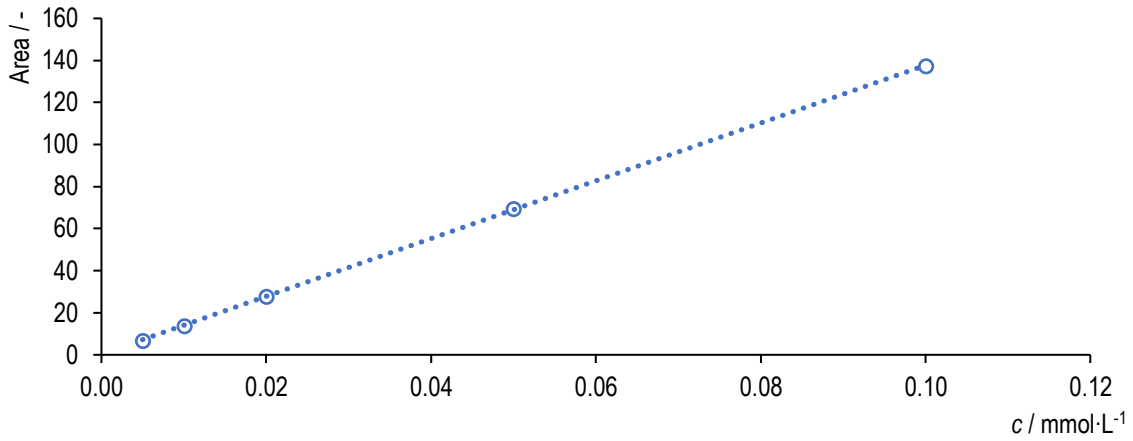

Figure v: Calibration of sodium gluconate (y = 1373.5·x + 0.3452, R^2 = 0.9999).

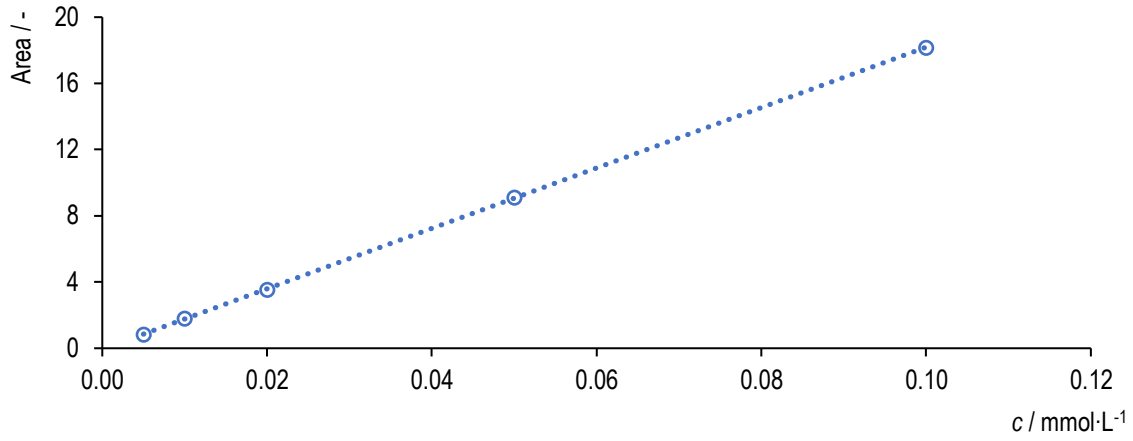

Figure vi: Calibration of D-mannitol (y = 182.46·x + 0.0577, R^2 = 0.9999).

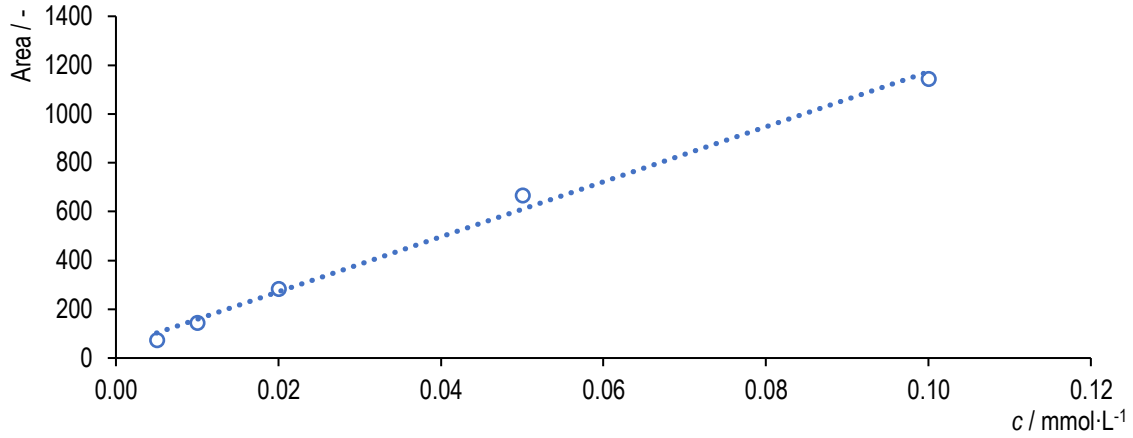

Figure vii: Calibration of sodium pyruvate (y = 11264·x + 46.166, R^2 = 0.9933).

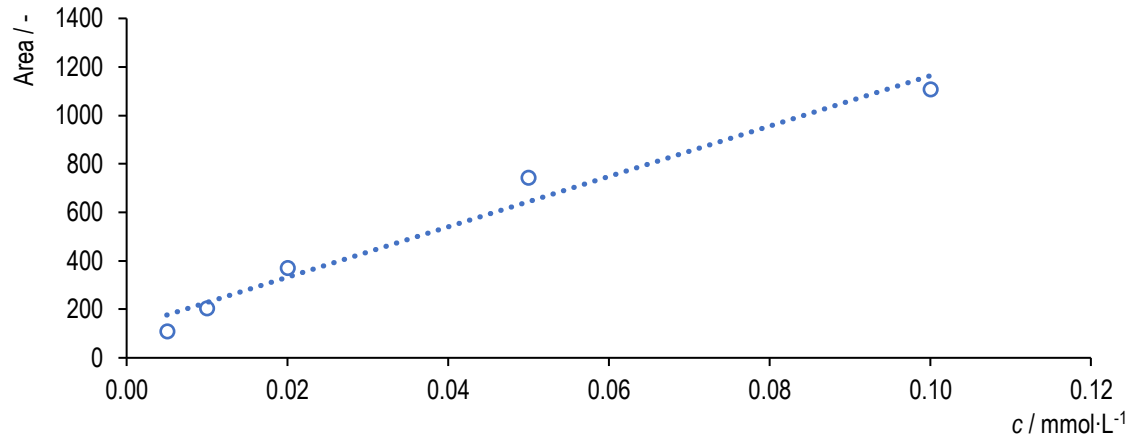

Figure viii: Calibration of *N*-acetylneuraminic acid (y = 10388·x + 124.6, R^2 = 0.9712).

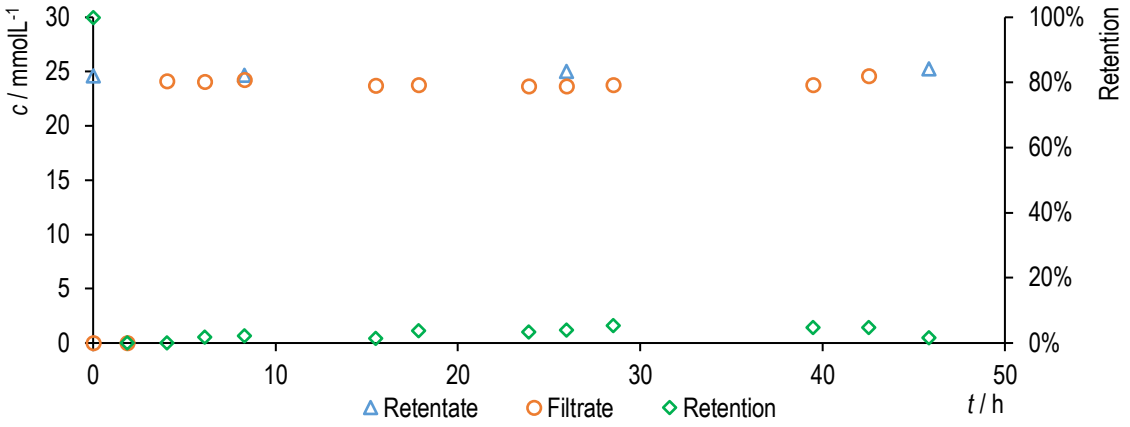

Figure ix: Concentration of D-glucose in samples of retentate, filtrate and retention over the filtration time using PILs BD2.

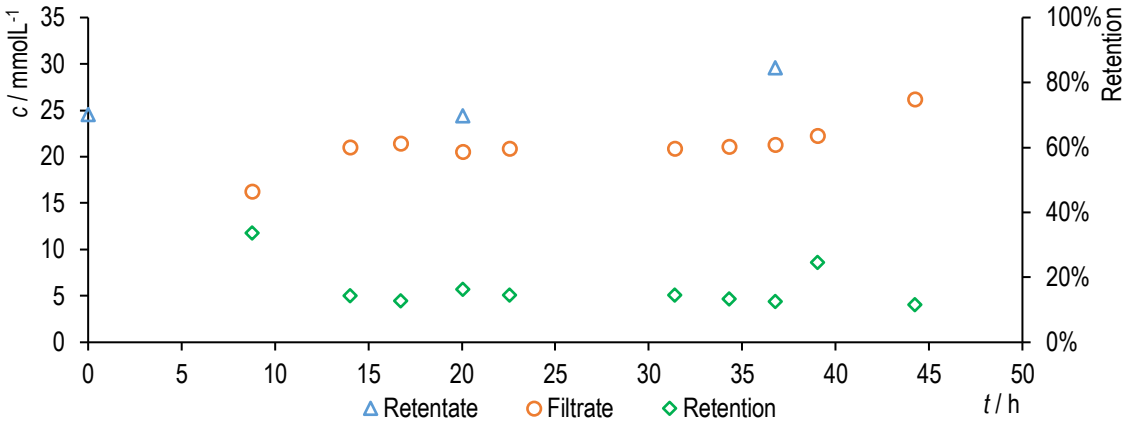

Figure x: Concentration of sucrose in samples of retentate, filtrate and retention over the filtration time using PILs BD2.

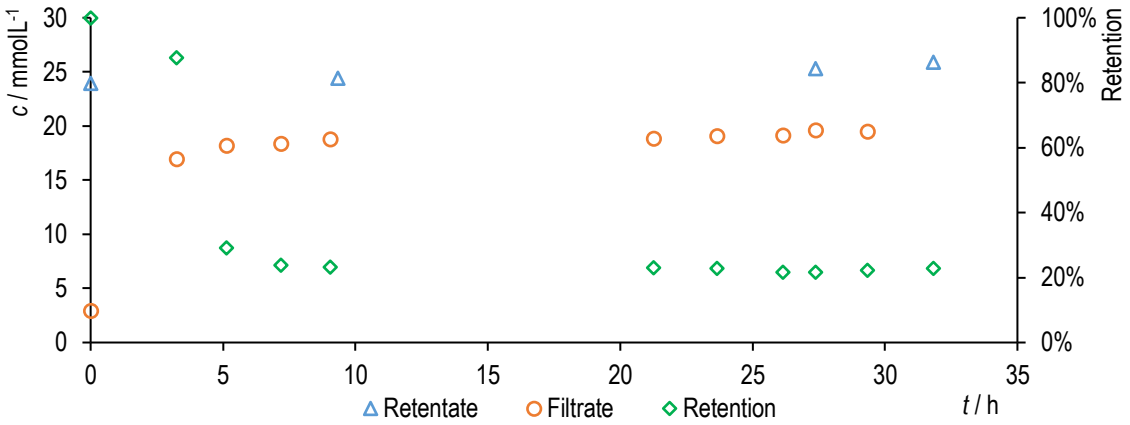

Figure xi: Concentration of raffinose in samples of retentate, filtrate and retention over the filtration time using PILs BD2.

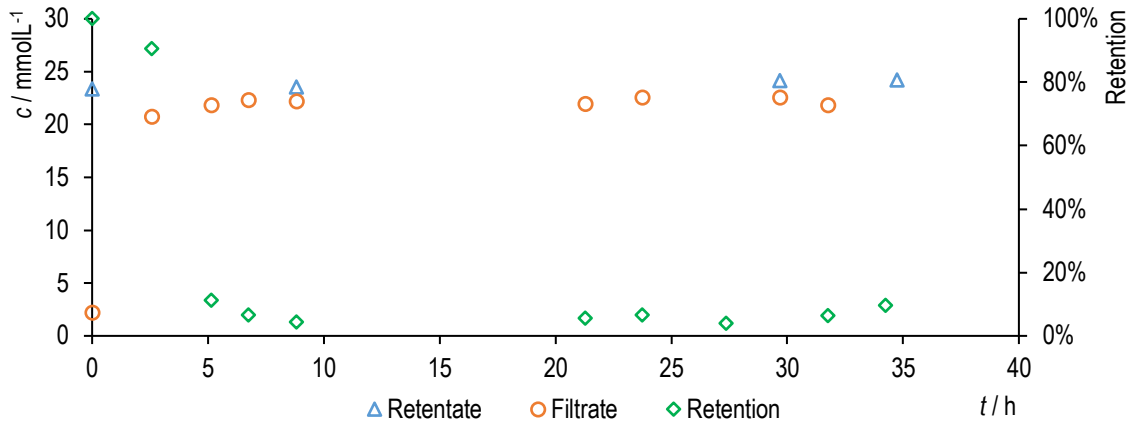

Figure xii: Concentration of D-mannose in samples of retentate, filtrate and retention over the filtration time using PILs BD2.

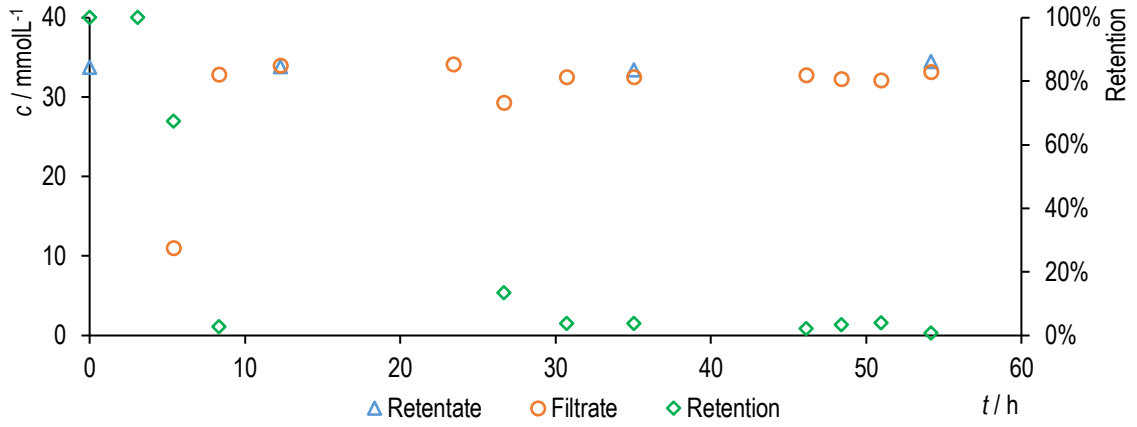

Figure xiii: Concentration of *N*-acetylneuraminic acid in samples of retentate, filtrate and retention over the filtration time using PILs BD2.

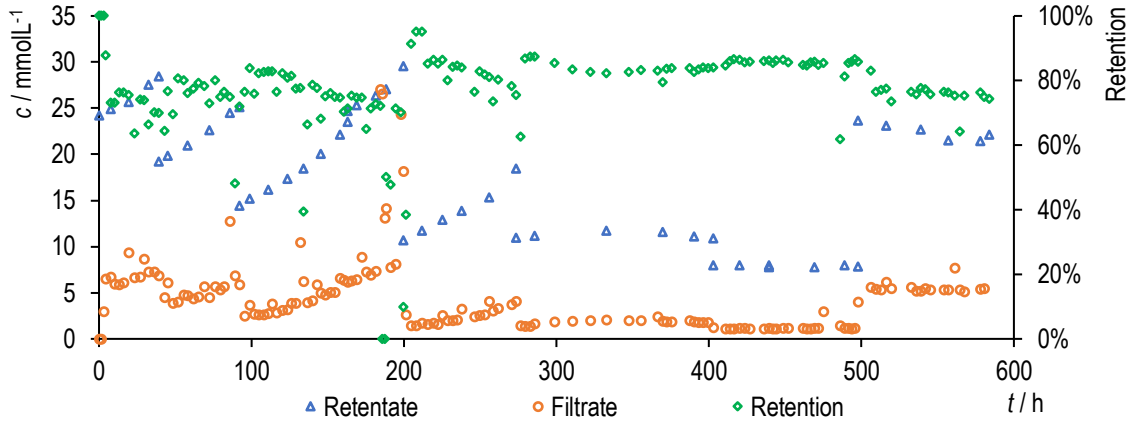

Figure xiv: Filtration of calcium gluconate in dead-end mode using PILs BD2.

A3. Atomic Force Microscopy

Appropriate pieces were taken of the casted membrane sheets and stocked on glass coverslips using epoxy resin to ensure a rigid mount. A NE100 (*Park Systems*, Korea) in dynamic mode was used to obtain the AFM topographies. Equipped with metal coated silicon cantilevers (type ACTA, AppNano, aluminum-coating, 300 kHz and HA-HR, SpectraInstruments, gold-coating, 380 kHz), setpoint and oscillation amplitude were chosen to minimize tip-sample interaction by soft tapping mode or non-contact mode. Investigation of several sample locations ensured the significance of observations.

A4. UV/VIS

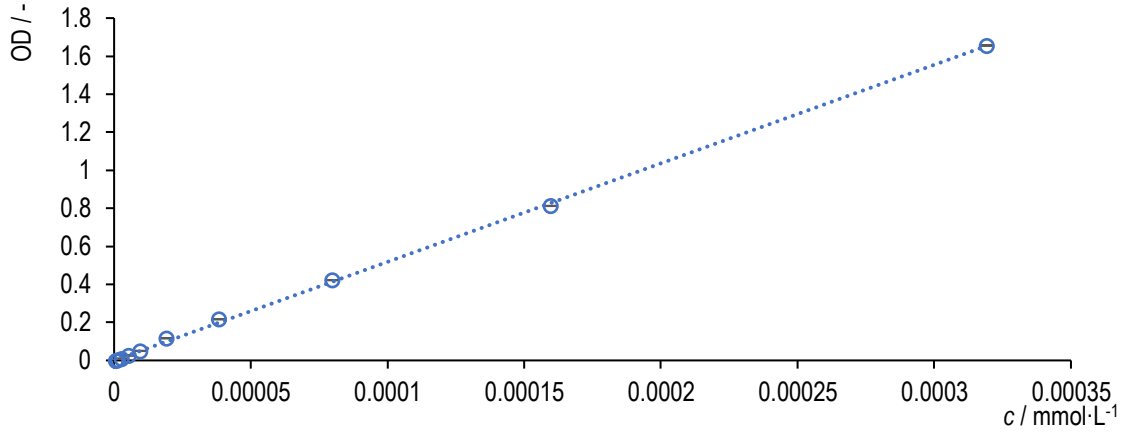

Figure xv: Calibration of Rimazol Brilliant Blue R (λ = 596 nm, y = 5181.3·x, R^2 = 0.9996).

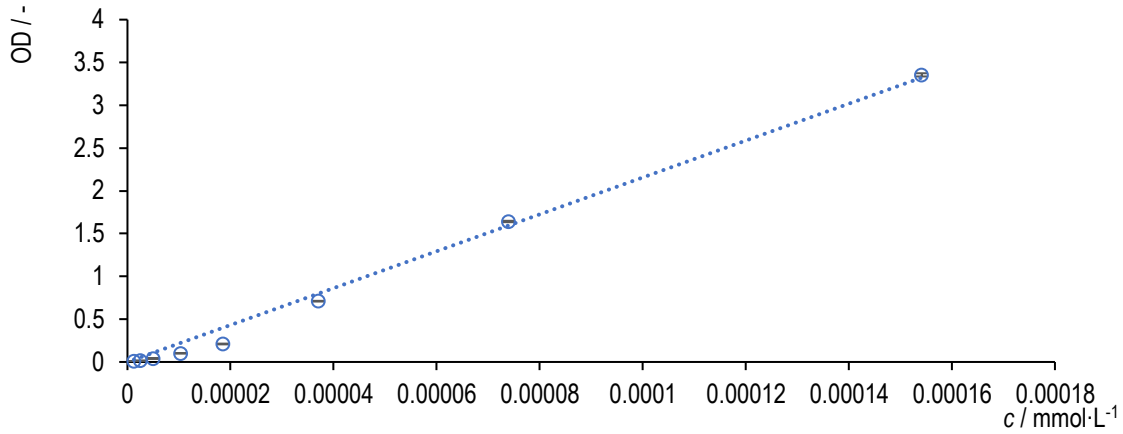

Figure xvi: Calibration of Malachite Green (λ = 617 nm, y = 21554·x, R^2 = 0.9932).

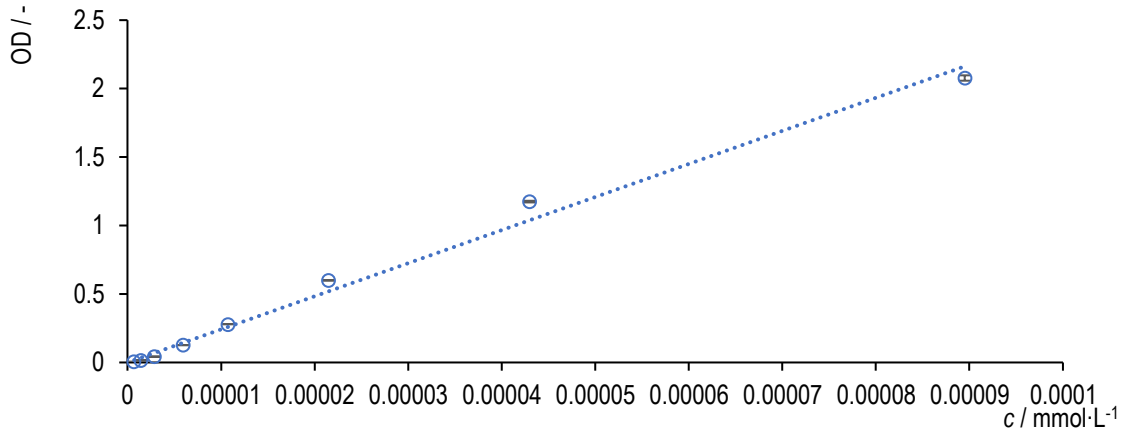

Figure xvii: Calibration of Acridineorange (λ = 492.5 nm, y = 24162·x, R^2 = 0.991).

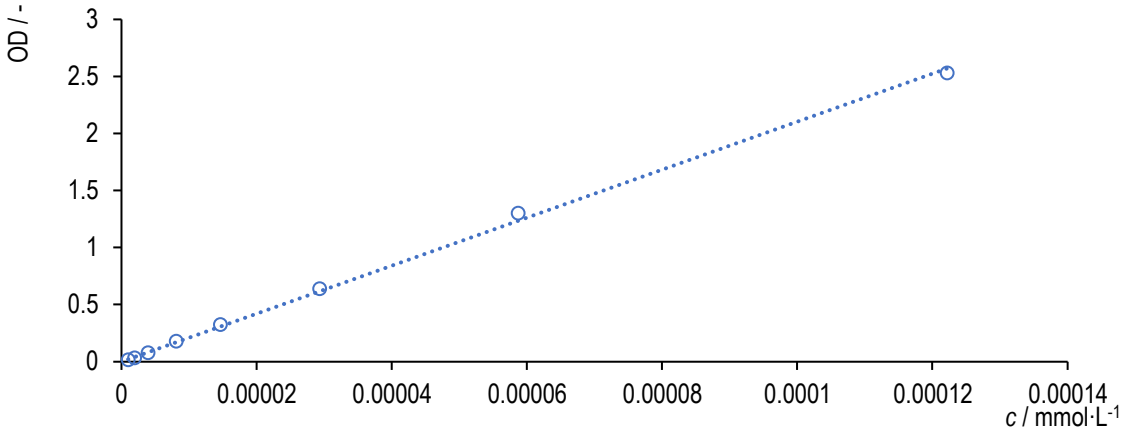

Figure xviii: Calibration of Methyl Orange (λ = 460.5 nm, y = 21037·x, R^2 = 0.9987).

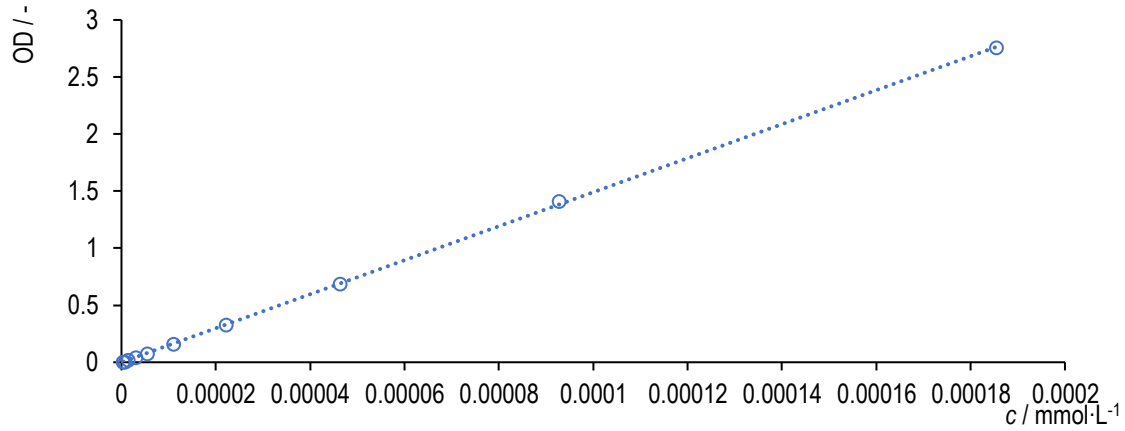

Figure xix: Calibration of Bromphenyl Red (λ = 429 nm, y = 14902·x, R^2 = 0.9998).

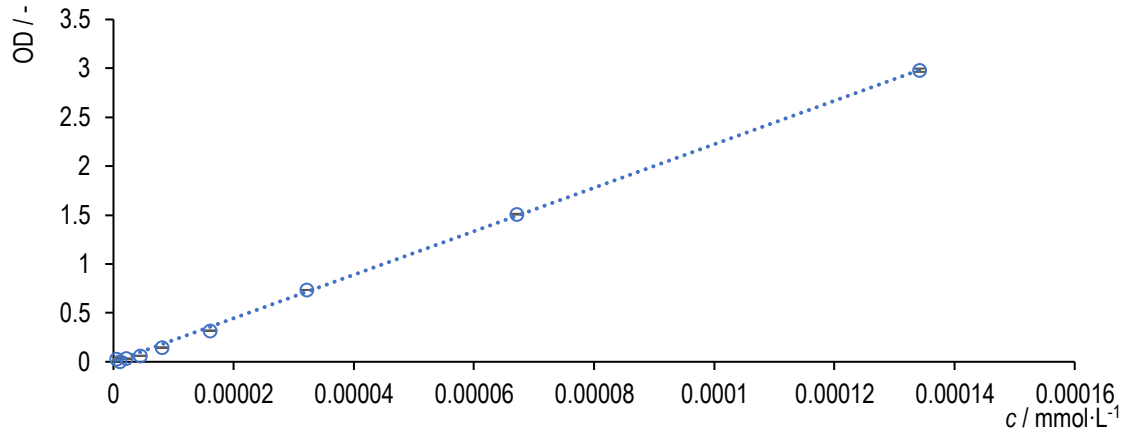

Figure xx: Calibration of Nile Blue (λ = 601.5 nm, y = 22238·x, R^2 = 0.9993).

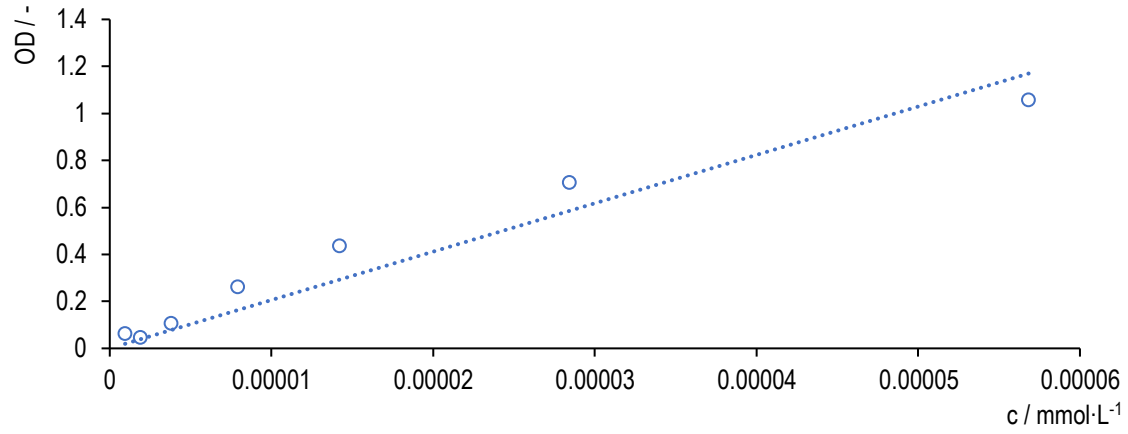

Figure xxi: Calibration of Methyl Orange in basic conditions (y = 20584·x, R^2 = 0.9682, pH = 12).

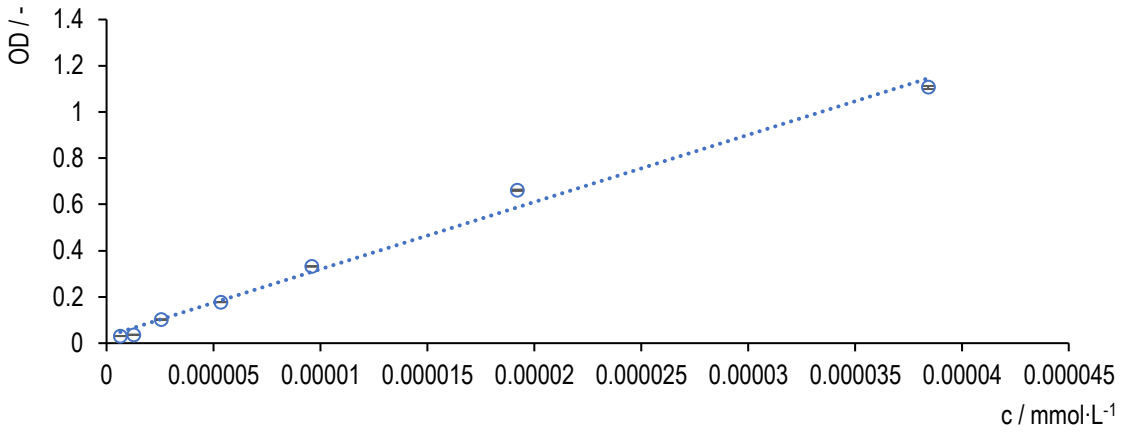

Figure xxii: Calibration of Acridine Orange in acidic conditions (y = 29051·x, R^2 = 0.9908, pH = 1).

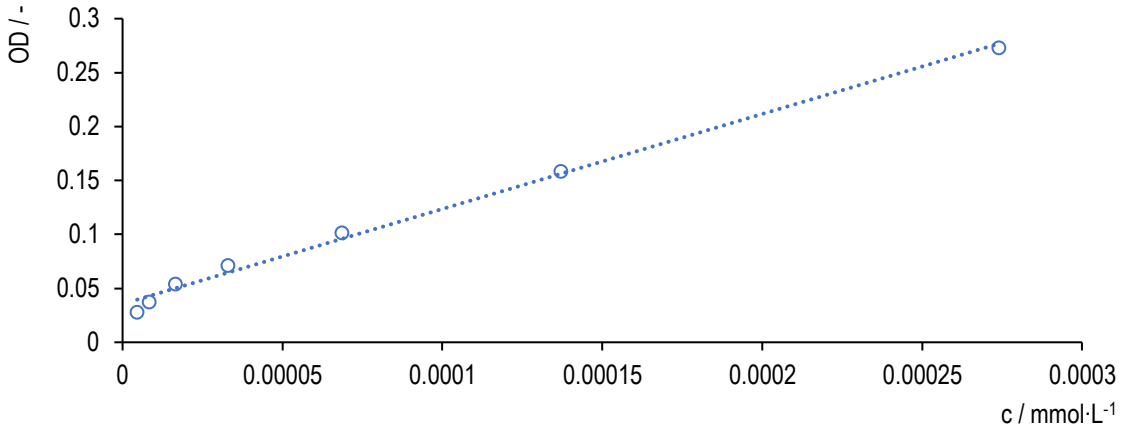

Figure xxiii: Calibration of Rimazol Brilliant Blue R in acidic conditions (y = 880.35·x, R^2 = 0.9936, pH = 1).

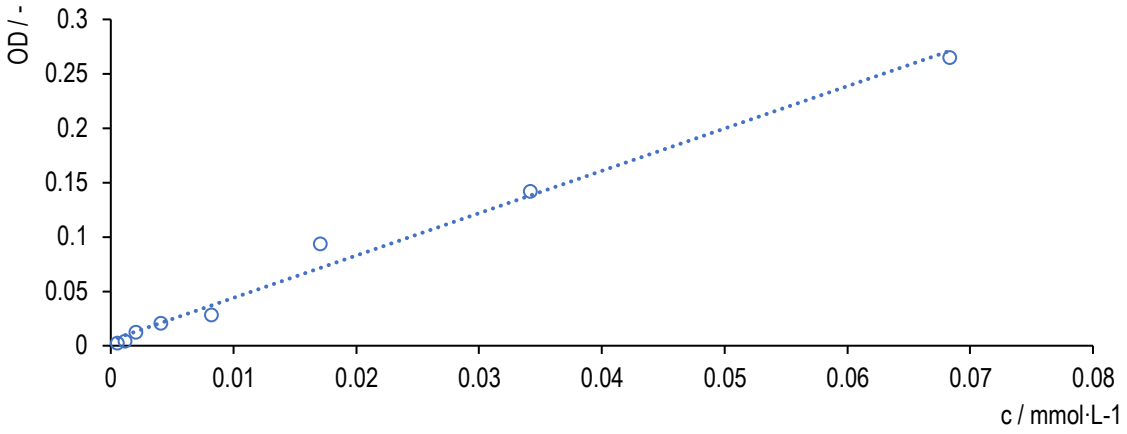

Figure xxiv: Calibration of Brom Phenyl Red in basic conditions (y = 3.8928·x, R^2 = 0.9888, pH = 12).

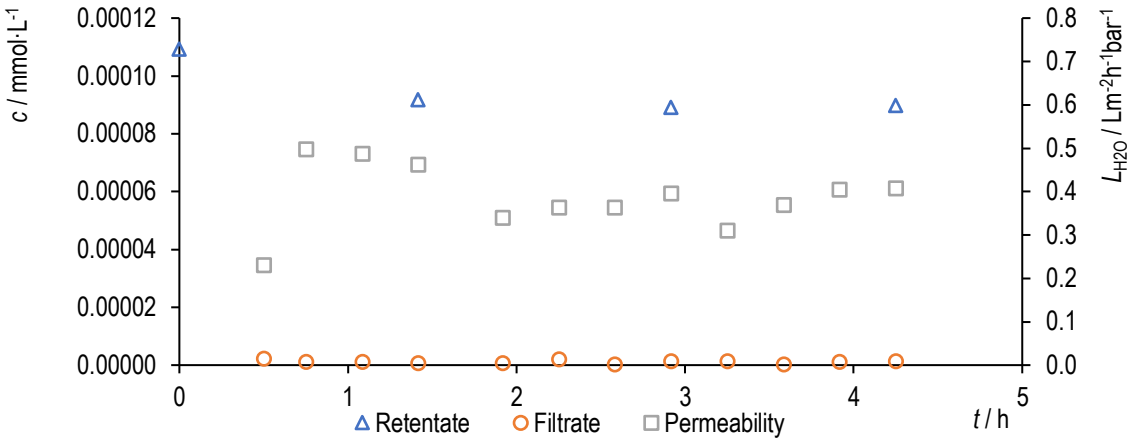

Figure xxv: Filtration of Rimazol Brilliant Blue R with PILs BD2.

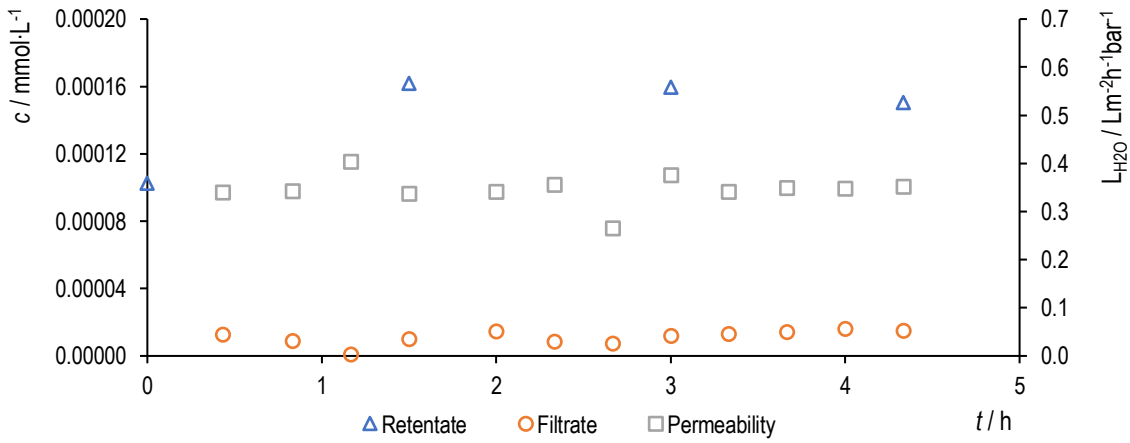

Figure xxvi: Filtration of Malachite Green with PILs BD2.

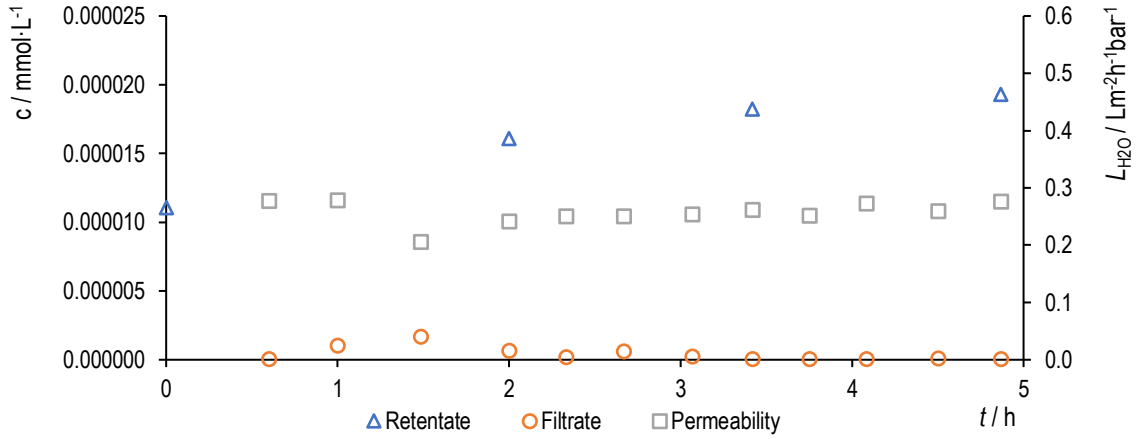

Figure xxvii: Filtration of Acridine Orange with PILs BD2.

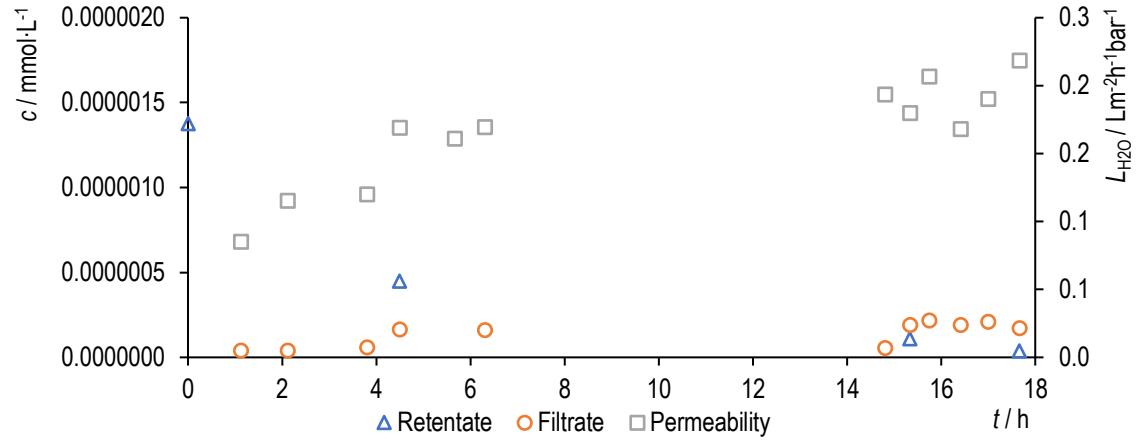

Figure xxviii: Filtration of Methyl Orange with PILs BD2.

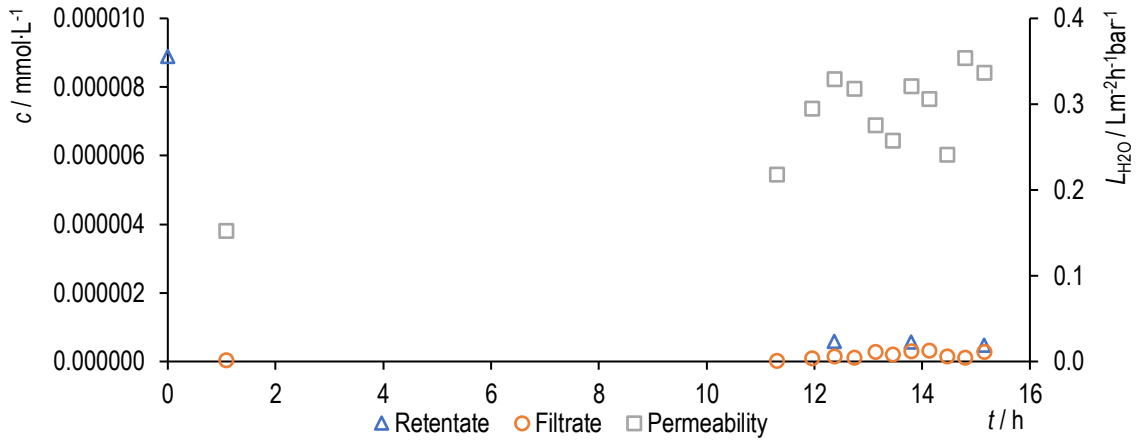

Figure xxix: Filtration of Bromphenol Red with PILs BD2.

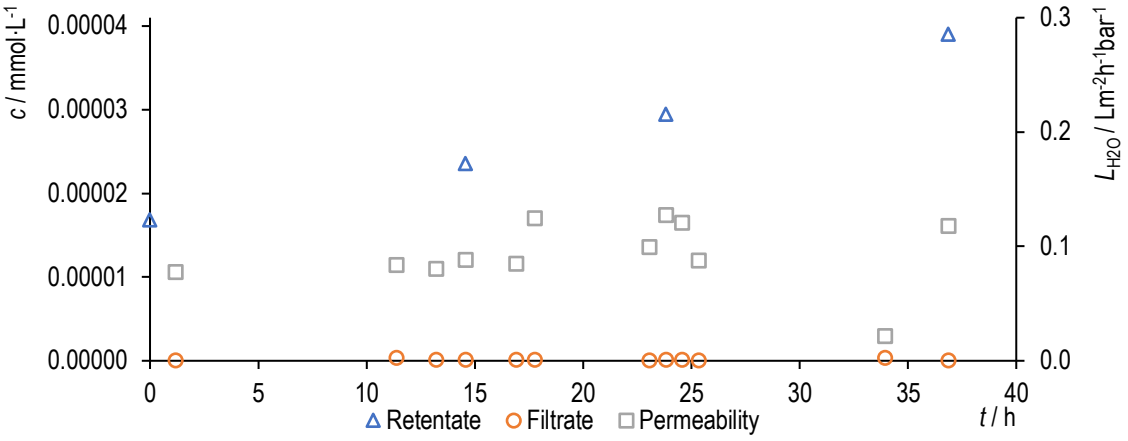

Figure xxx. Filtration of Nile Blue with PILs BD2.

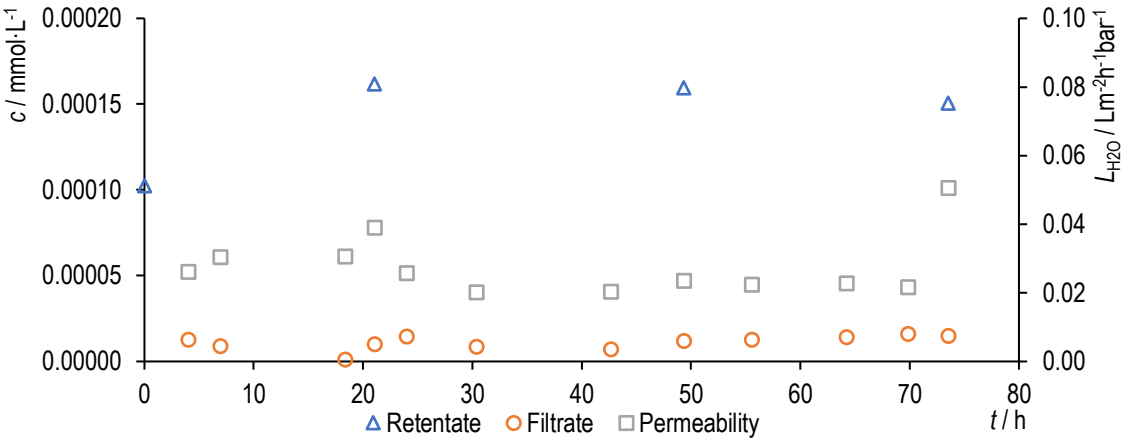

Figure xxxi: Filtration of Malachite Green with PILs BE1.

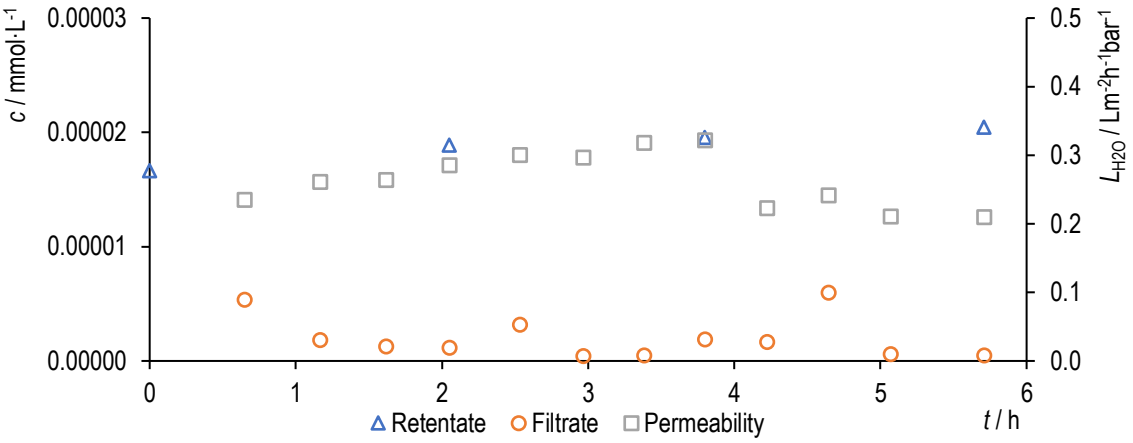

Figure xxxii: Filtration of Acridine Orange with PILs BE1.

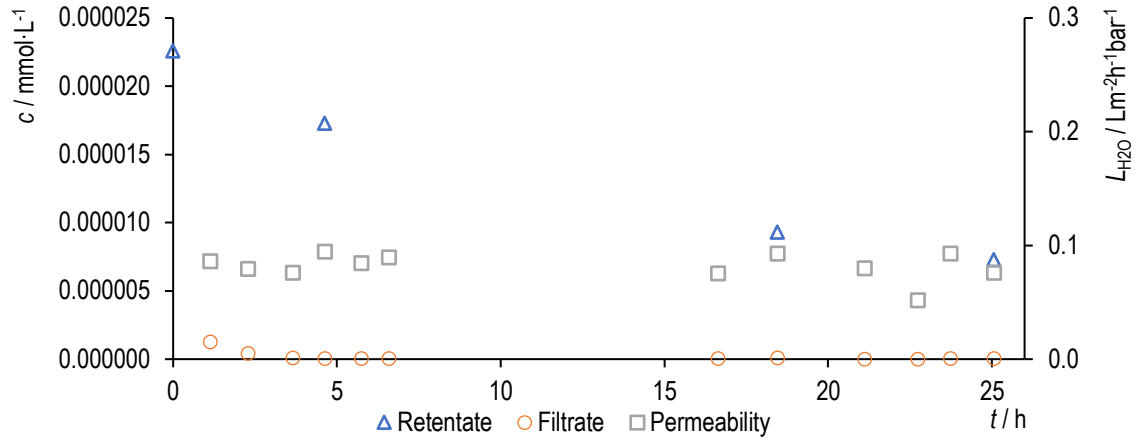

Figure xxxiii: Filtration of Methyl Orange with PILs BE1.

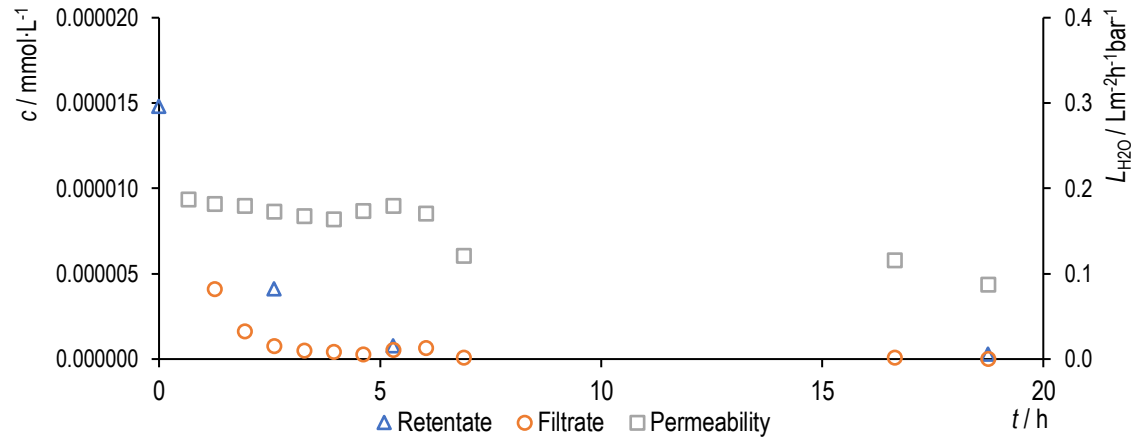

Figure xxxiv: Filtration of Bromphenol Red with PILs BE1.

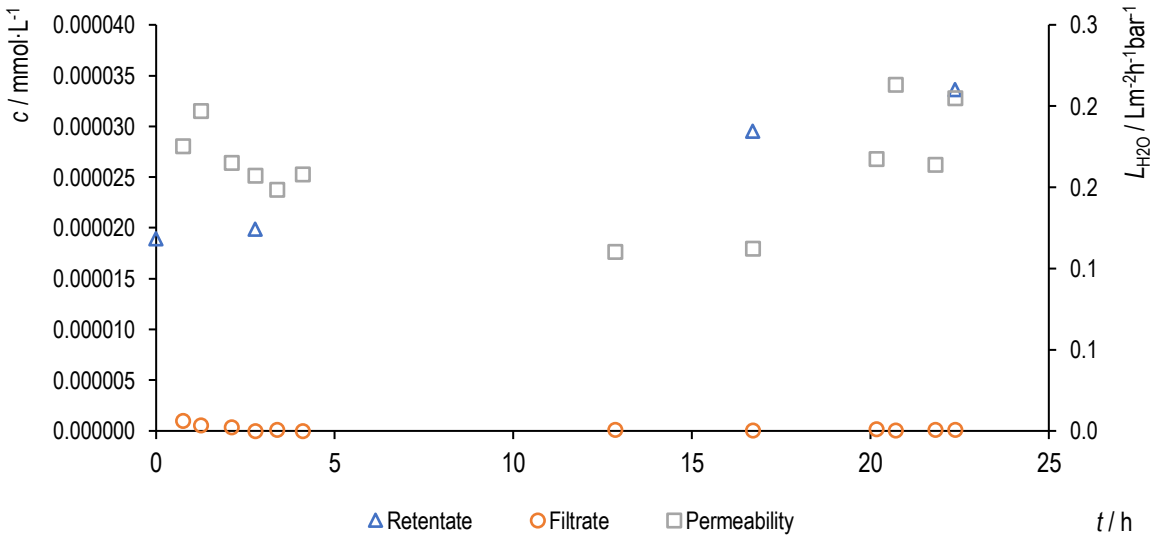

Figure xxxv. Filtration of Nile Blue with PILs BE1.

A5. Electrodialysis

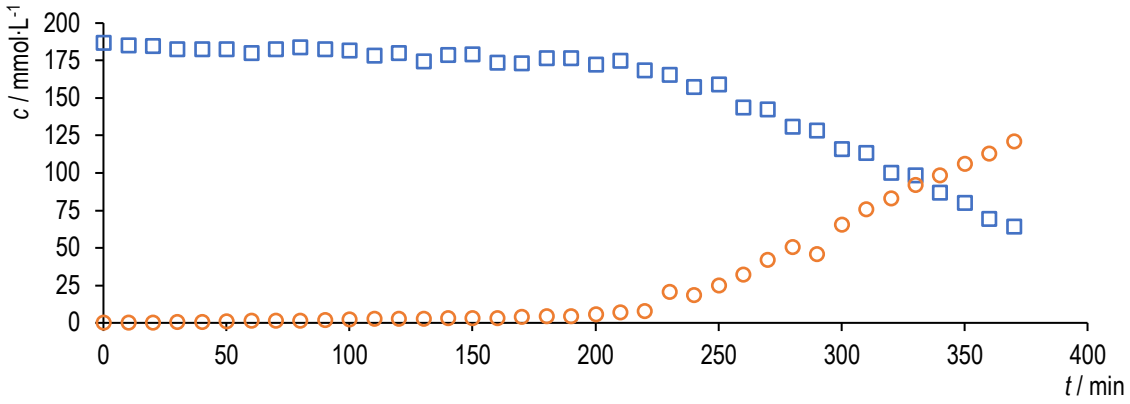

Figure xxxvi: Concentration of acetic acid (circles) and sodium acetate (squares) in electrodialysis using two PILs BD2 at 3 V (0-60 min), 6 V (60-120 min), 10 V (120-180 min) and 15 V (180-370 min).

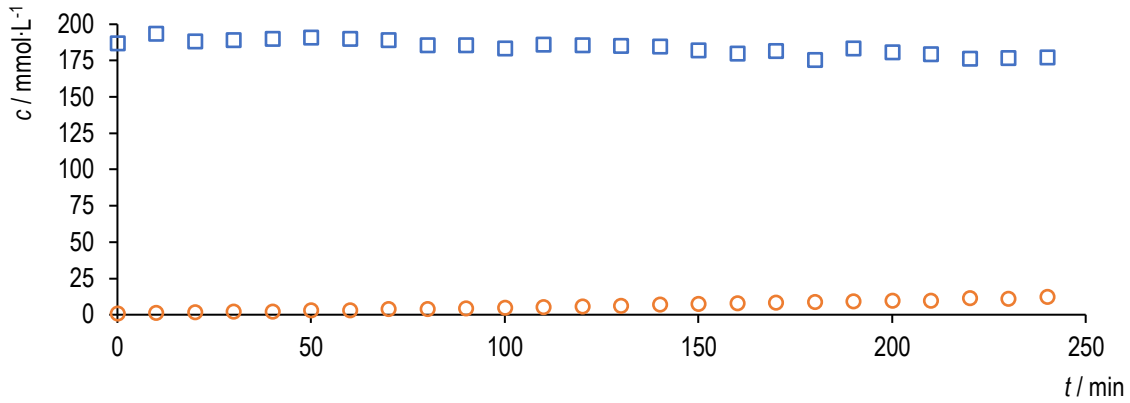

Figure xxxvii: Concentration of acetic acid (circles) and sodium acetate (squares) in electrodialysis using three PILs BD2 at 3 V (0-60 min), 6 V (60-120 min), 10 V (120-180 min) and 15 V (180-240 min).

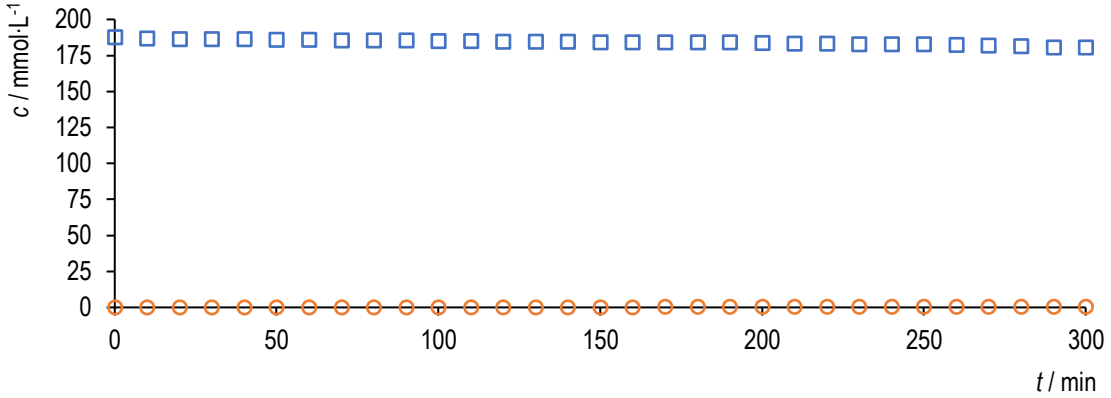

Figure xxxviii: Concentration of acetic acid (circles) and sodium acetate (squares) in electrodialysis using PILs BD3 at 3 V (0-60 min), 6 V (60-120 min), 10 V (120-180 min) and 15 V (180-300 min).

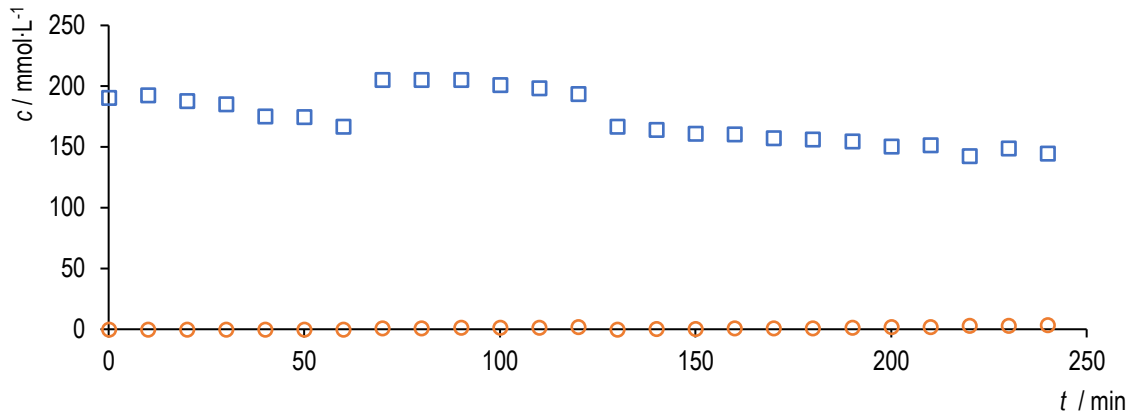

Figure xxxix: Concentration of acetic acid (circles) and sodium acetate (squares) in electrodialysis using PILs BE1 at 3 V (0-60 min), 6 V (60-120 min), 10 V (120-180 min) and 15 V (180-240 min).

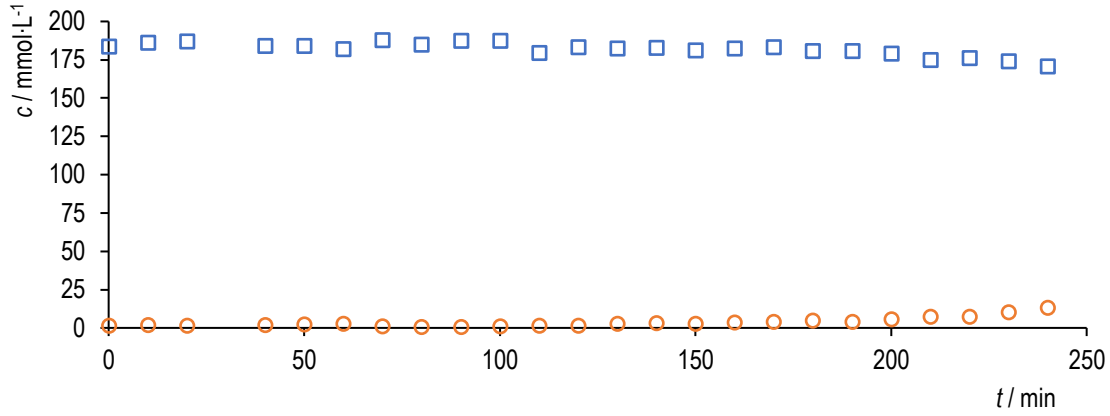

Figure xl: Concentration of acetic acid (circles) and sodium acetate (squares) in electrodialysis using two PILs BE1 at 3 V (0-60 min), 6 V (60-120 min), 10 V (120-180 min) and 15 V (180-240 min).

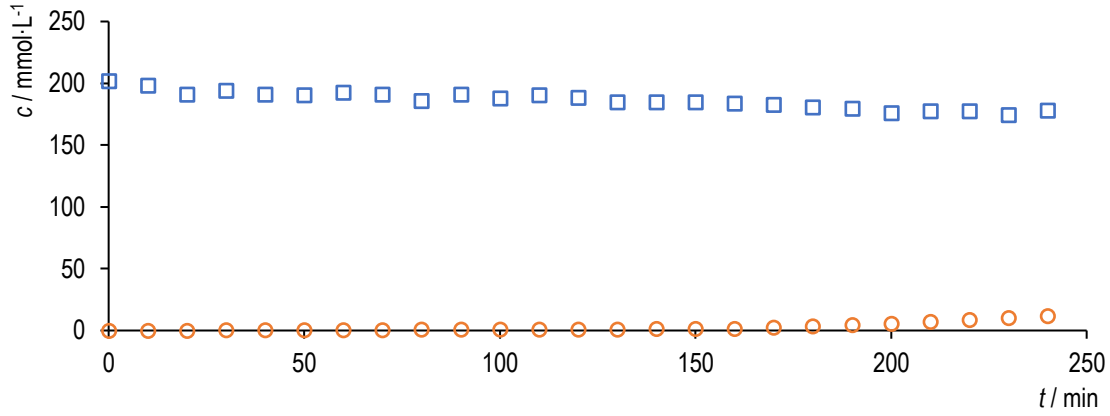

Figure xli: Concentration of acetic acid (circles) and sodium acetate (squares) in electrodialysis using three PILs BE1 at 3 V (0-60 min), 6 V (60-120 min), 10 V (120-180 min) and 15 V (180-240 min).

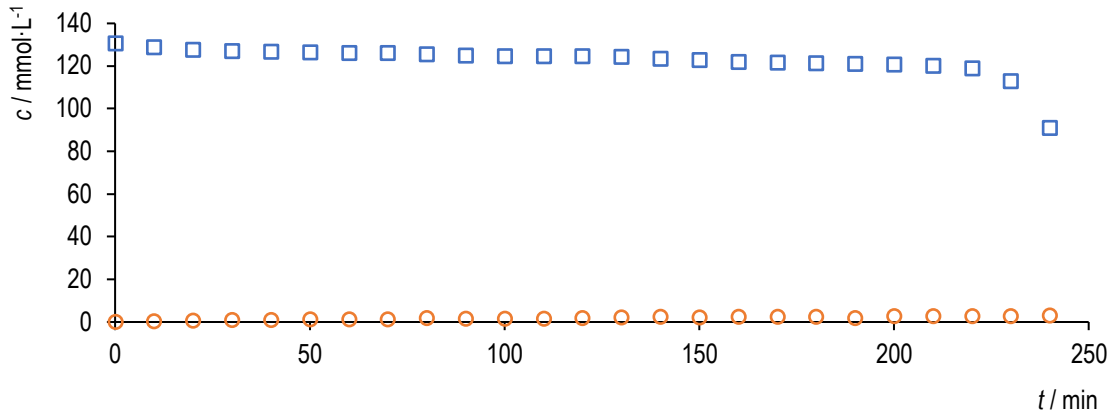

Figure xlii: Concentration of sodium gluconate (circles) and gluconic acid (squares) in electrodialysis using PILs BD2 at 3 V (0-60 min), 6 V (60-120 min), 10 V (120-180 min) and 15 V (180-240 min).

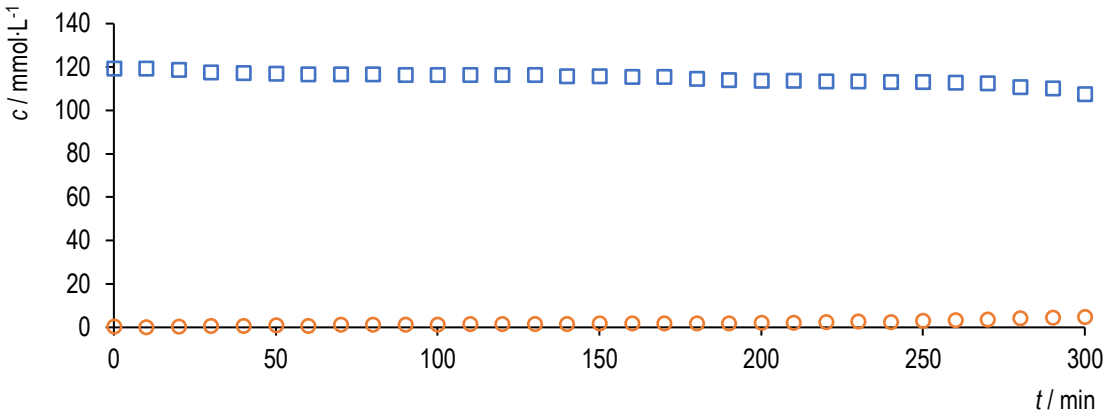

Figure xliii: Concentration of potassium gluconate (circles) and gluconic acid (squares) in electrodialysis using PILs BD2 at 3 V (0-60 min), 6 V (60-120 min), 10 V (120-180 min) and 15 V (180-300 min).

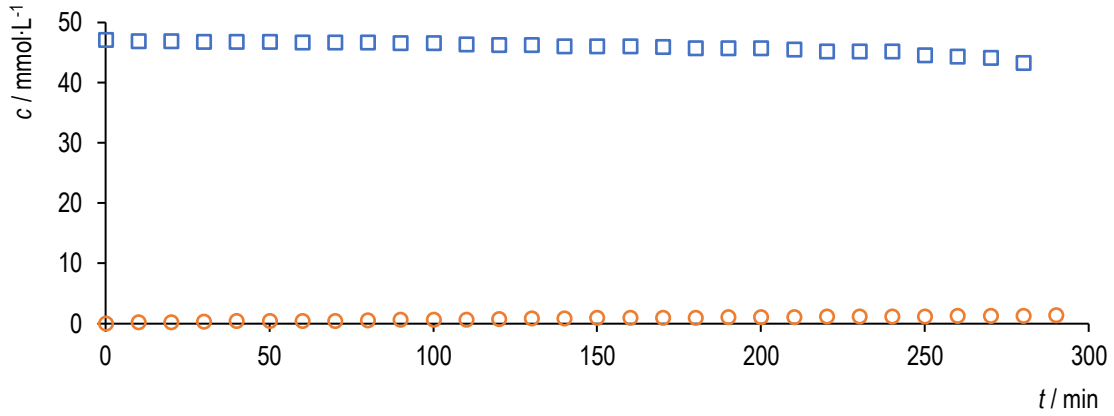

Figure xliv: Concentration of calcium gluconate (circles) and gluconic acid (squares) in electrodialysis using PILs BD2 at 3 V (0-60 min), 6 V (60-120 min), 10 V (120-180 min) and 15 V (180-300 min).

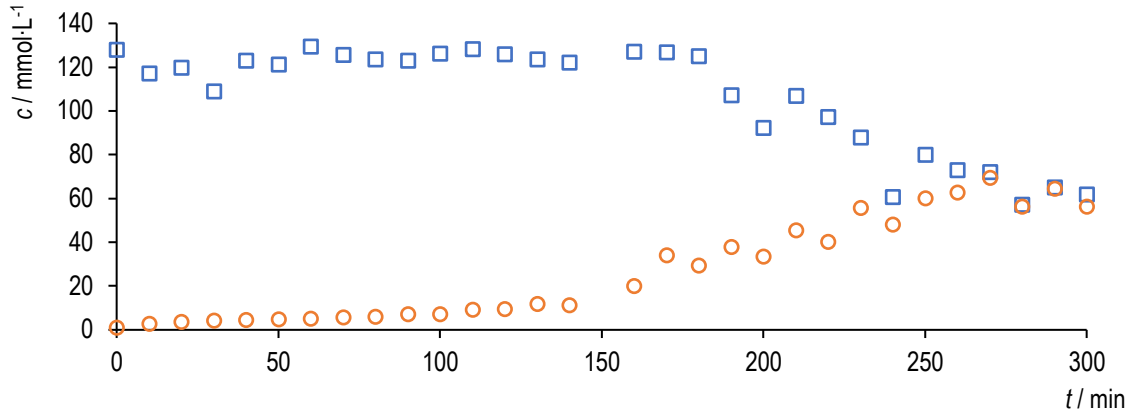

Figure xlv: Concentration of sodium gluconate (circles) and gluconic acid (squares) in electrodialysis using PILs BE1 at 3 V (0-60 min), 6 V (60-120 min), 10 V (120-180 min) and 15 V (180-300 min).

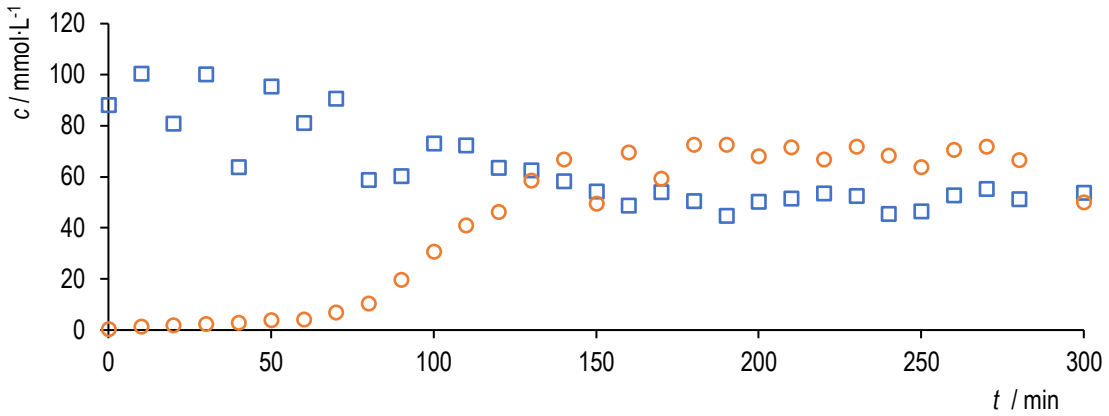

Figure xlvi: Concentration of potassium gluconate (circles) and gluconic acid (squares) in electrodialysis using PILs BE1 at 3 V (0-60 min), 6 V (60-120 min), 10 V (120-180 min) and 15 V (180-300 min).

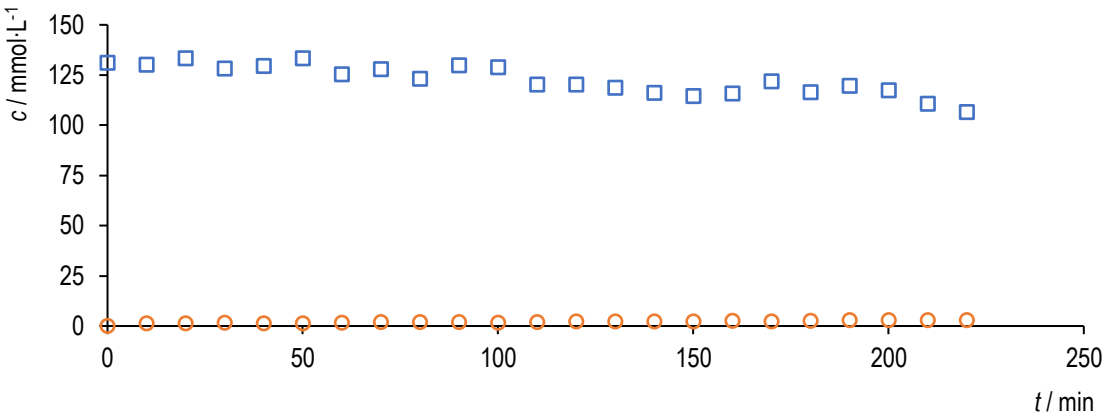

Figure xlvii: Concentration of calcium gluconate (circles) and gluconic acid (squares) in electrodialysis using PILs BE1 at 3 V (0-60 min), 6 V (60-120 min), 10 V (120-180 min) and 15 V (180-220 min).

Curriculum Vitae

Name	Fridolin O. Sommer born August 1st, 1994 in Leverkusen, Germany

Professional Career

Since 02/2021	Experienced Consultant Strategy & Management, CYLAD Consulting, Hamburg
06/2017 – 09/2020	Research assistant, Analytical and Industrial Chemistry, University of Rostock

Education

Since 04/2020	Master Economics, FernUnversität Hagen
10/2018 – 09/2019	Bachelor Economics, University of Rostock
06/2017 – 09/2020	Doctoral student in the group of Prof. Dr. Udo Kragl at the University of Rostock: (*Membranes based on polymerized vinylalkylimidazolium bromides – From ionic liquid monomers to membrane application*)
10/2015 – 04/2017	*Master of Science* in Chemistry, Technical University of Dortmund (*Investigations of β-myrcene with glucamines*)
10/2012 – 09/2015	*Bachelor of Science* in Chemistry, Technical University of Dortmund (*Rhodium-catalyzed hydroaminomethylation of functionalized amines*)

Publications

J. Claus[1], F. O. Sommer[1], U. Kragl, *Solid State Ionics* **2018**, 314, 119-128.

F. O. Sommer, J.-S. Appelt, I. Barke, S. Speller, U. Kragl, *Membranes* **2020**, *10*, 11, 308.

[1]Both authors contributed equally.

Presentations

Oral	*UV polymerized ionic liquids in membranes* F. O. Sommer, U. Kragl 8th International Conference on Ionic Liquids **2019**, Beijing, China
	Membranes based on UV-polymerized ionic liquids F. O. Sommer, J. S. Appelt, I. Barke, S. Speller, U. Kragl 4th Indo-German Workshop on "Advances in Materials, Reactions & Separation Processes" **2020**, Berlin

Poster

Advanced routes towards PILs membranes
F. O. Sommer, U. Kragl
JCF Forum **2017**, Rostock

Membranes based on polymerized ionic liquids
F. O. Sommer, U. Kragl
ProcessNet-Jahrestreffen Mechanische Flüssigkeitsabtrennung **2019**, Bamberg
ProcessNet-Jahrestreffen Fluidverfahrens- und Membrantechnik **2019**, Potsdam

Membranes based on UV-polymerized vinylimidazolium ionic liquids
F. O. Sommer, J.-S. Appelt, I. Barke, S. Speller, U. Kragl
5th International Conference on Ionic Liquid-Based Materials **2019**, Paris, France
Forschungscamp **2019**, Rostock
DGMT Membrane Symposium 17th Poster Day **2020**, Essen

Eidesstattliche Erklärung

Doktorandinnen/Doktoranden-Erklärung gemäß $ 4 Absatz 1 Buchstaben g und h der Promotionsordnung der Mathematisch-Naturwissenschaftlichen Fakultät der Universität Rostock

Name: Sommer, Fridolin Otto

Anschrift: Lichtburgring 3, 13355 Berlin

Ich habe eine Dissertation zum Thema

> Membranes based on polymerized vinylalkylimidazolium bromides – From ionic liquid monomers to membrane application

an der Mathematisch-Naturwissenschaftlichen Fakultät der Universität Rostock angefertigt. Dabei wurde ich von Herrn

> Prof. Dr. Udo Kragl

betreut.

Ich gebe folgende Erklärung ab:

1. Die Gelegenheit zum vorliegenden Promotionsvorhaben ist mir nicht kommerziell vermittelt worden. Insbesondere habe ich keine Organisation eingeschaltet, die gegen Entgelt Betreuerinnen/Betreuer für die Anfertigung von Dissertationen sucht oder die mir obliegenden Pflichten hinsichtlich der Prüfungsleistungen für mich ganz oder teilweise erledigt.
2. Ich versichere hiermit an Eides statt, dass ich die vorliegende Arbeit selbstständig angefertigt und ohne fremde Hilfe verfasst habe. Dazu habe ich keine außer den von mir angegebenen Hilfsmitteln und Quellen verwendet und die den benutzten Werken inhaltlich und wörtlich entnommenen Stellen habe ich als solche kenntlich gemacht.

Rostock, den _____ _____

(Unterschrift)

Ich habe fertig.

Giovanni Trapattoni